

VOLUME 5 / ISSUE 1 / 2022

PAGES 1-146

**EXPERIMENTAL
BIOMEDICAL RESEARCH**

ISSN 2618-6454

[http:// www.experimentalbiomedicalresearch.com](http://www.experimentalbiomedicalresearch.com)

EXPERIMENTAL BIOMEDICAL RESEARCH
VOLUME 5/ ISSUE 1 / JAN-FEB-MAR / 2022

EDITOR-IN-CHIEF

Professor, M.D., Hayrettin Ozturk, Dept. Pediatric Surgery and Pediatric Urology, Bolu Abant Izzet Baysal University, Medical School, Bolu, Turkey

SECTION EDITORS

Associate Professor, M.D., Gulali Aktas, Dept. Internal Medicine, Bolu Abant Izzet Baysal University, Medical School, Bolu, Turkey

Professor, M.D., Yusuf Yagmur, Dept. General Surgery, Medical Park, Gaziantep, Turkey

Professor, M.D., Mete Kaya, Dept. Pediatric Surgery, Health Sciences University, Sevket Yilmaz Education and Research Hospital, Bursa, Turkey

Associate Professor, M.D., Erkan Kilinc, Dept. Physiology, Bolu Abant Izzet Baysal University, Medical School, Bolu, Turkey

Assistant Professor, Ph.D., Muhammad Akhlaq, Dept. of Pharmaceutics, Faculty of Pharmacy, Gomal University, D.I.K Khyber Pakhtoonkhwah, Pakistan

Professor, M.D., Yalcin Karagoz, Dept. Biostatistics, Cumhuriyet University, Medical School, Sivas, Turkey

ASSOCIATE EDITORS

Assistant Professor, M.D., Emine Ozsari, Dept. Chest Diseases, Bolu Abant Izzet Baysal University, Medical School, Bolu, Turkey

Assistant Professor, M.D., Fatih Hilmi Cetin, Dept. Child and Adolescent Mental Health, Selcuk University, Medical School, Konya, Turkey

Associate Professor, M.D., Ummugul Uyeturk, Dept. Oncology, Bolu Abant Izzet Baysal University, Medical School, Bolu, Turkey

Specialist, M.D., Songul Peltek Ozer, Dept. Pathology, Bolu AIBU Training and Research Hospital, Bolu, Turkey

EDITORIAL BOARD MEMBERS

Professor, MBBS, DCH. M.D., Muslim Uddin Sabuj, Child Health Specialist, Head of the Department, Chattagram International Medical College (CIMC), Bangladesh

Professor, M.D., med. Amir Minovi, Chair and Director, Department of Otorhinolaryngology, St. Elisabeth-Krankenhaus Academic Teaching Hospital Cologne University Cologne, Germany

Professor, M.D., Turan Aslan, Dept. Infectious Diseases and Clinical Microbiology, Balikesir University, Medical School, Bolu, Turkey

Liping Li, M.D., Ph.D., Eunice Kennedy Shriver National Institute of Child Health and Human Development, National Institute of Health, Bethesda, MD, USA

Associate Prof., M.D., Nedaa Skeik, Vascular Medicine, Minneapolis Heart Instit., MN, USA

Professor, M.D., Fahri Yilmaz, Dept. Pathology, Sakarya University, Medical School, Sakarya, Turkey

Associate Prof., M.D., Serdar Ceylaner, Dept. Genetic, Intergen Genetic Diseases Diagnostic Research and Application Center, Ankara, Turkey

Associate Professor, M.D., Gulali Aktas, Dept. Internal Medicine, Bolu Abant Izzet Baysal University, Medical School, Bolu, Turkey

Associate Prof., M.D., Suleyman Ipekci, Dept. Endocrinology, Selcuk University, Faculty of Medicine, Konya, Turkey

Professor, M.D., Amir Hossain, Chattagram International Medical College (CIMC), Chittagong, Bangladesh

Professor, M.D., Kahraman Ozturk, Dept. of Hand Surgery, Health Sciences University, Istanbul, Turkey

Professor, M.D., Ahmet Ural, Department of Otorhinolaryngology, Bolu Abant Izzet Baysal University, Medical School, Bolu, Turkey

Associate Prof., M.D., Mukremin Uysal, Dept. Oncology, Afyon Kocatepe University, Medical School, Afyon, Turkey

Associate Prof., M.D., Mehmet Ozen, Dept. Hematology, Ufuk University, Medical School, Ankara, Turkey

Professor, M.D., Yasar Bukte, Dept. Radiology, Health Sciences University, Istanbul, Turkey

Professor, M.D., Nebil Yildiz, Dept. Neurology, Bolu Abant Izzet Baysal University, Medical School, Bolu, Turkey

Professor, M.D., Ramazan Topsakal, Dept. Cardiology, Erciyes University, Medical School, Kayseri, Turkey

Associate Prof., M.D., Hikmet Tekce, Dept. Internal Medicine-Nephrology, Bolu Abant Izzet Baysal University, Medical School, Bolu, Turkey

Professor, M.D., Hasan Orucoglu, Dept. Endodontics, Faculty of Dentistry, Bolu Abant Izzet Baysal University, Bolu, Turkey

Professor, M.D., Fuat Akpınar, Dept. Orthopedics and Traumatology, Istanbul Medeniyet University, Istanbul, Turkey

Associate Prof., M.D., Furkan Erol Karabekmez, Dept. Plastic and Reconstructive Surgery, Health Sciences University, Ankara, Turkey

Professor, M.D., Muhammed Guzel Kurtoglu, Dept. Microbiology, Bolu Abant Izzet Baysal University, Medical School, Bolu, Turkey

Associate Prof., M.D., Memis Hilmi Atay, Dept. Hematology, Ondokuz Mayıs University, Medical School, Samsun, Turkey

Professor, Ph.D., Erol Ayaz, Dept. Parasitology, Bolu Abant Izzet Baysal University, Medical School, Bolu, Turkey

Professor, M.D., Gokhan Kirbas, Dept. Chest Diseases, Dicle University, Medical School, Diyarbakir, Turkey

Associate Prof., M.D., Basri Cakiroglu, Dept. Urology, İstanbul Atlas University, Medical School, İstanbul, Turkey

Professor, M.D., Kemal Nas, Dept. Physical Medicine and Rehabilitation, Sakarya University, Medical School, Sakarya, Turkey

Professor, M.D., Huseyin Buyukbayram, Dept. Chest Diseases, Dicle University, Medical School, Diyarbakir, Turkey

Associate Professor, M.D., Akif Hakan Kurt, Dept. Pharmacology, Bolu Abant Izzet Baysal University, Medical School, Bolu, Turkey



Experimental Biomedical Research is licensed under a [Creative Commons Attribution 4.0 International License](https://creativecommons.org/licenses/by/4.0/)

AUTHOR GUIDELINES

INSTRUCTIONS FOR AUTHORS

Author Guidelines

Instructions for Authors

Experimental Biomedical Research publishes articles in English. Since the journal does not offer translation services, if the language of the manuscripts is not enough, the editors may refuse the manuscript or ask the author to seek language editorial services to bring the manuscript to minimum standards for the review process. If your manuscript is accepted it will be checked by our copyeditors for spelling and formal style before publication.

If you would like to submit a Review, please contact Editor-in Chief at info@experimentalbiomedicalresearch.com.

Online Submission

The articles must be submitted by the corresponding author via the Online Submissions System. If authors encounter technical problems with online submission, they may contact with support team at info@experimentalbiomedicalresearch.com.

Corresponding author

The corresponding author's must do: complete submission of manuscript files; storage of the article and all related documents and giving original data when necessary; contributions of the authors and explanations of conflict of interest disclosures; approval for submission; and the final proof control.

ORCID ID

[ORCID](https://orcid.org/) IDs of the corresponding author and other authors must be submitted during the registration process. This section is mandatory.

As part of our commitment to ensuring an ethical, transparent and fair peer review process, Experimental Biomedical Research is a publisher who signed ORCID open letter. ORCID provides a unique and persistent digital identifier that distinguishes researchers from every other researcher, even those who share the same name, and, through integration in key research workflows such as manuscript and grant submission, supports automated linkages between researchers and their professional activities, ensuring that their work is recognized.

The collection of ORCID iDs from corresponding authors is now part of the submission process of this journal. If you already have an ORCID iD you will be asked to associate that to your submission during the online submission process. We also strongly encourage all co-authors to link their ORCID ID to their accounts in our online peer review platforms. It takes seconds to do: click the link when prompted, sign into your ORCID account and our systems are automatically updated. Your ORCID iD will become part of your accepted publication's metadata, making your work attributable to you and only you. Your ORCID iD is published with your article so that fellow researchers reading your work can link to your ORCID profile and from there link to your other publications.

If you do not already have an ORCID iD please follow this [link](#) to create one.

Author Declaration, Funding and Financial Conflicts of Interest

Authors should provide a cover letter declares: that the article submitted has not been published elsewhere and is not under review; that the submission has been approved by all co-authors and, if necessary, by the responsible authorities and the institute. The publisher will not be responsible in cases of any claims for compensation.

All authors should disclose commercial ties or consulting, stock or share interests or patent license arrangements that can be viewed as a conflict of interest in relation to the manuscript presented ([Author Declaration Form & Conflict Of Interest Statement](#)).

Permissions

Obtaining permission from the copyright owner/ owners is obligatory for figures, tables or texts that previously published elsewhere if the authors want to add them to their manuscripts. Without this evidence, any material used in the article will be deemed to be an original product of the authors.

Units of measurement

The *International System of Units* (SI) is the modern form of the metric system, and is the most widely used system of measurement. Therefore, units of measurement should be presented using the International System of Units in Experimental Biomedical Research.

Abbreviations

Abbreviations are defined at the first mention and are then used continuously. The authors should always be used standard abbreviations and generic names of the drugs. Additionally, the abbreviations presented in the Tables and Figures must be compatible with SI. If registered trademarks are used, the name and country of the manufacturer must be given in parentheses following the generic name on the first use.

Preparation of Manuscript

Title Page

The title page should include: manuscript title, the name(s), the affiliation(s) and address (es) of the author(s).

The corresponding author information should include the e-mail address, the 16-digit ORCID ID, telephone number(s) and full mailing address.

Disclosure of conflict of interest, funding organizations and acknowledgments of people, grants, funds, etc. should be placed in the last section on the title page.

Abstract

Abstracts must not exceed 250 words. The abstract should describe with subheadings; *Aim, Method, Results, and Conclusions*. Abstracts should not contain any unexplained abbreviations or references. It is crucial that the abstract be an accurate summary of the contents of the paper.

Keywords

4 to 6 keywords are sufficient which can be recommended by the "[Index Medicus Subject Headings](http://www.nlm.nih.gov/mesh/meshhome.html)": MeSH (<http://www.nlm.nih.gov/mesh/meshhome.html>).

Main Text

The main text should describe with subheadings; *Introduction, Methods and Materials, Results, Discussion and Conclusions*. Manuscripts should be submitted in Microsoft Office Word formats and arranged as 12-point Times New Roman for text.

References to literature, figures and tables should be placed in the order of their citation in the text. The Author(s) should not use italics, bold or underlined words in the texts. Please use only generic names of drugs.

Introduction: Introduction to a research report should provide a context for the study and specify the particular aims of the reported study. In this section, the emphasis should be on brevity, for the introduction is not meant to be a detailed review but merely a capsule summary that provides a rationale for the second and most important part which is a clear statement as to why the study was undertaken.

Methods and Materials : In this section, the researcher should clearly write the methods used. The materials section should contain the information requested when the reported results need to be expanded and elaborated. It is also important to carry out appropriate statistical tests and to state the sources of the drugs and chemicals used.

Results: In this section, the authors should clearly written information collected using the methods described to achieve the objectives of the study.

Discussion: The discussion section is critical, the information collected is evaluated in relation to the objectives of the study and the context in which the study begins, and any inconsistency between the results is explained and elaborated.

References: It is important that the authors cite appropriate and up-to-date articles for information and comments in the text.

Conflicts of Interest

Authors must declare all relevant interests that could be perceived as conflicting. Authors should explain why each interest may represent a conflict. If no conflicts exist, the authors should state this. Submitting authors are responsible for coauthors declaring their interests.

References

Number references in the order they are mentioned in the text; do not alphabetize. Reference citations in the text should be identified by numbers in square brackets. In listing references (Format AMA), follow NLM Style Guide, abbreviating names of journals according to Index Medicus. Indicate each author's family name followed by a space and initials closed up without periods. Author names should be separated with a comma, never using the conjunction "and" between entries. All authors must be listed for papers with 1 to 3 authors. For papers with more than 3 authors, only the first 3 authors must be listed, followed by et al.

For online journals or articles published online ahead of print, provide the DOI number, if possible, rather than the URL. URLs used in references will not be made hyperlinks.

Journal article

List the first three authors;

Bothra J, Shah H, Tiwar C. Classic Wilms' tumor with raised alpha-fetoprotein levels: A case report and literature review. *Pediatr Urol Case Rep.* 2017; 4(1):238-42.

More than three authors followed by et al.

Nondel B, Lazarus J, Howlett J, et al. Donated staghorn kidney stone in an HIV positive pediatric kidney transplant recipient. *Pediatr Urol Case Rep.* 2017; 4(4):350-55.

Chapter in a book

Luck H. Catalase. In: Bergmeyer HU, editor. *Methods of Enzymatic Analysis.* New York: Academic Press; 1971. p. 885-93.

Online document

Doe J. Title of subordinate document. In: *The dictionary of substances and their effects.* Royal Society of Chemistry. [cited 2016 Dec 27]. Available from:[http://www.rsc.org/dose/title of subordinate document](http://www.rsc.org/dose/title%20of%20subordinate%20document).

The authors are responsible for the accurate and in full presentation in accordance with the journal's style of references.

Preparation of Figures and Tables

The figures and tables should be uploaded electronically by a separate file and should be stated consecutively in the text. Each table should have an explanatory heading, and if numerical measurements are made, the units should be added to the column header. Figures should be presented in vector image formats (Illustrator, EPS, WMF, FreeHand, CorelDraw, PowerPoint, Excel etc.) or in bitmap formats (Photoshop, TIFF, GIF, JPEG, etc.). Bitmap images should be at least 300 dpi resolution.

Supplementary Materials

Authors can submit one file of supplementary material such as audio files, video clips, or datasets. A section titled "Supplementary Material" should be included before the references list with a concise description for each supplementary material file. Authors are responsible for providing the final supplementary materials files that will be published along with the article.

English Language Editing

Editors and reviewers should ensure the clarity of English language of the article in assessment of the manuscript.

If any help needed in writing in English one can consider the following:

- Ask for help from a co-worker who is a native English speaker in sake of clarity of the text.
- Applying to a professional english language editing service to improve the quality of the language and grammar of the text.

Authors should aware that the use of a language editing service does not warrant an article to be accepted for publication in this journal.

ETHICAL STANDARDS

Ethical Responsibilities of Authors

Experimental Biomedical Research journal will follow the **Committee on Publication Ethics (COPE)** guidelines on how to deal with potential acts of misconduct. For this reason, authors should protected the journal trust, the professionalism of the scientific authorship, and must refrain from misrepresenting the consequences of research that could destroy all scientific effort.

Plagiarism checking

Articles sent to Experimental Biomedical Research journal are checked for possible plagiarism by using an appropriate software (**iThenticate**). However, corresponding and co-authors are responsible for any fraud, intentional or unintentional malpractice.

Research involving human participants and/or animals

Experimental Biomedical Research adopt ICMJE Recommendations on Protection of Research Participants. For more information, [click here!](#)

In addition to ICMJE recommendations, we also support 3Rs principals (**Replacement, Reduction and Refinement**) for humans and animals usage in research. Briefly 3Rs are mentioned below, and more information can be [accessed here!](#)

Replacement: approaches which avoid or replace the use of animals

Reduction: approaches which minimise the number of animals used per experiment

Refinement: approaches which minimise animal suffering and improve welfare

All work should be done with the permission of local human subjects or animal care committees (institutional and national) and clinical trials should be registered to legislation. The official numbers from these committees must be found in the Materials and Methods section (or text describing the experimental procedures).

1) Statement of human rights

The studies involving human participants should state that the research has been endorsed by the institutional and / or national research ethics committee and that it is conducted in accordance with the ethical standards set out in the [Helsinki Declaration of 1964](#), and that subsequent changes are also met (1).

2) Statement on the welfare of animals

If you have done experimental research on animals, authors should indicate whether the international, national and / or institutional guidelines for the care and use of the animals are followed, and whether the work has been approved by an institutional research ethics committee.

Informed consent

If manuscripts report the results of an experimental research of human subjects, all authors must fulfill the **International Committee of Medical Journal Editors (ICMJE)** requirements on confidentiality and informed consent from patients and study participants. Therefore;

1- Informed consent is obtained from all participants before they are included in the work.

2- Distinguishing details of the participants examined (name, date of birth, identification numbers and other information) should not be published in print, photographs and genetic profiles.

3-Where someone is deceased, please make sure that you have written permission from the family or estate.

4-If the identification features are changed to protect anonymity as in genetic profiling, the authors should assure that the changes do not distort scientific meaning.

Authors may use this [Patient Consent Form](#), which sent to the journal if requested.

The journal reserve the right to reject manuscripts that do not comply with the above-mentioned guidelines.

Publication charges

There are no submission fees or page charges for Experimental Biomedical Research journal.

Copyright Policy

Copyright (c): Author(s)

For all licenses, authors retain copyright and full publication rights without restriction.

License-Creative Commons License: CC BY: Articles published in *Experimental Biomedical Research* are open-access, distributed under the terms of the Creative Commons Attribution Non-Commercial License (<http://creativecommons.org/licenses/by-nc/4.0>), which permits unrestricted non-commercial use, distribution, and reproduction in any medium, provided the original work is properly cited.

Proofs

Accepted articles are sent as portable document format (PDF) files, along with proof by e-mail to the relevant author for approval. Corrections to PDF evidence should be limited to posting errors only, and no significant additions / deletions should be made. Authors are responsible for all statements made in their work, including changes made by the copy editor and authorized by the author concerned. Authors are strongly advised to thoroughly examine the PDF evidence and return the proofs within 3 days.

Experimental Biomedical Research

E-mail: info@experimentalbiomedicalresearch.com

Completed authorship forms may be mailed to this address.

Reference

1-World Medical Association. Declaration of Helsinki: ethical principles for medical research involving human subjects. <http://www.wma.net/en/30publications/10policies/b3/index.html>. Accessed October 14, 2010.

Editorial Assessment and Peer Review Policy-Process

Experimental Biomedical Research is an online-only, international, peer-reviewed, open access journal and is committed to maintaining the high quality of the peer-review process. Additionally, the peer review process ensures that the articles published, meet the accepted standards of the discipline. Experimental Biomedical Research (Editor) reviews new submissions according to its guidelines. When they meet all criteria, they are sent to two referees (double blind) and all manuscripts are read by reviewers, and revisions to the manuscript may be required. If the decision conflicts between two reviewers, it will be sent to third peer reviewer. The typical review will take in 2-4 weeks. When the manuscript is received from peer reviewer there will be one of the following outcome: 1) accepted manuscript without revisions, 2) invite authors to resubmit the manuscript after minor or major changes while the final decision is kept pending, 3) or reject the manuscript. When the manuscript is returned for revision prior to acceptance, the revised manuscript must be submitted within 30 days after the author's receipt of the referee's reports. Editorial review again (re-peer review/accepted/rejected). The final decision is sent to the authors.

Peer Review Policy-Process

Manuscript Submission

- New submission via online system
- Cover letter, author and co-author details, manuscript and separate files

Pre- Quality Associate Editorial Assessment

- Plagiarism check
- Qualification in the English language editing
- Ensuring that the manuscript adheres to the stylistic and bibliographic requirements outlined in the Author Guidelines (Experimental Biomedical Research Submission and Publication Checklist)
- Sent back to author for approval of edits

Peer Review

- Double-blind peer review undertaken by experts in the field
- When the manuscript is received from peer reviewer there will be one of the following outcome: 1) accepted manuscript without revisions, 2) invite authors to resubmit the manuscript after minor or major changes while the final decision is kept pending, 3) or reject the manuscript.
- Revision made by authors on the basis of reviewer recommendations (revisions must be highlighted and accompanied by a letter in response to each comment by the reviewers)
- In case of revisions, the revised article will be sent to the reviewers who will decide on a new recommendation for revision, acceptance or rejection.

Copy Editing

- Professional checking for the composition and organization (formatting) of the paper against the journal guidelines
- Reference styling and proof corrections

- Author's confirmation of the final edited manuscript before publication
- In this version, corrections to PDF evidence should be limited to posting errors only, and no significant additions / deletions should be made

Publishing

- Accepted article is sent for generating the galley proof
- Online publication of the manuscript

Copyright Notice

Copyright (c): Author(s)

Experimental Biomedical Research journal is licensed under a [Creative Commons Attribution-NonCommercial 4.0 International License](https://creativecommons.org/licenses/by/4.0/).

Privacy Statement

The names and email addresses entered in this journal site will be used exclusively for the stated purposes of this journal and will not be made available for any other purpose or to any other party.



Experimental Biomedical Research is licensed under a [Creative Commons Attribution 4.0 International License](https://creativecommons.org/licenses/by/4.0/)

Effects of the ATP-dependent K (+)-channel effectors pinacidil and glibenclamide on liver tissue in an experimental model of epilepsy: A histopathological study

Selma Erdogan Duzcu¹, Ayhan Cetinkaya², Hayriye Soyuturk³, Serif Demir⁴

¹Department of Pathology, Bolu Abant Izzet Baysal University, Faculty of Medicine, Bolu, Turkey

²Department of Physiology, Bolu Abant Izzet Baysal University, Faculty of Medicine, Bolu, Turkey

³Interdisciplinary Neuroscience, Bolu Abant Izzet Baysal University, Institute of Graduate Studies, Bolu, Turkey

⁴Department of Physiology, Duzce University, Faculty of Medicine, Duzce, Turkey

ABSTRACT

Aim: It is known that most of the antiepileptic drugs have negative effects on the liver. Pinacidil is a nonselective opener of KATP channels, including the plasma membrane and mitochondria. Glibenclamide is an ATP -dependent K channel blocker ensuring the intake of calcium. Our aim in this experimental study was to examine the effects of pinacidil and glibenclamide on the liver tissue of rats with focal epilepsy.

Method: Sixty male Sprague Dawley rats (2-4 months old, 200-250 gr) were used in the study. The rats were divided into 4 groups, 15 in each group. The groups were divided into control group, penicillin group, penicillin + pinacidil group and penicillin + glibenclamide group. The craniums of the rats in the control group were opened and normal saline was given; Penicillin (2 µl 500 IU) was intracortically administered to other groups and an experimental epilepsy model was created. At the end of the study, liver tissue of rats was taken and evaluated in terms of vacuolar degeneration, lymphocyte infiltration, vascular congestion, sinusoidal dilatation, necrosis, and Kupffer cell proliferation, radial alignment of hepatic cords, central vein and portal vein dilatation in hepatocytes.

Results: Venous congestion, cytoplasmic vacuolization, Kupffer cell proliferation, portal vein dilatation and necrosis were distinct in the group to which pinacidil was administered, and distortion was present in the radial sequence ($p < 0.001$). In addition, inflammation, venous congestion and hepatocyte necrosis were found to be lower in the glibenclamide given group compared to the control group ($p < 0.001$).

Conclusion: It can be suggested that pinacidil treatment caused negative results in liver histopathological parameters, whereas glibenclamide was more protective by reducing inflammation, venous congestion and hepatocyte necrosis.

Key words: Epilepsy, liver, pinacidil, glibenclamide, ATP dependent K (+)-channel, histopathology, rat.

✉ Dr. Selma Erdogan Duzcu

Department of Pathology, Bolu Abant Izzet Baysal University, Faculty of Medicine, Bolu, Turkey

E- mail: serdoganduzcu@hotmail.com

Received: 2021-05-25 / Revisions: 2021-07-12

Accepted: 2021-07-17 / Published online: 2022-01-01

Introduction

Epilepsy is one of the frequent central nervous system disorders, affecting many organs and

system [1]. Unbalanced potassium homeostasis is one of the important factors playing a role in the pathogenesis of epileptic seizures [1]. The concentration of extracellular potassium increases during the seizures, and the potential of cellular membrane decreases [1]. Therefore, the studies examining the pathophysiological mechanisms are critical [1]. Drug toxicity may occur owing to the role of liver in the

elimination of drugs and potential toxins [2]. Inflammation occurs through the activation of inflammasome that is a significant factor for hepatocyte damage and hepatic stellate cell activation, and acute and chronic liver diseases occur [3]. Most of anti-epileptic drugs may cause hepatotoxicity [2].

ATP-sensitive K channels (KATP) are present in many cells and tissues such as pancreas β cells, skeletal muscles, neurons, glial cells, kidney and liver [4]. KATP channels play key roles in hyperglycemia, hypoglycemia, ischemia and hypoxia [4]. ATP-dependent potassium channels consists of two sub-units as Kir6.x and sulphonylurea receptor [5]. They are found in the mitochondrial inner membrane of rat liver [6]. They directly take part in the glucose metabolism of in the intra-cellular ATP concentrations with liver KATP channels [4]. Moreover, they have different physiological and pharmacological functions based on KATP channels' subunits [4]. However, the information on the roles of K channels in hepatocytes is limited [5].

Pinacidil is a nonselective opener of KATP channels, including the plasma membrane and mitochondria [7, 8]. Pinacidil has been shown to have significant cardioprotective and vasorelaxant effects cardiac ischemia/reperfusion injury, arrhythmia and hypertension [7, 8].

Pinacidil is a vasodilator agent used in the treatment of hypertension [9]. Pinacidil have also been shown to prevent hypoxia in rat cardiac myocytes [8].

Glibenclamide is an ATP -dependent K channel blocker ensuring the intake of calcium [10, 11]. It is one of the most commonly-administered anti-diabetic drugs from the sulphonylurea group [3, 12]. Having been used for type 2 diabetes since 1960s, it has been reported to have anti-inflammatory and anti-oxidant effects [3, 10].

In the literature, there is no study revealing the effects of pinacidil and glibenclamide on the liver tissue of rats in which a focal epilepsy model was created. Therefore, in this study, we aimed to histopathologically investigate the effects of pinacidil and glibenclamide on liver morphology by creating experimental epilepsy in rats.

Materials and methods

Sixty male Sprague Dawley rats (2-4 months old, 200-250 gr) were used in the study. The Institutional Animal Care and Use Committee of Bolu Abant Izzet Baysal University (Number: 2018/36/A1) approved for the study. All procedures complied with the Guide for the Care and Use of Laboratory Animals (1996). These rats were kept in the environment that was illuminated/dark for 12, had a room temperature of $22 \pm 2^\circ\text{C}$ and relative humidity of 60-70% and they were fed ad libitum (with water and food).

Epilepsy animal model and groups

Experimental focal epilepsy model was performed by intracortical administration of penicillin to the animals in the experimental groups under ketamine-xylazine anesthesia (10/90 mg/kg, intraperitoneally).

Group 1: used as negative control group. The craniums of the rats in this group were opened and 2 μl of normal saline was intracortically administered.

The craniums of the rats in group 2, group 3 and group 4 were opened as in the group 1 and 2 μl of 500 IU penicillin was intracortically administered.

Group 2: dimethyl sulfoxide (DMSO) was intravenously administered 15 minutes after the focal penicillin model was formed in the brain.

Group 3: KATP channel opener pinacidil monohydrate (0.1 mg/kg, Sigma-Aldrich, CAS:

85371-64-8) was intravenously administered 15 minutes after the focal penicillin model was formed in the brain. The solvent of this drug was DMSO.

Group 4: KATP channel blocker glibenclamide (0.1mg/kg, Sigma-Aldrich, CAS: 10238-21-8) was intravenously administered 15 minutes after the focal penicillin model was formed in the brain. The solvent of this drug was DMSO. On the eighth day of work, the animals were euthanized by cervical dislocation under deep anesthesia using 5% halothane. Then, the liver tissues obtained from rats were fixed in 10% formaldehyde for histopathological examination.

Histopathological examination

Sections from liver tissues were followed in a manner to view the broadest surfaces, and then embedded into paraffin. 3 μ m sections were cut from the paraffin blocks and stained with hematoxylin eosin. Sections were assessed by a pathologist under LEICA DM 2000 LED light microscope.

Vacuolar degeneration, lymphocyte infiltration, vascular congestion, sinusoidal dilatation, necrosis, Kupffer cell proliferation, radial alignment of hepatic cords, central vein and portal vein dilatation in hepatocytes were assessed in the pathological examination of liver tissue and semi-quantitatively scored with points from 0 to 3 [13, 14]. Based on this score, absence of pathology was scored as 0, while presence of mild (focal) pathology was scored as 1, presence of moderate (multifocal) pathology was scored as 2, and presence of severe (diffuse) pathology scored as 3. Sections were stained with hematoxylin eosin were photographed at different scales through the Infinity 3 Analyze Release 6.5 system.

Statistical analyses

Number and percentage values were used for the descriptive statistics. To determine whether

there was a significant difference between the groups, Kruskal-Wallis test was used. In cases where there were differences between the groups, paired comparisons (post hoc) test was used to determine the groups as the sources of this difference. Significance level was used as $p<0.05$. Analyses were performed on Statistical Package for the Social Sciences (SPSS) v.21 by IBM.

Results

Two rat each in the groups 1, 2 and 3 died on the fourth day and were excluded from the study. While no epileptic activity was observed in the control group by electrophysiological evaluation of the experimental groups, it was shown by spike waves that the epilepsy model was formed in the other groups.

The histopathological parameters of the groups are presented in table 1. In addition, examples of microscopic images of the groups are presented in figures 1-4. The inflammatory cells in the portal area had a significant difference ($p<0.001$). The penicillin group (PE) had a significant increase compared to the control group. Moreover, compared to the PE group, penicillin+glibenclamide (PE+GLI) group had a significantly less inflammation. A significant difference regarding the sinusoidal dilatation values was present ($p<0.001$). Penicillin group had a significance increase compared to the control group.

A significance difference regarding the venous congestion values was present between the groups ($p<0.001$). PE and penicillin+pinacidil (PE+PI) groups had a significant increase in the venous congestion compared to the control group. PE+PI and PE+GLI group had a statistically significant decrease in venous congestion compared to the penicillin group. PE+PI group had a more distinctive congestion compared to the PE+GLI group.

Table 1. Distribution of histopathological parameters among the groups.

Parameters		Groups				
		Control (N=13) N (%)	PE (N=13) N (%)	PE + PI (N=13) N (%)	PE + GLI (N=15) N (%)	<i>p</i>
Inflammation	0	4 (30.8)	0 (0.0)	0 (0.0)	0 (0.0)	0.001
	1	9 (69.2)	6 (46.2)	10 (76.9)	15 (100.0)	
	2	0 (0.0)	4 (30.8)	2 (15.4)	0 (0.0)	
	3	0 (0.0)	3 (23.1)	1 (7.7)	0 (0.0)	
Average rank		17.73 ^a	38.04 ^b	30.19 ^{a,b}	24.50 ^a	
Sinusoidal dilatation	1	12 (92.3)	0 (0.0)	6 (46.2)	6 (40.0)	0.001
	2	1 (7.7)	10 (76.9)	4 (30.8)	9 (60.0)	
	3	0 (0.0)	3 (23.1)	3 (23.1)	0 (0.0)	
Average rank		14.35 ^a	39.96 ^b	28.88 ^{a,b}	26.90 ^{a,b}	
Congestion	1	5 (38.5)	0 (0.0)	0 (0.0)	9 (60.0)	0.001
	2	8 (61.5)	2 (15.4)	6 (46.2)	5 (33.3)	
	3	0 (0.0)	11 (84.6)	7 (53.8)	1 (6.7)	
Average rank		18.27 ^a	41.92 ^b	35.77 ^b	15.83 ^a	
Vacuolization	0	11 (84.6)	0 (0.0)	0 (0.0)	4 (26.7)	0.001
	1	2 (15.4)	4 (30.8)	8 (61.5)	7 (46.7)	
	2	0 (0.0)	9 (69.2)	3 (23.1)	4 (26.7)	
	3	0 (0.0)	0 (0.0)	2 (15.4)	0 (0.0)	
Average rank		10.77 ^a	38.81 ^b	34.50 ^b	26.13 ^b	
Necrosis	0	10 (76.9)	4 (30.8)	2 (15.4)	10 (66.7)	0.001
	1	3 (23.1)	4 (30.8)	8 (61.5)	5 (33.3)	
	2	0 (0.0)	5 (38.5)	2 (15.4)	0 (0.0)	
	3	0 (0.0)	0 (0.0)	1 (7.7)	0 (0.0)	
Average rank		18.81 ^a	34.62 ^{b,c}	36.38 ^b	21.17 ^c	
Kupffer cell proliferation	0	12 (92.3)	3 (23.1)	0 (0.0)	3 (20.0)	0.001
	1	1 (7.7)	4 (30.8)	12 (92.3)	11 (73.3)	
	2	0 (0.0)	6 (46.2)	0 (0.0)	1 (6.7)	
	3	0 (0.0)	0 (0.0)	1 (7.7)	0 (0.0)	
Average rank		11.27 ^a	35.27 ^b	34.15 ^b	29.07 ^b	
Distortion in radial alignment	0	11 (84.6)	10 (76.9)	5 (38.5)	14 (93.3)	0.010
	1	2 (15.4)	2 (15.4)	6 (46.2)	0 (0.0)	
	2	0 (0.0)	0 (0.0)	1 (7.7)	1 (6.7)	
	3	0 (0.0)	1 (7.7)	1 (7.7)	0 (0.0)	
Average rank		24.35 ^a	26.88 ^{a,b}	36.96 ^b	22.57 ^a	
Central vein dilatation	0	7 (53.8)	4 (30.8)	3 (23.1)	4 (26.7)	0.192
	1	5 (38.5)	4 (30.8)	6 (46.2)	10 (66.7)	
	2	1 (7.7)	5 (38.5)	4 (30.8)	1 (6.7)	
Average rank		20.81	31.31	31.58	26.47	
Portal vein dilatation	0	9 (69.2)	7 (53.8)	1 (7.7)	10 (66.7)	0.003
	1	4 (30.8)	3 (23.1)	6 (46.2)	2 (13.3)	
	2	0 (0.0)	3 (23.1)	5 (38.5)	3 (20.0)	
	3	0 (0.0)	0 (0.0)	1 (7.7)	0 (0.0)	
Average rank		20.46 ^a	26.69 ^{a,b}	39.85 ^b	23.60 ^a	

* Kruskal Wallis test ** letters a, b indicate the paired comparison (post-hoc) test results.

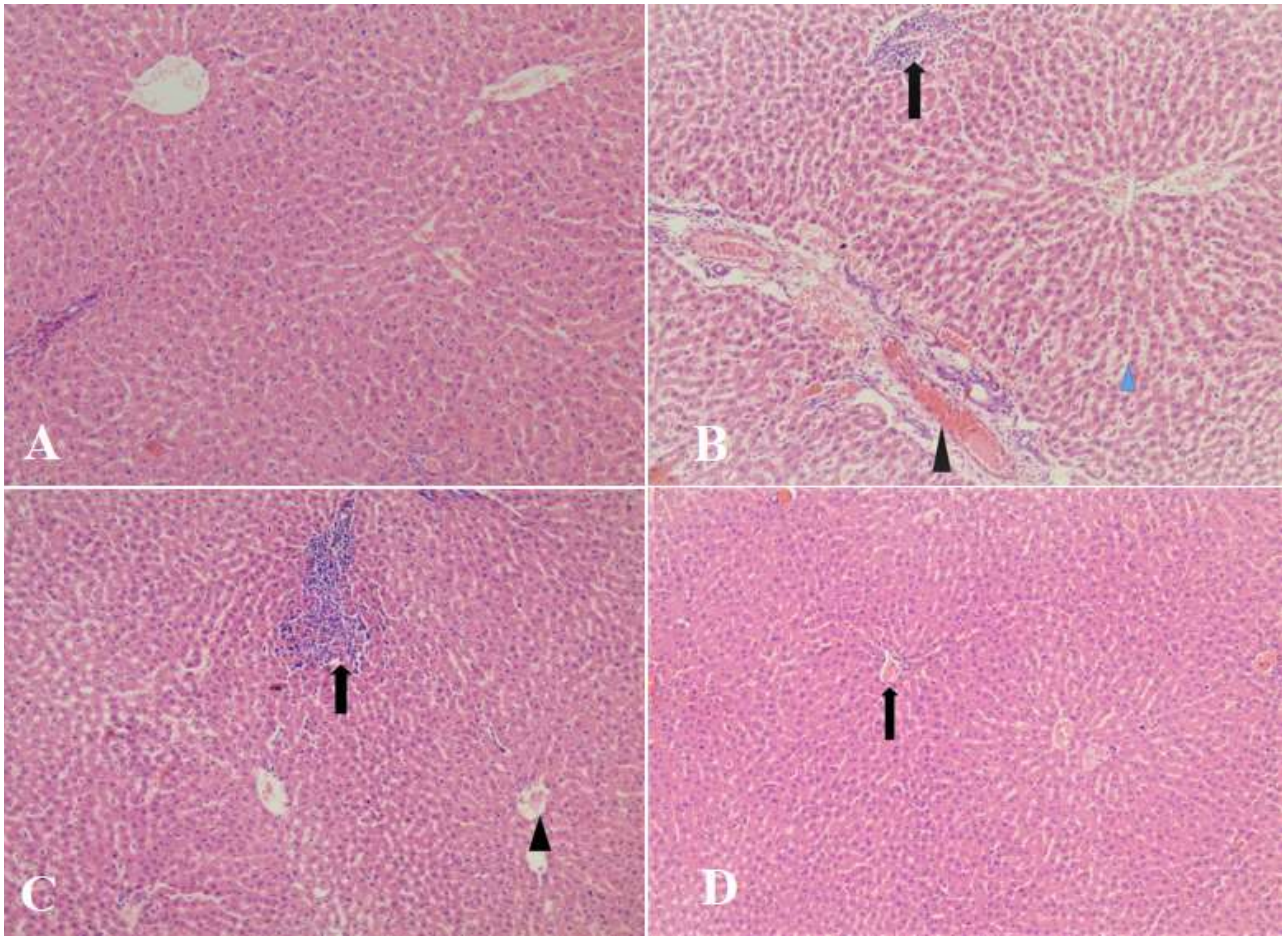


Figure 1. A. Control group, regular radial alignment present, inflammation and necrosis absent, HEX100. B. PE group; distinctive inflammation in the portal area (black arrow), portal venous congestion (tip of black arrow), sinusoidal dilatation (tip of blue arrow), HEX100. C. PE+PI group; distinctive portal inflammation (black arrow), central vein dilatation (tip of black arrow), HEX100. D. PE+GLI group; mild congestion in the central vein (black arrow), no distinctive inflammation present, HEX100.

The groups had a significant difference in terms of cytoplasmic vacuolization values ($p<0.001$). Cytoplasmic vacuolization statistically and significantly increased in other groups compared to the control group.

The groups had a significant difference in terms of necrosis values ($p=0.001$). Necrosis statistically and significantly increased in PE and PE+PI groups compared to the control group. PE+PI group had more necrosis compared to the PE+GLI group.

The groups had a significant difference in terms of Kupffer cell proliferation values ($p<0.001$). Kupffer cell proliferation statistically and

significantly increased in other groups compared to the control group.

The groups had a significant difference in terms of the values of radial sequence distortion ($p=0.010$). Compared to the control group and PE+GLI group, radial sequence of PE+PI group had a statistically significant distortion. The groups had no significant difference in terms of central vein dilatation ($p=0.192$).

The groups had a significant difference in terms of portal venous dilatation values ($p=0.003$). Portal vein dilatation statistically and significantly increased in PE+PI group compared to the control group. PE+PI group

had more portal vein dilatation compared to the PE+GLI group.

Discussion

Penicillin is administered intracortically or parenterally to form the experimental epilepsy model, and chemical convulsions are formed [15]. Based on the hypoxic processes in the cells of all systems, seizures may cause reversible and irreversible damages [15].

KATP channels are important for electrical activity [1]. KATP channels close when intracellular ATP concentration is high, and open in case of ischemia [4]. These channels consist of four pore-forming subunits Kir6.x (Kir6.1 or Kir6.2) and four regulatory subunit sulfonylurea receptors SUR (SUR1, SUR2A, or SUR2B) [4]. SUR1 and Kir6.2 are sensitive to diazoxide, the activator of KATP channels, and Kir6.2 with SUR2A is sensitive to pinacidil [4]. Genetic, physiological and pharmacological findings have demonstrated that K channels also have a role in epilepsy management and neuronal excitability [16, 17]. Thus, it has been reported that KATP channels may be a potential treatment for novel drugs [16, 17]. Acar et al. showed that pinacidil reduced epileptic activity, but glibenclamide did not have an effect [16]. Another study reported that glibenclamide showed an anticonvulsant effect by inhibiting generalized tonic clonic and absence seizures [18].

Ateş et al. examined the impact of epileptic seizure experienced by rats during their pregnancy on the liver of newborn rat [15]. Under the electron microscope, expansion and decrease in the number of mitochondria was seen and assessed in favor of latency in the hepatogenesis [15].

Inflammation, venous congestion, cytoplasmic vacuolization in hepatocytes, necrosis and Kupffer cell proliferation increased in the livers

of rats that were exposed to epilepsy seizure through the intracortical administration of penicillin, and inflammatory impact was seen in the livers of rats that suffered epileptic seizures, indicating hepatotoxic effect.

Pinacidil is an ATP-dependent mitochondrial K channel opener [19]. Pinacidil has been reported to have cardioprotective impacts by protecting the cardiac tissues from mitochondrial damage in ischemia reperfusion that occurs in vivo and in vitro [19]. In addition, pinacidil suppressed the inflammation around the incision line, as seen in a study conducted with rats [20]. However, the literature did not have data on the morphological effects of pinacidil on liver. This study indicated distinctive venous congestion, cytoplasmic vacuolization, Kupffer cell proliferation, portal vein dilatation and necrosis in the PE+PI group, and distortion was seen in the radial alignment. Compared to the control group, hepatotoxic impact was seen, but no significant difference with PE group was seen.

Glibenclamide inhibits ATP-sensitive potassium channels in pancreas beta cells [11]. Glibenclamide reduces proinflammatory cytokine generation, vasogenic edema and caspase-3 activation in bacterial infection cases among diabetic patients [3]. It has a protective role against the inflammation-related damage in the respiratory system, digestive system, kidneys, bladder and heart, in ischemia reperfusion damage and septic shock [3, 10]. Its anti-inflammatory impact is inhibited by the NLRP3 inflammasome, and it makes its contributions by reducing the generation of proinflammatory cytokines, preventing the spread of inflammatory cells into the inflammation area and boosting the nitric oxide generation [12].

Dwivedi et al. found that glibenclamide decreased thioacetamide-related

inflammasome activation, inflammatory lymphocyte infiltration, collagen deposition, necrotic hepatocytes and fibrosis [3]. Sokolovska et al. indicated that glibenclamide treatment reduced the liver tissue damage among the rats that had streptozotocin-related diabetes [11]. Liu et al. examined the effects of glibenclamide on the liver tissue damage related to acute radiation on rats [10]. Glibenclamide was found to decrease hepatocyte vacuolization, hepatocellular edema and hepatic sinusoids [10]. Administration of glibenclamide before the radiation stimulated the Akt-NF- κ B pathway and decreased reactive oxygen derivatives, creating a protective impact on the hepatocytes [10].

Malhi et al. indicated that ATP-dependent K channels had an important role in the arrangement of hepatocyte proliferation [5]. A limited DNA synthesis was seen in cell culture and pinacidil increased DNA synthesis, while glibenclamide inhibited DNA synthesis [5]. Ymazaki et al. conducted a study on pigs and examined the impact of nicorandil and glibenclamide on ischemia reperfusion damage [6]. Glibenclamide corrected the hepatocyte damage like nicorandil, but no difference was found when compared to the control group [6]. Hai et al. indicated that nicorandil (KATP channel opener) was protected from ischemia reperfusion damage through apoptosis inhibition [21].

This study indicated that glibenclamide decreased inflammation, venous congestion and hepatocyte necrosis, and that glibenclamide might have a hepatoprotective effect, which is in line with the literature. Pinacidil, whose impacts on the liver morphology has not been detailed in the literature, created hepatotoxic impact compared to the control group, but no significant difference with the data of PE group was found.

The study was solely based on histopathologic examination, and biochemical and other clinical tests were not present. We see this situation as the limitation of our study.

Conclusion

As a results, it can be suggested that pinacidil treatment caused negative results in liver histopathological parameters, whereas glibenclamide was more protective by reducing inflammation, venous congestion and hepatocyte necrosis. In addition to, studies that will reveal the impact mechanisms of ATP-dependent K channel opener and blocker drugs for liver will be beneficial for the therapeutic use of these drugs.

Funding: *The author(s) received no financial support for the research, authorship, and/or publication of this article.*

Conflict of Interest: *The authors declare that they have no conflict of interest.*

Ethical statement:

The study was approved by Local Clinical Research Ethics Committee Number: (2018/36/A1), and written informed consent was obtained from each subject.

Open Access Statement

This is an open access journal which means that all content is freely available without charge to the user or his/her institution under the terms of the Creative Commons Attribution Non-Commercial License (<http://creativecommons.org/licenses/by-nc/4.0>). Users are allowed to read, download, copy, distribute, print, search, or link to the full texts of the articles, without asking prior permission from the publisher or the author.

Copyright (c) 2021: Author (s).

References

- [1] Venediktova NI, Gorbacheva OS, Belosludtseva N V, et al. Energetic, oxidative and ionic exchange in rat brain and liver mitochondria at experimental audiogenic epilepsy (Krushinsky–Molodkina model). *J Bioenerg Biomembr.* 2017;49(2):149–58.
- [2] Poorrostami A, Farokhi F, Heidari R. Effect of hydroalcoholic extract of ginger on the liver of epileptic female rats treated with lamotrigine. *Avicenna J Phytomedicine.* 2014;4(4):276–86.
- [3] Dwivedi DK, Jena GB. Glibenclamide protects against thioacetamide-induced hepatic damage in Wistar rat: investigation on NLRP3, MMP-2, and stellate cell activation. *Naunyn Schmiedebergs Arch Pharmacol.* 2018;391(11):1257–74.
- [4] Zhou M, Yoshikawa K, Akashi H, et al. Localization of ATP-sensitive K⁺ channel subunits in rat liver. *World J Exp Med.* 2019;9(2):14–31.
- [5] Malhi H, Irani AN, Rajvanshi P, et al. K(ATP) channels regulate mitogenically induced proliferation in primary rat hepatocytes and human liver cell lines: Implications for liver growth control and potential therapeutic targeting. *J Biol Chem.* 2000;275(34):26050–57.
- [6] Yamazaki H, Oshima K, Sato H, et al. The effect of nicorandil on ischemia-reperfusion injury in a porcine total hepatic vascular exclusion model. *J Surg Res.* 2011;167(1):49–55.
- [7] Kopustinskiene DM, Liobikas J, Skemiene K, et al. Direct effects of K ATP channel openers pinacidil and diazoxide on oxidative phosphorylation of mitochondria in situ. *Cell Physiol Biochem.* 2010;25(2–3):181–86.
- [8] Iguchi K, Saotome M, Yamashita K, et al. Pinacidil, a KATP channel opener, stimulates cardiac Na⁺ / Ca²⁺ exchanger function through the NO / cGMP / PKG signaling pathway in guinea pig cardiac ventricular myocytes. *Naunyn Schmiedebergs Arch Pharmacol.* 2019;392(8):949–59.
- [9] Shaheen O, Patel J, Avant GR, et al. Effect of cirrhosis and debrisoquin phenotype on the disposition and effects of pinacidil. *Clin Pharmacol Ther.* 1986;40(6):650–55.
- [10] Liu H, Wang S, Wu Z, et al. Glibenclamide, a diabetic drug, prevents acute radiation-induced liver injury of mice via up-regulating intracellular ROS and subsequently activating Akt-NF-κB pathway. *Oncotarget.* 2017;8(25):40568–82.
- [11] Sokolovska J, Isajevs S, Sugoka O, et al. Comparison of the effects of glibenclamide on metabolic parameters, GLUT1 expression, and liver injury in rats with severe and mild streptozotocin-induced diabetes mellitus. *Med.* 2012;48(10):532–43.
- [12] Zhang G, Lin X, Zhang S, et al. A Protective Role of Glibenclamide in Inflammation-Associated Injury. *Mediators Inflamm.* 2017;2017:3578702.
- [13] Sabbah WS, Hanafy SM, Arafa MAA. Biochemical and histological study on the effect of levetiracetam on the liver and kidney of pregnant albino rats. *Folia Morphol.* 2019;78(4):809–17.
- [14] Ahmed OM, Fahim HI, Ahmed HY, et al. The preventive effects and the mechanisms of action of navel orange peel hydroethanolic extract, naringin, and naringenin in N-Acetyl-p-aminophenol-induced liver injury in wistar rats. *Oxid Med Cell Longev.* 2019;2019:2745352.
- [15] Ates U, Baka M, Uyanıkgil Y, et al. Histological study of liver tissue from

- newborn rats of mothers. *Ege Tıp Derg.* 2004;43(2):73–77.
- [16] Kobayashi K, Nishizawa Y, Sawada K, et al. K⁺ Channel Openers Suppress Epileptiform Activities Induced by 4-Aminopyridine in Cultured Rat Hippocampal Neurons. *J Pharmacol Sci.* 2008;108(4):517–28.
- [17] Acar Y, Özmerdivenli R, Demir Ş, et al, Ankaralı S, Beyazçiçek Ö, et al. Agonist and Antagonist Effects of ATP-Dependent Potassium Channel on Penicillin Induced Epilepsy in Rats. *Kafkas J Med Sci.* 2016;6(1):38–45.
- [18] Pithadia AB, Navale A, Mansuri J, et al. Reversal of experimentally induced seizure activity in mice by glibenclamide. *Ann Neurosci.* 2013;20(1):10–12.
- [19] Yu T, Fu XY, Liu XK, et al. Protective effects of pinacidil hyperpolarizing cardioplegia on myocardial ischemia reperfusion injury by mitochondrial K⁺ ATP channels. *Chin Med J (Engl).* 2011;124(24):4205–10.
- [20] Cao S, Qin Y, Chen J, et al. Effects of pinacidil on changes to the microenvironment around the incision site, of a skin/muscle incision and retraction, in a rat model of postoperative pain. *Mol Med Rep.* 2015;12(1):829–36.
- [21] Hai S, Takemura S, Minamiyama Y, et al. Mitochondrial K⁺ATP channel opener prevents ischemia-reperfusion injury in rat liver. *Transplant Proc.* 2005;37(1):428–31.

Riluzole and ranolazine application of prostate cancer: Cancer related testicular and liver tissue damage

Pinar Koroglu Aydin¹, Ilknur Bugan²

¹Department of Histology and Embryology, Haliç University, Faculty of Medicine, Istanbul, Turkey

²Department of Biology, Istanbul University, Faculty of Science, Vezneciler, Istanbul, Turkey

ABSTRACT

Aim: In this study, utilizing the in vivo Copenhagen rat model possessing prostate cancer, we studied the possible impact of tumorigenesis on testes and liver morphology and whether riluzole (RIL) and ranolazine (RNL) treatment would have any affect or not.

Method: Male Copenhagen rats were divided into four groups: 1) Control group, 2) Cancer group, 3) Cancer + 10 µM Riluzole 4), and Cancer + 2.5 µM / 5 µM Ranolazine group. The tissue samples of testes and liver were taken and processed for light microscopy, including staining with hematoxylin and eosin.

Results: In the cancer group, degenerated seminiferous tubules, cell remnants in the lumen were shown in the testis, and a decrease in the spermatogenic cell line was found. The deterioration in these parameters was milder in the treatment groups and an increase in the number of normal tubules was found. In the cancer group, pyknotic nucleus, mononuclear cell infiltration, hyperemia, vacuolization, disrupted arrangement of hepatocyte plates, sinusoidal dilatations, and degenerated hepatocytes were observed in the liver. However, there was a slight damage in cancer + 10 µM RIL, cancer + 2.5 µM RNL, and cancer + 5 µM RNL groups. Properly hepatocyte arrangement and sinusoidal enlargement were observed.

Conclusions: This treatment can be considered a promising protective adjuvant candidate for testes and liver tissue in prostate cancer or cancer therapy-related damage.

Key words: Dunning prostate cancer model, testes, liver, riluzole, ranolazine, mat-lylu cells.

✉ Pinar Koroglu Aydin

Department of Histology and Embryology,
Haliç University, Faculty of Medicine, Istanbul, Turkey

E- mail: pinarkoroglu@halic.edu.tr

Received: 2021-06-22 / Revisions: 2021-08-17

Accepted: 2021-09-21 / Published online: 2022-01-01

Introduction

The drug repurposing consist of the investigation of off-target effects of existing drugs for new therapeutic purposes. Some drugs are currently in clinical use and may be renamed off-label as anticancer agents or in cancer-related several problems.

Riluzole (RIL) is a Food Drug Administration (FDA) approved drug for the treatment of amyotrophic lateral sclerosis. RIL also has neuroprotective, anticonvulsant, analgesic, anesthetic, anti-ischemic, and sedative properties. They searched the effects of cell growth and tumorigenesis to repurpose it for the treatment of cancer. RIL is accepted to act by indirectly inhibiting glutamate signaling. However, the specific effects of RIL in breast cancer cells are not well understood [1]. It has been found out that RIL acts as an anti-invasive on rat prostate cancer cells [2].

Cancer cells use a variety of growth signaling pathways to acquire an advantage over normal cells in terms of proliferation. Many types of cancer also express glutamate receptors, suggesting that glutamate may play an important mission. Glutamate signaling is used by breast, prostate, and skin cancers to increase their growth. Because glutamate signaling is so important for tumor growth, it is thought that it will be crucial to investigate the mechanisms underlying glutamate signaling and discover strategies to interrupt this signaling to prevent tumor growth. Glutamate secretion was first shown to be inhibited in brain tissue by a drug, RIL. It has been shown to block sodium channels and glutamate signaling. Breast cancer cells that are triple negative are treated RIL was found to inhibit cell proliferation. In addition, for brain, skin, breast, and prostate cancers, it has been shown to inhibit cancer cell proliferation in culture or in xenograft models. In a melanoma clinical trial, riluzole reduced tumor size in certain patients. RIL also demonstrated some clinical advantages in a phase II trial person with melanoma [3].

Ranolazine (RNL) is an FDA-approved anti-anginal drug with an anti-ischemic activity that has also been shown to have anti-arrhythmic properties due to prevention of the late sodium current in cardiomyocytes [4,5]. It has been suggested that RNL has been shown to be an antagonist against any experimental heart function failure, including doxorubicin cardiotoxicity, by decreasing the reactive oxygen species content. In studies conducted with the prostate and breast cancer in vivo models, it has been revealed that RNL can have an anti-metastatic effect [6,7].

RIL is predominantly metabolized by the hepatic microsomal cytochrome P450 in extrahepatic tissues [8]. In parallel, RNL is metabolized by the cytochrome P-450 system

in the liver [9]. Regarding this issue, many factors such as various mediator molecules that play a role in the immune response during the development process of cancer, chemotherapeutic drugs used in cancer therapy, and ionizing radiation used in radiotherapy can cause damage to organs such as the liver and testes in our study [10-12].

In a study examining the pharmacological blockade of lipid oxidation with RNL in prostate cancer models, oral administration of RNL (100 mg/kg for 21 days) was shown to result in decreased tumor CD8+ T-cells, increased macrophages, and decreased blood myeloid immunosuppressive monocytes [13]. The Dunning rat prostate cancer model has now become a useful model that is utilized in the research of androgen-independent prostate cancer and metastasis biology in in vitro and in vivo [14]. In this study, the Dunning model was formed in Copenhagen rats using strongly metastatic Mat-LyLu cells via subcutaneous injection [15].

In our study, we aimed (1) to show the liver and testicular damage that we predicted to occur in the prostate cancer model, (2) to evaluate how effect of our drugs on these tissues, occur damage by histopathological assessments.

No study in the literature addresses testicular or liver damage in experimental or clinical models with cancer or prostate cancer. In our study, it is predicted that RIL and RNL, which continue to be used for non-cancer-related different treatments, will provide advantages in terms of cost and time with the repositioning strategy as a drug in the damage caused by cancer.

Materials and methods

Cell culture

Mat-LyLu cells were grown in RPMI culture medium (RPMI-1640, Gibco; Life Technologies, USA), supplemented with 1%

fetal bovine serum (FBS) (Gibco), 2 mM L-glutamine (Gibco; Life Technologies, USA), and 250 nM dexamethasone (Sigma; Sigma-Aldrich, USA) Cells were cultured at 37°C in the humidified 5% CO₂ incubator [16].

Animals and prostate cancer model

Male Copenhagen rats (provided from Tubitak Marmara Research Center, Kocaeli, Turkey) were used. The animals were kept in 12:12-hr day-night cycle at 22-25°C and fed with pellet food and water. To induce tumors (in cancer group and cancer + RIL or RNL groups), 2x10⁵ Mat-LyLu cells were inoculated subcutaneously into the right flank of each rat with isoflurane (Abbott; Queenborough, UK). After the body weights were recorded, Mat-LyLu injection was inoculated subcutaneously into the upper right front extremity of each rat in the experimental groups. The volume of cell suspension to be injected into the rats was adjusted to be in the range of 0.10 – 0.50 ml. All operations performed on animals (from maintenance to dissection) were carried out under the ethical regulations and specific permission of Istanbul University (I.U. HADYEK, number: 2010/116).

Administration of drugs and experimental design

In the project study, the use of at least 6 subjects for the control group, cancer and treatment groups was calculated by performing power analysis with the pass 2008 program, in order to create a Dunning cancer model at $\alpha=0.05$ significance level, to obtain 0.8% power.

Male Copenhagen rats were divided into four experimental sets. There are 6 rats in each all group. 1) Control group: Physiological saline (0.9% NaCl) was applied to rats with gavage (1 ml solutions) every other day without tumor inoculation, 2) Cancer group: After the

inoculation of Mat-LyLu cells, 0.9% NaCl was applied to rats orally, 3) Cancer+RIL group: 10 μ M RIL (in an equal volume of physiological saline) was administrated with gavage every other day for 22 days, following inoculation of Mat-LyLu cells, 4) Cancer+RNL group: Respectively, 2.5 μ M and 5 μ M RNL doses was applied in the same way and duration.

Monitoring of primary tumors and dissection

The primary tumorigenesis was monitored daily. The dimension of the primary tumor was measured with calipers every day. “Tumor volume” was evaluated as (shortest diameter) 2 \times (longest diameter) 1/2 [17]. At the 22nd day after the cell inoculation, the primary tumor, testes and liver were dissected.

Histopathological evaluations

The testes and liver tissues were immersed in Bouin's fixative and processed routinely. The hematoxylin and eosin (H&E) tissues were analyzed. At a magnification of x200, five identical locations were chosen and analyzed. Normal, regressive, degenerative, or atrophic tubules were classified as normal, regressive, degenerative, or atrophic tubules based on Hess' data [18]. Normal tubules have normal spermatogenesis and blood testes barrier morphology. Seminiferous tubules with one or more defects make up regressive tubules. Degenerative tubules indicates irregular arrangements and atrophic tubules perform only sertoli cells.

The semi-quantitative histological assessment of liver damage was done using modified histological criteria described earlier [19]. Five similar areas were chosen and investigated at \times 400 magnification. The hepatic injury, based on the disrupted arrangement of hepatocyte plates, sinusoidal dilatation, hyperemia, vasocongestion, mononuclear cell infiltration,

pyknotic nucleus, degenerated hepatocytes were scored by using a scale ranging from 0 to 3 (0: none; 1: mild; 2: moderate; and 3: severe) for each criterion. The score was done for all groups. They were photographed by an Olympus CX41 microscope fitted with an Olympus DP71 digital camera DP71, Tokyo, Japan). The images were observed under a light microscopy on the 10x magnification.

Statistical analysis

Graph-Pad Prism 3.0 (GraphPad Software, San Diego, CA, USA) program was used and the data were analyzed by using one-way analysis of variance (ANOVA). The difference between

the groups were determined with Tukey's multiple comparison tests.

Results

Primary tumorigenesis and monitoring of primary tumors

The primary tumors were first palpable on the 12th day (in cancer group) and the 16th day (RIL treatment group) and their volumes increased. There was an insignificant decrease in the tumor weights within the cancer + RIL group compared to the cancer group. RNL administration was decreased insignificantly in the tumor weights compared to the cancer group (Figure 1).

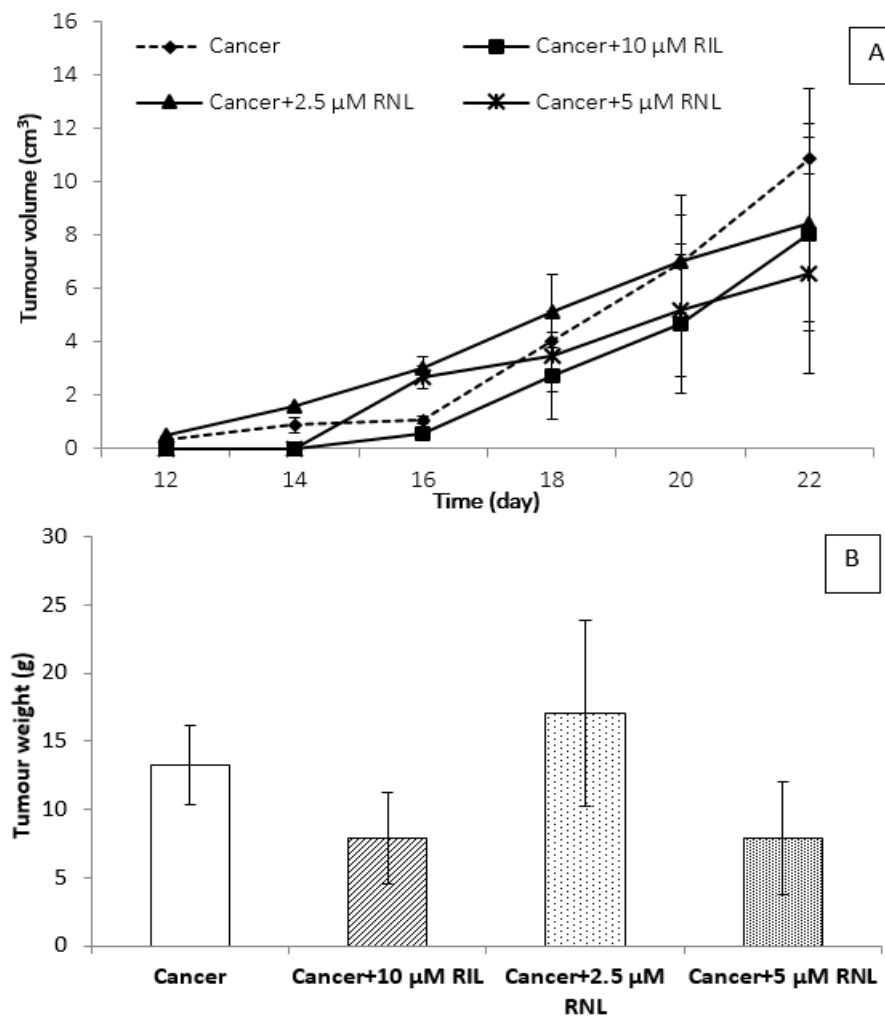


Figure 1. The development of primary tumor after inoculation of Mat-LyLu cells, **A.** Time courses of tumor volume and effects of RIL and RNL (2.5 µM and 5 µM) compared with cancer group. **B.** Tumor weights at the end of the experiment in groups.

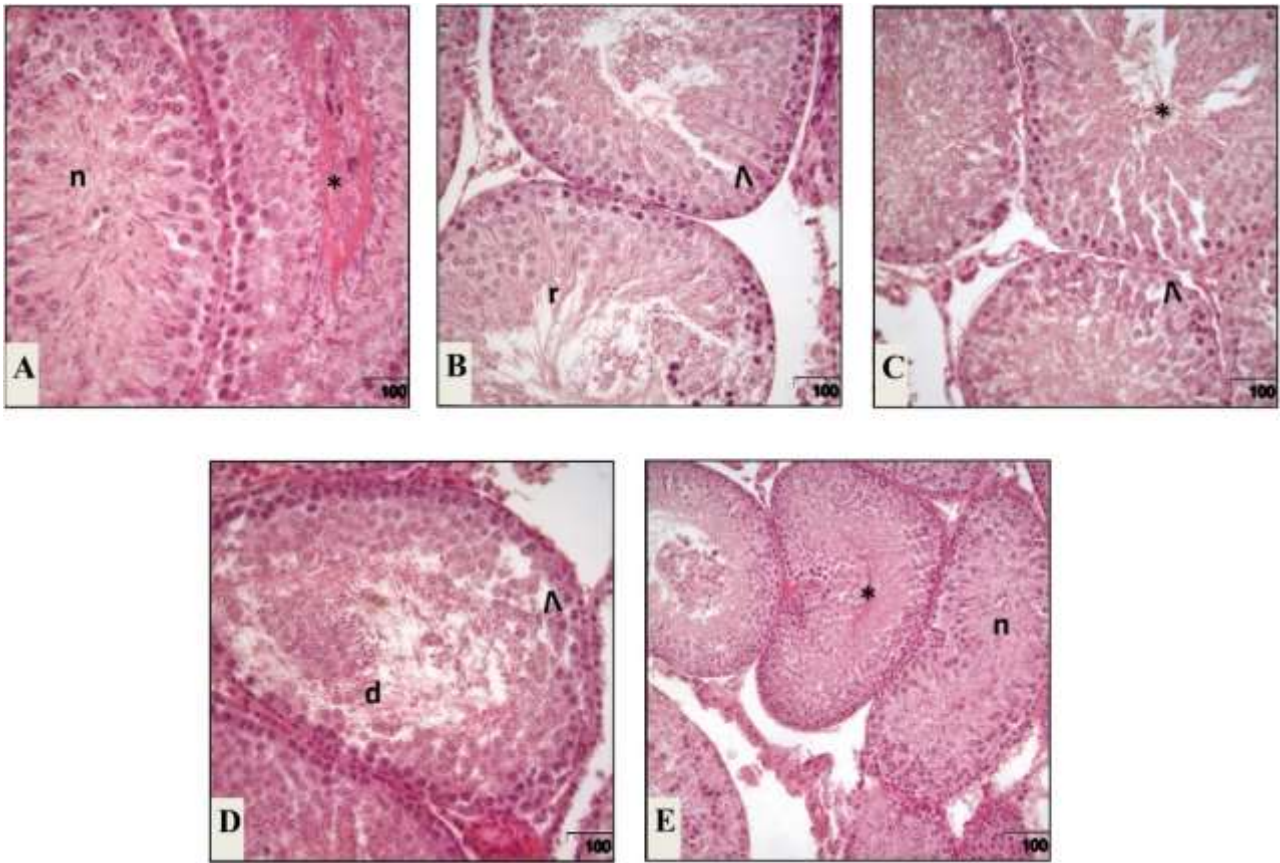


Figure 2. Testes tissue histological appearance: control group (A), cancer group (B), cancer + 10 μ M RIL group (C), cancer + 2.5 μ M RNL group (D), cancer + 5 μ M RNL group. (E). Normal morphology in seminiferous tubules (n), spermatogenic cells (^), spermatozoa (*) in lumen of the seminiferous tubules, degenerative (d) and regressive (r) seminiferous tubules, H&E staining, Bar: 100 μ m, x10 magnification.

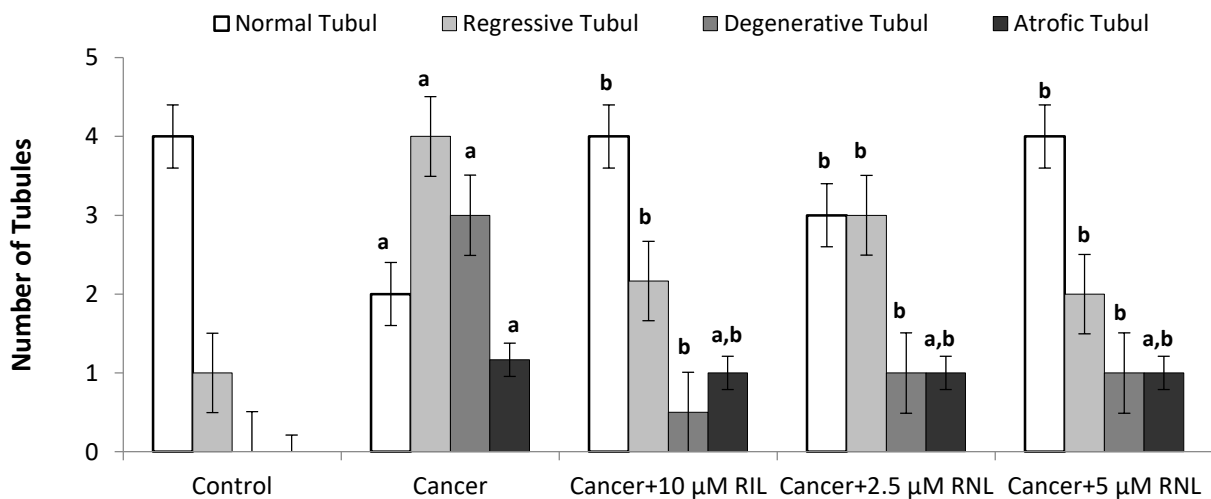


Figure 3. The histopathological scoring of the testes in the experimental groups. ap <0.05, compared to the control group, bp < 0.05, compared to the cancer group.

Histopathological evaluations and damage score

Testes tissue

When H&E stained testicular sections are examined, in the control group, normal testes' histology was observed (Figure 2A). In the cancer group, degenerated seminiferous tubules, cell debris in the lumen were shown and decreased in the spermatogenic cell line (Figure 2B). The number of degenerative tubules was surged and the spermatogenic cells decreased, and the regressive tubules were also shown in the cancer group. There was a mild disruption in seminiferous tubules, spermatozoa in the lumen, and spermatogenic cells in the cancer + 10 μ M RIL, cancer + 2.5 μ M RNL, and cancer + 5 μ M RNL group. The number of normal tubules was raised in these treatment groups (Figure 2C, D, and E).

The semi-quantitative evaluation of testicular tissue sections made under the light microscope is given in Figure 3. While it was observed that the seminiferous tubule structure was predominantly normal in the control group, a decrease in the number of normal tubules was remarkable in all other groups. The number of regressive tubules and degenerative tubules were found to be increased in the cancer group compared to the control group. The number of normal tubules was diminished while the number of degenerative tubules was increased and there were atrophic tubules in the cancer group compared to the healthy control group. Additionally, the number of normal tubules was increased and the number of regressive, degenerative tubules decreased significantly in cancer + RIL, cancer + RNL groups; the atrophic tubules decreased compared to the cancer group. It was detected that there is a statistically significant difference ($p < 0.05$).

Liver tissue

When H&E stained liver sections are examined, the control group depicts a normal hepatic parenchymal histology and hepatocyte structure with normal lobular architect and hepatocytes arranged in cords encircling the central canal. (Figure 4A). In the cancer group, pyknotic nucleus, mononuclear cell infiltration, hyperemia, vacuolization, disrupted arrangement of hepatocyte plates, sinusoidal dilatations, and degenerated hepatocytes were observed (Figure 4B). When RIL or RNL treatment was applied, histological appearances showed similarity within the control groups. There was a slight damage in cancer + 10 μ M RIL, cancer + 2.5 μ M RNL, and cancer + 5 μ M RNL groups. Properly hepatocyte arrangement and sinusoidal enlargement were observed (Figure 4C, D, and E).

The semi-quantitative evaluation of liver tissue sections that was assessed under a light microscope is given in Figure 5. There was a significant increase in the cancer groups compared to the control group. RIL and RNL treatment groups were significantly reduced in the liver histological damage compared to the cancer control group ($p < 0.05$).

Discussion

Within the scientific literature, it was exhibited that the cancer disease caused by other disease mechanisms has a higher mortality rate compared to the sole self-occurring cancer mechanism. Thus, it is predicted that the deaths due to cancer will increase significantly in the coming years. Depending on these reasons, the research to diagnose cancer early on and accurately to prevent and follow up the cancer treatment and its side effects resulting from the cancer treatment gain significance day by day [20].

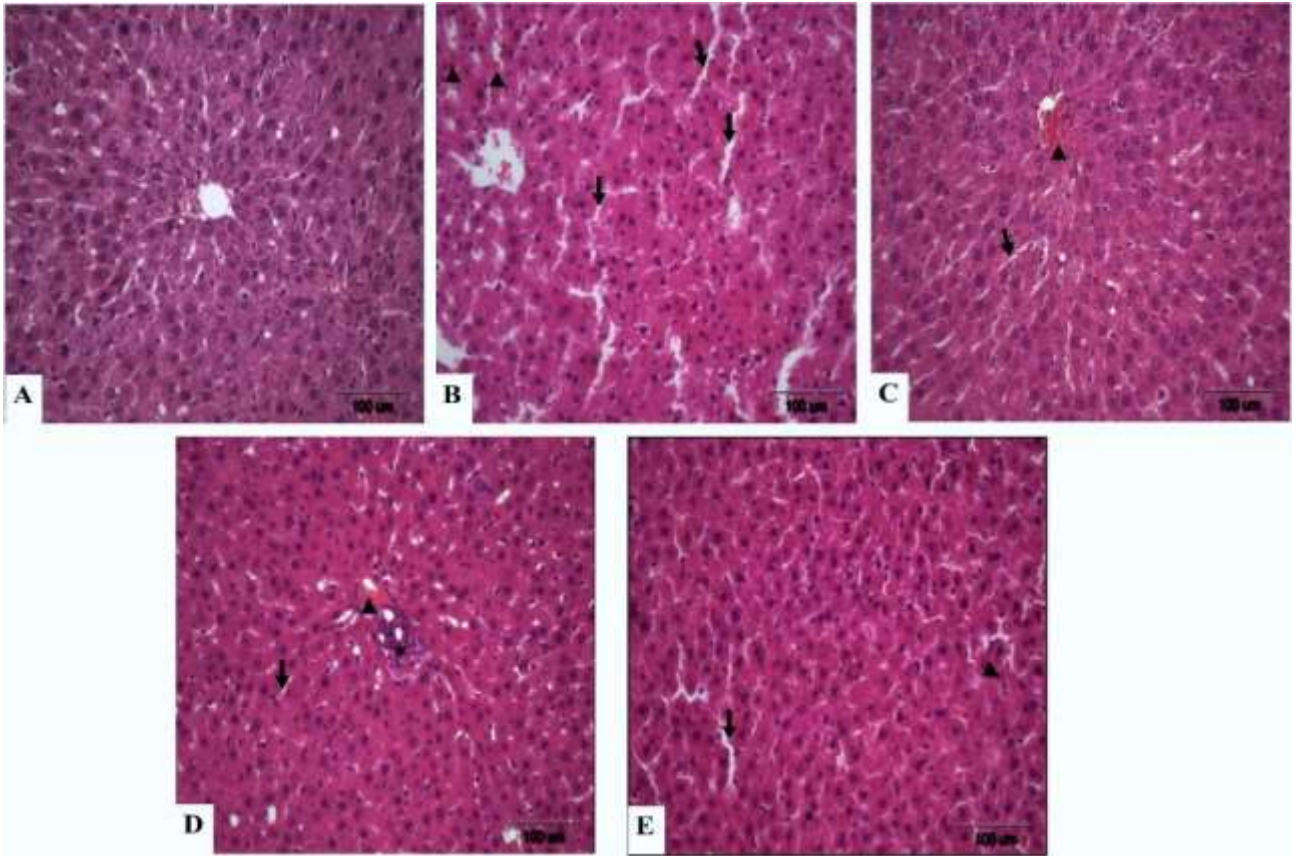


Figure 4. Liver tissue histological appearance: control group (A): cancer group (B), cancer + 10 μ M RIL group (C), cancer + 2.5 μ M RNL group (D), cancer + 5 μ M RNL group (E): sinusoidal dilatation (\rightarrow), hyperemia (\blacktriangleright), mononuclear cell infiltration (*), H&E staining, Bar:100 μ m, x10 magnification.

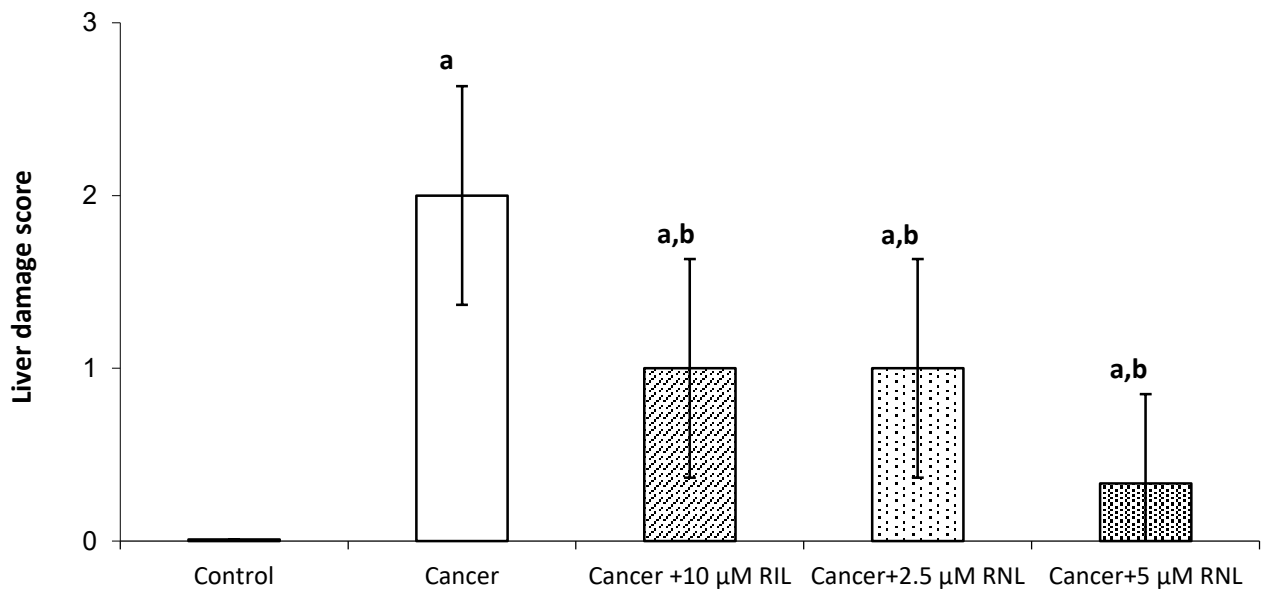


Figure 5. The histopathological scoring of the liver in the experimental groups. ap < 0.05, compared to the control group, bp < 0.05, compared to the cancer group.

Although the effects of many drugs or agents in the cancer models have been examined in studies to date, the effects of RIL and RNL treatment on testicular and liver tissue in experimental prostate cancer have not been investigated with an *in vivo* model before. In our study, we aimed to show the infertility as we anticipated that occurs by the prostate cancer, since the toxicity that it will create in the liver tissue and the therapeutic potential may occur by repositioning of these drugs.

In our study, the primary tumors were observed in about 10 days after subcutaneous inoculation of Mat-LyLu cells into rats [16]. The essential sequels of the systemic administration of RIL and RNL to prostatic tumor-bearing rats were as follows: (1) these treatments mostly prevented testicular and liver damage occurring by the prostate cancer model. (2) In the cancer + 10 μ M RIL and cancer + 5 μ M RNL group, there was a decrease in the growth of primary tumors insignificantly. Since prostate tissue is not directly affected in the Dunning prostate cancer model, we only evaluated the primary tumor weight for the cancer formation process. The Dunning prostate cancer model was not an orthotopic model, it was administered via subcutaneous injection and the target tissue was not prostate. That's why the first metastasis site was lung tissue in the Dunning model, we discussed the cancer related damage in the testis and liver tissues due to this.

RIL, the only drug approved by the FDA for treating amyotrophic lateral sclerosis, inhibits cancer proliferation through its inhibitory effect on glutamatergic signaling [21, 22]. It has been reported that RIL treatment inhibits the growth of brain tumor. The effects of RIL on these cells have been reported to be related to the inhibition of glucose transporter, a poor prognostic indicator [21]. It demonstrated that RIL inhibits cell growth in breast cancer [23].

According to a different *in vitro* study, it has been determined that 5 μ mol/L RIL (and 20 μ mol/L RNL) have anti-invasive effects on MAT-LyLu cells, and suggested RIL (and RNL) may ultimately be “repurposed” as an anti-metastatic drug against PCa [2]. It has been reported that RIL inhibits cell cycle progression and induces apoptosis in tumor cells [24]. The androgen-dependent transcription factor and androgen receptor enhance prostate cancer but inhibiting androgen-dependent or androgen biosynthesis induce remission for only a short time. RIL exerts its anti-tumorigenic effects [25].

RNL, a piperazine derivative sold under the trade name of Ranexa, a selective inhibitor of late sodium current, is a drug used in the treatment of stable angina patients who cannot be adequately controlled with first-line antianginal agents or cannot tolerate these treatments for any reason [26]. RNL has proven to be effective in treating experimental heart failure. It was shown that RNL attenuates trastuzumab-induced heart dysfunction in mice and reduces trastuzumab-induced apoptosis via decreasing the occurrence of caspase-3 fragmentation. RNL limits the production of reactive oxygen species in this experimental model [27]. It was demonstrated that RNL mitigates obesity-induced non-alcoholic fatty liver disease and increases hepatic pyruvate dehydrogenase activity. RNL treatment reverses obesity-induced hepatic steatosis [28]. Matrigel invasion of Mat-LyLu cells and secondary tumorigenesis (*in vivo* lung metastases) were inhibited by RNL [2,16].

Various mediator molecules of the immune system during the development of cancer, chemotherapeutic drugs used in cancer therapy, and ionizing radiation used in radiotherapy can cause damage to organs such as the liver and testes [10, 11,12]. It suggested that the liver

damage can also be caused by drugs, particularly the anti-tubercular drugs, general anesthetics, paracetamol, and some anti-cancer drugs [29].

The main reason for studying testicular tissue was its close functional association to the prostate, both being parts of the male reproductive system. More so, oxidative stress which is coupled to increased reactive oxygen species and DNA damage in sperm is the leading cause of testicular damage. This situation is directly linked to fertility potentials and can result in infertility [30]. The causes of male-induced fertility problems are cancer and testicular damage. It is known that the prostate tissue has an important contribution to fertility, especially the seminal fluid that provides the transport of sperm at the time of ejaculation [31]. In a case report of a 48 year old patient who was investigated for the metastasis of prostate adenocarcinoma of the prostate, 9 years after the initial diagnosis, prostate specific antigen was gradually elevated and a tumor in the left testicle developed. It has been suggested that testicular metastases may develop, although not frequently, in advanced prostate cancer cases [32].

Prostate cancer cells maintain various stages of the metastasis process through stromal cells, immune cells, and other cells within the tumor microenvironment, as well as cytokines and chemokines secreted by the metastatic site. These proteins exert their effects through autocrine or paracrine mechanisms. The most common site of metastasis for prostate cancer is bone (84% of cases), followed by distant lymph nodes (10.6%), liver (10.2%), and lungs (9.1%). Testicular metastases of primary prostate carcinoma are very rare, ranging from 0.18% to 0.5%, and it is said that their diagnosis can pose great difficulties. The mechanism of metastasis from prostate to testis may vary [33].

To demonstrate the protective effect of the RIL and RNL on testicular damage in rat prostate cancer will be useful in identifying new positive therapeutic options in clinical infertility trials. The histology of the seminiferous tubules in testicular tissues is evaluated as normal, regressive, degenerative, and atrophic [18]. In the present study, the histological evaluation of the testes of rats bearing prostate cancer showed an increase in the abnormal tubules and disorganization. We believe that the histopathological signs of damage observed in the cancer-control group may be an indicator of the development of the infertility process in the prostate cancer model. We can say that the administration of RIL and RNL protects the testicular tissue against infertility which may occur due to the histopathological damage caused by cancer.

The main reason for examining liver tissue is that it is the tissue that we expect to be most affected by toxic damage in the cancer process. The liver is an important organ exposed to attack by reactive oxygen species. The liver is involved in many basic physiological events. Glucose homeostasis, protein, lipid, lipoprotein, and bile acid production, as well as biotransformation, detoxification, conjugation, and excretion of endogenous and exogenous compounds are among the major functions of the liver [34].

There is no information in the literature about liver toxicity in prostate cancer. It was suggested that prostate cancer is a prominent metastatic dormant cancer. It has the worst prognosis when found in the liver compared to other metastatic sites. These metastatic nodules result in an adverse reaction in the pro-metastatic microenvironment; decline, as decided by both dormancy from the nodules name [35]. In our study, there was a significant increase in liver histological damage in cancer-

control groups compared to the healthy control group. RIL and RNL treatment groups were significantly reduced in liver histological damage compared to the cancer-control group. We can say that RIL and RNL application protects the liver tissue which may occur due to the histopathological damage caused by cancer. There are some limitations not studied. This is a part of study, with a small sample size. Animal experiments were planned by considering the minimum number and power analysis that would give a statistically significant result on the grounds of ethical committee obligations. Pharmacological doses were determined based on our previous in vitro findings. In future studies, it is foreseen that the study with different doses and drug combinations will be investigated more extensively with projects with larger budgets.

Conclusions

In conclusion, the effect of RIL and RNL application on testicular and liver damage in the prostate cancer model was first investigated in vivo. Nowadays, the drug repositioning subject has gained attention for researchers and pharmaceutical companies. Drug repositioning involves the investigation of existing drugs for new therapeutic purposes. Some drugs are already in clinical use and can be repurposed as anticancer agents. Especially, some agents have troubling adverse effects that dramatically reduce the life quality of cancer patients, so drug repositioning is a promising strategy [36, 37]. In addition to reducing time and cost, off-label drugs are also a low-risk strategy due to their off-target effects. When comparing repositioning and traditional drug development subject, their safety verified as repositioned drugs passed all clinical tests in Phase I, Phase II, and Phase III. Furthermore, some repositioned agents can be as molecular entities

and have more affiliations to be launched once a new indication is discovered [38, 39]. Our microscopic evaluations reveal that RIL and RNL have a protective effect on the testes and liver in the metastatic prostate cancer model. Based on our results, it has been determined that the two drugs (RIL, RNL), which are used for other purposes in the clinic, have a positive effect against the damage to the testes and liver caused by the prostate cancer. The current study could be a model investigation for future work on developing agents for decreasing testicular and liver damage caused by prostate cancer and other types of cancer.

Funding: *This study was supported by TUBITAK (The Scientific and Technological Research Council of Turkey), project number 110T890.*

Conflict of Interest: *The authors declare that they have no conflict of interest.*

Ethical statement:

The study was confirmed by Non-Interventional Ethics Committee of University of Istanbul (I.U. HADYEK decision no: 116; date: 2010).

Open Access Statement

This is an open access journal which means that all content is freely available without charge to the user or his/her institution under the terms of the Creative Commons Attribution Non-Commercial License (<http://creativecommons.org/licenses/by-nc/4.0>). Users are allowed to read, download, copy, distribute, print, search, or link to the full texts of the articles, without asking prior permission from the publisher or the author.

Copyright (c) 2021: Author (s).

References

- [1] Dolfi SC, Medina DJ, Kareddula A, et al. Riluzole exerts distinct antitumor effects from a metabotropic glutamate receptor 1-specific inhibitor on breast cancer cells. *Oncotarget*. 2017; 8(27):44639-53.
- [2] Rizaner N, Uzun S, Fraser SP, et al. Riluzole: Anti-invasive effects on rat prostate cancer cells under normoxic and hypoxic conditions. *Basic Clin Pharmacol*. 2020;127(4):254-64.
- [3] Raghubir M, Nowshin Rahman C, Fang J, et al. Osteosarcoma growth suppression by riluzole delivery via iron oxide nanocage in nude mice. *Oncol Rep*. 2020;43(1): 169–76.
- [4] Hale SL, Shryock JC, Belardinelli L, et al. Late sodium current inhibition as a new cardioprotective approach. *J Mol Cell Cardiol*. 2008;44(6):954-67.
- [5] Antzelevitch C, Nesterenko V, Shryock JC, et al. The role of late I_{Na} in development of cardiac arrhythmias. *Handb Exp Pharmacol*. 2014; 221:137-68.
- [6] Nelson M, Yang M, Millican-Slater R, et al. Nav1.5 regulates breast tumor growth and metastatic dissemination in vivo. *Oncotarget*. 2015;6 (32):32914–29.
- [7] Bugan I, Kucuk S, Karagoz Z, et al. Anti-metastatic effect of ranolazine in an in vivo rat model of prostate cancer, and expression of voltage-gated sodium channel protein in human prostate. *Prostate Cancer Prostatic Dis*. 2019; 22 (4):569-79.
- [8] Ajroud-Driss S, Saeed M, Khan H, et al. Riluzole metabolism and CYP1A1/2 polymorphisms in patients with ALS. *Amyotroph Lateral Scler*. 2007; 8(5):305-309.
- [9] Cheng JW. Ranolazine for the management of coronary artery disease. *Clinical Therapeutics*. 2006; 28(12):1996-2007.
- [10] Thu YM, Richmond A. NF- κ B inducing kinase: a key regulator in the immune system and in cancer. *Cytokine Growth Factor Rev*. 2010;21(4):213-26.
- [11] Valiño-Rivas L, Vaquero JJ, Sucunza D, et al. NIK as a Druggable Mediator of Tissue Injury. *Trends Mol Med*. 2019; 25 (4):341-60.
- [12] Farhood B, Khodamoradi E, Hoseini-Ghahfarokhi M, et al. TGF- β in radiotherapy: mechanisms of tumor resistance and normal tissues injury. *Pharmacol Res*. 2020; 155:104745.
- [13] Guth A, Monk E, Agarwal R, et al. Targeting Fat Oxidation in Mouse Prostate Cancer Decreases Tumor Growth and Stimulates Anti-Cancer Immunity. *Int J Mol Sci*. 2020; 21(24): 9660.
- [14] Pienta KJ, Abate-Shen C, Agus DB, et al. The current state of preclinical prostate cancer animal models. *Prostate*. 2008;68 (6):629-39.
- [15] Tennant TR, Kim H, Sokoloff M, et al. The Dunning model, *Prostate*. 2000; 43 (4):295-302.
- [16] Bugan I, Karagoz Z, Altun S, et al. Gabapentin, an analgesic used against cancer-associated neuropathic pain: Effects on prostate cancer progression in an in vivo rat model. *Basic Clin Pharmacol Toxicol*. 2016; 118(3): 200–207.
- [17] Wang T, Huang W, Cheng F. Baclofen a GABAB receptor agonist, inhibits human hepatocellular carcinoma cell growth in vitro and in vivo. *Life Sci*. 2008; 82 (9-10):536–41.
- [18] Hess RA, Linder RE, Strader LF, et al. Acute effects and long term sequelae of 1,3-dinitrobenzene on male reproduction in the rat II. quantitative and qualitative histopathology of the testis. *J Androl*. 1988; 9(5): 327- 42.

- [19] Bhattacharya A, Dhar P, Mehra RD. Preliminary morphological and biochemical changes in rat liver following postnatal exposure to sodium arsenite. *Anat Cell Biol*. 2012; 45 (4): 229-40.
- [20] Siegel RL, Miller KD, Jemal A. Cancer statistics, CA: Cancer J. Clin. 2019; 69(1):7-34.
- [21] Sperling S, Aung T, Martin S, et al. Riluzole: a potential therapeutic intervention in human brain tumor stem-like cells. *Oncotarget*. 2017; 20(57):96697-96709.
- [22] Taguchi YH, Wang H. Genetic Association between Amyotrophic Lateral Sclerosis and Cancer. *Genes (Basel)*. 2017; 8(10):243.
- [23] Speyer C, Nassar MA, Hachem AH, et al. Riluzole mediates anti-tumor properties in breast cancer cells independent of metabotropic glutamate receptor 1. *Breast Cancer Res Treat*. 2016; 157:217-28.
- [24] Lemieszek MK, Stepulak A, Sawa-Wejksza K, et al. Riluzole Inhibits Proliferation, Migration and Cell Cycle Progression and Induces Apoptosis in Tumor Cells of Various Origins. *Anti-Cancer Agents Med Chem*. 2018;18 (4):565-72.
- [25] Wadosky KM, Shourideh M, Goodrich DW, et al. Riluzole induces AR degradation via endoplasmic reticulum stress pathway in androgen-dependent and castration-resistant prostate cancer cells. *Prostate*. 2019;79 (2):140-150.
- [26] Rayner-Hartley E, Sedlak T. Ranolazine: A Contemporary Review. *J Am Heart Assoc*. 2016;5(3):e003196.
- [27] Riccio G, Antonucci S, Coppola C, et al. Ranolazine Attenuates Trastuzumab-Induced Heart Dysfunction by Modulating ROS Production. *Front physiol*. 2018; 9:38.
- [28] Al Batran R, Gopal K, Aburasayn H, et al. The antianginal ranolazine mitigates obesity-induced nonalcoholic fatty liver disease and increases hepatic pyruvate dehydrogenase activity. *JCI Insight*. 2019; 4 (1): e124643.
- [29] Teschke R. Hepatotoxicity: Molecular Mechanisms and Pathophysiology. *Int J Mol Sci*. 2019; 20 (1): 211.
- [30] Smith R, Kaune H, Parodi D, et al. Increased sperm DNA damage in patients with varicocele relationship with seminal oxidative stress. *Hum Reprod*. 2006; 21(4): 986–993.
- [31] Hoppe BS, Harris S, Rhoton-Vlasak A, et al. Sperm preservation and neutron contamination following proton therapy for prostate cancer study. *Acta Oncol*. 2017;56(1):17-20.
- [32] Campara Z, Simic D, Aleksic P, et al. Metastasis of prostate adenocarcinoma to the testis. *Med Arch*. 2016; 70(4): 318-20.
- [33] Raghuvanshi K, Deshmukh H, Raval A, et al. Cancer prostate metastasis to testis: A rare encounter, 2018; 1(2): 94-96.
- [34] Vdoviaková K, Vdoviaková K, Petrovová E, et al. Importance rat liver morphology and vasculature in surgical research. *Med Sci Monit*. 2016; 22: 4716-28.
- [35] Ma B, Wells A, Wei L, et al. Prostate cancer liver metastasis: Dormancy and resistance to therapy, *Seminars in Cancer Biology*. 2021; 71: 2-9.
- [36] Biber A, Durusu IZ, Özen C. In vitro anticancer effect of tricyclic antidepressant nortriptyline on multiple myeloma. *Turk J Biol*. 2018; 42 (5):414-21.
- [37] Turanli B, Grötli M, Boren J, et al. Drug Repositioning for Effective Prostate Cancer Treatment. *Front physiol*. 2018; 9:500.
- [38] Xue H, Li J, Xie H, et al. Review of Drug Repositioning Approaches and Resources. *Int J Biol Sci*. 2018;14 (10):1232-44.

- [39]Ozdemir A, Ark M. A novel ROCK inhibitor: off-target effects of metformin. Turk J Biol. 2021; 45 (1):35-45.

The link between learning performance, immobility in the forced swim test, and hippocampal glia

Tuba Ozcan¹, Yildirim Sara^{1,4}, Kutluk Bilge Arikan^{2,4}, Bengi Unal^{3,4}, Cagri Temucin Unal^{3,4}

¹Department of Medical Pharmacology, Hacettepe University, Faculty of Medicine, Ankara, Turkey

²Department of Mechanical Engineering, TED University, Faculty of Engineering, Ankara, Turkey

³Department of Psychology, Çanakkale Onsekiz Mart University, Faculty of Arts and Sciences, Çanakkale, Turkey

⁴Neuroscience and Neurotechnology Center of Excellence (NÖROM), Ankara, Turkey

ABSTRACT

Aim: To obtain maximal translational insights from animal models of depression, we need to know the meaning of behavioral parameters of animal models. The extent of construct and face validities of behavioral despair in the form of behavioral immobility in forced swim test (FST) is disputed. In this study, learning performance in a dual solution T-Maze and immobility on the 2nd day of FST was compared to shed light on this debate. Furthermore, we aimed to inspect the relationship between hippocampal glial densities and behaviors observed.

Method: Twelve adult male Sprague Dawley rats were tested in the dual-solution T-Maze and in FST. Subsequently, hippocampal slices were obtained, astrocyte and microglia cells were stained, and the densities were calculated for each subject.

Results: The rats utilized different learning strategies to solve the T-Maze. But irrespective of strategy, the rats that exhibited an overall efficiency in their learning performance, remained immobile for longer durations on the 2nd day of the FST. No significant relationship was detected between hippocampal microglia and behavioral indices in T-Maze and FST. However, we detected a significant positive correlation with CA1 astrocyte density and T-Maze learning and dentate gyrus CA1 astrocyte density and headshake behavior in FST.

Conclusions: The subjects showing a better cognitive performance in the T-Maze were immobile longer in the FST. This observation raises doubts about immobility as depression index and posits that it might reflect better learning. Our results also suggest that hippocampal glia cell types are differentially involved in cognition and affect.

Key words: Forced swim test, behavioral despair, learning, t-maze, glia, hippocampus.

✉ Bengi Unal

Department of Psychology, Çanakkale Onsekiz Mart University, Faculty of Arts and Sciences, Çanakkale, Turkey.

Neuroscience and Neurotechnology Center of Excellence (NÖROM), Ankara, Turkey

E- mail: bengi.unal@comu.edu.tr

Çagri Temucin Unal

Department of Psychology, Çanakkale Onsekiz Mart University, Faculty of Arts and Sciences, Çanakkale, Turkey.

Neuroscience and Neurotechnology Center of Excellence (NÖROM), Ankara, Turkey

E- mail: cagri.unal@comu.edu.tr

Received: 2021-08-05 / Revisions: 2021-09-19

Accepted: 2021-09-22 / Published online: 2022-01-01

Introduction

Depressive disorders are characterized by mood disturbances that affect an individual's daily functioning and constitute a large burden for individuals and societies they live in. According to the World Health Organization (2018) report [1], major depressive disorder, the most frequent form of depressive disorders constitutes the number one cause of disability. A recent report by Kessler et al. (2012) [2] indicates a 16.6 % lifelong prevalence of major depressive disorder in the United States. Given the chronic harm depressive disorders have in the modern world, it becomes of paramount importance to generate valid and reliable preclinical models of depressive disorders [3], undoubtedly an arduous task [4].

Forced swim test (FST) is a widely used animal model to gauge depression-like behavior in rodents [5]. The test consists of two trials separated apart by 24 hours. In these trials, the animals are placed in a water filled cylinder from which escape is not possible. The first trial, which typically lasts for 15 minutes, is considered to be the stress induction phase while the second trial typically lasts for 5 minutes. Immobility is considered to be an index of behavioral despair reflecting a depressive behavioral phenotype; in this state the rodents do not exhibit any movement other than keeping their heads above water. Even during periods of extended immobility, the rodents can exhibit various struggling behaviors to different degrees [6].

It has been repeatedly shown that antidepressant treatment in between the two trials reduced behavioral immobility, findings bolstering the predictive validity of the forced swim test [7]. In a similar vein, exposure to enriched environments, electroconvulsive shock, and REM deprivation also reduce immobility durations in the second test [8].

Complementing this picture, increasing stress levels through increased water depth [9], increased time spent in water [10], and prior stressors [6, 11] make the animals more susceptible to behavioral despair.

However, forced swim test as a preclinical depression model is not immune to serious criticisms. First of all, depression in humans is characterized by a plethora of cognitive, behavioral, and emotional symptoms and FST falls short of capturing this complexity [5]. A serious challenge to FST comes from the antidepressant response's time profile of reduced mobility; while antidepressants take 2-4 weeks to have their antidepressive effects in humans [12], a single day of antidepressant treatment in between the two trials suffices to reduce immobility in FST [3]. The findings alluded to pose serious challenges to the construct and predictive validity of FST as a preclinical model of depression [13, 14].

Phenomenologically speaking, increased immobility seen in the second trial might as well represent a passive coping strategy. There is evidence that this reduced mobility might reflect a learning process where animals learn that active coping behaviors like climbing and swimming do not result in the removal of the stressor [10, 14, 15, 16, 17, 18, 19]. While remaining immobile does not speed up the removal of the stressor, it is more energy preserving compared to active coping behaviors.

The current paper addresses how immobility in the forced swim test relates to behavioral and anatomical indices of cognitive functioning in rodents. In our behavioral experiments, we investigated the relationship between the learning performance in a dual solution t-maze task where animals were reinforced with food for entering the target arm and the propensity to exhibit immobility in the forced swim test. For

the anatomical parameters, we focused on the hippocampus as it is an integral brain region for the formation of cognitive maps which is imperative for spatial learning and navigation [20, 21] and shows distinct anatomical and functional alterations in affective disorders as a member of the limbic circuitry [22, 23, 24]. We focused on hippocampal microglia and astrocytes as recent studies point out to the important involvement of these cell types in the formation of neural circuits and synaptic plasticity [e.g. 25, 26]. Our findings indicate that immobility on the second forced swimming test day is associated with quicker acquisition of the T-maze task. Interestingly, the pace of T-maze acquisition was related to higher astrocyte counts in the CA1 region of the hippocampus bolstering the anatomical validity of our learning paradigm. Given our results, the ubiquitous observation that depression in humans is largely related to cognitive dysfunction poses a challenge to the validity of the forced swim test as a model of depression.

Materials and methods

Animals and housing

Twelve male Sprague Dawley rats weighing 250-350 gr. obtained from Kobay Experimental Animals Laboratory Inc (Ankara, Turkey) were used in this study. The rats were randomly assigned to three cages, with four rats per cage (40 cm x 34 cm x 17 cm). All rats were housed in an artificially-lit room with access to water and food *ad libitum* at a temperature of 18-24 °C. The standardized 12:12 hr light-dark cycle (lights on 07:00 AM) was maintained throughout the study.

All experiments were performed with the approval of the Kobay DHL Inc. Animal Research and Ethics Committee (protocol number: 268).

Behavioral testing

The behavioral sessions were carried out in an adjacent room during the daytime between 10:00 a.m. and 4:00 p.m. There were three resting days between two experiments. After a handling procedure had been applied once a day for a week, the rats were subjected to the T-Maze procedure. Then, the rats were exposed to the Forced Swim Test (FST) procedure for two consecutive days. On the same day as the FST procedure ended, transcardial perfusion and fixation were performed to remove the brains for the histological applications.

T-Maze

Tolman's T-Maze [27] procedures were carried out to assess rats' spatial learning abilities and spatial navigational strategies following a food deprivation period. For this, the rats' diet was restricted to 4 gr/day, starting one week before the experiment. The body weight of each subject was gradually reduced to 90% of the basal weight before the start of the training phase and the weights were stabilized at this level throughout the experiment by recording the weight of the rats every day. A plus-shaped maze was used in the experiment, which was placed 90 cm above the floor (arms: 45 cm length, 12.5 cm width, 7 cm height; center area: 12.5 cm), constructed of black-colored MDF material. A styrofoam panel was used to block the entrance to one arm, rendering a T-shaped maze. At the end of each arm, a perforated food cup (1 cm in diameter) was fixed 3 cm away from the distal end of the arm filled with the food reward (Nestlé CORN FLAKES™) that provided ubiquitous smell of the food from each arm so that smell of the food reward did not provide a navigational cue during the experiment. Separate food wells, which did not allow for visual localization of the reward were attached on top of each perforated food cup at

the end of the maze arms, and these were used for discriminatory baiting as further explained below

The experiment consisted of three different phases: habituation phase on the first day, training phase and probe trial on the second day. In the habituation phase, each rat explored freely all the four arms of the maze containing the food reward for 10 minutes. By doing so, rats were acclimated to the maze and discovered that if they roam around the maze and travel to the end of the arms, they can find the food reward while getting over their natural neophobicity.

The training phase and probe trial were carried out respectively on the second day. While on habituation day, all of the arms were baited with the food reward; on the second day only one of the four arms randomly selected for each animal was baited. It was expected from the subjects in the training phase to learn the rewarded arm of the maze, regardless of the strategy they use. To illustrate, if the subject was positioned from the south arm, the opposite north arm was blocked with the panel. A bait was placed where the subject can reach either the east arm or west arm (see: Figure 1). In addition, the same amount of bait covered with a perforated container was placed in every arm as to eliminate the effect of the food odor. Each rat had to turn 90 ° when they reach the center of the maze to the left (i.e., to the west arm if the start arm was the south arm) or to the right (i.e., to the east arm if the start arm was the south arm) once to reach the bait. If the rat turned to the reward arm when released into the maze the rat was allowed to consume a piece of bait. Contrary, if the rat turned to the wrong arm the rat was removed from the maze within three seconds. The floor and walls were cleaned between each trial with a cloth dampened with alcohol diluted with water to wipe out possible

clues such as feces, urine, or food bits on the maze surface.

During the training phase the rats were given a maximum of 35 trials for the training to learn the location of the baited arm in the T-Maze. When the rats got nine out of the 10 consecutive attempts correctly, the probe trial was initiated. The starting arm, where the rat had been placed in the training phase, was rotated 180° to the opposite arm that became the new starting arm for the single probe trial. The rats were classified into the “allocentric” or “egocentric” group on the basis of their performance during the probe trial: the rats who turned to the same reward arm as in the training and reached the bait despite the 180° rotation of the start arm were labeled as allocentric/place learners, the rats who turned to the previously unbaited opposite arms were labeled as egocentric/response learners.

In the training phase, the maximum number of consecutive correct choices and the number of trials that each rat took to achieve the criterion (nine of 10 correct) were counted by two independent observers from the recorded videos. Also, the total duration to complete the probe trial was calculated for each rat. These measurements were used to quantify the learning speed of the rats as an indicator of cognitive performance.



Figure 1. T-maze training of rats during the experiments where rats underwent habituation (Left panel), training (Middle panel), and testing (Right panel) trials. Note that the blocked arms oppose each other during training and testing.

Forced Swim Test (FST)

FST procedure was initiated three days after when the rats were returned ad libitum access to food. In accordance with the standard protocol of the FST (Porsolt et al., 1997), a Plexiglass cylinder tank (50 cm in height, 20 cm in diameter) was filled with 30 cm tap water (25°C) so that the tails of the rats did not touch the bottom of the container. A digital camera (Logitech C270) was positioned to record the setup. All rats were acclimated to the test room for half an hour before starting the trials. On the first day, each rat was kept in the water filled cylinder tank with no possible escape for 15 minutes as the first phase of the experiment. The test phase was applied to each rat 24 h later, on the second day in which the duration of water exposure was reduced to 5 minutes. Throughout the experiment, the tank was cleaned and refilled with fresh tap water at 25°C. The rats were kept in a single cage and it was ensured that they remained dry immediately after the trials. The rats were considered immobile when moved only enough to keep their heads afloat above the water. Two independent observers counted the total duration of immobility on the second day of the FST, the number of diving and head shaking behaviors for each rat by examining the recorded videos.

Histological procedure: Preparation of brain slices

Following the conclusion of the behavioral experiments, animals were deeply sedated with an i.p. injection of urethane 1.25 gr/kg and perfused transcardially with 0.1M phosphate buffer (PB) solution followed by 4% paraformaldehyde (PFA) in 0.1M PB. The removed brains (N=12) were kept in the fixation overnight and were preserved with 30% sucrose in 0.1M PB for later processing. The brains were cut into 100 µm thick coronal

sections containing Dentate Gyrus and CA1 subregions of the dorsal hippocampus with vibratome based on The Rat Brain in Stereotaxic Coordinates by Paxinos and Watson (2007) [28].

Immunohistochemistry for glial markers

100 µm thick brain sections were washed 3 times with 0.1M PB, and then permeabilized with 10% methanol and 1% sodium borohydride for one hour. The sections were blocked in 10% normal goat serum and 0.5% Triton X for 24h for non-specific target binding. Subsequently, the sections were subjected to immunohistochemistry for glial fibrillary acidic protein (GFAP) which is an astrocyte marker, and ionized calcium binding adaptor molecule 1 (IBA-1) protein which is a microglia marker. A series of sections were incubated in rabbit-anti-GFAP+ and primary antibody diluted 1: 1000 for 24h. Another section series from the same brains were incubated in the rabbit- anti-IBA1 antibody diluted 1: 1000 for 24h. All the sections washed three times with 0.1M PB were then recovered from the secondary goat-anti-rabbit antibody diluted 1: 500 for 4h, after which the antibodies were conjugated with the horseradish peroxidase (HRP) enzyme. This binding reaction was visualized with NovaRED™ (Vector Labs, Burlingame, CA).

The stained sections were dehydrated with ethanol and cleared with xylene. Afterwards, they were coated with DEPEX, fixed on glass microslides and were coverslipped. The pictures of the Dentate Gyrus and CA1 subregions of the dorsal hippocampus were taken with the Motic B210 3MP digital microscope with 4X, 10X, 40X objective lenses. The region of interest (ROI) and the density of astrocytes and microglia cells on the micrographs were calculated via the ImageJ program for further statistical analysis.

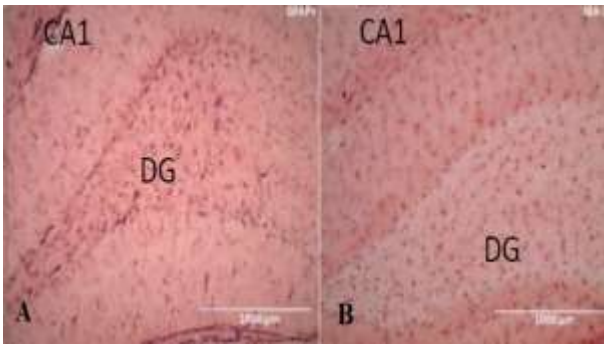


Figure 2. Two sections taken with 10X lens including dentate gyrus (DG) and CA1 subregions of the dorsal hippocampus. (A) The section stained for the astrocyte marker glial fibrillary acidic protein (GFAP +) (1: 1000 rabbit-anti-GFAP antibody, 1: 500 goat-anti-rabbit antibody). (B) The following brain section taken from the same brain, IBA-1 staining which is a protein specific to microglial cells was applied (1:1000 rabbit-anti-IBA1 antibody, 1: 500 goat-anti-rabbit antibody).

Statistical analysis

Microsoft Excel and SPSS v.21 were used for the data analysis. To compare the groups, Wann-Whitney U non-parametric tests were used to investigate the relationships between behavioral parameters in T-maze, FST, and anatomical variables, Pearson correlations were carried out.

Results

The initial parameter that was recorded about the subjects concerned their performance on the T-Maze. Based on their choice in the probe trial of the T-Maze (as explained in detail in the methods section), the 12 rats were classified as allocentric/place learners – relying on the hippocampus-based strategy (n = 8), and as egocentric/response learners (n = 4) – relying on the striatum-based strategy for navigation. In addition to the strategy, we have extracted several other parameters from the T-Maze performance of the subjects:

- The number of trials out of the max. 35 training trials that it took the subject to reach to

the learning criterion (i.e., how many trials did it take rats to achieve 9 correct choices out of 10 consecutive attempts),

- Max. number correct choices to reach the learning criterion (for e.g., if an animal reached 9/10 criterion by making 2 successive correct choices, followed by an incorrect attempt and then by 7 uninterrupted correct choices; the animal got a score of “7” for this indice),

- The duration (in sec) to complete the probe trial.

A summary of the T-Maze performance of the subjects is given in Fig. 3. From the FST performance, the indices we have extracted were the total duration of immobility, the frequency of active struggling behaviors (pedaling, jumping, diving), the frequency of head-shake behavior on the second day of the FST.

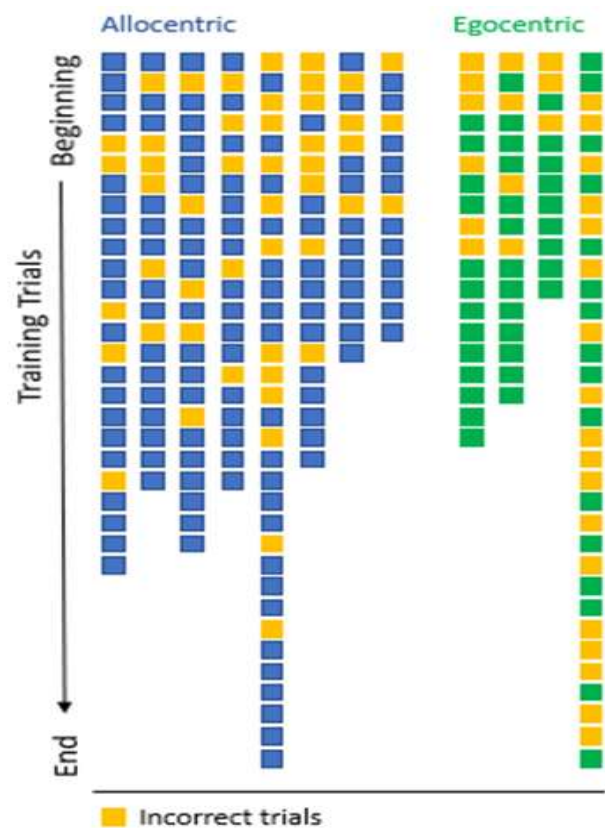


Figure 3. The graphical summary of T-Maze performance of each subject in the experiment. Each

column corresponds to the data from a single rat. Blue squares indicate the correct trials for allocentric/place learners and the green squares indicate the correct trials for egocentric/response learners. Trials with incorrect choices (i.e., failure to locate the baited arm) are indicated with yellow squares for both allocentric and egocentric strategy groups.

Immunohistochemical parameters that were used in the current study were the densities (# cells / 100 μm^2) of GFAP+ astrocyte glia cells and IBA-1+ microglia cells in the dentate gyrus and CA1 subregions of the hippocampus.

Comparison of T-Maze performance between allocentric/place learners and egocentric/response learners

To test the relationship between studied parameters in T-Maze, the first groups of rats utilizing different learning strategies in T-Maze were compared. Since the sample size is limited and there are more rats utilizing allocentric learning strategy compared ($n=8$) to egocentric learners ($n=4$), we ran Mann-Whitney U non-parametric tests.

It was found that the groups did not differ significantly in terms of total number of trials to reach the criterion for learning ($U = -0.681$, $p = 0.57$). The groups also were not significantly different from each other in terms of max. number of consecutive correct choices ($U = 0.347$, $p = 0.808$). Finally, the duration to complete the probe trial was contrasted between the groups, there was no statistical difference between the allocentric/place and egocentric/response learners ($U = -0.818$, $p = 0.497$).

But irrespective of the learning strategy, we have detected a significant positive correlation between the total number of trials it took subjects to reach to learning criterion (i.e., correct choice in 9 out of 10 successive trials) and time it took the subject to complete the

probe trial ($r(12) = .821$, $p = 0.002$) (Fig. 4). In other words, the rats which learned the location of the baited arm in the T-Maze rapidly also demonstrated faster choice and reward consumption response in the probe trial.

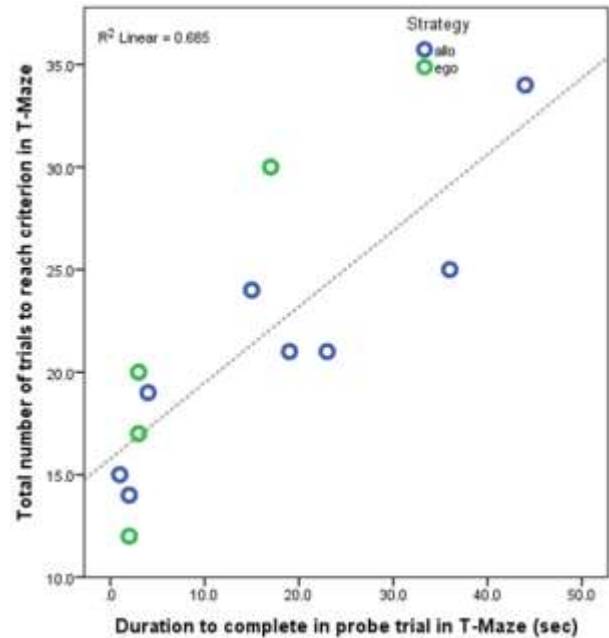


Figure 4. The graph depicting the positive correlation between the total number of trials in T-Maze to reach the criterion for learning and duration to complete the probe trial. Regardless of the strategy, a positive correlation was present between these T-Maze parameters. Blue circles correspond to allocentric/place learners (allo) and green circles correspond to egocentric/response learners (ego).

A marginally significant positive correlation was also detected between the total number of trials it took subjects to reach to learning criterion and max. number of consecutive correct choices in training in T-Maze ($r(12) = -.575$, $p = .051$).

Comparison of T-Maze and FST behavioral performances:

-To investigate the relationship between studied parameters in T-Maze and FST tasks, firstly, the groups of rats utilizing different learning strategies in T-Maze were compared. Since the sample size is limited and there are

more rats utilizing allocentric learning strategy compared (n =8) to egocentric learners (n = 4), we ran Mann-Whitney U non-parametric tests. When T-Maze strategy and FST immobility was compared, no significant differences were detected ($U = -1.361, p = .214$). Moreover, T-Maze learning strategy was not significantly related to frequency of headshake behavior on the second day of FST ($U = 0.597, p = .570$).

-To investigate a possible link between behavioral performance in T-Maze and FST, Pearson bivariate comparisons were carried out between T-Maze parameters (total number of training trials, duration to complete the probe trial and the max. number of consecutive correct choices) with FST parameters (duration of immobility on the 2nd day of FST, headshake frequency on the 2nd day).

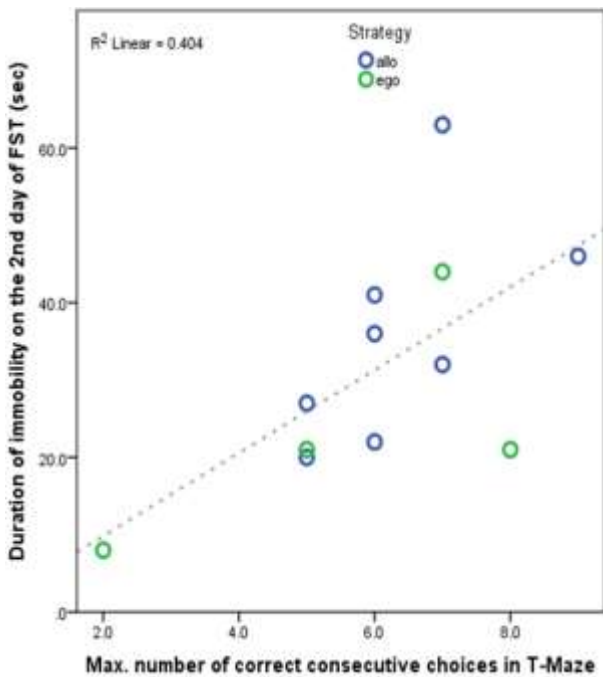


Figure 5. The graph depicting the positive correlation between the max. number of consecutive correct choices in T-Maze and the duration of immobility on the 2nd day of the FST. Regardless of the strategy, a positive correlation was present between these T-Maze and FST parameters. Blue circles correspond to allocentric/place learners (allo) and green circles correspond to egocentric/response learners (ego).

The relationship between duration of immobility on the 2nd day of FST, the total number of training trials and the duration to complete the probe trial were not significant ($r(12) = -.249, p = .435$); $r(12) = -.310, p = .354$, respectively). But a significant positive correlation was detected between duration of immobility on the 2nd day of FST and the max. number of consecutive correct trials in T-maze ($r(12) = .636, p = .026$) (Figure 5).

Comparison of T-Maze and FST behavioral performances with the astrocyte and microglia densities in hippocampal subfields:

In the last set of analyses, the behavioral parameters from the T-Maze and FST were contrasted against the microglial densities across DG and CA1 hippocampal subfields. To calculate the GFAP+ and Iba1+ glial cells, at least 3 hippocampal sections/rat clearly stained with the appropriate antibody for the glial marker proteins were imaged under 10X magnification. The digital images of the hippocampus then transferred to ImageJ. The hippocampal DG and CA1 regions were demarcated on the imaged sections and stained cells that were clear in the focal plane were counted using “Cell Counter” Image J Program. The density of Iba1+ microglia in DG and CA1 hippocampal subfields were not statistically different in allocentric/place learners and egocentric/response learners ($U = 1.134, p = .315$; $U = -1.443, p = .2$, respectively). The density of GFAP+ astrocytes were also not statistically different in the DG between the groups ($U = -1.701, p = .109$) but a significant difference emerged between the groups in the CA1 subfield ($U = 2.193, p = .032$): egocentric/response learner subjects had a higher density of GFAP+ astrocytes in CA1 ($Mdn_{ego} = 0.0030/100 \mu m^2, Mdn_{allo} = 0.0022/100 \mu m^2$) than allocentric/place learners.

When the glial cell densities were compared with the T-Maze performance, the density of Iba1+ microglia were not significantly correlated with the total number of training trials, the max. number of consecutive correct choices and duration to complete the probe trial (For the DG: $r = -.514$, $p = .106$; $r = -.241$, $p = .475$; $r = -.418$, $p = .230$, respectively. For the CA1: $r = .499$, $p = .208$; $r = -.332$, $p = .422$; $r = .611$, $p = .145$, respectively.)

The GFAP+ astrocyte density in the CA1 hippocampal subfield, however, was significantly negatively correlated with the total number of training trials ($r = -.664$, $p = .036$), and duration to complete the probe trial ($r = -.761$, $p = .017$) but not with the maximum number of consecutive correct choices ($r = .419$, $p = .228$). But this relationship was subfield specific as we did not observe a significant relationship between DG GFAP+ astrocyte density and the total number of training trials, the max. number of consecutive correct choices and duration to complete the probe trial in T-Maze ($r = .218$, $p = .520$; $r = .188$, $p = .579$; $r = .130$, $p = .720$).

Microglia and astrocyte densities in hippocampal subfields were also compared with the FST parameters of immobility duration and headshake frequency. Irrespective of the hippocampal subfields, Iba1+ microglia density was not significantly correlated with either of the immobility duration and headshake frequency (For the DG: $r = -.561$, $p = .072$; $r = .177$, $p = .602$, respectively. For the CA1: $r = -.423$, $p = .297$; $r = .276$, $p = .508$, respectively.) In terms of GFAP+ astrocytes, we detected a marginally significant negative correlation with DG GFAP+ cell density and the headshake frequency on the 2nd day of FST ($r = -.596$, $p = .053$) but not with duration of immobility ($r = .478$, $p = .137$). CA1 astrocyte density was not correlated with either of the headshake

frequency or duration of immobility ($r = .053$, $p = .884$; $r = .296$, $p = .406$).

Discussion

The present study investigated the relationship between learning in a T-maze that is open to solution through multiple learning strategies and behavioral despair as measured by immobility on the second FST day. Microglia and astrocyte cell densities were calculated for different hippocampal subfields also as the glial cells as cell types and hippocampus as a brain region is thought to play sophisticated roles in mood and cognition [29].

The results can be briefly summarized as follows. In terms of behavioral efficacy, both egocentric and allocentric strategies were comparable. Overall, the faster the rats reached learning criterion, the faster they also completed the probe trial used to classify them as egocentric and allocentric learners. The egocentric and allocentric learners did not exhibit differences in terms of their immobility scores on FST day 2. Nonetheless, a positive relationship between the number of consecutive correct trials and immobility on FST day 2 emerged from our analysis indicative of a tendency to remain more immobile in animals that learned the T-maze task more effectively. This relationship becomes more meaningful in light of the marginally significant relationship between the learning trials required to reach criterion and the number of consecutive correct trials before animals reached the criterion. As alluded to before also, reaching learning criterion earlier was associated with faster completion of the probe trial. Overall, the behavioral results indicate that the better the animals learn the T-maze, the more immobile they tend to remain on FST day 2.

At the anatomical level, microglia counts in hippocampal CA1 and DG subregions did not

show any relation to learning while astrocyte counts appeared to be higher in the CA1 region of the egocentric learners but not in the DG subregion. Interestingly, CA1 astrocyte counts overall showed a negative correlation with the total number of training trials required to reach learning criterion and duration to complete probe trials. In other words, astrocyte numbers in CA1 are associated with better learning performance. DG astrocyte on the other hand showed a negative correlation with the number of headshakes, an index of struggling behavior in FST [30].

The multiple memory systems hypothesis poses that different memory systems can cooperate or compete for the solution of a particular cognitive task [31]. The T-maze task utilized in the current study could be solved in two ways: 1) by formation of a cognitive map, a strategy largely dependent on the hippocampus and 2) by learning a set of response sequences taking the organism as a reference point that is largely dependent on the striatum. The former strategy is referred to as the allocentric strategy while the latter is referred to as the egocentric strategy [31]. The current study suggests that both strategies can result in comparable behavioral performance as apparent from the lack of differences in the acquisition rates of both egocentric and allocentric learners. Intriguingly, egocentric and allocentric learners did not differ in their level of immobility in FST day 2. This result has some phenomenological implications. Human clinical literature suggests that patients with major depressive disorder have smaller hippocampal volumes [22, 23] along with functional hippocampal alterations [24]. From the perspective of multiple memory systems theory, the compromised system would not be able to compete for expression with the intact system [32]. Complementing this, stress exposure, a major risk factor for depressive

disorder, in animals bolsters egocentric strategies [33]. The absence of differences in immobility in FST day 2 casts doubts about the serviceable function of FST as an animal model of depression. Just to the contrary, the rats that possessed higher efficacy in their learning in the T-maze tended to display higher immobility during FST day 2. These results are more fitting with the notion that immobility during FST day 2 reflects a learning phenomenon [10] rather than a state of behavioral despair. Indeed, De Pablo and colleagues [17, 34] have found that post-FST1 anisomycin treatment that interferes with the protein synthesis; hence the consolidation of learning [35] was associated with a reduction in immobility during FST day 2. The so called short term ameliorating effects of antidepressants [36] on FST day 2 might actually be related to the fact that acute antidepressants have the potential to impair cognitive functioning [37].

Our anatomical results are less straightforward when it comes to interpretation. We did not observe any relationship between CA1 and DG microglia counts with T-maze and FST performances. Whether there are differences in other regions is a question that awaits an answer. Moreover, the absence of effects in this study does not negate that hippocampal microglia play crucial roles when it comes to learning. For instance, brain-derived neurotrophic factors released from microglial cells have been shown to be of critical importance for spatial learning in the hippocampus [25, 26]. On the other hand, the pro-inflammatory responses of microglia, which are hampered by the activation of nicotinic acetylcholine receptors bearing $\alpha 7$ subunits [38, 39], have been shown to impair cognition [40]. These findings actually support the thinking that microglia population might serve as a double edged sword when it comes to

their effects on cognition and this very nature might have masked the meaningful variances in our studies.

While the role of the astrocyte population is a multifaceted, their presence is not associated with an undesired state such as inflammation apart from traumatic brain injury related astrogliosis [41] which does not occur in the intact, normal brain. Some of their conventional roles include providing metabolic support to neurons and pH homeostasis (42) and contribution to the neurovascular demands [43]. Aside from the traditional roles known, recent decades have shown that astrocytes play a role in regulating synaptic communication between neurons, releasing glutamate when necessary [44]. This function is also regulated by acetylcholine [45], a neuromodulator intricately involved in cognitive functions [46]. Pabst and colleagues [47] have found that the optogenetic activation of the septohippocampal pathway recruits hilar interneurons through astrocytes producing long-lasting hyperpolarizations in the pyramidal neurons. In line with the crucial roles of astrocytes, astrocyte numbers in our study was related to more efficacious learning in the t-maze. There are two major culprits to the credibility of this account though. One is the finding that CA1 astrocyte counts were higher in the CA1 of egocentric learners. The other pertains to the absence of a relationship between astrocyte counts and FST day 2 performance which we are tempted to relate to memory of the FST day 1. Expecting a higher CA1 astrocyte count in allocentric learners is a straightforward logic and it is very plausible that astrocytes in CA1 play a crucial role in determining the glucose balance between the hippocampus and the striatum as these seem to be coordinated in accordance with the memory system usage [48]. The latter culprit pertaining to the absence

of evidence for astrocyte involvement in immobility during FST 2 might be explained by the fact that FST involves a stressful learning situation as evidenced by the natural tendency of rodents to avoid water especially when it threatens their thermoregulation [5]. In this respect, differences might emerge in the ventral hippocampal regions that are implicated in stressful situations [49] and not studied in the current set of experiments, which constitutes a weakness. Another flaw pertains to our low sample size. Nonetheless, seeing the effects we saw despite the limited sample size points out also to their strength. Future studies implementing bigger sample sizes and utilizing parametric statistics will yield a richer answer to the exact cognitive mechanisms involved in t-maze learning and how this relates to what is being actually learned during FST.

As alluded to before, there is evidence to the contrary to our studies. Treatments used to prevent and/or avert depression in humans such as environmental enrichment, electroconvulsive shock, and REM duration are shown to diminish immobility during FST day 2 [8]. However, false positive results with psychostimulants, negative results with some selective serotonin reuptake inhibitors, lower immobility being related to lower defecation rates as reviewed by Armario in 2021 [5] pose a challenge to the view that FST immobility reflects pure behavioral despair as well as reduced immobility observed after inactivating molecular learning switches using anisomycin [17, 34]. Ateşyakar and colleagues [50] have found low cognitive competence to be associated with increased immobility in FST day 2, a finding that seem to contradict our findings. Nevertheless, the discrepancies might be explained by the availability of different cognitive strategies in solving the cognitive tasks. For instance, the radial arm maze task

implemented by Ateşyakar and colleagues [50] is typically solved using allocentric strategies rather than egocentric strategies [51] while the T-maze configuration used in our studies provide more liberty to the animals [e.g., 31]. In conclusion, our studies support the notion that FST day 2 immobility is mainly a reflection of memory mechanisms while they do not rule out other factors such as behavioral despair and coping strategies. It is hoped that more detailed future studies will shed light on the exact contribution of these different mechanisms to immobility in FST.

Acknowledgments: *The authors would like to express their gratitude to Metin Yeşiltepe MD, Buse Nur Türkmen, Can Çetinkaya, and Cemre Kürşat for their technical assistance and beneficial suggestions.*

Funding: *This work has been supported by The Scientific and Technological Research Council of Turkey (TUBITAK) 3501 grant (218K570) to Çağrı Temuçin Ünal.*

Conflict of Interest: *The authors declare that they have no conflict of interest.*

Ethical statement:

The study was confirmed by Local Ethics Committee (protocol number: 268).

Open Access Statement

This is an open access journal which means that all content is freely available without charge to the user or his/her institution under the terms of the Creative Commons Attribution Non-Commercial License (<http://creativecommons.org/licenses/by-nc/4.0>). Users are allowed to read, download, copy, distribute, print, search, or link to the full texts of the articles, without asking prior permission from the publisher or the author.

Copyright (c) 2021: Author (s).

References

- [1] World Health Organization (2018). Depression fact sheet.
- [2] Kessler RC, Petukhova M, Sampson NA, et al. Twelve-month and lifetime prevalence and lifetime morbid risk of anxiety and mood disorders in the United States. *Int J Methods Psychiatr Res.* 2012;21(3):169-84.
- [3] Nestler EJ, Gould E, Manji H. Preclinical models: status of basic research in depression. *Biol Psychiatry.* 2002;52(6):503-28.
- [4] Stanford SC. Some Reasons Why Preclinical Studies of Psychiatric Disorders Fail to Translate: What Can Be Rescued from the Misunderstanding and Misuse of Animal ‘Models’?. *Altern Lab Anim.* 2020;48(3):106-15.
- [5] Armario A. The forced swim test: Historical, conceptual and methodological considerations and its relationship with individual behavioral traits. *Neurosci Biobehav Rev.* 2021;128:74-86.
- [6] Bogdanova OV, Kanekar S, D'Anci KE, et al. Factors influencing behavior in the forced swim test. *Physiol Behav.* 2013;118:227-39.
- [7] Slattery DA, Cryan JF. Using the rat forced swim test to assess antidepressant-like activity in rodents. *Nat Protoc.* 2012;7(6):1009-14.
- [8] Porsolt RD, Anton G, Blavet N, et al. Behavioural despair in rats: a new model sensitive to antidepressant treatments. *Eur J Pharmacol.* 1978;47(4):379-91.
- [9] Borsini F, Volterra G, Meli A. Does the behavioral “despair” test measure “despair”? *Physiol Behav.* 1986;38(3):385-86.
- [10] West AP. Neurobehavioral studies of forced swimming: the role of learning and memory in the forced swim test. *Prog Neuropsychopharmacol Biol Psychiatry.* 1990;14(6):863-77.

- [11] Prince CR, Anisman H. Acute and chronic stress effects on performance in a forced-swim task. *Behav Neural Biol.* 1984;42(2):99-119.
- [12] van Calker D, Zobel I, Dykieriek P, et al. Time course of response to antidepressants: predictive value of early improvement and effect of additional psychotherapy. *J Affect Disord.* 2009;114(1-3):243-53.
- [13] Castagné V, Porsolt RD, Moser P. Use of latency to immobility improves detection of antidepressant-like activity in the behavioral despair test in the mouse. *Eur J Pharmacol.* 2009;616(1-3):128-33.
- [14] Molendijk ML, de Kloet ER. Immobility in the forced swim test is adaptive and does not reflect depression. *Psychoneuroendocrinology.* 2015;62:389-91.
- [15] Hawkins J, Hicks RA, Phillips N, et al. Swimming rats and human depression. *Nature.* 1978;274(5670):512-13.
- [16] Borsini F, Meli A. Is the forced swimming test a suitable model for revealing antidepressant activity? *Psychopharmacology (Berl).* 1988;94(2):147-60.
- [17] De Pablo JM, Parra A, Segovia S, et al. Learned immobility explains the behavior of rats in the forced swimming test. *Physiol Behav.* 1989;46(2):229-37.
- [18] de Kloet ER, Molendijk ML. Coping with the Forced Swim Stressor: Towards Understanding an Adaptive Mechanism. *Neural Plast.* 2016;2016: 6503162.
- [19] Commons KG, Cholanians AB, Babb JA, et al. The rodent forced swim test measures stress-coping strategy, not depression-like behavior. *ACS Chem Neurosci.* 2017;8(5):955-60.
- [20] Eichenbaum H. The role of the hippocampus in navigation is memory. *J Neurophysiol.* 2017;117(4):1785-96.
- [21] Lisman J, Buzsáki G, Eichenbaum H, et al. Viewpoints: how the hippocampus contributes to memory, navigation and cognition. *Nat Neurosci.* 2017;20(11):1434-47.
- [22] Bremner JD, Narayan M, Anderson ER, et al. Hippocampal volume reduction in major depression. *Am J Psychiatry.* 2000;157(1):115-18.
- [23] McKinnon MC, Yucel K, Nazarov A, et al. A meta-analysis examining clinical predictors of hippocampal volume in patients with major depressive disorder. *J Psychiatry Neurosci.* 2009;34(1):41-54.
- [24] Milne AM, MacQueen GM, Hall GB. Abnormal hippocampal activation in patients with extensive history of major depression: an fMRI study. *J Psychiatry Neurosci.* 2012;37(1):28-36.
- [25] Parkhurst CN, Yang G, Ninan I, et al. Microglia promote learning-dependent synapse formation through brain-derived neurotrophic factor. *Cell.* 2013;155(7):1596-609.
- [26] Torres L, Danver J, Ji K, et al. Dynamic microglial modulation of spatial learning and social behavior. *Brain Behav Immun.* 2016; 55:6-16.
- [27] Tolman EC, Ritchie BF, Kalish D. Studies in spatial learning. II. Place learning versus response learning. *J Exp Psychol.* 1946;36(3):221.
- [28] Paxinos G, Watson C. The rat brain in stereotaxic coordinates: hard cover edition. Elsevier. Hard Cover Edition. 6th Edition - November 2, 2006.
- [29] Santello M, Toni N, Volterra A. Astrocyte function from information processing to

- cognition and cognitive impairment. *Nat Neurosci.* 2019;22(2):154-66.
- [30] Lino-de-Oliveira C, De Lima TC, et al. Structure of the rat behaviour in the forced swimming test. *Behav Brain Res.* 2005;158(2):243-50.
- [31] Gold PE. Coordination of multiple memory systems. *Neurobiol Learn Mem.* 2004;82(3):230-42.
- [32] Gasbarri A, Pompili A, Packard MG, et al. Habit learning and memory in mammals: behavioral and neural characteristics. *Neurobiol Learn Mem.* 2014;114:198-208.
- [33] Packard MG. Anxiety, cognition, and habit: a multiple memory systems perspective. *Brain Res.* 2009;1293:121-28.
- [34] De Pablo JM, Ortiz-Caro J, Sanchez-Santed F, et al. Effects of diazepam, pentobarbital, scopolamine and the timing of saline injection on learned immobility in rats. *Physiol Behav.* 1991;50(5):895-99.
- [35] Davis HP, Squire LR. Protein synthesis and memory: a review. *Psychol Bull.* 1984;96(3):518-59.
- [36] Petit-Demouliere B, Chenu F, Bourin M. Forced swimming test in mice: a review of antidepressant activity. *Psychopharmacology (Berl).* 2005;177(3):245-55.
- [37] Skandali N, Rowe JB, Voon V, et al. Dissociable effects of acute SSRI (escitalopram) on executive, learning and emotional functions in healthy humans. *Neuropsychopharmacology.* 2018;43(13):2645-51.
- [38] De Simone R, Ajmone-Cat MA, Carnevale D, et al. Activation of $\alpha 7$ nicotinic acetylcholine receptor by nicotine selectively up-regulates cyclooxygenase-2 and prostaglandin E 2 in rat microglial cultures. *J Neuroinflammation.* 2005;2(1):4.
- [39] Pavlov VA, Tracey KJ. The cholinergic anti-inflammatory pathway. *Brain Behav Immun.* 2005;19(6):493-99.
- [40] Terrando N, Eriksson LI, Ryu JK, et al. Resolving postoperative neuroinflammation and cognitive decline. *Ann Neurol.* 2011;70(6):986-95.
- [41] Shandra O, Winemiller AR, Heithoff BP, et al. Repetitive diffuse mild traumatic brain injury causes an atypical astrocyte response and spontaneous recurrent seizures. *J Neurosci.* 2019;39(10):1944-63.
- [42] García-Cáceres C, Balland E, Prevot V, et al. Role of astrocytes, microglia, and tanycytes in brain control of systemic metabolism. *Nat Neurosci.* 2019;22(1):7-14.
- [43] Liu CY, Yang Y, Ju WN, et al. Emerging roles of astrocytes in neuro-vascular unit and the tripartite synapse with emphasis on reactive gliosis in the context of Alzheimer's disease. *Front Cell Neurosci.* 2018;12:193.
- [44] Bezzi P, Gundersen V, Galbete JL, et al. Astrocytes contain a vesicular compartment that is competent for regulated exocytosis of glutamate. *Nat Neurosci.* 2004;7(6):613-20.
- [45] Navarrete M, Perea G, Fernandez de Sevilla D, et al. Astrocytes mediate in vivo cholinergic-induced synaptic plasticity. *PLoS Biol.* 2012;10(2):e1001259.
- [46] Ünal ÇT. A Summary of Electrophysiological Research of Basal Forebrain Cholinergic Neurons. *İzmir Sosyal Bilimler Dergisi.* 2020; 2 (1): 9-15.
- [47] Pabst M, Braganza O, Dannenberg H, et al. Astrocyte Intermediaries of Septal Cholinergic Modulation in the Hippocampus. *Neuron.* 2016;90(4):853-65.
- [48] McNay EC, Gold PE. Food for thought: fluctuations in brain extracellular glucose provide insight into the mechanisms of memory modulation. *Behav Cogn Neurosci Rev.* 2002;1(4):264-80.

- [49] Gulyaeva NV. Ventral hippocampus, Stress and psychopathology: Translational implications. *Neurochem J.* 2015;9(2):85-94.
- [50] Atesyakar N, Canbeyli R, Unal G. Low cognitive competence as a vulnerability factor for behavioral despair in rats. *Behav Processes.* 2020;174:104103.
- [51] Olton DS, Collison C, Werz MA. Spatial memory and radial arm maze performance of rats. *Learn Motiv.* 1977;8(3):289-314.

Bisphenol A levels in bowel endometrioma diagnosed serums: A case control study

Filiz Ardic¹, Humeyra Celik², Huseyin Yesilyurt³, Serap Mutlu Ozcelik Otcu⁴

¹Department of Obstetrics and Gynecology, Ağrı Patnos State Hospital, Ağrı, Turkey

²Department of Physiology, Bolu Abant İzzet Baysal University, School of Medicine, Bolu, Turkey

³Department of Obstetrics and Gynecology, Ankara City Hospital, Ankara, Turkey

⁴Department of Obstetrics and Gynecology, University of Health Sciences, Gazi Yaşargil Training and Research Hospital, Diyarbakır, Turkey

ABSTRACT

Aim: To investigate the bisphenol A (BPA) levels, which may be a risk factor in the etiology of endometrioma, in patients diagnosed laparoscopically with endometrioma with and without bowel involvement.

Method: In the prospective cross-sectional case control study, 47 cases were included in the study, which were admitted to the gynecology and infertility services with and without bowel involvement endometrioma who were operated and diagnosed histopathologically. 43 patients were included in the control group. For serum BPA value, blood samples taken immediately before the operation were studied in laboratory. Patients and controls were compared with controls in terms of serum BPA values.

Results: The mean age of the patients was 35 ± 2 in the endometriosis group and 36 ± 2 in the control group which was and not statistically significant. There was no statistical difference between the patient and control groups in terms of menstruation periods. Serum BPA levels were significantly higher in the bowel involvement group compared to the non-bowel involvement group, as the distribution width was higher due to excessive values, and only 5 patients with bowel involvement did not reach statistically significant levels. Serum BPA level was 1084 ± 1132 ng/L in the endometriosis group and 269 ± 99 ng/L in the control group which was statistically significant ($p < 0,001$).

Conclusions: BPA levels were showing very wide range especially in the patient group. Serum BPA levels was statistically significantly higher in the endometrioma group compared to the control group. Therefore, in the etiology of endometriosis BPA may take a definite place.

Key words: Endometrioma, endometriosis, intestine, bowel, bisphenol-A.

✉ Humeyra Celik

Department of Physiology, Bolu Abant İzzet Baysal University, School of Medicine, Bolu, Turkey

E-mail: humeyra.colaker@gmail.com

Received: 2021-06-23 / Revisions: 2021-10-14

Accepted: 2021-10-24 / Published online: 2022-01-01

Introduction

Endometriosis is a chronic inflammatory disease characterized by the endometrial gland and stroma outside the endometrium [1]. Its

clinical symptoms are dysmenorrhea, dyspareunia, non-cyclic pelvic pain, and subfertility and cause 30-50% infertility and 10-15% morbidity in premenopausal reproductive women [2]. Even if endometriosis is a benign gynecological disease, it carries a risk of epithelial ovarian cancer [3]. Although endometriosis is classified as genital and extragenital [4], the most common position of extragenital endometriosis is the bowels [5,6].

Where there is still conflicting information about its prevalence, pathogenesis, natural course, and optimal treatment, and today it is believed that environmental toxins may also be one of its pathogenesis.

Environmental toxins that induce the dysregulation of hormone systems that regulate reproductive, cardiovascular, neurological and immune processes in humans are called endocrine-disrupting chemicals (EDC) [7]. People exposed to EDCs have been shown to have an increased risk of developing diseases such as cancer, diabetes, obesity, infertility [8-12]. Bisphenol A (BPA); is one of the commonly used EDCs [13]. 70% of the produced BPA is used in polycarbonate plastics and 25% in epoxy resins [14], polycarbonates are included in the structure of various plastic products such as feeding bottles, tin cans, and water bottles [15]. Epoxy resins, on the other hand, are used for coating the inner surface of metal cans used in the packaging of food and beverages and different types of food transport containers. If the process does not occur correctly in constructing these packaging materials, the migration of BPA-type resins and reaction products to food is formed [16]. Considering that packaged convenience foods are consumed very intensively in our age, studies on substances that migrate from packaging materials to food become important for food safety and human health.

Due to its estrogen (E2)-like structure, BPA shows estrogenic effects by binding to α -receptors and weakly β -estrogen receptors (ER) *in vivo* and *in vitro* environment [17]. Although BPA binds to nuclear estrogen receptors with less affinity than 17 β -estrogen (E2), it binds to non-nuclear estrogen receptors with similar affinity as E2 [18]. BPA could act as an anti-estrogen that blocks the estrogenic

response by competing with endogenous E2 [19] and showing an antiandrogenic effect by binding directly to androgen receptors blocking endogenous androgen activity [19,20].

In recent years, it has been known that BPA can negatively affect the endocrine system even at lower doses [21]. BPA taken by various means is metabolized in the liver glucuronidation pathway. BPA loses its estrogenic effect when sulfated. The approximate half-life of BPA is 6 hours, and almost all of it is excreted in urine within 24 hours. Although rapidly metabolized, BPA could accumulate in tissues for a long time and participate in the conjugation – deconjugation cycle [22]. It is believed that BPA is exposed to toxic effects, especially during the fetal and neonatal period, when liver detoxification enzymes are not yet developed, and its effects are revealed through this period [23].

One of the theories put forward to explain the etiology of endometriosis, the cause of which is not precisely known, is induction theory. This theory suggests that some exogenous and endogenous hormonal and biological factors cause the transformation of undifferentiated cells into endometrium tissue [24]. *In vitro* studies have said that ovarian surface epithelium has the potential to undergo transformation to form endometriotic lesions in response to estrogen [25]; prenatal exposure of mice to BPA can reveal an EM-like phenotype in female offspring [26]. The demonstration that BPA exposure causes endometriosis-like lesions has led to the hypothesis that BPA may play a role in endometriosis pathogenesis. Therefore, we wanted to shed light on whether BPA can be included in endometrioma pathogenesis by examining the serum levels of BPA, which is an environmental toxin patient with and without bowel involvement.

Materials and methods

Study design

For this study, Clinical Ethics Committee approval with the decision number 120/2017 was obtained from Health Sciences University Ankara Dr. Zekai Tahir Burak Women's Health Health Application and Research Center. Data were obtained at gynecology clinics of the same hospital, carried out from 2017 to 2018.

A total of 90 patients, 47 female patients and 43 healthy women aged 29-38, were included in the study according to inclusion and exclusion criteria (Table 1). The control group was created from women who were admitted to our hospital for routine follow-up or pap smear. The endometrioma group was formed from people who were diagnosed with endometrioma during laparoscopy or laparotomy and reported endometrioma as a result of the pathological examination in their material.

Table 1. Inclusion and exclusion criteria.

Inclusion criteria	Exclusion criteria
-Being between the ages of 29-40 -Getting written consent	-Taking any hormonal medication in the last 6 months -Having applied assisted reproductive techniques in the last 6 months -Endometrioma / cyst detected in USG -Having dysmenorrhea / dyspareunia -Having menstrual irregularity BMI > 35

The information of patients was obtained by conducting a face-to-face interview. Body mass index was calculated by measuring height and weight during the hospitalization of patients. The cases in the follicular phase of the menstrual cycle and at the end of menstruation were included in the study. Dyspareunia and

dysmenorrhea were questioned. New onset and non-recurrent pains were not considered dyspareunia. Patients who described the new onset of dysmenorrhea or pain for other reasons were not included in the group. All patients in control and endometrioma groups were married. One patient in the endometrioma group, despite being married for one year, did not have children and was accepted as infertile. Since this patient did not receive any hormonal therapy, the patient was included in the endometrioma group.

ELISA

After verbal consent was obtained from all of the patients in the study group, 10 ccs of venous blood were collected at the end of 8 hours of fasting to evaluate serum BPA levels on the morning of the operation. The blood taken was immediately taken into a glass tube after being centrifuged at 3000 rpm for 20 minutes. The tubes were paraffinized and stored at -80 ° C without exposure to any plastic material and sunlight. BPA levels in serum were analyzed with the sandwich ELISA detection method following the instructions prepared by the kit manufacturer (Pars BioChem NanjingG Pars BioChem CO, LTD). In ELISA analysis, samples were read in a Rayto microplate RT 2100 C reading device. The kits have a 50 ng / L sensitivity, and the BPA threshold value was accepted as 150-4000 ng / L.

Statistical analysis

The numerical data measured were presented as mean and standard deviation (SD), median (median), minimum and maximum values. Kolmogorov-Smirnov and Shapiro-Wilk tests were used to determine whether the numerical values obtained from the measurement were compatible with the normal distribution. Since numerical values did not conform to the normal distribution, data belonging to independent groups were compared using the Mann-

Whitney U test. Non-parametric Spearman correlation analysis was used for correlations between numerical values. Nominal or ordinal data obtained by census were presented as numbers and percentages. In statistical analysis, p value below 0.05 was considered statistically significant.

Results

47 age-matched female patients with endometriosis and 43 healthy women were included in the study as the endometrioma group and control group. The mean age of the endometrioma and control groups was 35 ± 2 years, and no statistical difference was found between them ($p = 0.127$) (Table 2)

maximum: 236-4450 ng / L), especially in the endometrioma group (Table 2).

When patients with endometriosis with and without bowel involvement were compared; it was observed that there was no significant difference between the two subgroups in terms of age, menarche age and duration of menstruation ($p > 0.05$ for each) (Table 3). However, endometrioma size was found to be significantly higher in patients with bowel involvement compared to those without involvement ($p = 0.041$) (Table 3).

Serum BPA levels were observed to be very high in the group with bowel involvement compared to the non-involvement group (median values; 1805 ng / L and 464 ng / L,

Table 2. Comparison of the characteristic features between the endometrioma and control groups.

Parameters	Endometrioma group (n=47)		Control group (n=43)		P value
	Mean \pm SD	Median (Min-Max)	Mean \pm SD	Median (Min-Max)	
Age (Year)	35 ± 2	35 (29-38)	35 ± 2	35 (32-38)	0,127
Menarche age (Year)	12 ± 1	13 (11-15)	13 ± 1	13 (11-15)	0,001
Menstruation (Day)	6 ± 2	6 (4-9)	6 ± 1	6 (4-8)	0,739
Bisphenol A (ng/L)	1084 ± 1132	488 (236-4450)	269 ± 99	233 (155-505)	<0,001

Menarche ages of the endometrioma group was found to be significantly lower than the control group ($p = 0.001$) (Table 2). No statistically significant difference was found between the endometrioma and control groups in terms of menstrual periods (6 ± 2 days and 6 ± 1 days, respectively, $p = 0.739$) (Table 4).

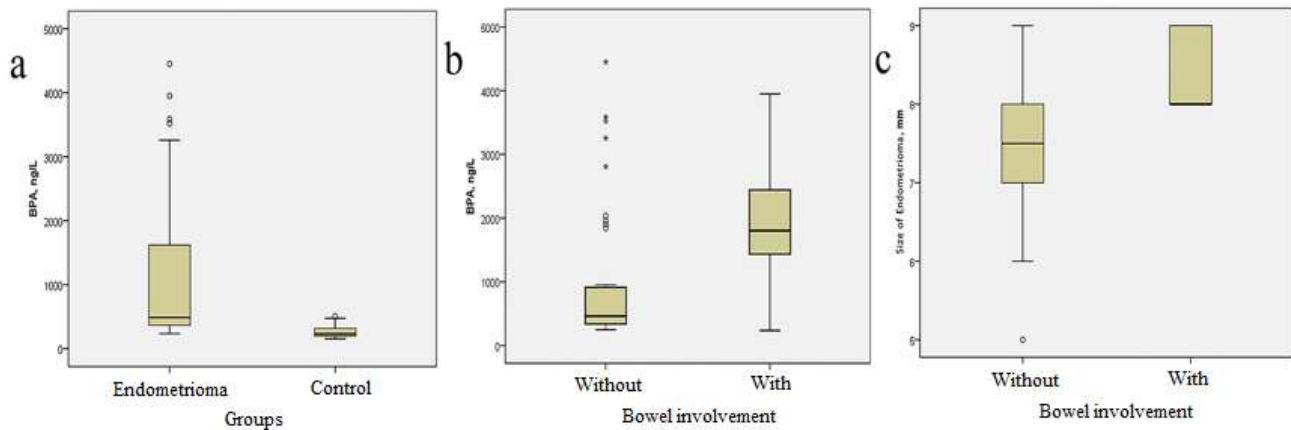
Serum human BPA levels of the endometrioma group (1084 ± 1132 ng / L) were found to be significantly higher than the control group (269 ± 99 ng / L) ($p < 0.001$) (Table 2). BPA levels showed a very wide range (minimum-

respectively), it was observed that the difference between the two groups could not reach a statistically significant level since because the distribution was too high due to extreme values and there were patients only 5 with bowel involvement (Table 3). However, the size of endometrima was found to be significantly higher in patients with intestinal involvement compared to those without involvement ($p = 0.041$) (Figure 1).

A weak negative correlation was found between serum BPA level and patient age in the

Table 3. Comparison of the variables for endometrioma group with and without bowel involvement.

Parameters	Bowel Involvement (-) (n=42)		Bowel Involvement (+) (n=5)		P Value
	Mean \pm SD	Median (Mean-Max)	Average \pm SD	Median (Min-Max)	
Age (Year)	35 \pm 2	35 (29-38)	36 \pm 2	36 (33-37)	0,429
Menarche age (Year)	12 \pm 1	13 (11-15)	12 \pm 1	12 (11-13)	0,603
Duration of menstruation (Day)	6 \pm 2	6 (4-9)	5 \pm 1	6 (4-7)	0,390
Endometrioma (mm)	7 \pm 1	8 (5-9)	8 \pm 1	8 (8-9)	0,041
Bisphenol A (ng/L)	978 \pm 1071	464 (250-4450)	1973 \pm 1366	1805 (236-3950)	0,190

**Figure 1.** a) Graph of serum bisphenol A values of endometrioma and control groups. b) Graph of serum bisphenol A values of endometrioma group with and without bowel involvement. c) Endometrioma size graph of the endometrioma group with and without intestinal involvement.

endometrioma group ($r=-0,307$; $p=0,036$) (Table 4). However, there was no significant correlation between BPA and age in the control group ($p=0,413$). No significant correlation was found between serum BPA levels and menarche age, menstrual duration, and endometrioma size in both the endometrioma group and the control group ($p>0,05$) (Table 4).

Discussion

In the world, 10-15% of women of reproductive age are affected by endometriosis, and endometriosis is considered a significant cause of morbidity [27]. Considering the demographic characteristics, it is known that

endometriosis is diagnosed in the reproductive period [28] and that early menarche age is a risk factor for endometriosis [29], and that menstrual bleeding is prolonged. In the study, the average age of endometrioma group with endometriosis being in the reproductive period and not being different from controls [30] and the early menarche age compared to controls [30, 31] are consistent with the literature. The information that the duration of menstrual bleeding is long in patients with endometriosis [32] is not compatible with the result of the study, but similar studies are encountered when evaluated daily (6 days) [33].

Table 4. Spearman's correlation coefficients (r) and significance levels (p) between serum **Bisphenol A** level and other variables in the endometrioma and control groups.

Groups			Age	Menarche age	Duration of menstruation	Size of endometrium
Endometrioma	Bisphenol A	r	-0,307*	0,030	-0,206	0,070
		p	0,036	0,840	0,165	0,641
Control	Bisphenol A	r	0,128	0,027	-0,012	-
		p	0,413	0,862	0,939	-

Many risk factors have been identified for endometriosis, such as genetics, age, race, obesity, exposure to the hormone, and environmental conditions. BPA is also considered one of the most widely used environmental factors today, and that can be considered a risk factor in the formation of endometriosis. Due to the E2-like nature of BPA, it binds to α -receptors in vivo and in vitro and weakly to β -estrogen receptors (ER), demonstrating estrogenic effects [17]. Although BPA binds to nuclear estrogen receptors with lower affinity than 17 β -estradiol (E2), it binds to non-nuclear estrogen receptors with similar affinity to E2 [18]. BPA could act as an anti-estrogen that blocks the estrogenic response by competing with endogenous E2 and binding directly to androgen receptors [19], blocking endogenous androgen activity and showing an antiandrogenic effect [19,20]. In recent years, it has been known that BPA can negatively affect the endocrine system even at low doses [21]. In our study, serum BPA levels were significantly higher, although there was an extensive distribution in the endometrioma group. Although a weak negative correlation was observed between serum BPA levels and patient age in the endometrioma group, no correlation was found between serum BPA

levels and menarche age, menstrual duration, and endometrioma size in the endometrioma group and the control group. The detection of the high amount of BPA in the serum of patients with endometriosis in accordance with the study of Cobellis et al. [34] suggests that BPA is involved in the pathophysiology of endometriosis. The difference of between Cobellis et al. and the present study is BPA analysis method. Cobellis et al. assessed serum BPA levels by chromatography but our method is ELISA.

The area that extragenital endometriosis most commonly observed is the bowels [6] and 3.8-37% of patients with endometriosis have bowel endometriosis [35]. As the etiopathogenesis of intestinal endometriosis is multifactorial (retrograde menstruation, coelomic metaplasia, lymphatic dissemination, etc.) [36], the bowel contact of endocrine disrupting chemicals taken with food gives BPA a position in terms of pathogenesis. In our study, patients with endometriosis with and without intestinal involvement were compared; the size of endometrioma was significantly larger in patients with bowel involvement compared to those without involvement. Serum BPA levels were observed to be very high in the group with bowel involvement compared to the group

without involvement (median values; 1805 ng / L and 464 ng / L, respectively), measurement of extreme values, too much distribution width, and the presence of only five patients with bowel involvement caused the difference between the two groups to not reach a statistically significant level. The high presence of BPA, which enters the body with food intake, in those with intestinal involvement is significant in terms of the place where BPA is absorbed into the body. Especially for the endometrioma group with bowel endometriosis, avoiding BPA may affect the course of the disease. Our study is original in terms of showing bowel involvement and serum BPA values.

BPA taken in various ways is mainly metabolized in the liver glucuronidation pathway and loses its estrogenic effect when BPA is sulfated. The half-life of BPA is 6 hours, and although it is rapidly metabolized, BPA can accumulate in tissues for a long time and be included in the conjugation-deconjugation cycle. Although almost all of the BPA is excreted in the urine in 24 hours [22], high urinary BPA levels in patients diagnosed with laparoscopic endometriosis [37], and significantly higher total urinary BPA levels in patients diagnosed with non-ovarian endometrioma [38] indirectly support the results of our study. On the other hand, there are other studies in the literature in which the urinary BPA values in endometriosis were examined, and no significant results were obtained [39, 40]. However, the evaluation of these studies in patients diagnosed with endometriosis radiologically limited the discussion. Studies showing how exposure to BPA causes changes in the organism shed light on the pathophysiology of BPA endometriosis. In the study in which BPA was given to an

endometriotic animal model created by injecting uterine tissue into the pelvis, and its effects were examined, it has been shown that BPA increased distal lesion volumes (300 and 900 ppm BPA), increased the number of atretic and dead follicles (30, 300 and 900 ppm BPA), activate estrogen receptor genes and disrupt ovarian functions [41]. In another study investigating the effects of BPA in the *in vitro* endometriosis model, it was reported that BPA showed agonistic activity against estrogen receptor alpha and beta [42]. In another study conducted to investigate the role of BPA in the pathophysiology of endometriosis, it was observed that high urinary BPA levels and high thiobarbituric acid-reactive products were associated with each other in women diagnosed with endometriosis. It was stated that BPA could achieve its effects by increasing oxidative stress in the formation of endometriosis [43]. Since liver detoxification enzymes have not developed yet, it suggests that exposure to the toxic effects of BPA, especially in the intrauterine and neonatal period, reveals the effects of BPA through this period [44]. It has been determined that BPA given to pregnant Balb-C mice starting from the 1st day of pregnancy and up to the 7th postpartum day causes endometriosis-like structures in the adipose tissue surrounding the genital areas of the offspring. In addition, cystic ovary, cystic endometrial hyperplasia, atypical hyperplasia, and adenomatous hyperplastic structures were seen more in animals exposed to BPA than controls [26]. Although endometriosis is diagnosed in the reproductive period, the fact that the effects of BPA are shown as a result of chronic exposure and through estrogenic receptors does not change the fact that it creates the primary pathology at a very early stage of life.

As a result of our study, endocrine disrupting chemicals have gained importance regarding the pathogenesis of endometriosis. The present study is a clinical study but should be supported the effects of BPA in experimental studies, besides it should be investigate that what is relationship between BPA and bowel endometriosis. Studies aimed at enlightening the pathogenesis of endometriosis could create new treatment options and prevent infertility and cancers due to endometriosis.

Funding: *The author(s) received no financial support for the research, authorship, and/or publication of this article.*

Conflict of Interest: *The authors declare that they have no conflict of interest.*

Ethical statement: *Clinical ethics committee approval with the decision number 120/2017 was obtained from Health Sciences University Ankara Dr. Zekai Tahir Burak Women's Health Health Application and Research Center.*

Open Access Statement

This is an open access journal which means that all content is freely available without charge to the user or his/her institution under the terms of the Creative Commons Attribution Non-Commercial License (<http://creativecommons.org/licenses/by-nc/4.0>). Users are allowed to read, download, copy, distribute, print, search, or link to the full texts of the articles, without asking prior permission from the publisher or the author.

Copyright (c) 2021: Author (s).

References

[1] Matarese G, De Placido G, Nikas Y, et al. Pathogenesis of endometriosis: natural immunity dysfunction or autoimmune disease? *Trends Mol Med.* 2003;9(5):223–28.

- [2] Haydardedeoglu B, Zeyneloglu HB. The impact of endometriosis on fertility. *Womens Health.* 2015;11:619–23.
- [3] Kim HS, Kim TH, Chung HH, et al. Risk and prognosis of ovarian cancer in women with endometriosis: a meta-analysis. *Br J Cancer.* 2014;110(7):1878–90.
- [4] Nezhat C, Falik R, McKinney S, et al. Pathophysiology and management of urinary tract endometriosis. *Nat Rev Urol.* 2017;14(6): 359-72.
- [5] Sourial S, Tempest N, Hapangama DK. Theories on the pathogenesis of endometriosis. *Int J Reprod Med.* 2014;2014:179515.
- [6] Veeraswamy A, Lewis M, Mann A, et al. Extragenital endometriosis. *Clin Obstet Gynecol.* 2010;53(2):449-66.
- [7] Kabir ER, Rahman MS, Rahman I. A review on endocrine disruptors and their possible impacts on human health. *Environ Toxicol Pharmacol.* 2015;40(1):241–58.
- [8] Heindel JJ, Newbold R, Schug TT. Endocrine disruptors and obesity. *Nat Rev Endocrinol.* 2015;11(11):653–61.
- [9] Sweeney MF, Hasan N, Soto AM, et al. Environmental endocrine disruptors: effects on the human male reproductive system. *Rev Endocr Metab Disord.* 2015;16(4):341–57.
- [10] Costa EM, Spritzer PM, Hohl A, et al. Effects of endocrine disruptors in the development of the female reproductive tract. *Arq Bras Endocrinol Metab.* 2014;58(2):153–61.
- [11] Chevalier N, Fenichel P. Endocrine disruptors: new players in the pathophysiology of type 2 diabetes? *Diabetes Metab.* 2015;41(2):107–15.
- [12] Knowler KC, To SQ, Leung YK, et al. Endocrine disruption of the epigenome: a breast cancer link. *Endocr Relat Cancer.* 2014;21(2):33–55.

- [13] Ballesteros G, Soledat P, Perez-Bendito D. Analytical methods for the determination of bisphenol A in food. *J Chromatogram A.* 2009; 1216(3): 449-69.
- [14] Tsai W-T. Human health risk on environmental exposure to Bisphenol-A: a review. *J Environ Sci Health C Environ Carcinog Ecotoxicol Rev.* 2006; 24(2): 225-55.
- [15] Matsumoto A, Kunugita N, Kitagawa K, et al. Bisphenol A levels in human urine. *Environ Health Perspect.* 2003; 111(1): 101.
- [16] García RS and Losada PP. Determination of bisphenol A diglycidyl ether and its hydrolysis and chlorohydroxy derivatives by liquid chromatography–mass spectrometry. *J Chromatogr A.* 2004; 1032(1-2): 37-43.
- [17] Caserta D, Mantovani A, Marci R, et al. Environment and women's reproductive health. *Hum Reprod Update.* 2011; 17(3): 418-33.
- [18] Alonso-Magdalena P, Laribi O, Ropero AB, et al. Low doses of bisphenol A and diethylstilbestrol impair Ca²⁺ signals in pancreatic α -cells through a nonclassical membrane estrogen receptor within intact islets of Langerhans. *Environ Health Perspect.* 2005; 113(8): 969.
- [19] Moriyama K, Tagami T, Akamizu T, et al. Thyroid hormone action is disrupted by bisphenol A as an antagonist. *J Clin Endocrinol Metab.* 2002; 87(11): 5185-90.
- [20] Wetherill YB, Fisher NL, Staubach A, et al. Xenoestrogen action in prostate cancer: pleiotropic effects dependent on androgen receptor status. *Cancer Res.* 2005; 65(1): 54-65.
- [21] Lopez-Cervantes J and Paseiro-Losada P. Determination of bisphenol A in, and its migration from, PVC stretch film used for food packaging. *Food Addit Contam.* 2003; 20(6): 596-606.
- [22] Lee J, Choi K, Park J, et al. Bisphenol A distribution in serum, urine, placenta, breast milk, and umbilical cord serum in a birth panel of mother–neonate pairs. *Sci Total Environ.* 2018; 626: 1494-1501.
- [23] Ginsberg G and Rice DC. Does rapid metabolism ensure negligible risk from bisphenol A? *Environ Health Perspect.* 2009; 117(11): 1639.
- [24] Vinatier D, Orazi G, Gosson M, et al. Theories of endometriosis. *Eur J Obstet Gynecol Reprod Biol.* 2001; 96(1): 21-34.
- [25] Matsuura K, Ohtake H, Katabuchi H, et al. Coelomic metaplasia theory of endometriosis: evidence from in vivo studies and an in vitro experimental model. *Gynecol Obstetric Invest.* 1999; 47(1): 18-22.
- [26] Signorile PG, Spugnini EP, Mita L, et al. Pre-natal exposure of mice to bisphenol A elicits an endometriosis-like phenotype in female offspring. *Gen Comp Endocrinol.* 2010; 168(3): 318-25.
- [27] Vercellini P, Vigano P, Somigliana E, et al. 'Endometriosis: Pathogenesis and treatment', *Nat Rev Endocrinol.* 2014; 10(5), 261–75.
- [28] Tanbo T and Fedorcsak P. 'Endometriosis-associated infertility: aspects of pathophysiological mechanisms and treatment options', *Acta Obstet Gynecol Scand.* 2017; 96(6) 659–67.
- [29] Shafir, A. L. Farland LV, Shah DK, et al. 'Risk for and consequences of endometriosis: A critical epidemiologic review'. *Best Pract and Res Clin Obstet and Gynaecol.* 2018; 51:1–15.
- [30] Nnoaham KE, Webster P, Kumbang J, et al. 'Is early age at menarche a risk factor for endometriosis? A systematic review and meta-analysis of case-control studies', *Fertil Steril.* 2012; 98(3):702-12.

- [31] Matalliotakis I M, Cakmak H, Fragouli YG, et al. 'Epidemiological characteristics in women with and without endometriosis in the Yale series'. *Arch Gynecol Obstet.* 2008; 277(5): 389–93.
- [32] Moini A, Malekzadeh F, Amirchaghmaghi E, et al. 'Risk factors associated with endometriosis among infertile Iranian women'. *Arch Med Sci.* 2013 Jun 20;9(3):506-14.
- [33] Darrow SL, Vena JE, Batt RE, et al. Menstrual cycle characteristics and the risk of endometriosis. *Epidemiology.* 1993;4(2):135-42.
- [34] Cobellis L, Colacurci N, Trabucco E, et al. Measurement of bisphenol A and bisphenol B levels in human blood sera from healthy and endometriotic women. *Biomed Chromatogr.* 2009 ;23(11):1186-90.
- [35] Redwine DB. Ovarian endometriosis: a marker for more extensive pelvic and intestinal disease. *Fertil Steril.* 1999;72(2):310-15.
- [36] Yong PJ, Bedaiwy MA, Alotaibi F, et al. Pathogenesis of bowel endometriosis. *Best Pract Res Clin Obstet Gynaecol.* 2021;71:2-13.
- [37] Rashidi BH, Amanlou M, Lak TB, et al. A case-control study of bisphenol A and endometrioma among subgroup of Iranian women. *J Res Med Sci.* 2017;22:7.
- [38] [38] Upson K, Sathyanarayana S, De Roos AJ, et al. A population-based case-control study of urinary bisphenol A concentrations and risk of endometriosis. *Hum Reprod.* 2014 ;29(11):2457-64.
- [39] Itoh H, Iwasaki M, Hanaoka T, et al. Urinary bisphenol-A concentration in infertile Japanese women and its association with endometriosis: A cross-sectional study. *Environ Health Prev Med.* 2007;12(6):258-64.
- [40] Buck Louis GM, Peterson CM, Chen Z, et al. Bisphenol A and phthalates and endometriosis: the Endometriosis: Natural History, Diagnosis and Outcomes Study. *Fertil Steril.* 2013;100(1):162-9.e1-2.
- [41] Jones RL, Lang SA, Kendzierski JA, et al. Use of a Mouse Model of Experimentally Induced Endometriosis to Evaluate and Compare the Effects of Bisphenol A and Bisphenol AF Exposure. *Environ Health Perspect.* 2018;126(12):127004.
- [42] Li Y, Perera L, Coons LA, et al. Differential in Vitro Biological Action, Coregulator Interactions, and Molecular Dynamic Analysis of Bisphenol A (BPA), BPAF, and BPS Ligand-ER α Complexes. *Environ Health Perspect.* 2018;126(1):017012.
- [43] Peinado FM, Lendínez I, Sotelo R, et al. Association of Urinary Levels of Bisphenols A, F, and S with Endometriosis Risk: Preliminary Results of the EndEA Study. *Int J Environ Res Public Health.* 2020;17(4):1194.

Meloxicam, a selective COX-2 inhibitor, displays anticonvulsive effects in pentylenetetrazole-induced acute seizures in mice through GABA and glutamate mediated mechanism

Bilal Sahin¹, Recep Akkaya², Sebahattin Karabulut³

¹Department of Physiology, Sivas Cumhuriyet University, School of Medicine, Sivas, Turkey

²Department of Biophysics, Sivas Cumhuriyet University, School of Medicine, Sivas, Turkey

³Department of Medical Services and Techniques, Vocational School of Health Services, Sivas Cumhuriyet University, Sivas, Turkey

ABSTRACT

Aim: To investigate the possible anticonvulsive effect of the selective COX-2 inhibitor meloxicam in pentylenetetrazole (PTZ)-induced epileptic seizures in mice and to examine its possible role on inhibition and excitation balance in the brain.

Method: 30 BALB-c albino mice (16-18 weeks old) weighing 30-33 gr were used. Animals were randomly divided into five groups (n = 6 for each group). Group 1: control, group 2: received saline (10 ml/kg, i.p.) 30 minutes before PTZ (60 mg/kg i.p.) administration, group 3: received saline (10 ml/kg, i.p.) 30 minutes after PTZ (60 mg/kg i.p.) injection, group 4: received 60 mg/kg meloxicam i.p., 30 minutes before PTZ (60 mg/kg i.p.) administration. Group 5: received meloxicam (60 mg/kg i.p.) 30 minutes after PTZ injection (60 mg/kg, i.p.). The animals were observed for 30 minutes and the seizure stages and first myoclonic jerk times (FMJ) were recorded. After 24 hours, brain tissues were removed and the cortex and hippocampus were separated for biochemical assessments. ELISA method was used to measure GABA and glutamate levels.

Results: Administration of meloxicam before PTZ induced seizure, reduced seizure stages and prolonged FMJ duration ($p < 0.05$). Pre-treatment with meloxicam increased GABA levels in the cortex and decreased glutamate levels in the hippocampus ($p < 0.05$). Post-treatment of meloxicam after PTZ-induced seizure increased GABA levels in the hippocampus ($p < 0.05$).

Conclusion: The results of our experimental study suggest that meloxicam has anti-convulsive effects and these effects may be mediated by GABA and glutamate, which are the main indicators of inhibition and excitation balance in the brain.

Key words: Meloxicam, COX-2, epilepsy, GABA, glutamate, mice.

✉ Bilal Sahin

Department of Physiology, Sivas Cumhuriyet University,
School of Medicine, Sivas, Turkey

E-mail: bilalsahin@cumhuriyet.edu.tr

Received: 2021-06-23 / Revisions: 2021-08-13

Accepted: 2021-08-28 / Published online: 2022-01-01

Introduction

Epilepsy is a short-term paroxysmal disorder of brain function characterized by sudden, abnormal and hypersynchronous discharges and seizures observed in a group of neurons in

the central nervous system [1]. Although many studies have been conducted to understand the underlying mechanism and to develop pharmacological treatment, our knowledge about the biological disorders that cause epilepsy is limited [2]. Because of this deficit, currently available anti-epilepsy treatment is symptomatic and ineffective in 30% of cases [3]. Therefore, more effective therapies should be developed to target epileptogenesis. Various molecular and cellular changes accompanying

epilepsy include inflammatory processes in the brain as well as inhibitory-stimulatory processes and an imbalance in the antioxidant system [4]. Studies aiming to elucidate the processes that lead to epilepsy have suggested that inflammation plays an important role both as a cause and a consequence of seizure development [5]. Additionally, several anti-inflammatory drugs have been reported for antiepileptic activities [6,7]. In contrast, there is inverse evidence on the relationship between inflammation and epilepsy [2]. Consequently, further research is needed to understand this relationship.

Cyclooxygenase-2 (COX-2) has received much attention for its important role in the development of various inflammatory processes over the past two decades, and therefore it involves in the formation of seizures and the development of epilepsy. The COX enzyme group consists of oxygenases that convert arachidonic acid to prostaglandins (PGs), which are pro-inflammatory mediators as COX-1 and COX-2 [8]. While COX-1 is mainly expressed in almost all tissue types, COX-2 is an inducible isoform-inducible enzyme that is primarily localized in immune cells such as macrophages and leukocytes, and it is upregulated in pathological conditions like neuronal death and neuronal hyper-excitability and is predominantly expressed in the brain [9]. In addition, COX-1 is thought to be involved in the homeostatic production of PG while COX-2 generally produces PGs related to pathophysiological processes [10]. In this context, COX-2 inhibitor drugs are used for treatments to reduce inflammation in both acute and chronic conditions [11]. In the past few years, a serious research has been done on the applicability of COX-2 as a treatment target in various neuro-inflammatory diseases, including epilepsy.

The animal models for epilepsy have been frequently used to examine the potentiality of anti-convulsing effects of COX-2 inhibition and its effect on seizure activity and development. It has been observed that the findings differ in different seizure and treatment conditions. Meloxicam, a selective COX-2 inhibitor, is used clinically to ease inflammation, swelling, stiffness, and joint pain that is associated with juvenile rheumatoid arthritis, osteoarthritis, and rheumatoid arthritis as part of class drugs called nonsteroidal anti-inflammatory (NSAID)[2]. Meloxicam inhibits prostaglandin biosynthesis in inflammation through COX-2 inhibiting effect [12]. In previous studies, meloxicam was observed to increase the first myoclonic jerk (FMJ) time in acute pentylenetetrazole (PTZ) epilepsy model [13] and to reduce the levels of myeloperoxidase and malondialdehyde and to reintegrate the brain glutathione content [14]. Finally, in a study of kindling model epilepsy in mice, meloxicam reduced inflammation and oxidative stress, and thus it showed anti-epileptic effects [15]. Therefore, for the first time in this study, in PTZ-induced acute seizure mouse model, we examined whether pre- and post-treatment of meloxicam would affect seizure susceptibility through GABAergic and glutamatergic balance in the hippocampus and cortex.

Materials and methods

Animals

Male adult BALB-c Albino 30-33 g mice (16-18 weeks old) purchased from Sivas Cumhuriyet University were used for experiments. The animals were placed in a room with an ambient temperature of $22\pm 3^{\circ}\text{C}$, with a stable humidity between 35–60% and with water and food ad libitum. All experimental procedures were performed under

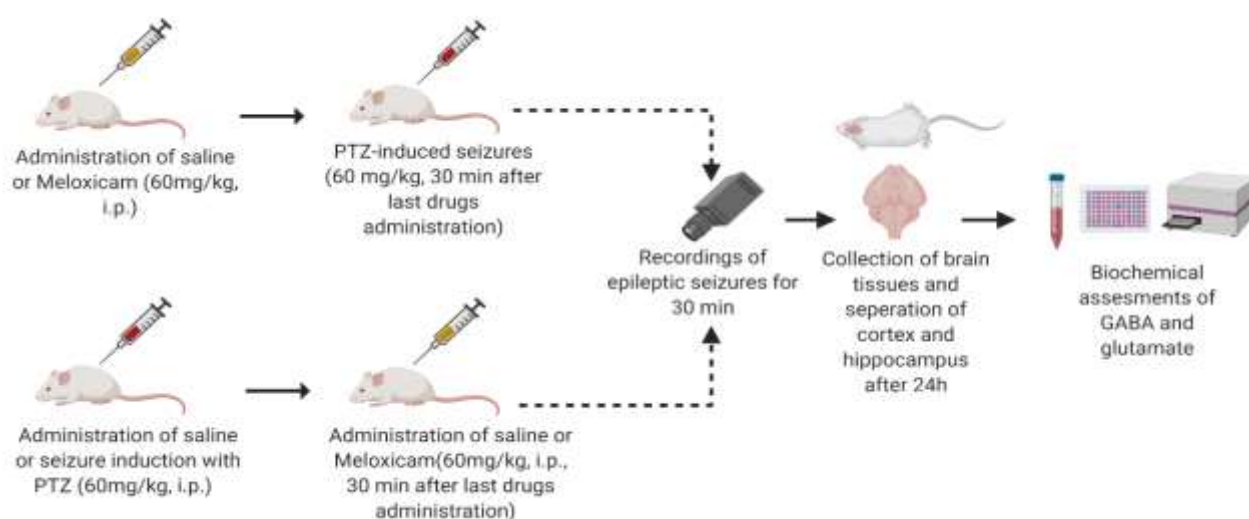


Figure 1. Experimental design of the study (created with BioRender.com).

the guidelines of the Local Ethics Committee of Sivas Cumhuriyet University (Registry Number: 65202830-050.04.04 dated 24.02.2020). The animals were acclimated to laboratory conditions prior to the assay.

Chemicals

Pentylenetetrazole and meloxicam were dissolved in physiological saline. Solutions were freshly prepared for the experiment days. All chemicals used in the studies were of analytical purity. All drugs were purchased from Sigma-Aldrich Co., St Louis, MO, USA.

Experimental protocols

Thirty mice were randomly divided into five clusters for behavioral and biochemical evaluations ($n = 6$ for each groups). Group 1 was control, group 2 was given intraperitoneal saline (10 ml/kg, i.p.) before 30 min PTZ (60 mg/kg i.p.) [16,17], group 3 was given intraperitoneal saline (10 ml/kg, i.p.) after 30 min PTZ injection (60 mg/kg i.p.), group 4 was injected 60 mg/kg meloxicam i.p. before 30 min PTZ (60 mg/kg i.p.), and group 5 was administered 60 mg/kg meloxicam i.p. after 30

min PTZ injection (60 mg/kg i.p.). To determine seizure stages, the Racine convulsion scale (RCS) was used as follows:

- Phase 0 = no response after PTZ administration
- Phase 1 = short or long-term ear and facial twitching
- Phase 2 = myoclonic body jerks and severe myoclonic reflexes
- Phase 3 = clonic forelimb convulsions, severe rearing-up on hind-legs and transition to clonic seizure
- Phase 4 = short or long-term tonic clonic seizures
- Phase 5 = Severe recurrent generalized tonic-clonic seizures
- Phase 6 = lethal seizure/death

For 30 min., mice were observed both for assessing seizure stage and recording the time of the first myoclonic jerk (FMJ) with Phase 3 seizures [18]. Animals were sacrificed and the hippocampus and cortex tissues were removed for the assessment of biochemical parameters. The experimental design is shown in detail in Figure 1.

Biochemical analysis of glutamate and gamma amino butyric acid (GABA)

The cortical and hippocampal regions of brain tissues were homogenized at (pH 7.4) in ice-cold Phosphate Buffered Saline (PBS) solution by using a manual homogenizer, and then they were centrifuged at 12.000g for 10 min at 4°C. The supernatants of the centrifuged homogenates were removed. Mice ELISA commercial kits (YL Biont, Shanghai, China, detection range: 24.69-2000pg/mL) were used to measure glutamate and GABA levels from cortical and hippocampal supernatants according to the manufacturer's instructions. In summary, standard and tissue samples were added to the plate and were incubated for 60 minutes at 37°C. Following the wash stage, staining solutions were added and were

incubated for 15 minutes at 37°C. Stop solution was added and it was read as 450 nm. To determine the total protein content of samples, Bradford method was used to optimize outcomes from the hippocampus and cortex[19].

Statistical analysis

The data were presented as mean ± SEM (standard error of the mean). For all data, the one-way analysis of variance (ANOVA) with Tukey post hoc comparisons test was used. The criterion for the statistical significance less than 5% was accepted.

Results

The effect of Meloxicam on epileptic behaviour

The epileptic seizure scores were significantly

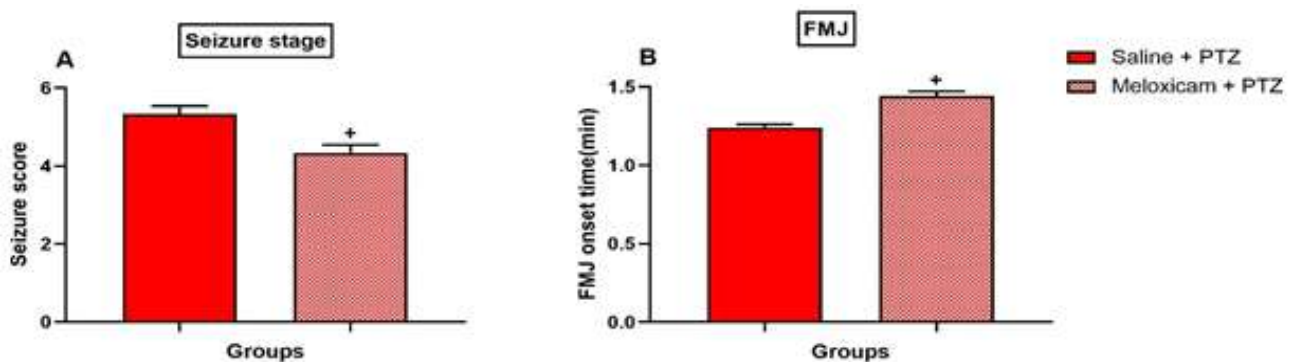


Figure 2A, B. The effect of Meloxicam on seizure stage and FMJ time

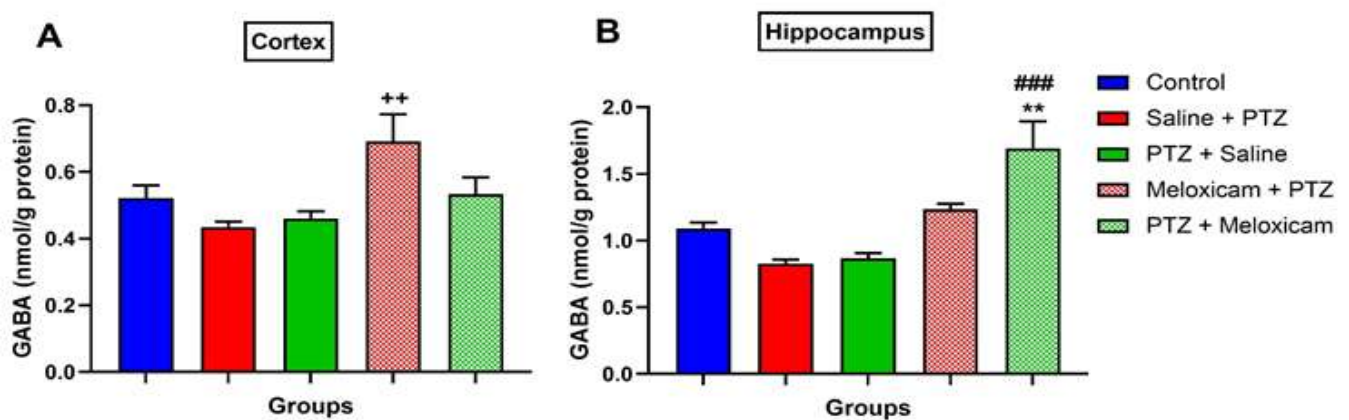


Figure 3A, B. Effect of meloxicam on GABA levels. (A), Cortex (B), Hippocampus. Values are presented as mean ± SEM. ** $p < 0.01$ compared with control group. ++ $p < 0.01$, +++ $p < 0.001$ compared with saline+PTZ group. ### $p < 0.01$, #### $p < 0.001$ compared with PTZ+saline group.

lower in meloxicam+PTZ group by comparison with the saline+PTZ group ($p < 0.05$). (Figure 2A).

The FMJ time was significantly higher in meloxicam+PTZ group (1.44 ± 0.03 min) by comparison with saline+PTZ group (1.24 ± 0.02 min) ($p < 0.05$). (Figure 2B). No seizure-related death was observed in mice during PTZ - induced acute seizure experiments.

The effect of Meloxicam on GABA levels in cortex and hippocampus

In the cortex, there was no statistically significant difference between saline+PTZ and PTZ+saline group by comparison with control group (0.52 ± 0.04 8 nmol/g protein) ($p > 0.05$). On the other hand, there was a significant difference between meloxicam+PTZ group (0.69 ± 0.8 nmol/g protein) by comparison with the saline+PTZ group (0.43 ± 0.01 nmol/g protein) ($p < 0.05$). Otherwise, there was no statistically significant difference between PTZ+meloxicam and PTZ+saline group ($p > 0.05$) (Figure 3A). In the hippocampus, GABA levels were significantly higher in

PTZ+meloxicam group (1.69 ± 0.20 nmol/g protein) by comparison with the control (1.08 ± 0.04 nmol/g protein) ($p < 0.05$) and PTZ+saline (0.86 ± 0.03 nmol/g protein) ($p < 0.001$) groups (1.23 ± 0.04 nmol/g protein) ($p < 0.01$).

Furthermore, GABA levels were higher in meloxicam+PTZ group (1.22 ± 0.04 nmol/g protein) by comparison with saline+PTZ group (0.83 ± 0.03 nmol/g protein) ($p < 0.05$). However, no statistically significant difference was found between PTZ+meloxicam (1.62 ± 0.16 nmol/g protein) and PTZ+saline group in the hippocampus ($p > 0.05$) (Figure 3B).

No seizure-related death was observed in mice during PTZ-induced acute seizure experiments.

The effect of Meloxicam on glutamate levels in cortex and hippocampus

In the cortex, no statistically significant difference was found between saline+PTZ and meloxicam+PTZ groups ($p > 0.05$). Similarly, there was no statistically significant difference between PTZ + saline and PTZ + meloxicam

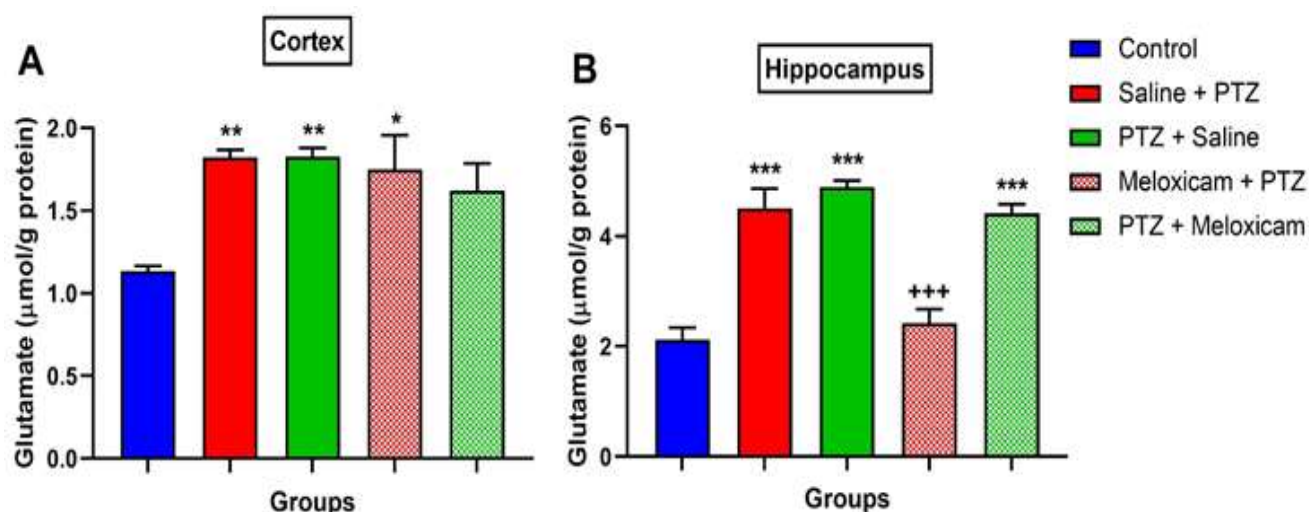


Figure 4. Effect of meloxicam on glutamate levels. (A), Cortex (B), Hippocampus. Values are presented as mean \pm SEM. ** $p < 0.01$ compared with control group. ++ $p < 0.01$, +++ $p < 0.001$ compared with saline+PTZ group. ### $p < 0.01$, #### $p < 0.001$ compared with PTZ+saline group.

groups ($p > 0.05$). Contrarily, glutamate levels were significantly higher in the saline+PTZ (1.82 ± 0.04 nmol/g protein) and PTZ+saline group (1.82 ± 0.05 nmol/g protein) by comparison with the control group (1.13 ± 0.03 nmol/g protein) ($p < 0.01$). Moreover, glutamate levels were higher in the meloxicam+PTZ group (1.75 ± 0.20 nmol/g protein) by comparison with the control group ($p < 0.05$). However, in the cortex, no significant difference was found in PTZ+meloxicam group (1.62 ± 0.16 nmol/g protein) by comparison with the control group ($p > 0.05$) (Figure 4A). In the Hippocampus, glutamate levels in saline+PTZ (4.50 ± 0.35 nmol/g protein), PTZ+saline (4.88 ± 0.12 nmol/g protein) and PTZ+meloxicam groups (4.41 ± 0.16 nmol/g protein) were higher than the control group (2.12 ± 0.22 nmol/g protein) ($p = 0.0001$). However, glutamate levels in meloxicam+PTZ group (2.42 ± 0.25 nmol/g protein) were significantly lower than saline+PTZ group ($p < 0.001$) (Figure 4B). In addition, there was no statistically significant difference between PTZ+saline and PTZ+meloxicam groups ($p > 0.05$).

Discussion

In the present study, it is shown that administration of meloxicam, a COX-2 inhibitor, before and after PTZ-induced acute seizures in mice reduces seizure stages and increases FMJ, and therefore it shows an anticonvulsant activity. Preliminary administration of meloxicam has increased GABA levels both in the cortex and hippocampus, and it has decreased glutamate levels in the hippocampus. On the other hand, administration of meloxicam after seizure induction has no effect on glutamate levels, but it has increased GABA levels in the hippocampus. These findings suggest that the

anticonvulsant activity of meloxicam in acute PTZ-induced seizures in mice may be mediated through the levels of GABA and glutamate, two of the most important molecules in the inhibition and excitation processes in brain.

In brain, COX-2 is expressed in discrete neuronal populations, particularly in the cortex and hippocampus [20]. In many reports, it has been stated that COX-2 plays a significant role in some neurological disorders such as Alzheimer's disease [21], traumatic brain injury [22], cerebral ischemia [23], and epilepsy [24]. The effect of COX-2 inhibitors on seizure type and seizure activity may vary according to different seizure and treatment conditions. Pre-treatment with selective COX-2 inhibitors nimesulide and rofecoxib for 45 minutes prior to seizure induction has demonstrated the diverse efficacy of COX-2 inhibitors in 3 different types of seizure models in mice. These inhibitors have showed anti-convulsing activities by increasing the mean onset time of seizures and by reducing seizure duration in bicuculline- and picrotoxin-induced seizures; on the other hand, they have revealed no effect in maximal electroshock-induced seizures [7]. It shows that the administration of the COX-2 inhibitor rofecoxib at 2 mg/kg and 4 mg/kg increases the seizure threshold, but it does not show that there are any anticonvulsive effects at a low dose, and consequently, there is a dose-dependent effect [25]. Pre-treatment with the selective COX-2 inhibitor, celecoxib, also shows the anticonvulsant effects in 60 minutes before seizure induction in the PTZ-induced rat model [26]. Similarly, in our study, pre-treatment with meloxicam shows the anticonvulsant effect in 30 minutes before seizure induction. Moreover, selective COX-2 inhibitor, etoricoxib, shows an anticonvulsant effect both in PTZ-induced rat model and genetic Wag/Rij absence epilepsy rat model.

However, a number of studies suggest that pre-treatment with COX-2 inhibitors could have a proconvulsive effect [27,28].

Animal models of epilepsy, including PTZ-induced acute seizures, are widely used to identify molecules with anticonvulsant potential and to investigate their efficacy. PTZ exerts its convulsive effect by inhibiting the GABA_A receptor. Decreased GABAergic activity and increased glutamatergic system activity are shown as the most frequent causes of seizures [29]. GABA_A receptor and a ligand-gated chloride channel mediate inhibitory transmission at synapses. In the present work, we have found that PTZ-induced epileptic seizure activity decreases due to the pre- and post-treatment with the COX-2 inhibitor meloxicam. COX-2 mRNA and protein induction, for the first time, have been revealed in the hippocampus and cerebral cortex tissues of rats in a seizure model induced by a maximum electroconvulsive shock [20]. In the same study, it is also shown that COX-2 induction is regulated by glutamatergic N-methyl-D-aspartate (NMDA) receptor-dependent synaptic activity. Several studies have demonstrated that meloxicam prevents ischemia-induced excitotoxicity by changing the transcript levels of different genes of the glutamatergic system, especially NMDA and AMPA receptor subunits [30–32].

PGE₂, the major product of COX-2, binds EP1 receptor with a higher affinity which is a subfamily of G protein-coupled receptors (GPCRs). It has been suggested that COX-2 inhibitors exhibit an anticonvulsant activity by reducing PGE₂ production and lead to a decrease in EP receptor activation, and as a result, they reduce calcium ion entry and the release of the excitatory neurotransmitter glutamate, thereby blocking seizures [33]. These findings are consistent with this current

study in which meloxicam decreases glutamate levels in the hippocampus. Activation of COX-2 also increases oxidative stress by increasing the production of free radicals. Increased oxidative stress causes continuous apoptosis of GABAergic neurons, leading to an increase in glutamate-mediated excitation in neuronal network [34]. Selective COX-2 inhibitor, NS-398, causes up-regulation in the expression of GABA_A receptors, thus, it prevents epileptic seizures by reducing neuronal excitability via MAPK/ERK pathway in hippocampus in pilocarpine-induced status epilepticus in rats [35]. Similarly, in our study, both pre- and post-treatments with meloxicam have increased GABA levels in the cortex and hippocampus. The data suggest that meloxicam shows its anti-convulsive effect by increasing GABAergic activity with pre- and post- treatments and by reducing glutamatergic activity in hippocampus via pre- treatment.

Conclusion

In conclusion, meloxicam shows an anti-epileptic effect on mice both in pre- and post-treatments through GABA and glutamate in PTZ-induced acute seizure models. However, there is a need for further research to understand the underlying mechanisms.

Funding: *The author(s) received no financial support for the research, authorship, and/or publication of this article.*

Conflict of Interest: *The authors declare that they have no conflict of interest.*

Ethical statement:

All experimental procedures were performed under the guidelines of the Local Ethics Committee of Sivas Cumhuriyet University (Registry Number: 65202830-050.04.04 dated 24.02.2020).

Open Access Statement

This is an open access journal which means that all content is freely available without charge to the user or his/her institution under the terms of the Creative Commons Attribution Non-Commercial License (<http://creativecommons.org/licenses/by-nc/4.0>). Users are allowed to read, download, copy, distribute, print, search, or link to the full texts of the articles, without asking prior permission from the publisher or the author.

Copyright (c) 2021: Author (s).

References

- [1]Taskiran AS, Ergul M, Gunes H, et al. The Effects of Proton Pump Inhibitors (Pantoprazole) on Pentylentetrazole-Induced Epileptic Seizures in Rats and Neurotoxicity in the SH-SY5Y Human Neuroblastoma Cell Line. *Cell Mol. Neurobiol.* 2021;41(1):173–83.
- [2]Rawat C, Kukal S, Dahiya UR, et al. Cyclooxygenase-2 (COX-2) inhibitors: future therapeutic strategies for epilepsy management. *J Neuroinflammation.* 2019;16(1):197.
- [3]Chen Z, Brodie MJ, Liew D, et al. Treatment outcomes in patients with newly diagnosed epilepsy treated with established and new antiepileptic drugs a 30-year longitudinal cohort study. *JAMA Neurol.* 2018;75(3):279–86.
- [4]Borowicz-Reutt KK, Czuczwar SJ. Role of oxidative stress in epileptogenesis and potential implications for therapy. *Pharmacol Reports.* 2020;72(5):1218–26.
- [5]Vezzani A, French J, Bartfai T, et al. The role of inflammation in epilepsy. *Nat Rev Neurol.* 2011;7(1):31–40.
- [6]Dhir A, Naidu PS, Kulkarni SK. Neuroprotective effect of nimesulide, a preferential COX-2 inhibitor, against pentylentetrazol (PTZ)-induced chemical kindling and associated biochemical parameters in mice. *Seizure.* 2007;16(8):691–97.
- [7]Dhir A, Naidu PS, Kulkarni SK. Effect of cyclooxygenase-2 (COX-2) inhibitors in various animal models (bicuculline, picrotoxin, maximal electroshock-induced convulsions) of epilepsy with possible mechanism of action. *Indian J Exp Biol.* 2006;44(4):286–91.
- [8]Takemiya T, Suzuki K, Sugiura H, et al. Inducible brain COX-2 facilitates the recurrence of hippocampal seizures in mouse rapid kindling. *Prostaglandins Other Lipid Mediat.* 2003;71(3–4):205–16.
- [9]Zhang J, Goorha S, Raghov R, et al. The tissue-specific, compensatory expression of cyclooxygenase-1 and -2 in transgenic mice. *Prostaglandins Other Lipid Mediat.* 2002;67(2):121–35.
- [10]Kulkarni SK, Dhir A. Cyclooxygenase in epilepsy: From perception to application. *Drugs of Today.* 2009;45(2):135–54.
- [11]Löscher W, Klitgaard H, Twyman RE, et al. New avenues for anti-epileptic drug discovery and development. *Nat Rev Drug Discov.* 2013;12(10):757–76.
- [12]Edfawy M, Hassan MH, Mansour A, et al. Meloxicam modulates oxidative stress status, inhibits prostaglandin E2, and abrogates apoptosis in carbon tetrachloride-induced rat hepatic injury. *Int J Toxicol.* 2012;31(3):276–86.
- [13]Darvishi H, Rezaei M, Khodayar MJ, et al. Differential effects of meloxicam on pentylentetrazole- and maximal electroshock-induced convulsions in mice. *Jundishapur J Nat Pharm Prod.* 2017;12(2). e.36412.
- [14]Hakan T, Toklu HZ, Biber N, et al. Effect of COX-2 inhibitor meloxicam against

- traumatic brain injury-induced biochemical, histopathological changes and blood-brain barrier permeability. *Neurol Res.* 2010;32(6):629–35.
- [15] Elgarhi R, Shehata MM, Abdelsameea AA, et al. Effects of Diclofenac Versus Meloxicam in Pentylentetrazol-Kindled Mice. *Neurochem Res.* 2020;45:1913–19.
- [16] Akkaya R, Karabulut S, Taskiran AS. Investigation of the effect of REM sleep deprivation on epileptic seizures caused by pentylentetrazole in mice. *Exp Biomed Res.* 2020;3(3):149–56.
- [17] Li B, Wang L, Sun Z, et al. The Anticonvulsant Effects of SR 57227 on Pentylentetrazole-Induced Seizure in Mice. *PLoS One.* 2014;9(4):93158.
- [18] Racine RJ. Modification of seizure activity by electrical stimulation. I. After-discharge threshold. *Electroencephalogr Clin Neurophysiol.* 1972;32(3):269-79.
- [19] Ernst O, Zor T. Linearization of the Bradford protein assay. *J Vis Exp.* 2010;(38):1918.
- [20] Yamagata K, Andreasson KI, Kaufmann WE, et al. Expression of a mitogen-inducible cyclooxygenase in brain neurons: Regulation by synaptic activity and glucocorticoids. *Neuron.* 1993;11(2):371–86.
- [21] Melnikova T, Savonenko A, Wang Q, et al. Cyclooxygenase-2 activity promotes cognitive deficits but not increased amyloid burden in a model of Alzheimer's disease in a sex-dimorphic pattern. *Neuroscience.* 2006;141(3):1149-62.
- [22] Cernak I, O'Connor C, Vink R. Activation of cyclo-oxygenase-2 contributes to motor and cognitive dysfunction following diffuse traumatic brain injury in rats. *Clin Exp Pharmacol Physiol.* 2001;28(11):922-25.
- [23] Nakayama M, Uchimura K, Zhu RL, et al. Cyclooxygenase-2 inhibition prevents delayed death of CA1 hippocampal neurons following global ischemia. *Proc Natl Acad Sci U. S. A.* 1998;95(18):10954–59.
- [24] Vezzani A, Granata T. Brain inflammation in epilepsy: Experimental and clinical evidence. *Epilepsia.* 2005;46(11):1724–43.
- [25] Akula KK, Dhir A, Kulkarni SK. Rofecoxib, a selective cyclooxygenase-2 (COX-2) inhibitor increases pentylentetrazol seizure threshold in mice: Possible involvement of adenosinergic mechanism. *Epilepsy Res.* 2008;78(1):60–70.
- [26] Oliveira MS, Furian AF, Royes LFF, et al. Cyclooxygenase-2/PGE2 pathway facilitates pentylentetrazol-induced seizures. *Epilepsy Res.* 2008;79(1):14–21.
- [27] Jeong KH, Kim JY, Choi YS, et al. Influence of aspirin on pilocarpine-induced epilepsy in mice. *Korean J Physiol Pharmacol.* 2013;17(1):15–21.
- [28] KunzNote T, Oliw EH. Nimesulide Aggravates Kainic Acid-Induced Seizures in the Rat. *Pharmacol Toxicol.* 2001;88(5):271–76.
- [29] Li HH, Lin PJ, Wang WH, et al. Treatment effects of the combination of ceftriaxone and valproic acid on neuronal and behavioural functions in a rat model of epilepsy. *Exp Physiol.* 2021;106(8):1814-28.
- [30] Montori S, Dos-Anjos S, Martínez-Villayandre B, et al. Age and meloxicam attenuate the ischemia/reperfusion-induced down-regulation in the NMDA receptor genes. *Neurochem Int.* 2010;56(8):878–85.
- [31] Llorente IL, Burgin TC, Pérez-Rodríguez D, et al. Unfolded protein response to global ischemia following 48 h of reperfusion in the rat brain: The effect of age and meloxicam. *J Neurochem.* 2013;127(5):701–10.
- [32] Montori S, Dosanjós S, Ríos-Granja MA, et al. AMPA receptor downregulation induced by ischaemia/reperfusion is attenuated by

age and blocked by meloxicam. *Neuropathol. Appl Neurobiol.* 2010;36(5):436–47.

[33] Lin TY, Lu CW, Wang CC, et al. Cyclooxygenase 2 inhibitor celecoxib inhibits glutamate release by attenuating the PGE2/EP2 pathway in rat cerebral cortex endings. *J Pharmacol Exp Ther.* 2014;351(1):134–45.

[34] Dhir A, Naidu PS, Kulkarni SK. Effect of naproxen, a non-selective cyclo-oxygenase inhibitor, on pentylenetetrazol-induced kindling in mice. *Clin Exp Pharmacol Physiol.* 2005;32(7):574–84.

[35] Zhang HJ, Sun RP, Lei GF, et al. Cyclooxygenase-2 inhibitor inhibits hippocampal synaptic reorganization in pilocarpine-induced status epilepticus rats. *J Zhejiang Univ Sci B.* 2008;9(11):903–915.

The variation of 5'-carboxycytosine localization within the nucleus of normal and cancerous cells

Selcen Celik Uzuner 

Department of Molecular Biology and Genetics, Faculty of Science, Karadeniz Technical University, Trabzon, Turkey

ABSTRACT

Aim: Cytosine modifications are the common epigenetic marks during cellular processes. The pattern of cytosine modifications varies depending on the tissues and the developmental stages. The interactions within the epigenome are complex, and co-existence of cytosine modifications provides understanding on their collaborative or distinct functions. This study aims to disclose the intra-nuclear co-location of 5'-carboxycytosine with other modified cytosine bases in normal and cancerous cells.

Methods: Co-localization patterns were assessed using an immunostaining protocol enhanced with enzyme treatments, and microscope images were analyzed using Image J co-localization plug in.

Results: Findings showed that most of 5'-carboxycytosine is associated with oxidized forms of 5'-methylcytosine; however, some extent of individual localization was detected following different antigen retrievals.

Conclusion: These suggest that antigenicity reveals variation in the detection of the co-existence of cytosine modifications. The spatial organization of chromatin may be expected to affect this variation and it needs further investigation.

Key words: Epigenetics, cytosine modifications, immunofluorescence, co-localization, cancer.

✉ Selcen Celik Uzuner

Department of Molecular Biology and Genetics, Faculty of Science, Karadeniz Technical University, Trabzon, Turkey

E-mail: selcen.celik@ktu.edu.tr

Received: 2021-07-10 / Revisions: 2021-10-19

Accepted: 2021-10-24 / Published online: 2022-01-01

Introduction

Epigenetic mechanisms are involved in the regulation of gene expression. The mechanisms include reversible chemical modifications of histone proteins and DNA. DNA methylation occurring on cytosine bases (5'-methylcytosine, 5mC or 5mC) is a well-described modification. DNA methylation has been shown to be associated with gene regulation in development and alterations in its pattern were

found in different diseases, such cancer and neurodegenerative diseases [1-3]. The pattern of epigenetic mechanisms is highly dynamic depending on the cellular processes. For instance, methyl groups have been supposed to be removed from methylated cytosines during the preparations for DNA repair machinery, and the methylation mark has been erased gradually by the conversion of methyl to other chemical groups, such hydroxyl and formyl [4, 5]. These oxidized forms of cytosine methylation including hydroxymethylation (5hmC), formylation (5fC) and carboxylation (5caC) catalyzed by Ten-Eleven-Translocation (TET) enzymes, are supposed to be intermediates of active demethylation process in particular during DNA repair [6-8]. Additionally, there is

an increasing evidence revealing the potential function of these modifications in the regulation of gene expression as well [9-11]. The patterns of cytosine modifications have been found to change in tissue-specific manner and also during different steps of development [12-18]. The findings that show the patterns of cytosine modifications are likely associated with disease progresses support their biological significance.

Immunofluorescence is a powerful tool to reveal both quantitative and qualitative profile of cytosine modifications. The spatial organization of modifications within the nuclei can be assessed, and co-existence patterns of modifications are also evaluated by fluorescence-based microscopies. This provides understanding whether there are complex interactions between modifications suggesting their co-function during cellular processes. This study aimed to reveal the co-localization of 5'-carboxycytosine (5caC) with 5meC, 5hmC and 5fC in cancer and normal cells using the newly developed immunofluorescence protocol with different antigen retrieval approaches. Antigen retrieval is one of the most important steps in immunostaining of DNA epitopes as it utilizes the accessibility of DNA epitopes (*i.e.* cytosine modifications) to be labelled by the specific antibodies. The usual application for antigen retrieval is acid treatment; however previous studies showed that acid treatment alone did not unmask some extent of methylated cytosines and also other modifications from protein content [19-22]. The protocol was enhanced with the additional use of trypsin and pepsin enzymes that have different proteolytic activities [19, 20]. The sequential treatment of cells with acid, trypsin and pepsin revealed increased amounts of staining in each modification. But amount of the epigenetic

marks is not the only parameter that is supposed to be altered after methodological improvements. This study aims to disclose the intra-nuclear co-location of 5'-carboxycytosine with other modified cytosine bases in normal and cancerous cells. In this study, the new immunostaining protocol further showed that a majority of 5caC (more than 70%) was co-localized with 5meC, 5hmC or 5fC in the cells. But antigen retrievals with additional enzyme treatments provided a significant amount of 5caC that independently localized from cytosine methylation in normal cells. The co-existence pattern of 5caC with 5fC was not affected using acid and/or enzymes in normal cells, whereas it was significantly changed after the treatments with enzymes in both cancer cells. Therefore, 5caC's localization within the nucleus highly depends on solvent-exposure of regions of carboxymethylated cytosines in cells, and the detection of immune-localization of DNA modifications is highly associated with three-dimensional structure of chromatin-DNA complex that is organized within the chromatin layers with different response to enzymatic reactions. These findings suggest that classical immunofluorescence protocol with acid use alone can likely overestimate the co-localization of 5caC with other cytosine modifications depending on the cell type. Therefore, technical limitation can prevent the detection of 5caC that is separately located within the cell nucleus.

Materials and methods

Cell culture

CF-1 embryonic fibroblasts (American Type Cell Collection ATCC, Cat No SCRC-1040, VA, US), AR42J pancreatic cancer cells (ATCC, Cat No CRL-1492) and HeLa cervical cancer cells (ATCC, Cat No CCL-2) were used. Cells were cultured in DMEM (Wisent Inc., Cat

No 319-005-CL, Quebec, Canada), RPMI (Wisent, Cat No 350-000-CL) or in EMEM (Wisent, Cat No 320-026-CL), respectively. Complete media included 10% of foetal bovine serum (FBS) (Capricorn Scientific GmbH, Cat No FBS11-A, Ebsdorfergrund, Germany) and 1% streptomycin-penicillin (Wisent, Cat No 450-201-EL), and cells were cultured in chamber slides (Ibidi GmbH, Cat No 81201, Martinsried, Germany) at 37°C with 5% CO₂.

Immunostaining protocol

Cells were fixed and stained as described previously [20]. The protocol briefly included permeabilization of fixed cells, antigen retrieval, and incubations with primary and secondary antibodies. Antigen retrieval (AR) process included 4N hydrochloric acid (Merck KGaA, Cat No 100319, Darmstadt, Germany) alone or 0.25% trypsin-EDTA (Wisent, Cat No 325-043-EL) after acid or acid followed by 0.25% trypsin-EDTA and pepsin (Sigma Aldrich Co., Cat No P7000, St. Louis, USA). Acid was treated for 10 min at room temperature (RT), and enzymes were treated for 1 min at 37°C. Pepsin concentrations used were 0.1 mg/ml, 0.5 mg/ml or 1 mg/ml as these conditions were defined for each cell in the previous study [20]. The applied pepsin conditions for AR step are summarized in Table 1.

Table 1. Pepsin concentrations applied after acid and trypsin for each co-localization in cells.

Cell	Co-localization		
	5caC and 5meC (mg/ml)	5caC and 5hmC (mg/ml)	5caC and 5fC (mg/ml)
CF-1	0.1	0.1	1
AR42J	0.1	0.1	0.1
HeLa	N/A	1	1

After pepsin treatment, cells were washed with 1xPBS (phosphate-buffered saline) (Biomatik, Cat No A3602, Ontario, Canada) for 3 times. Cells were blocked with 50 % goat serum at 4°C overnight followed by the treatment with primary antibodies for 1) anti-5meC (mouse anti-5meC; Active Motif Inc. Cat No 39649, Carlsbad, CA) at 1:400 for 1 h at RT, 2) anti-5hmC (rabbit anti-5hmC; Active Motif Cat No 39791) at 1:1000 overnight at 4°C, 3) anti-5fC (rabbit anti-5fC; Active Motif Cat No 61223) at 1:1000 overnight at 4°C and/or 4) anti-5caC (rabbit anti-5caC; Active Motif Cat No 61225) at 1:1000 overnight at 4°C. Primary antibodies were washed with 1xPBS followed by incubations with secondary antibodies (Alexa 488 mouse Abcam Cat No Ab150113, Cambridge, UK, Alexa 488 rabbit Abcam Cat No Ab150077 or Texas Red rabbit Abcam Cat No Ab6719). Secondary antibody conditions for each primary antibody were 1) 1 h at RT, 2) 1:1000 for 1 h at RT, 3) 1:1000 for 2 h at RT, and 4) 1:1000 4°C overnight, respectively. Cytosine methylation was also co-stained with MBD1 protein (methyl-binding protein-1) in mouse embryonic fibroblasts or with mitochondria in MDA-MB-231 cell line (ATCC, Cat No HTB-26). Anti-MBD1 antibody was purchased from Abcam (Cat No ab3753) and incubated at 4°C overnight after the treatment with anti-5meC antibody. MitoTracker Red CMXRos was purchased from ThermoFisher Scientific (Massachusetts, USA, Cat No M7512) and used at 400nM within the culture media for 45 min at 37°C. Cells then were fixed with 4% paraformaldehyde (w/v) (ChemSolute, Th. Geyer GmbH & Co., Cat No 8416-0500, and Germany) for half an hour at room temperature (RT), and visualized under the microscope. Non-immune IgG antibodies for rabbit (Abcam, Cat No ab172730) and mouse (Sigma,

Cat No I8765) were used to show negative staining. Representative green and red channel images after treatment with non-immune IgG are shown in Figure 1.

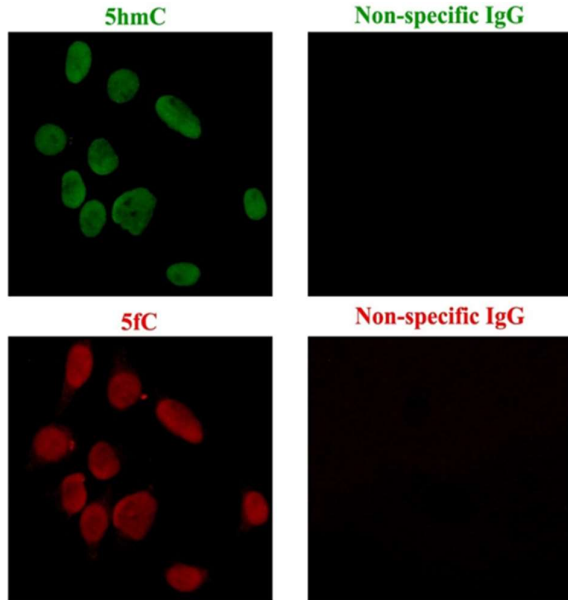


Figure 1. Representative non-specific IgG staining in parallel with 5hmC and 5fC staining in HeLa cells. Non-specific (non-immune IgG) treatment did not reveal any detectable staining both in green and red channels. Non-specific IgG control staining was included in each immunostaining in this study (not all data shown).

Co-localization analysis

Stained cells were visualized using a 40x objective of the inverted fluorescence microscope (AxioVert A1, Carl Zeiss, and Germany). Images were taken for both green and red filters. Images from both channels were analyzed using co-localization plug-in of Image J software (NIH, US). The steps for co-localization analysis briefly include i) subtraction of background, ii) conversion of both images to 8-bit grey scale, and iii) calculation of Mander's overlap coefficient using co-localization plug-in [23]. Co-existence of modifications was represented by Pearson's correlation coefficient, Mander's correlation

(overlap) coefficient, M1 and M2 values. Pearson's correlation coefficient represents the correlation between the intensities of two signals (green and red in this study), and this is a value between -1 (negative correlation) and +1 (positive correlation). Mander's correlation coefficient indicates the co-localization level of two signals within the nuclei and this parameter is between 0 and 1. Values close to 1 indicate high co-localization. M1 and M2 values represent split-coefficients for red and green channels, respectively.

Statistical analysis

Statistical comparisons for co-localization coefficients, M1 and M2 values were performed using UNIANOVA (univariate analysis of variance) of SPSS software (Version 23). Significance levels used were $p < 0.05$ (*), $p < 0.01$ (**), $p < 0.001$ (***) and $p < 0.0001$ (****). Each experiment was performed as triplicates and standard errors of the mean (\pm s.e.m) were used to evaluate deviation of the calculations between independent repeats.

Results

Evaluation of co-localization of different epitopes

First of all, co-localization profiles were examined using nuclear (including 5meC, 5hmC, MBD1-methyl-binding protein 1) and/or extra-nuclear epitopes (a marker for mitochondria) in different cell lines to interpret the relationship between the co-localization coefficient values, the co-localization plot pattern and the actual co-staining. The representative co-localization patterns show co-localization plots of red (channel 1, X axes of co-localization plot) and green (channel 2, Y axes of co-localization plot) channels with co-localization coefficients from high to low (from up to down) (Figure 2A-F) and microscopy

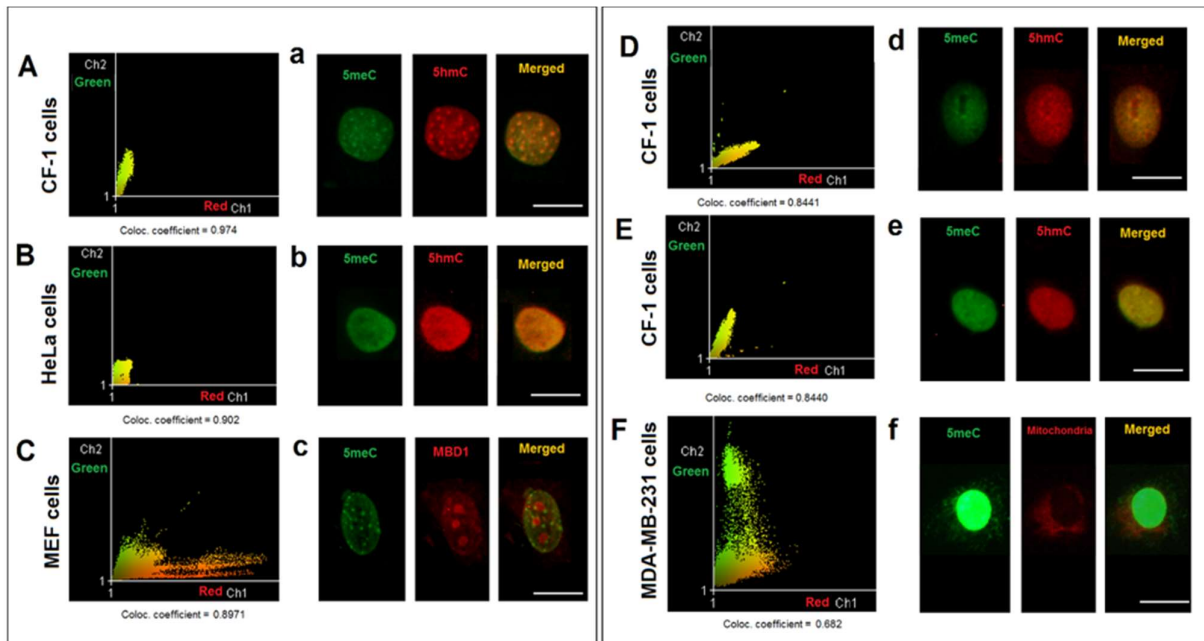


Figure 2. Examples of co-localisation profiles of two epitopes in different cell lines. **A, B, C, D, E** and **F** show the representative co-localisation plots for correlation coefficients from high to low, respectively. **a, b, c, d, e** and **f** show the representative microscopy images of individual and merged staining for **A, B, C, D, E** and **F**, respectively. **A (a), D (d)** and **E (e)** show 5meC-5hmC co-staining in CF-1 cells, **B (b)** show 5meC-5hmC co-staining in HeLa cells, **C (c)** show 5meC-MBD1 co-staining in mouse embryonic fibroblasts (MEF), **F (f)** show 5meC-mitochondria co-staining in MDA-MB-231 cells. Scale bar is 10 micron.

images of nuclei at each channel together with the merged images for co-localization throughout the nucleus (Figure 2a-f). The close and high coefficient values (between 0.84 and 0.97) can indicate different co-localization than each other (Figure 2A-E). For instance, some of MBD1 protein localized as distinct large foci regions independently from DNA methylation (5meC) (Figure 2c) that was represented by a distinct population in red channel (Figure 2C). Similarly, some of 5meC existed within the small foci that were not co-localized with MBD1 (Figure 2c). But the general co-localization value of those two markers is around 0.9. Another example includes co-staining of 5meC with a mitochondrial marker for membrane permeability (Figure 2F, f). A large population of 5meC within the cells was not associated with mitochondrial staining as represented by a distinct population in green channel; however, there was a small yellowish

region representing co-localization (Figure 2F). Co-localization coefficient of 5meC and mitochondria was around 0.7. The representatives suggest that the distribution of the existence of two markers within the plots can vary even if co-localization coefficients were close to each other. Besides, the plots and coefficients should be evaluated together with merged images to conclude about the co-existence profiles.

Co-localization of 5caC and 5meC

The majority of 5-carboxycytosine was found to be co-localized with DNA methylation (5meC) in both CF-1 and AR42J cells (Figure 3). In CF-1 normal fibroblast cells, the co-existence of 5caC and 5meC was decreased after enzyme use ($p < 0.001$) in the antigen retrieval step (Figure 3A -C). This suggests that protein compounds which are acid-resistant but enzyme-sensitive can result in overestimation

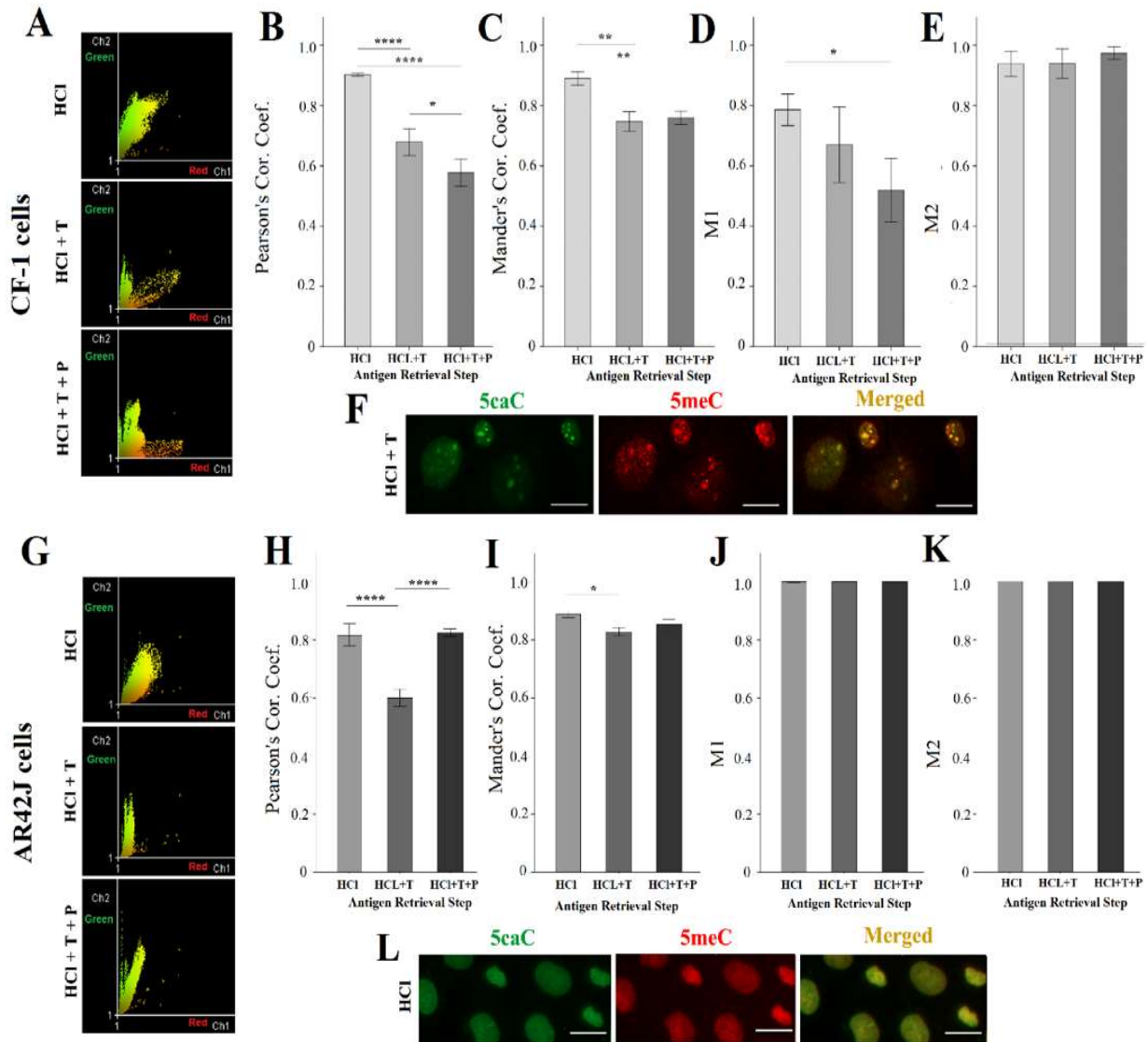


Figure 3. The co-localisation of 5caC and 5meC in CF-1 and AR42J cells. CF-1 cells (A-F) and AR42J (G-L) include co-localisation dot plots of 5caC (green) and 5meC (red) after acid alone (HCl), acid + trypsin (HCl + T) and acid + trypsin + pepsin (HCl + T + P) (A, G), bar graphs for the comparisons of Pearson's correlation coefficients (B, H), Mander's correlation coefficients (C, I), M1 values (D, J), M2 values (E, K) and representative microscopy images (F, L). Bar graphs show +/- standard error of the mean of independent triplicates. Scale bar is 10 micron. $p < 0.05$ (*), $p < 0.01$ (**) and $p < 0.0001$ (****)

of the co-localization degree of 5caC and 5meC. 68 % of 5meC was associated with 5caC and around 52 % of 5meC was significantly found to be independently from 5caC after sequential treatment of cells with acid, trypsin, and pepsin ($p < 0.05$) (Figure 3D). However almost 90% of 5caC was localized with methylated regions (Figure 3E), and this pattern was not affected by the choice of antigen

retrieval ($p > 0.05$). Both 5caC and 5meC existed within distinct focal regions within the nuclei, and many of foci were stained for both (Figure 3F). In AR42J cancer cells, the co-localization value of 5caC with 5meC was above 0.8 after HCl alone or followed by trypsin and pepsin (Figure 3G, H). However, only trypsin treatment after acid resulted in a significant decrease in the detection of co-localized 5meC

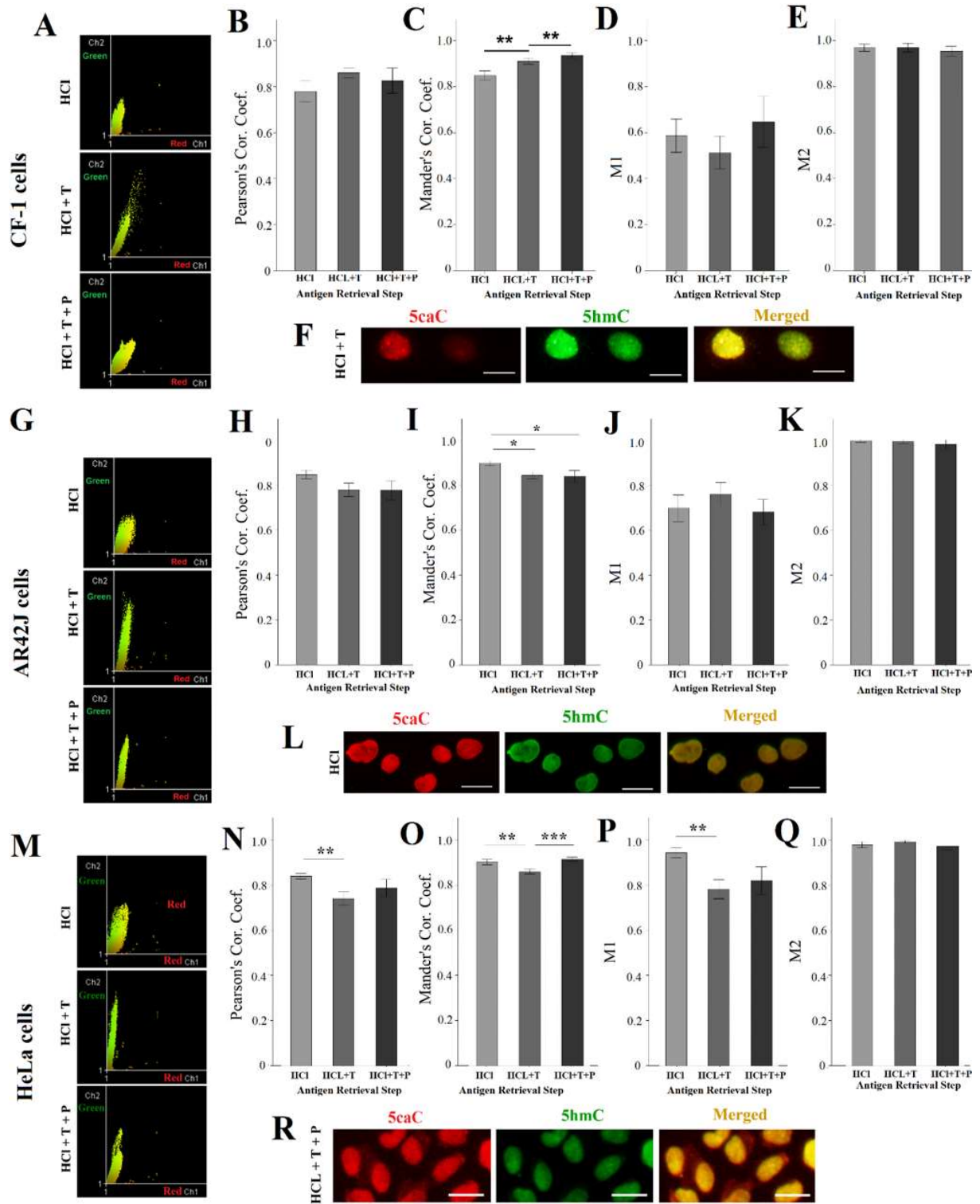


Figure 4. The co-localisation of 5caC and 5hmC in CF-1, AR42J and HeLa cells. CF-1 cells (A-F), AR42J (G-L) and HeLa cells (M-R) include co-localisation dot plots of 5caC (red) and 5hmC (green) after acid alone (HCl), acid + trypsin (HCl + T) and acid + trypsin + pepsin (HCl + T + P) (A, G, M), bar graphs for the comparisons Pearson's correlation coefficients (B, H, N), of Mander's correlation coefficients (C, I, O), M1 values (D, J, P), M2 values (E, K, Q) and representative microscopy images (F, L, R). Bar graphs show +/- standard error of the mean of independent triplicates. Scale bar is 10 micron. $p < 0.05$ (*), $p < 0.01$ (**)

and 5caC (Mander's correlation coefficient $p < 0.05$, Pearson's correlation coefficient $p < 0.0001$) (Figure 3H, I). Almost all 5meC's localization was associated with 5caC (Figure 3J), and all 5caC was co-localized with 5meC as well (Figure 3K). The use of enzymes did not result in a significant change in both M1 and M2 values ($p > 0.05$). Differentially from CF-1 cells, most of both 5meC and 5caC diffusely localized within the nucleus (Figure 3L).

Co-localization of 5caC and 5hmC

In CF-1 mouse embryonic fibroblasts, there was no difference in Pearson's correlation between 5caC and 5hmC, whereas analysis of Mander's correlation coefficient showed that co-localization values were high (more than 0.85) and enzyme use improved the detection of co-existence of 5caC with 5hmC ($p < 0.01$ for each) compared to acid treatment alone (Figure 4A,-C). However, antigen retrieval did not reveal a different pattern of M1 and M2 values (Figure 4D, E). Only half of the 5caC was co-localized with 5hmC (Figure 4D) but almost all 5hmC was found to be co-localized with 5caC (Figure 4E). 5caC and 5hmC were found within both diffuse and focal regions of nuclei (Figure 4F). In AR42J pancreatic cancer cells, Pearson's correlation was not different, Mander's co-localization values were more than 0.8, and each enzyme did reveal less co-localized pattern of 5caC and 5hmC ($p < 0.05$ for each) (Figure 4G-I). But enzymes did not significantly affect M1 and M2 values as around 70% of 5caC were co-localized with 5hmC throughout the nucleus (Figure 4J). Almost all 5hmC (99%) was found together with 5caC (Figure 4K). Differentially from CF-1 cells, both modifications existed within the nucleus as diffuse pattern (Figure 4L). In HeLa cells, trypsin treatment after acid resulted with a decrease in the detection of co-localization

($p < 0.01$ compared to acid alone, $p < 0.001$ compared to enhanced retrieval with pepsin) similar to Pearson's correlation coefficient, but all applications for antigen retrieval indicate that the co-localization degree for 5caC and 5hmC was around 0.9 (Figure 4M-O). The M1 value was decreased after the additional treatment of acid with trypsin ($p < 0.01$) but pepsin after trypsin did not affect the detection ($p > 0.05$) (Figure 4P). In general, around 85% of 5caC was co-existed with 5hmC (Figure 4P), but almost all 5hmC (98%) was co-localized with 5caC in HeLa cells (Figure 4Q). Both 5caC and 5hmC were mostly organized as diffuse pattern in the nuclei regardless of the type of antigen retrieval used (Figure 4R).

Co-localisation of 5caC and 5fC

In CF-1 cells, 5caC and 5fC was highly co-localized (more than 0.9) regardless of the use of antigen retrieval (Figure 5A-C). Similarly, almost all 5caC within the nucleus were co-localized with 5fC (Figure 5D), however trypsin treatment revealed a significant amount of 5fC (approximately 20%) that was not co-localized with 5caC ($p < 0.05$ compared to acid alone, $p < 0.01$ compared to the additional treatment with pepsin) (Figure 5E). 5caC and 5fC were mostly diffuse within the nucleus but some were localized in distinct focal regions (Figure 5F). In AR42J cells, trypsin alone ($p < 0.0001$) and trypsin followed by pepsin ($p < 0.001$) revealed less co-localization of 5caC with 5fC, but the average value was around 0.85 (Mander's and Pearson's correlations were similar to each other) (Figure 5G-I). Half of 5caC was found to co-localized with 5fC after sequential treatment of cells with acid, trypsin and pepsin compared to acid alone ($p < 0.0001$) and with trypsin ($p < 0.0001$) (Figure 5J) whereas almost all 5fC was co-localized with 5caC after any antigen retrieval application

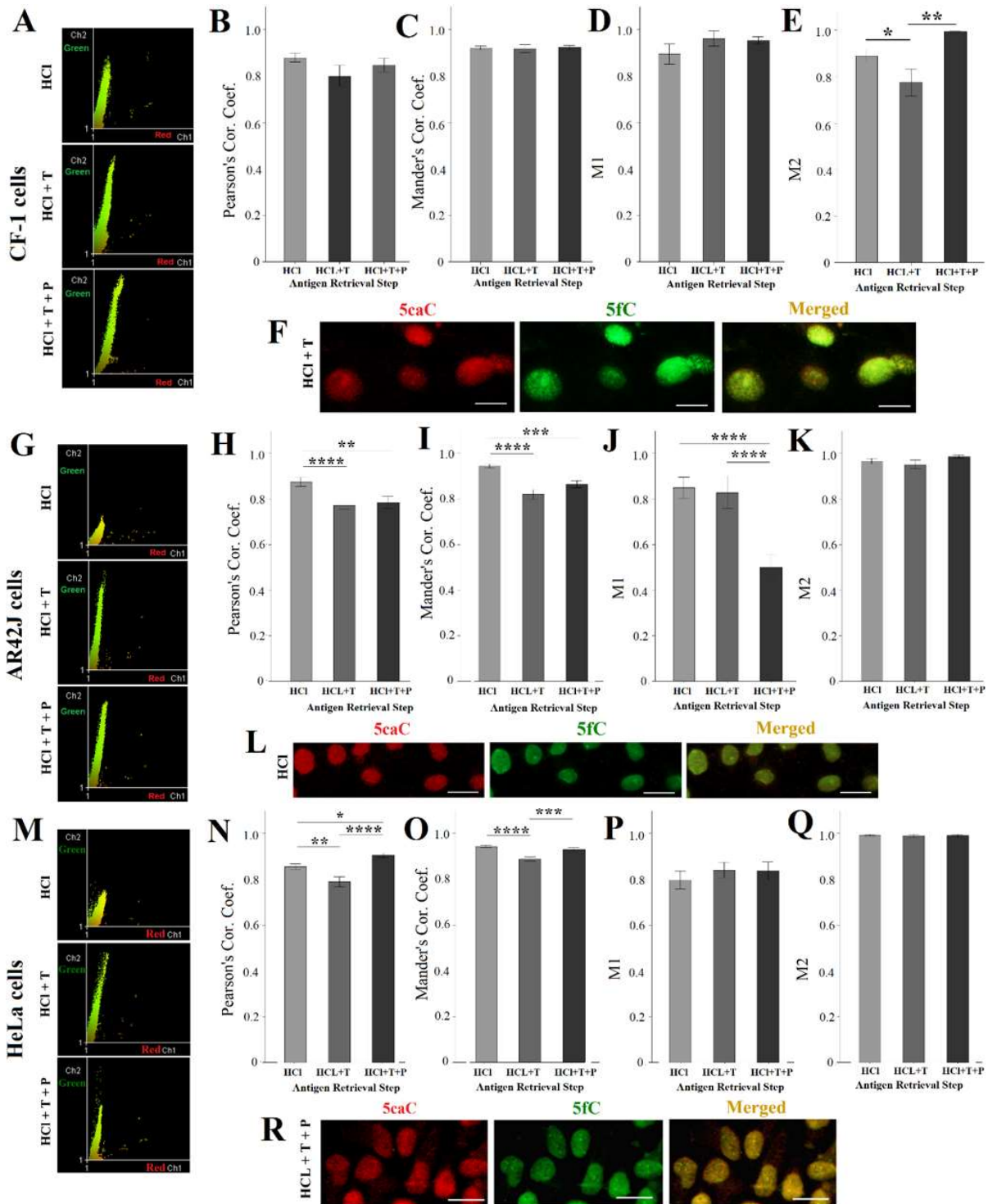


Figure 5. The co-localisation of 5caC and 5fC in CF-1, AR42J and HeLa cells. CF-1 cells (A-F), AR42J (G-L) and HeLa cells (M-R) include co-localisation dot plots of 5caC (red) and 5fC (green) after acid alone (HCl), acid + trypsin (HCl + T) and acid + trypsin + pepsin (HCl + T + P) (A, G, M), bar graphs for the comparisons of Pearson's correlation coefficients (B, H, N), Mander's correlation coefficients (C, I, O), M1 values (D, J, P), M2 values (E, K, Q) and representative microscopy images (F, L, R). Bar graphs show +/- standard error of the mean of independent triplicates. Scale bar is 10 micron. $p < 0.05$ (*), $p < 0.01$ (**), $p < 0.001$ (***) and $p < 0.0001$ (****).

(Figure 5K). 5caC was diffusely localized but 5fC showed few focal accumulations within the nucleus (Figure 5L). HeLa cells showed a similar co-localization pattern with AR42J cells as the use of trypsin significantly provided more independent localization of 5caC and 5fC from each other ($p < 0.0001$ compared to acid alone, $p < 0.001$ compared to acid, trypsin and pepsin) (Mander's and Pearson's correlations were similar to each other) (Figure 5M-O). Around 20% of 5caC was found to localize independent from 5fC (Figure 5P), but a negligible amount of 5fC (less than 1%) was independently localize from 5caC (Figure 5Q). Like the other cells, both modifications were mostly found in diffuse staining but some foci with 5fC accumulation were present within the nucleus (Figure 5R).

Discussion

This study attempted to understand the variety in the co-localization of 5'-carboxycytosine with 5'-methylcytosine and its other derivatives within the normal and cancer cells using a newly developed immunofluorescence protocol. Different antigenic retrieval methods were used to reveal whether there was diversity in the co-existence of cytosine modifications. Immunostaining is an advantageous method for *in situ* detection of DNA modifications; however, it has some technical limitations in terms of accessibility of DNA regions of interest. Antigen retrieval is a crucial step in immunostaining for DNA epitopes to remove protein content around DNA. The standard application for antigen retrieval of modified cytosines includes the treatment of permeabilized cells with hydrochloric acid (1-4N) [24-26]. Following acid treatment, the use of trypsin alone or its sequential use with pepsin were shown to enhance the staining level of cytosine modifications in normal and cancer

cells [20-22]. Trypsin and pepsin are proteolytic enzymes which hydrolyze hydrophilic and hydrophobic residues of proteins, respectively. These enzymes were used to target a diversity of proteins to be removed around DNA. Chromatin is a complex structure that composed of histones and DNA. DNA is also associated with non-histone proteins and this increases complexity of spatial organization of DNA and proteins. Epigenetic modifications can exist in euchromatic and heterochromatic regions, and this pattern is highly dynamic depending on the cell type and the cellular activities [27-35]. The intra-nuclear location of cytosine modifications therefore can be associated with their functions. The lack of complete antigen retrieval is problematic in immunostaining for understanding the locations within nuclear compartments as well as for measurement of the levels of modifications. Although there is no antigen retrieval strategy ensuring the complete binding of each antibody for cytosine modifications, enzyme treatments after acid that enhanced the detectable level of these as previously shown [20] did reveal the different patterns of co-localization in this study. The co-pattern of these modifications can suggest the associative function of modifications or distinct localization can indicate specific function of modifications depending on cell type or/and under specific conditions within the cells. However, the limitations of the study include the necessity for the higher resolution for visualization through confocal microscopy. The staining pattern of cytosine modifications can vary in cells and also in developmental stages. In this study, 5caC is co-localized with 5meC, 5hmC or 5fC at around 76-92 % range in the cells experienced (Table 2). Most of 5caC was found to co-exist with 5hmC in differentiated liver cells whereas it showed

Table 2. Summarised comparison of co-localisation of 5caC with 5meC, 5hmC and 5fC in different cells after various antigen retrieval

CELLS	Co-localisation with 5meC		Co-localisation with 5hmC		Co-localisation with 5fC	
	Mander's coefficient	P	Mander's coefficient	P	Mander's coefficient	P
CF-1	HCl - 0.90 ± 0.022 T - 0.68 ± 0.120 P - 0.58 ± 0.140	HCl vs T (↓) <i>p</i> <0.01 HCl vs P (↓) <i>p</i> <0.01	HCl - 0.85 ± 0.080 T - 0.91 ± 0.060 P - 0.93 ± 0.030	HCl vs T (↑) <i>p</i> <0.01 T vs P (↑) <i>p</i> <0.01	HCl - 0.92 ± 0.036 T - 0.92 ± 0.050 P - 0.92 ± 0.023	<i>p</i> >0.05
	Ave: 0.76 ± 0.170		Ave: 0.89 ± 0.070		Ave: 0.92 ± 0.070	
AR42J	HCl - 0.89 ± 0.042 T - 0.83 ± 0.041 P - 0.85 ± 0.073	HCl vs T (↓) <i>p</i> <0.05	HCl - 0.90 ± 0.044 T - 0.84 ± 0.060 P - 0.84 ± 0.080	HCl vs T (↓) <i>p</i> <0.05 HCl vs P (↓) <i>p</i> <0.05	HCl - 0.94 ± 0.040 T - 0.82 ± 0.080 P - 0.86 ± 0.050	HCl vs T (↓) <i>p</i> <0.0001 HCl vs P (↓) <i>p</i> <0.001
	Ave: 0.86 ± 0.06		Ave: 0.86 ± 0.06		Ave: 0.88 ± 0.080	
HeLa	N/A		HCl - 0.90 ± 0.048 T - 0.86 ± 0.044 P - 0.91 ± 0.330	HCl vs T (↓) <i>p</i> <0.01 T vs P (↑) <i>p</i> <0.0001	HCl - 0.95 ± 0.018 T - 0.89 ± 0.036 P - 0.93 ± 0.036	HCl vs T (↓) <i>p</i> <0.0001 T vs P (↑) <i>p</i> <0.001
			Ave: 0.88 ± 0.050		Ave: 0.92 ± 0.040	

HCl: hydrochloric acid, T: trypsin, P: pepsin, Ave: average, ↓ decrease, ↑ increase

distinct location in hepatic progenitor cells [36]. However, in embryonic stem cells 5caC was tend to co-localize with 5hmC more than with 5meC [37]. The level of co-existence decreased with brain development in the mouse [37]. 5caC and 5fC are mostly considered as temporary and unstable modifications of cytosines during stem cell development, but 5hmC is thought to be more persistent mark throughout the nucleus [37-39]. The amounts of 5caC, 5fC and 5hmC were shown to gradually decrease by each DNA replication in mouse embryos before implantation [17, 38]. Apart from the normal development process, the pattern of cytosine modifications has been also shown to be altered in cancer cells. In brain tumor cells, both 5hmC and 5caC were detected at significant levels and those were also co-localized within the nucleus, whereas HeLa cells were shown to not to have detectable 5caC signal [40] suggesting that 5hmC and 5caC can be the epigenetic hallmarks of tumors specifically developed from neural stem cells. However, this study used only standard acid treatment for antigenic retrieval of both markers. Additional enzyme treatments could enhance the staining performance. The amount of 5caC in HeLa cells was detectable

after any of antigen retrieval [20], and the present study also confirms the presence of 5caC in HeLa cells. Trypsin did reveal more content of 5caC independently localized from 5hmC and 5fC in these cells (represented by decreased Mander's co-localization coefficients). In both HeLa and AR42J cells, the detectable pattern of co-existence of 5caC and 5fC was significantly changed after the treatments with enzymes (Table 2). A decrease in the co-localization of 5caC with 5meC was detected in normal cells after enzyme treatments compared to AR42J cancer cells. In contrast, 5caC's co-localization with 5fC was not affected by the use of different antigen retrievals in normal fibroblasts. However, pepsin treatment provided almost 40 % of independent 5caC location from 5meC in CF-1 normal fibroblast cells. Therefore, 5caC's localization within the nucleus highly depends on solvent-exposure of carboxymethylated cytosines in normal cells suggesting its existence along different chromatin regions with different sensitivity against acid and/or enzymes (Table 2). These results can indicate that the detection of immune-localization of DNA modifications highly depends on three-

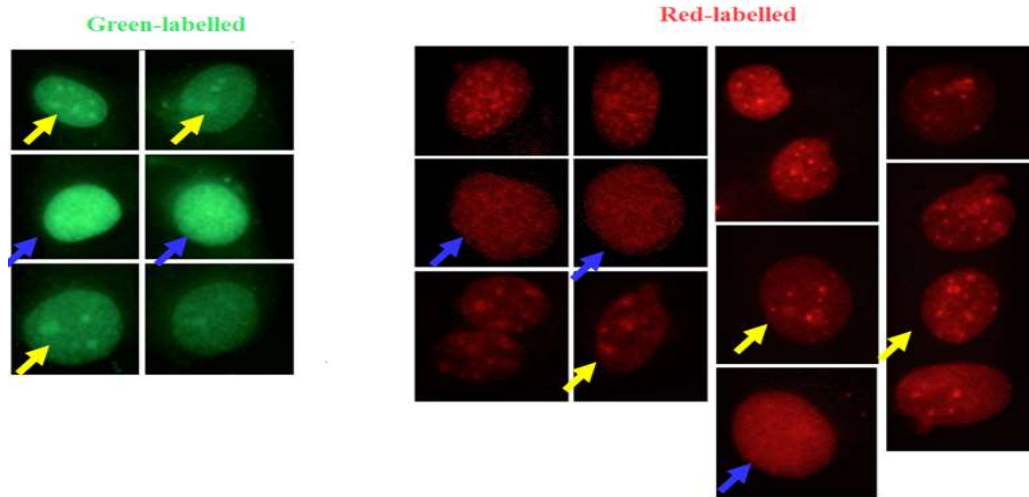


Figure 6. Staining pattern of 5caC after HCl and trypsin in CF-1 embryonic fibroblasts. CF-1 cells showed heterogeneity in 5caC staining as some cells had predominantly diffuse staining (blue arrows) but some had focal staining (yellow arrows).

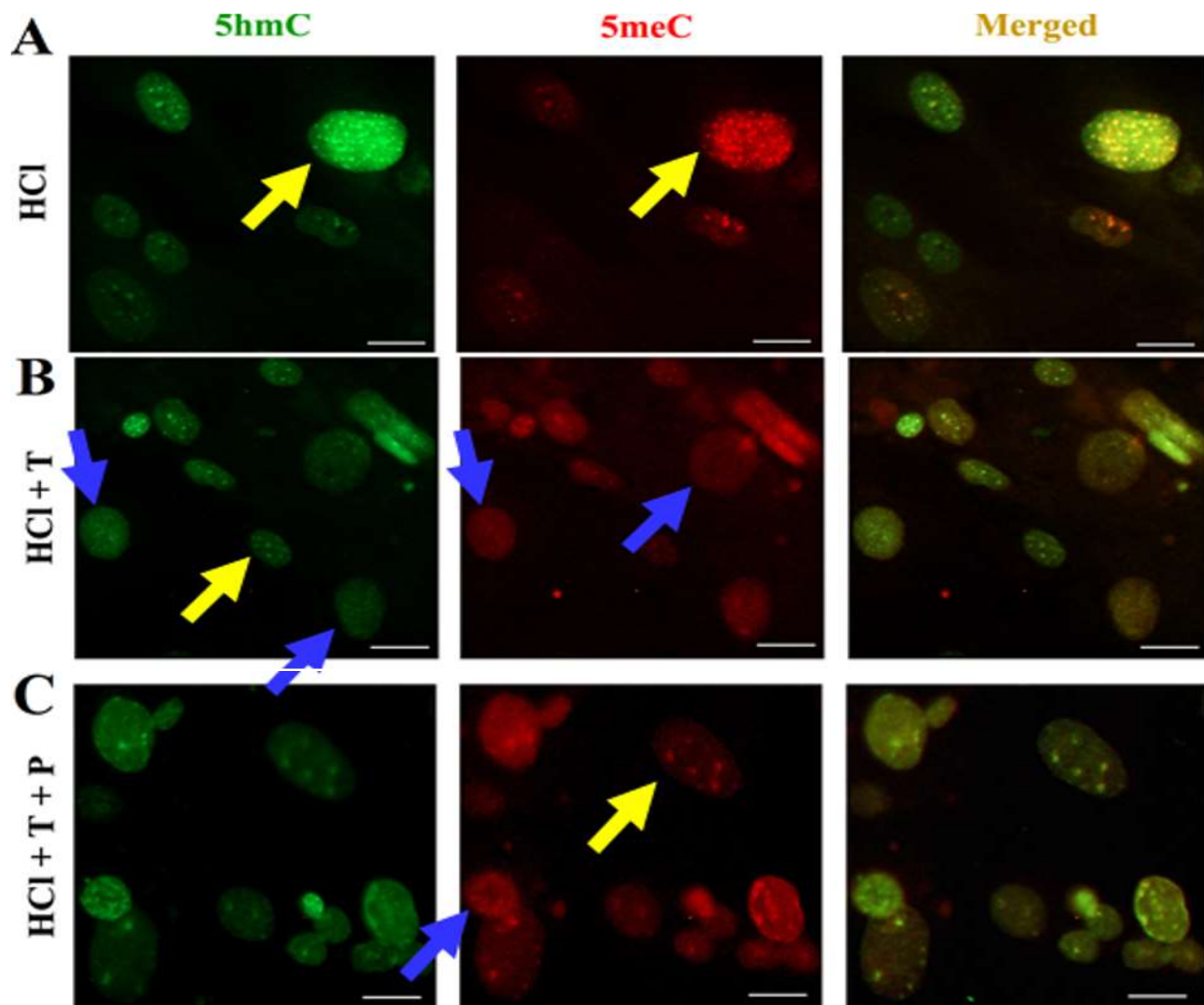


Figure 7. Staining pattern of 5meC and 5hmC in CF-1 cells after different antigen retrievals. CF-1 cells showed heterogeneity in 5meC and 5hmC staining as some cells had predominantly diffuse staining (blue arrows) but some had focal staining (yellow arrows).

dimensional structure of chromatin-DNA complex that is organized within the layers with different response to enzymatic reactions (Table 2). In general, compared to cancer cells, normal cells (mouse embryonic fibroblasts) showed more heterogeneity in terms of focal and/or diffuse staining of 5caC (Figure 6), 5hmC and 5meC (Figure 7).

Acknowledgements and Funding:

This study was supported by The Scientific and Technological Research Council of Turkey (TUBITAK) with the grant number 116Z733, and this study was also performed thanks to the equipment grant by Karadeniz Technical University (Grant Number: FAY-2015-141).

The author(s) received no financial support for the research, authorship, and/or publication of this article.

Conflict of Interest: *The authors declare that they have no conflict of interest.*

Ethical statement:

Ethics committee decision was not taken as it was a cell culture study.

Open Access Statement

This is an open access journal which means that all content is freely available without charge to the user or his/her institution under the terms of the Creative Commons Attribution Non-Commercial License (<http://creativecommons.org/licenses/by-nc/4.0>). Users are allowed to read, download, copy, distribute, print, search, or link to the full texts of the articles, without asking prior permission from the publisher or the author.

Copyright (c) 2021: Author (s).

References

- [1]Pihlstrom L, Berge V, Rengmark A, et al. Parkinson's Disease Correlates With Promoter Methylation in the alpha-Synuclein Gene. *Mov Disord.* 2015; 30(4): 577-80.
- [2]Ibn Sina A, Carrascosa L, Liang Z, et al. Epigenetically reprogrammed methylation landscape drives the DNA self-assembly and serves as a universal cancer biomarker. *Nat Com.* 2018;9(1):4915.
- [3]Tang X, Ruan S, Tang Q, et al. DNA methylation profiles in the hippocampus of an Alzheimer's disease mouse model at mid-stage neurodegeneration. *Int J Clin Exp Med.* 2018; 11(11): 11876-88.
- [4]Wu X, and Y Zhang, TET-mediated active DNA demethylation: mechanism, function and beyond. *Nat Rev Genet.* 2017; 18(9): 517-34.
- [5]Sadakierska-Chudy A, Kostrzewa RM, Filip M. A comprehensive view of the epigenetic landscape part I: DNA methylation, passive and active DNA demethylation pathways and histone variants. *Neurotox Res.* 2015;27(1):84-97.
- [6]He YF, Li BZ, Li Z, et al. Tet-Mediated Formation of 5-Carboxylcytosine and Its Excision by TDG in Mammalian DNA. *Science.* 2011; 333(6047): 1303-1307.
- [7]Cortellino S, Xu J, Sannai M, et al. Thymine DNA Glycosylase Is Essential for Active DNA Demethylation by Linked Deamination-Base Excision Repair. *Cell.* 2011;146(1): 67-79.
- [8]Ito S, Shen L, Dai Q, et al. Tet Proteins Can Convert 5-Methylcytosine to 5-Formylcytosine and 5-Carboxylcytosine. *Science.* 2011; 333(6047): 1300-1303.
- [9]Wu H, D'alessio AC, Ito S, et al. Genome-wide analysis of 5-hydroxymethylcytosine distribution reveals its dual function in transcriptional regulation in mouse embryonic stem cells. *Genes Dev.* 2011;25(7): 679-84.

- [10] Stroud H, Feng S, Kinney SM, et al. 5-Hydroxymethylcytosine is associated with enhancers and gene bodies in human embryonic stem cells. *Genome Biol.* 2011;12(6):R54.
- [11] Iurlaro M, Ficiz G, Oxley D, et al. A screen for hydroxymethylcytosine and formylcytosine binding proteins suggests functions in transcription and chromatin regulation. *Genome Biol.* 2013; 14(10):R119.
- [12] Tao H, Xie P, Cao Y, et al. The Dynamic DNA Demethylation during Postnatal Neuronal Development and Neural Stem Cell Differentiation. *Stem Cells Int.* 2018; 2018: 2186301.
- [13] Chamberlain A, Lin M, Lister RL, et al. DNA Methylation is Developmentally Regulated for Genes Essential for Cardiogenesis. *J Am Heart Assoc.* 2014; 19(3): e000976.
- [14] Szulwach K, Li X, Li Y, et al. 5-hmC-mediated epigenetic dynamics during postnatal neurodevelopment and aging. *Nat Neurosci.* 2011; 14(12): 1607-16.
- [15] Ruzov A, Tsenkina Y, Serio A, et al. Lineage-specific distribution of high levels of genomic 5-hydroxymethylcytosine in mammalian development. *Cell Res.* 2011; 21(9): 1332-42.
- [16] Niles K, Chan D, La Selle S, et al. Critical Period of Nonpromoter DNA Methylation Acquisition during Prenatal Male Germ Cell Development. *PloS One.* 2011; 6(9): e24156.
- [17] Inoue A, Shen L, Dai Q, et al. Generation and replication-dependent dilution of 5fC and 5caC during mouse preimplantation development. *Cell Res.* 2011;21(12):1670-76.
- [18] Kinney SM, Chin HG, Vaisvila R, et al. Tissue-specific Distribution and Dynamic Changes of 5-Hydroxymethylcytosine in Mammalian Genomes. *J Biol Chem.* 2011; 286(28): 24685-93.
- [19] Celik S, Y Li, O'Neill C. The Exit of Mouse Embryonic Fibroblasts from the Cell-Cycle Changes the Nature of Solvent Exposure of the 5'-Methylcytosine Epitope within Chromatin. *PloS One.* 2014; 9(4): e92523.
- [20] Celik-Uzuner S. Enhanced immunological detection of epigenetic modifications of DNA in healthy and cancerous cells by fluorescence microscopy. *Microsc Res and Tech.* 2019; 82(11):1962-72
- [21] Li Y, O'Neill C. Persistence of Cytosine Methylation of DNA following Fertilisation in the Mouse. *PloS One.* 2012; 7(1): e30687.
- [22] Li Y, and O'Neill C, 5'-methylcytosine and 5'-hydroxymethylcytosine Each Provide Epigenetic Information to the Mouse Zygote. *PloS One,* 2013; 8(5): e63689.
- [23] Zinchuk V, Zinchuk O, and Okada T, Quantitative colocalization analysis of multicolor confocal immunofluorescence microscopy images: Pushing pixels to explore biological phenomena. *Acta Histochem Cytochem.* 2007; 40(4): 101-11.
- [24] Ballestar E, Paz MF, Valle L, et al. Methyl-CpG binding proteins identify novel sites of epigenetic inactivation in human cancer. *EMBO J.* 2003; 22(23): 6335-45.
- [25] Globisch D, Münzel M, Müller M, et al. Tissue Distribution of 5-Hydroxymethylcytosine and Search for Active Demethylation Intermediates. *PloS One,* 2010; 5(12): e15367.
- [26] Lian CG, Xu Y, Ceol C, et al. Loss of 5-Hydroxymethylcytosine Is an Epigenetic Hallmark of Melanoma. *Cell.* 2012; 150(6): 1135-46.
- [27] Alioui A, Wheldon LM, Abakir A, et al. 5-Carboxylcytosine is localized to euchromatic regions in the nuclei of

- follicular cells in axolotl ovary. *Nucleus*. 2012; 3(6): 565-69.
- [28] Cowell I, Papageorgiou N, Padget K, et al. Histone deacetylase inhibition redistributes topoisomerase II β from heterochromatin to euchromatin. *Nucleus*. 2011; 2(1): 61-71.
- [29] Kang YK, Koo DB, Park JS, et al. Differential inheritance modes of DNA methylation between euchromatic and heterochromatic DNA sequences in ageing fetal bovine fibroblasts. *FEBS Lett*. 2001;498(1):1-5.
- [30] Kubiura M, Okano M, Kimura H, et al. Chromosome-wide regulation of euchromatin-specific 5mC to 5hmC conversion in mouse ES cells and female human somatic cells. *Chromosome Res*. 2012;20(7):837-48.
- [31] Papazvan R, Voronina E, Chapman JR, et al. Methylation of histone H3 at lysine 23 in meiotic heterochromatin. *Epigenetics Chromatin*. 2013; 6 (Suppl 1)(O13).
- [32] Wen B, Wu H, Loh YH, et al. Euchromatin islands in large heterochromatin domains are enriched for CTCF binding and differentially DNA-methylated regions. *BMC Genom*. 2012; 13:566.
- [33] Wongtawan T, Taylor JE, Lawson KA, et al. Histone H4K20me3 and HP1 alpha are late heterochromatin markers in development, but present in undifferentiated embryonic stem cells. *J Cell Sci*. 2011; 124(11): 1878-90.
- [34] Chantalat S, Depaux A, Hery P, et al. Histone H3 trimethylation at lysine 36 is associated with constitutive and facultative heterochromatin. *Genome Res*. 2011;21(9):1426-37.
- [35] Bernstein E, Duncan EM, Masui O, et al. Mouse polycomb proteins bind differentially to methylated histone H3 and RNA and are enriched in facultative heterochromatin. *Mol Cell Biol*. 2006; 26(7): 2560-69.
- [36] Ramsawhook AH, Lewis LC, Eleftheriou M, et al. Immunostaining for DNA Modifications: Computational Analysis of Confocal Images. *J Vis Exp*. 2017;(127):56318.
- [37] Wheldon LM, Abakir A, Ferjentsik Z, et al. Transient Accumulation of 5-Carboxylcytosine Indicates Involvement of Active Demethylation in Lineage Specification of Neural Stem Cells. *Cell Rep*. 2014; 7(5): 1353-61.
- [38] Inoue A, and Zhang Y, Replication-Dependent Loss of 5-Hydroxymethylcytosine in Mouse Preimplantation Embryos. *Science*. 2011;334(6053):194.
- [39] Iqbal K, Jin SG, Pfeifer GP, et al. Reprogramming of the paternal genome upon fertilization involves genome-wide oxidation of 5-methylcytosine. *PNAS*. 2011; 108(9): 3642-47.
- [40] Ramsawhook A, Lewis L, Coyle B, et al. Medulloblastoma and ependymoma cells display increased levels of 5-carboxylcytosine and elevated TET1 expression. *Clin Epigenetics*. 2017; 9:18.
- [41] Drohat AC, and Coey CT. Role of Base Excision "Repair" Enzymes in Erasing Epigenetic Marks from DNA. *Chem Rev*. 2016; 116(20): 12711-29.
- [42] Santos F, Peat J, Burgess H, et al. Active demethylation in mouse zygotes involves cytosine deamination and base excision repair. *Epigenetics Chromatin*. 2013;6(1):39.

Histological changes in mice tissues induced by gold nanoparticles with different surface coatings and sizes

Ilyas Ozcicek,^{1,2} Nilufer Ulas Ayturk³, Nese Aysit^{1,2}

¹Department of Medical Biology, School of Medicine, Istanbul Medipol University, Istanbul, Turkey

²Health Science and Technologies Research Institute (SABITA), Istanbul Medipol University, Istanbul, Turkey

³Department of Histology and Embryology, Faculty of Medicine, Çanakkale Onsekiz Mart University, Çanakkale, Turkey

ABSTRACT

Aim: Gold nanoparticles (AuNPs) have many biomedical applications due to their unique properties (e.g., chemical stability, optical properties, biocompatibility, easy synthesizability, and multiple functionalizations). This study aimed to synthesize two highly monodispersed and stable AuNPs of different sizes (AuNP₂₀ and AuNP₅₀), modified with polyethyleneimine (PEI) and polyethylene glycol (PEG), and systematically investigate their toxicological effects on histological changes in the organs of BALB/c mice.

Methods: AuNPs (AuNP₂₀ and AuNP₅₀) were synthesized, and their surfaces were coated with PEI and PEG. All necessary characterizations were performed. After the application of two different doses of intravenous injections (IV) of the AuNPs (0.5 and 5 mg Au/kg), their toxicological effects and histological changes in the various mice organs (e.g., liver, spleen, kidney, brain) were evaluated with multiple parameters 48 h post injection. Fourteen days after a single high dose (5 mg Au/kg) IV injection of AuNPs, transmission electron microscopy (TEM) analysis was performed to reveal their ultrastructural effects in the liver of the mice.

Results: Stable and highly monodispersed AuNPs were synthesized successfully. Since the liver is the most critical organ in nanotoxicological evaluations, changes in the parameters of AuNPs were shown to have remarkable effects. Although there were no differences in the impact caused between the two AuNPs sizes, the microstructure of the liver tissue treated with AuNP nanoparticles with PEI or PEG coatings was similar to that observed in the control group. Microstructural histological changes in the other organs (e.g., brain, kidney, and spleen) were relatively less than those found in the liver. The PEI and PEG surface coatings generally increased the biocompatibility of the AuNPs. According to the TEM analysis data, apparent cellular changes were observed after a long exposure period in the AuNP groups without an additional surface coating. Although slight cellular alterations were observed in the AuNP groups coated with PEG and PEI, the morphology of the hepatocyte cells was generally healthy.

Conclusion: The surface coating of the AuNPs was a more decisive parameter than the size of the nanoparticles in terms of *in vivo* histological toxicity. The stability, biocompatibility, and surface coating of the AuNPs were critical parameters for potential nanotheranostic applications.

Key words: Gold nanoparticles, nanotoxicity, histopathology, polyethyleneimine, polyethylene glycol, surface functionalization, mice.

✉ Ilyas Ozcicek

Department of Medical Biology, School of Medicine,
Istanbul Medipol University, Istanbul, Turkey

Health Science and Technologies Research Institute
(SABITA), Istanbul Medipol University, Istanbul, Turkey

E- mail: iozcicek@medipol.edu.tr

ilyasozcicek@gmail.com

Received: 2021-08-05 / Revisions: 2021-11-04

Accepted: 2021-11-30 / Published online: 2022-01-01

Introduction

Gold nanoparticles (AuNPs) have many biomedical applications due to their unique chemical, physical, and optical properties [1]. Nanocarrier systems have many advantages, such as a large surface area, multiple functionalization, and small sizes [2]. Because of these superior features, AuNPs have been widely preferred in biomedical research recently, with applications that include detection [3], biosensors [4], bio-imaging [5], photothermal therapy [6], drug delivery [7], and DNA or RNA delivery [8, 9]. Also, to the beneficial effects of nanomaterials, there is a critical need to investigate the potentially toxic effects of AuNPs in biological environments. The synthesis method, size, surface functionalization, biological exposure time, and concentration of nanoparticles are fundamental parameters in nanotoxicological evaluations [10].

In some cellular biology studies in which AuNPs were used without additional surface coating, the researchers showed that the nanoparticles often accumulated in larger endosomes as aggregates. Although these particles have primarily been evaluated as biocompatible in terms of cellular toxicity, small ones have been reported to reduce cellular viability [11-13]. On the other hand, in some cellular biology studies in which PEG-modified AuNPs were used, the authors observed that the particles were localized in smaller endosomes, with consequent aggregation minimization and increased particle uptake [14-16]. Again, PEI modification of AuNPs has been shown to increase the stability, biocompatibility, and cellular uptake of nanoparticles [17]. Previously, some *in vivo* studies have been conducted to evaluate the toxicity and histological effects of various AuNPs. Researchers have reported that smaller

nanoparticles cause more *in vivo* toxic effects, such as the swelling of hepatocyte cells [18]. Different PEG-coated AuNPs have been shown to reduce toxicity and increase stabilization and circulation time in the blood [19]. However, further *in vivo* studies are needed to determine the histological effects of the different AuNPs and their role in nanotoxicity.

This study aimed to synthesize two highly monodispersed and stable AuNPs of different sizes (AuNP₂₀ and AuNP₅₀) and modified with polyethyleneimine (PEI) and polyethylene glycol (PEG). Additionally, this study aimed to systematically investigate their toxicological effects on histological changes in the organs of BALB/c mice.

Materials and methods

AuNP synthesis, surface functionalization, and characterization

First, seed AuNPs (AuNP₂₀) were synthesized and then used to synthesize AuNPs of average size (AuNP₅₀). For the production of AuNP₂₀, a modified Turkevich synthesis method was used [20]. After 100 ml, 0.25 mM of chloroauric acid (H[AuCl₄]) solution (Sigma-Aldrich) was prepared, and trisodium citrate dihydrate (Sigma-Aldrich Corp.) was added at a concentration of 0.033% by increasing the rotational speed of the boiling solution. After the prepared seed AuNP solution was cooled, it was centrifuged (Thermo-Scientific, MicroCL 21R) at 7,000 g for 30 min. Then, it was dispersed in deionized water. Average-sized AuNPs (AuNP₅₀) were synthesized using the seeding-growth method [21]. After 100 ml, 0.25 mM chloroauric acid solution was prepared, and 2.4 ml of seed AuNPs were added and mixed. Trisodium citrate was added in the next step at a concentration of 0.15 mM, and 1 ml of 25 mM hydroquinone (Sigma-Aldrich Corp.) solution was added and mixed for 10

min. Then, the synthesized average-sized AuNPs (AuNP₅₀) were centrifuged at 7,000 g for 30 min and dispersed in deionized water.

For the PEI functionalization of all the synthesized AuNPs, a 2% PEI (Mw: 10,000–25,000, Sigma-Aldrich Corp.) stock solution was prepared. Then, it was added to the AuNPs solutions at a 0.005% final concentration and mixed [17]. After the PEI coating process, all the AuNPs solutions were centrifuged at 7,000 g for 30 min and then dispersed in deionized water. A 0.15 mM PEG-SH (Mw: 5,000, Nanocs) solution was prepared for PEG functionalization of all the synthesized AuNPs. Then, 100 µl of the solution was added to each ml of the synthesized AuNPs solution and mixed. After the PEG coating, all the AuNPs solutions were centrifuged at 7,000 g for 30 min and then dispersed in deionized water.

Inductively coupled plasma mass spectrometry (ICP-MS) measurements were applied (Perkin Elmer ICP-MS, Nexion 300X) to precisely quantify the amount of gold (Au) in all the synthesized AuNPs solutions. All AuNPs solutions were standardized to contain Au at 50 µg ml⁻¹ and 500 µg ml⁻¹ for subsequent animal studies. The synthesized AuNPs were characterized regarding zeta potential and size using a zeta sizer (Zetasizer Ultra-Malvern). The surface plasmon resonance (SPR) spectrum shifts were determined using a UV-visible spectrophotometer (Shimadzu UV-1800). Scanning electron microscope (SEM) images of the AuNPs were taken (SEM-Zeiss Geminisem 500).

Animals

A total of 27 male adult BALB/c mice were used for histological staining (n = 18) and transmission electron microscopy (TEM) studies (n = 9). The animal procedures were performed under the Istanbul Medipol

University Institutional Animal Care and Use Committee (IMU-HADYEK, Approval date/number: May 18, 2017/21). For histological staining, the AuNPs were dissolved in 250 µl of sterile PBS (Sigma-Aldrich Corp.) and injected in two different doses (0.5 and 5 mg Au/kg) from the tail veins of the mice. In contrast, all the AuNP groups were dissolved in 250 µl of sterile PBS again and injected as a single dose (5 mg Au/kg) from the tail vein of the mice for liver TEM studies. All mice were allowed free access to drinking water and diet. The cages were located in temperature-controlled normal room conditions and a light-dark period of 12 h.

General histological studies

Hematoxylin and eosin (H&E) staining was performed to evaluate the general toxicological effects of the various AuNPs groups on the histological changes in the mice organs (e.g., liver, spleen, kidney, brain). All the necessary organs were collected from the mice 48 h post injection and fixed in 10% formalin solution (Tekkim) to evaluate the toxicity of the AuNP groups. The tissues were kept at 60°C in increasing ethanol (Sigma-Aldrich Corp.) series (from 70–100%) for the dehydration process. Then, the transparency process was applied with two xylene (Tekkim) exchanges. The tissues were left at room temperature for 1 h. In the final step, all the tissue samples were embedded in paraffin (Tekkim) blocks, sectioned into 5 µm slices, and stained with H&E (Bio-Optica) for histological examinations.

TEM analysis of liver tissue

TEM analysis was conducted to reveal the toxicological effects of different AuNPs groups on the ultrastructural changes in the liver of the mice in more detail. All liver tissue samples

were collected from the mice 14 days post injection. The tissues were rapidly dissected and separated. A total of 1 ml of 2.5% glutaraldehyde (Sigma-Aldrich Corp.) was added to the tissue samples, and the fixation procedure was applied in the ice for 4 h. Glutaraldehyde was discarded after the fixation process, and washing steps were applied three times using sodium cacodylate trihydrate buffer (Sigma-Aldrich Corp.). Then, the tissue samples were post-fixed with 1% OsO₄ (EMS) for 1 h. The samples were treated with an increasing acetone series (from 10–100%) for 5 min following the buffer-washing steps. The tissue samples were then embedded using an Epoxy-Embedding Kit (Sigma-Aldrich) and kept for 24 h at 60°C. Ultrathin sections (50–60 nm thick) were taken from the liver tissue samples (Ultramicrotome-Leica EM FC7) and placed on copper TEM grids (EMS) for imaging and histological examinations in the final step.

Results

AuNP characterization

The main characteristic properties of the synthesized AuNP groups are shown in Table 1. Highly monodispersed and stable AuNPs were synthesized using the modified Turkevich

synthesis method and the seeding-growth method. The size of the AuNPs increased depending on the PEI and PEG coatings. Again, the polydispersity index (PDI) values remained below 0.2, with a high monodispersed level. It was shown with these results that a highly controlled and optimized protocol was applied. The changes in UV-visible peaks depended on the surface coatings for the seed- and medium-sized AuNPs. After PEI functionalization, there was a significant positive increase in zeta potentials. On the other hand, the zeta potential values remained negative after PEG modification. The synthesis of highly monodispersed and stable AuNPs was confirmed according to the SEM images shown in Figure 1. The PEI and PEG surface coatings were visible for all surface-modified AuNP groups. Additionally, the size measurements of the AuNPs were verified based on the SEM images.

General histological evaluations

H&E staining was performed to evaluate the general toxicological effects of different AuNPs groups in the mice organs (e.g., liver, brain, kidney, spleen) after 48 h post injection. All AuNP groups were administered to mice in two different doses (0.5 and 5 mg Au/kg animal weight) within the scope of general histological

Table 1. Main characteristic properties of synthesized gold nanoparticle groups.

AuNP Groups	Hydrodynamic diameter (nm)	Polydispersity index (PDI)	UV-visible peak (nm)	Zeta potential (mV)
AuNP ₂₀ ^a	20.07±0.15	0.12	520	-49.55
AuNP ₂₃ -PEI	23.45±0.20	0.16	522	+32.20
AuNP ₂₄ -PEG	24.82±0.30	0.18	523	-21.75
AuNP ₅₀	50.64±0.16	0.13	534	-36.16
AuNP ₅₄ -PEI	54.22±0.20	0.17	536	+29.15
AuNP ₅₆ -PEG	56.45±0.30	0.19	538	-31.15

^aSubscript represents the size of the AuNPs.

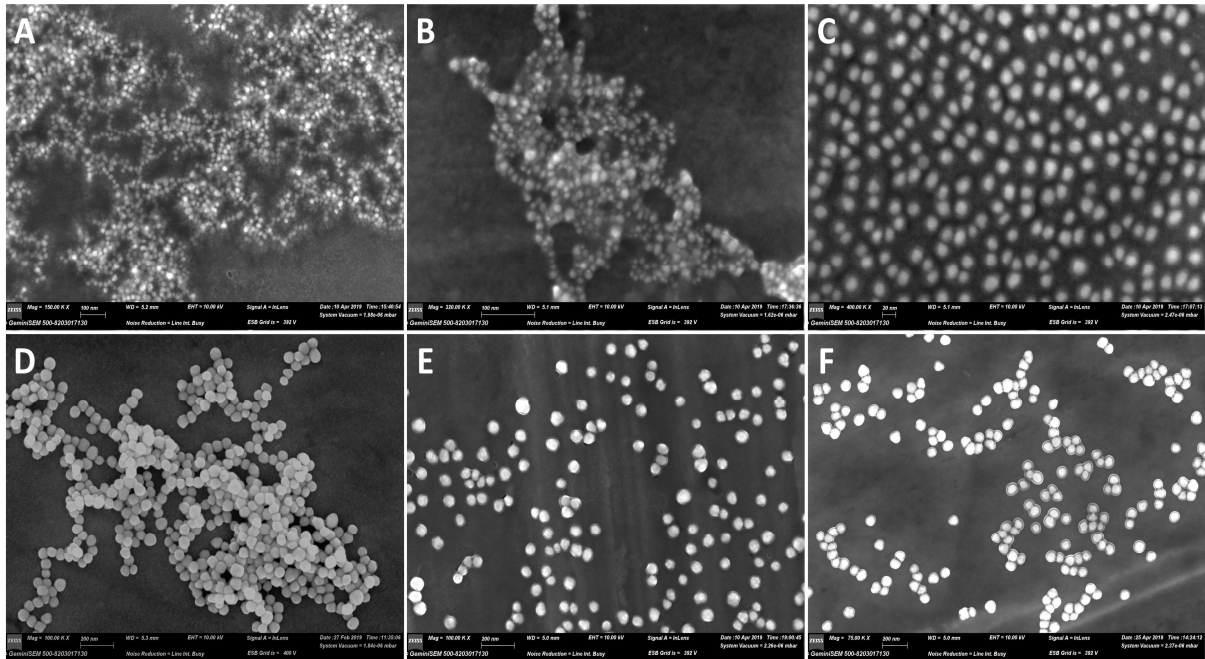


Figure 1. SEM images of synthesized gold nanoparticles. (A) AuNP₂₀. (B) AuNP₂₃-PEI. (C) AuNP₂₄-PEG. (D) AuNP₅₀. (E) AuNP₅₄-PEI. (F) AuNP₅₆-PEG

staining. The liver, the organ where nanomaterials accumulate the most, is also essential in nanotoxicity evaluations. Liver tissues were the most affected tissues after a 48 h exposure period (Figure 2). The hepatocytes and portal areas of the liver tissue had a regular appearance in the specimens within the control group (Figure 2 A).

After such a short-term exposure period to low concentrations of AuNPs, minimal histological changes (e.g., slightly degenerated hepatocytes with hyperchromatic nuclei, low level of lymphocyte infiltration, minimal increase in the cell numbers of Kupffer, enlarged sinusoids) were observed in the liver tissues from specimens in the experimental groups compared to the control group (Figure 2 B, C). The microstructure of the liver tissue was similar to the control group in the AuNP groups containing PEI or PEG surface coatings (Figure 2 B₂, B₃, C₂, C₃), although the observed changes did not depend on the AuNPs size. Liver parenchyma tissue was similar to normal,

especially in specimens treated with the PEI-coated AuNP groups. The results were similar when considering liver groups exposed to high concentrations of AuNP groups (Figure 2 D, E). On the other hand, microstructural histological changes for the liver tissue were observed more clearly due to short-term (48 h) AuNPs exposure at high concentrations. Again, fewer cellular degenerations were observed in the AuNP groups with additional PEG or PEI functionalization (Figure 2 D₂, D₃, E₂, E₃) than in the citrate-stabilized AuNP groups (Figure 2 D₁, E₁), although there were few size-related changes.

Microstructural histological changes observed in other organs (e.g., brain, kidney, and spleen) were relatively fewer than in the control groups after the short-term (48 h) AuNPs exposure period (Figure 3, 4, 5). Because of the blood-brain barrier in the brain, no noticeable histological alterations were observed after the 48 h exposure period to AuNPs. The results were similar for both high

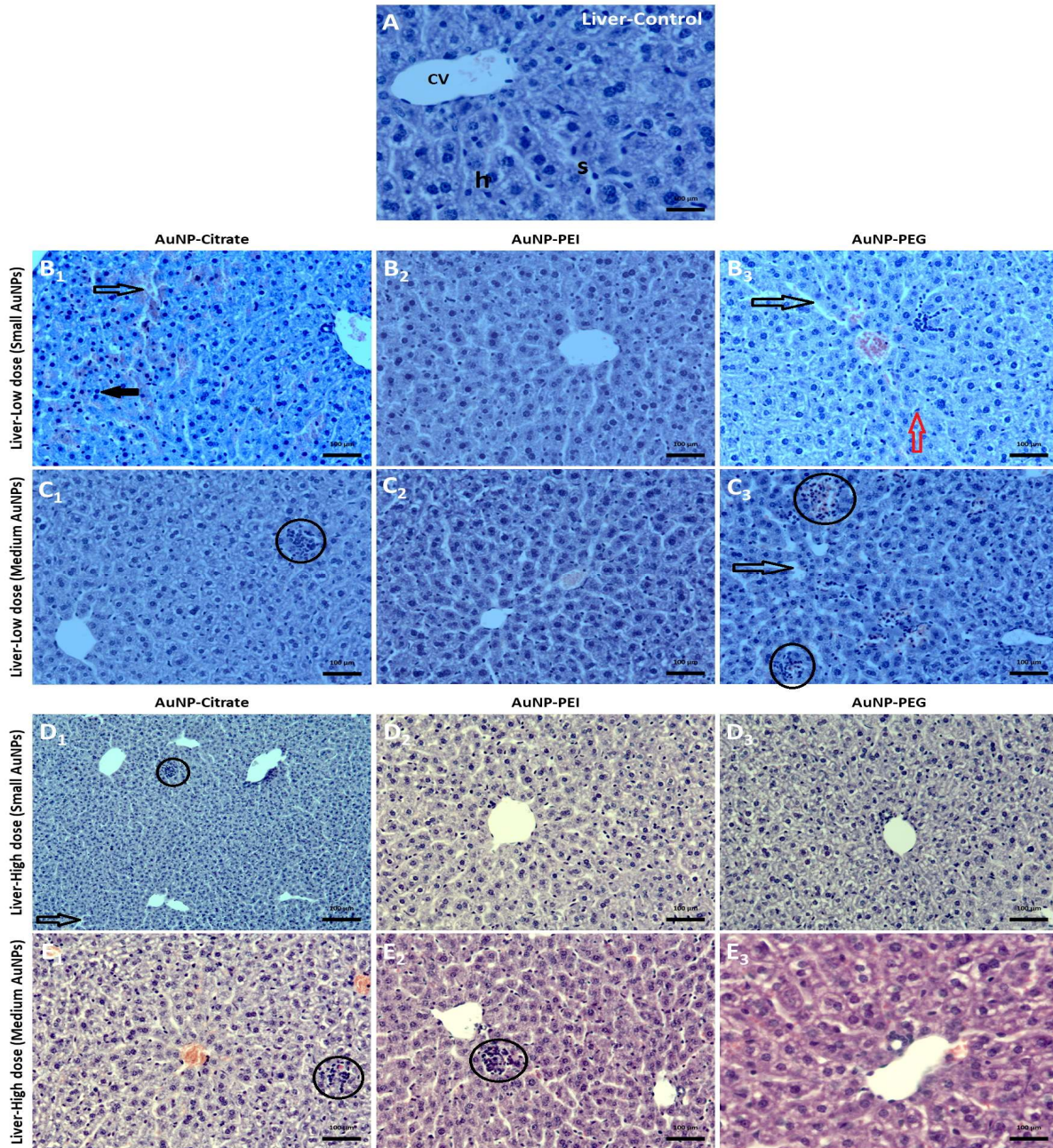


Figure 2. Histological evaluations of the AuNPs on the microstructural changes for the liver tissue in mice at 48 h after two different doses (0.5 and 5 mg Au/kg animal weight) i.v. injection of gold nanoparticles. (A) Control. (Figure B, C) Low dose. (Figure D, E) High dose. (B₁), (D₁) AuNP₂₀. (B₂), (D₂) AuNP₂₃-PEI. (B₃), (D₃) AuNP₂₄-PEG. (C₁), (E₁) AuNP₅₀. (C₂), (E₂) AuNP₅₄-PEI. (C₃), (E₃) AuNP₅₆-PEG. (H&E, 20× objective). Black filled arrow: hyperchromatic nucleus of hepatocytes, black circle: lymphocyte infiltration, black empty arrow: enlarged sinusoids, red empty arrow: Kupffer cell, CV: central vein, S: Sinusoidal capillary, h: hepatocyte.

and low AuNPs concentrations. Healthy neuronal and glial cell morphologies and typical axonal and dendritic structures were observed in all AuNP groups (Figure 3). No significant degenerations were observed in the kidney tissue from specimens from any of

the AuNP groups exposed to low and high Au concentrations. The renal cortex, glomerulus, and tubular structures generally had a healthy morphology (Figure 4). In contrast, slightly degenerated glomerular structures and slightly enlarged tubules were observed in the citrate-

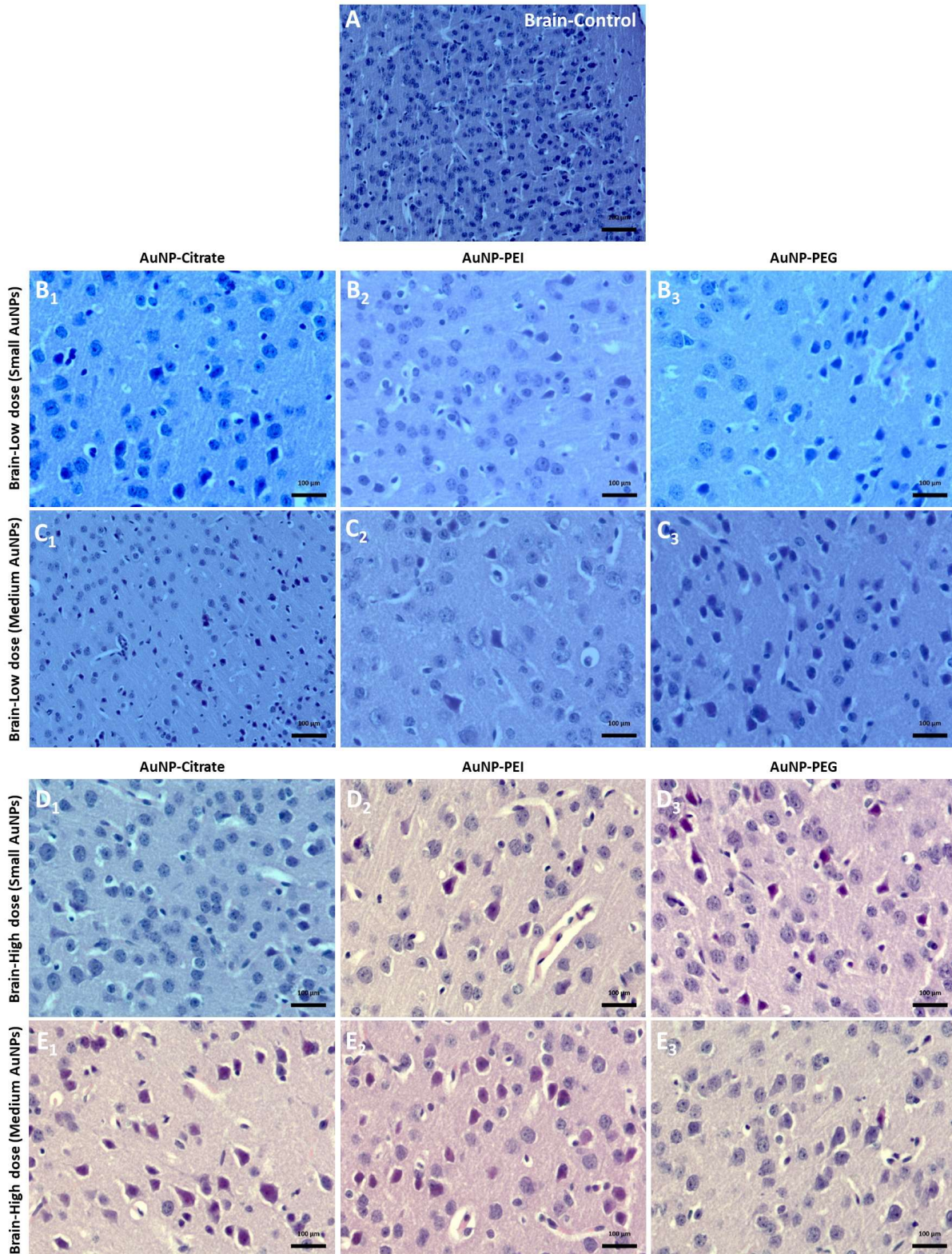


Figure 3. Histological evaluations of the AuNPs on the microstructural changes for the brain tissue in mice at 48 h after two different doses (0.5 and 5 mg Au/kg animal weight) i.v. injection of gold nanoparticles. (A) Control. (Figure B, C) Low dose. (Figure D, E) High dose. (B₁), (D₁) AuNP₂₀. (B₂), (D₂) AuNP₂₃-PEI. (B₃), (D₃) AuNP₂₄-PEG. (C₁), (E₁) AuNP₅₀. (C₂), (E₂) AuNP₅₄-PEI. (C₃), (E₃) AuNP₅₆-PEG. (H&E, 40× objective).

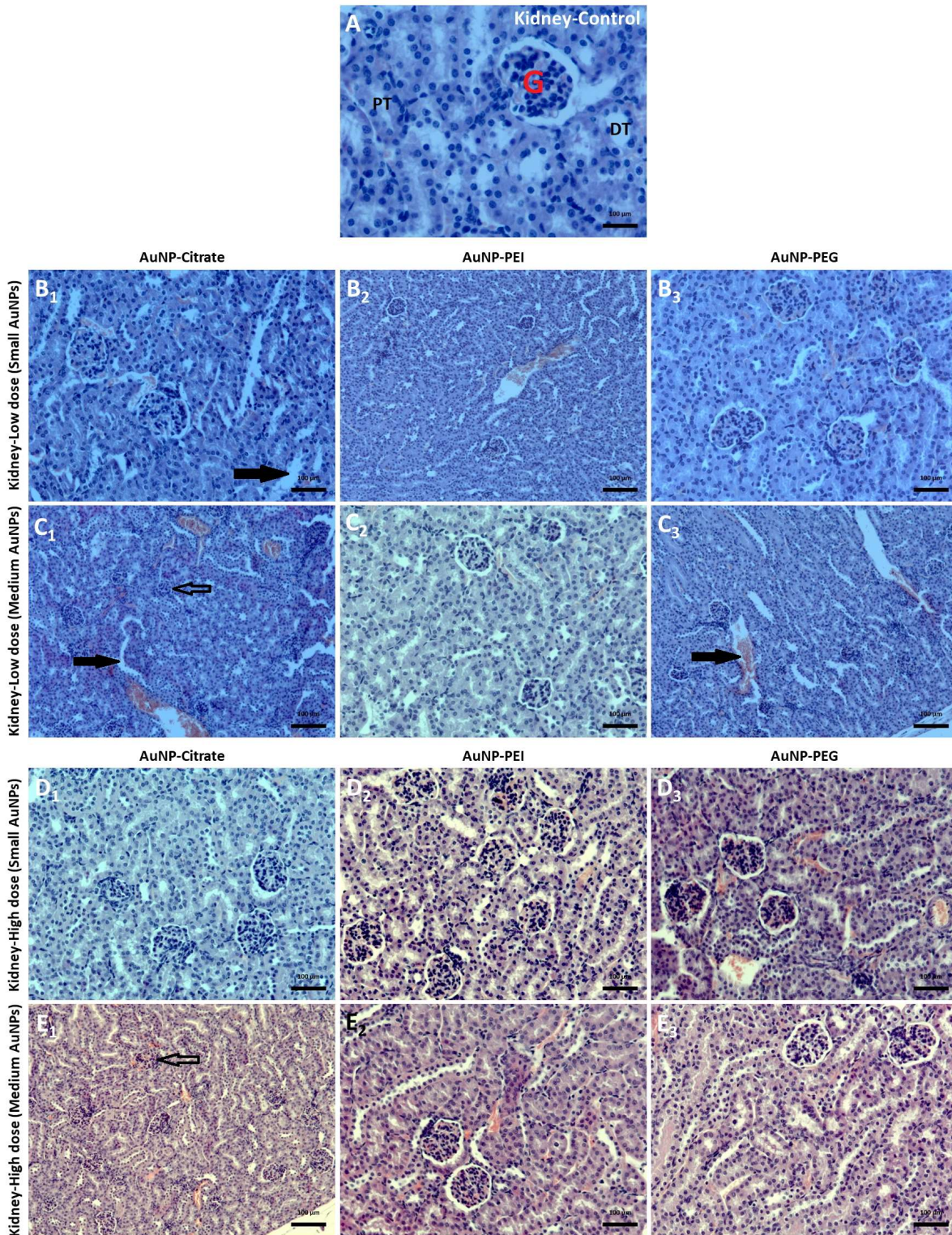


Figure 4. Histological evaluations of the AuNPs on the microstructural changes for the kidney tissue in mice at 48 h after two different doses (0.5 and 5 mg Au/kg animal weight) i.v. injection of gold nanoparticles. (A) Control. (Figure B, C) Low dose. (Figure D, E) High dose. (B₁), (D₁) AuNP₂₀. (B₂), (D₂) AuNP₂₃-PEI. (B₃), (D₃) AuNP₂₄-PEG. (C₁), (E₁) AuNP₅₀. (C₂), (E₂) AuNP₅₄-PEI. (C₃), (E₃) AuNP₅₆-PEG. (H&E, 20× objective). G: Glomerular structure, DT: Distal tubule, PT: proximal tubule, black empty arrow: degenerated glomerular structures, black filled arrow: enlarged tubules.

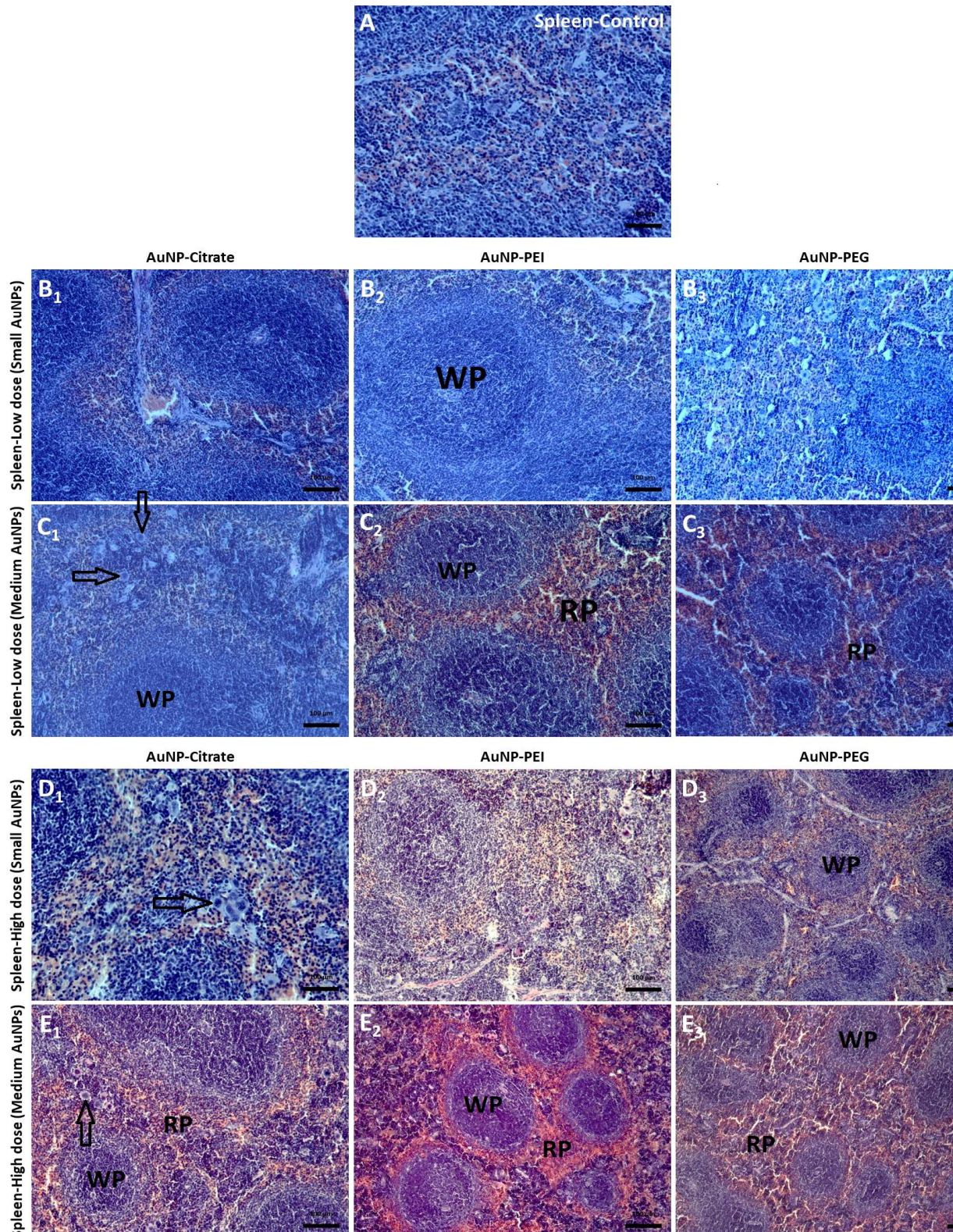


Figure 5. Histological evaluations of the AuNPs on the microstructural changes for the spleen tissue in mice at 48 h after two different doses (0.5 and 5 mg Au/kg animal weight) i.v. injection of gold nanoparticles. (A) Control. (Figure B, C) Low dose. (Figure D, E) High dose. (B₁), (D₁) AuNP₂₀. (B₂), (D₂) AuNP₂₃-PEI. (B₃), (D₃) AuNP₂₄-PEG. (C₁), (E₁) AuNP₅₀. (C₂), (E₂) AuNP₅₄-PEI. (C₃), (E₃) AuNP₅₆-PEG. (H&E, 10× objective). WP: White pulp, RP: Red pulp, black empty arrow: large macrophages.

stabilized AuNP groups. No histological changes were observed depending on the particle sizes. The spleen is another vital organ after the liver in terms of nanotoxicological evaluations. White and red pulp structures with regular appearances were generally observed (Figure 5) after the exposure period to low AuNPs concentrations. Lymphoid follicles surrounded by large macrophages were observed, especially in the citrate-stabilized AuNP₅₀ group (Figure 5 C₁). After exposure to high AuNP concentrations in the AuNP groups without additional surface coating, lymphoid follicles were surrounded by large macrophages (Figure 5 D₁, E₁). In contrast, in the groups of AuNPs containing PEI and PEG surface coating, spleen tissue morphologies were evaluated as normal (Figure 5 D₂, D₃, E₂, E₃).

Ultrastructural histological evaluations of the liver

TEM analysis was performed to reveal the effects of different AuNP groups on the ultrastructural changes in the liver of the mice in more detail on the 14th day after a single high dose (5 mg Au/kg) intravenous injection of AuNPs (Figure 6). Cellular structures were evaluated as normal and healthy in the control group (Figure 6A). In the AuNP groups, mainly in the medium-sized AuNPs group without additional surface coating, apparent cellular changes (e.g., enlarged cisternae, degraded granular or agranular endoplasmic reticulum, deformed nuclei, mitochondria) were observed after the long exposure period (Figure 6B, E). Although slightly enlarged cisterna structures were observed in the AuNP groups coated with PEG and PEI, the morphology of the hepatocyte cells was generally healthy (Figure 6C, D, F, G). AuNPs clusters were observed again in the cytoplasmic regions and within the cell nuclei (as indicated by arrows).

Discussion

Highly monodispersed and stable AuNPs were synthesized using the modified Turkevich synthesis method and the seeding-growth method. The PEI and PEG surface functionalization prevented the aggregation of the particles in the aqueous phase and made them more stable. The chemical surface and charge of the particles were also changed by the optimal and successful surface modifications of the AuNPs coated with PEI and PEG. With such features, the behavior of the particles in the biological environment was affected. There was a significant positive increase in the zeta potentials of the particles, especially after the PEI coating. When AuNPs are positively charged, they can easily and directly interact with negatively charged molecules (e.g., RNA and DNA). The advantage of effective potential applications for DNA delivery or siRNA-based gene silencing studies is offered with such an interaction. In the literature, researchers have shown that AuNPs with PEI surface coating are highly effective as gene silencing agents by conjugating with siRNA [22, 23].

Foreign molecules in the bloodstream are recognized by reticuloendothelial system (RES) components and are inactivated by being transported to the liver and spleen in *in vivo* biological environments. In particular, the liver is the organ where the nanoparticles entering the systemic circulation accumulate more frequently. Therefore, the liver is a vital organ that should always be considered in *in vivo* nanotoxicological evaluations [24]. Also, the spleen is an essential organ in the immune system and lymphoid maturation. With the assessment of liver and spleen cells, several toxic effects of nanoparticles are better understood. Significant level accumulation occurs in the liver and spleen, followed by the

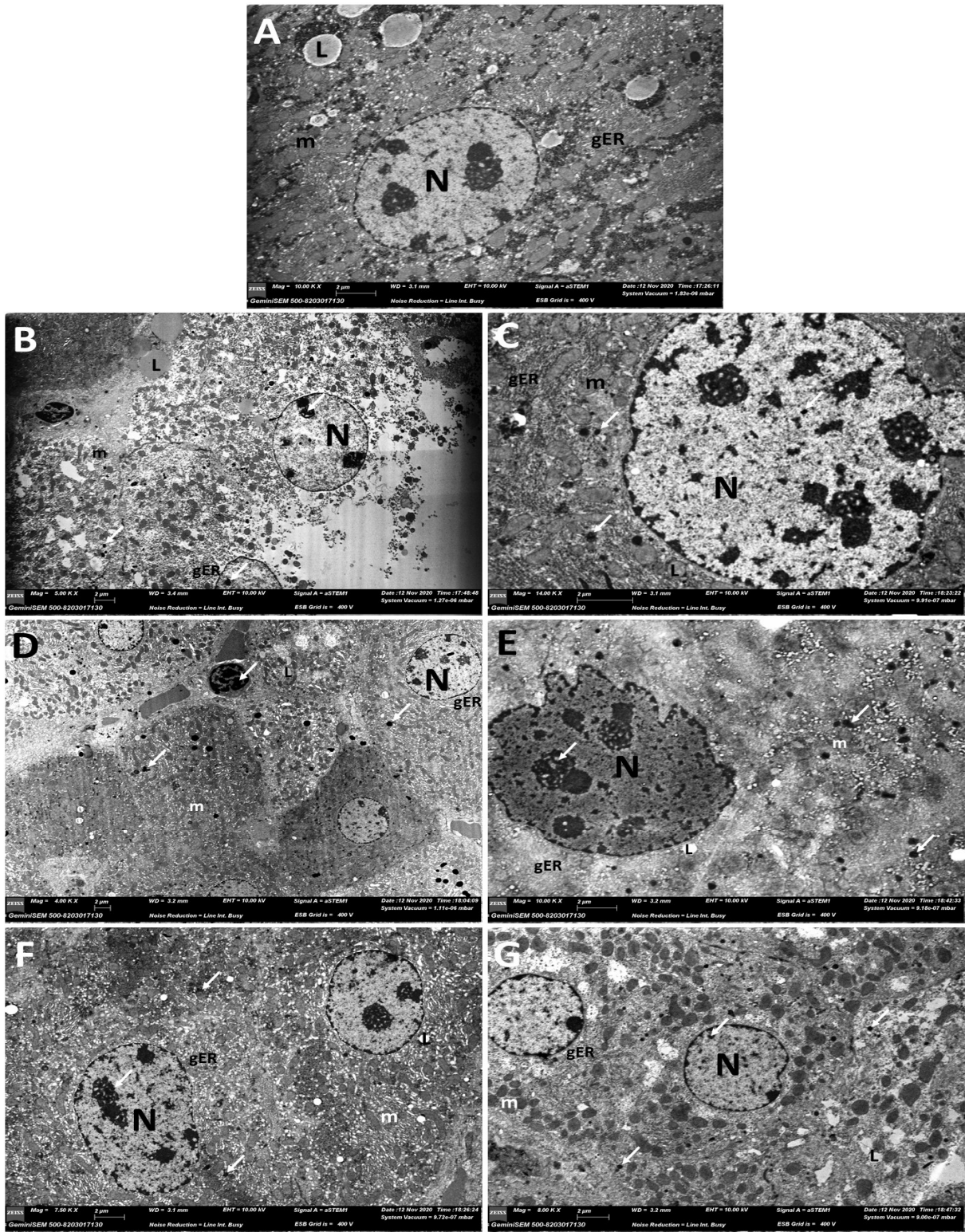


Figure 6. Ultrastructural histological evaluation of AuNPs using TEM for the liver tissue in mice on day 14 after a single dose (5 mg Au/kg animal weight) i.v. injection of gold nanoparticles. (A) Control. (B) AuNP₂₀. (C) AuNP₂₃-PEI. (D) AuNP₂₄-PEG. (E) AuNP₅₀. (F) AuNP₅₄-PEI. (G) AuNP₅₆-PEG. Some cellular compartments are represented by letters: N: Nucleus of the hepatocyte, L: Lipid droplet, m: Mitochondria, gER: Granular endoplasmic reticulum. Arrows show the gold nanoparticle aggregates localized in the various cellular compartments and the cell nucleus.

kidneys and circulatory system after intestinal nanoparticle absorption [25].

The liver tissue was the most toxicologically affected during the 48 h period according to our H&E staining results after two different doses of AuNPs exposure in mice. Although significant histological alterations were not observed depending on AuNPs size, the microstructure of the liver tissue was considered to be more similar to the control group in specimens treated with AuNPs containing PEI or PEG surface modification. Abdelhalim et al. showed that smaller particles cause more toxic effects (e.g., increase in the number of sinusoidal Kupffer cells, fatty changes in swollen hepatocytes, necrosis) in the liver of the rats after the injection of AuNPs with different diameters [18]. Histological changes in other organs were relatively less frequent when compared to liver tissues. Because of the presence of the blood-brain barrier, no noticeable changes were observed in the brain. No significant cellular degenerations in the kidney tissue were observed for any AuNP group exposed to low and high Au concentrations.

On the other hand, slightly degenerated glomerular structures and slightly enlarged tubules were observed in the AuNP-citrate groups. Ma et al. observed collagen accumulation in the renal parenchyma after administering AuNPs with different diameters and concentrations to mice, especially at high concentrations [26]. The spleen is another vital organ after the liver in terms of nanotoxicological considerations. After exposure to high AuNPs concentrations, lymphoid follicles surrounded by large macrophages were observed in the tissues of individuals treated with AuNP-citrate groups. Since the spleen is a critical lymphoid organ, this inflammatory physiological response

depends on the exposure of these particles. The PEI and PEG surface modifications generally increased the biocompatibility of the AuNPs. According to previously published results, different surface charges of AuNPs caused by changes in the chemical surface of the AuNPs can also trigger changes in liver and spleen tissues [27].

Apparent cellular changes and degenerations were observed after a long exposure period in the AuNP-citrate groups, according to our TEM analysis results. Although slight cellular changes were observed in the AuNP groups modified with PEG or PEI, the morphology of the hepatocyte cells was generally expected. We were allowed by TEM analysis of liver tissue to evaluate the cellular localization of the AuNPs. AuNPs clusters were observed in the cytoplasmic regions and cell nuclei, especially in surface-modified AuNP groups. Fraga et al. [28] showed that nanoparticles localized predominantly as endosomes in Kupffer cells after injection of 20 nm diameter citrate- and CALNN-pentapeptide-coated AuNPs into rats. Those researchers reported that they could not observe nanoparticles in the cytosol or nucleus of hepatocyte cells [28].

It is essential for nanoparticles to remain in sufficient quantities in the cytoplasm and nucleus, escaping from endosomal and lysosomal pathways without exocytosis. Additional surface modifications are needed to allow nanoparticles to escape through these pathways and enter the cell nucleus. Thus, a variety of potential nanotherapeutic applications can be implemented more effectively. Nanoparticles must also remain in organs for the required time and amount without causing toxic effects to have sufficient impact on cells for potential biomedical purposes.

Conclusions

In summary, we performed a systematic study to understand the histological effects of AuNPs with different surface coatings (PEI or PEG) and sizes (AuNP₂₀ and AuNP₅₀) in mice. Stable and highly monodispersed AuNPs were synthesized successfully. It has been concluded that the surface coating of AuNPs is a more decisive parameter than size in terms of *in vivo* histological toxicity. Histologically, it was observed that the liver was the most affected organ. PEI and PEG surface modifications increased the biocompatibility of the AuNPs. Stability, biocompatibility, and AuNP surface coating are critical parameters for potential nanotheranostic applications.

Acknowledgments: *The authors would like to thank the Scientific and Technological Research Council of Turkey (Grant no: 217S135) for providing financial support for this project.*

Funding: *The Scientific and Technological Research Council of Turkey (TUBITAK) (Grant no: 217S135).*

Conflict of Interest: *The authors declare that they have no conflict of interest.*

Ethical statement: *The animal procedures were performed under the Istanbul Medipol University Institutional Animal Care and Use Committee (IMU-HADYEK, Approval date/number: May 18, 2017/21).*

Open Access Statement: *This is an open access journal which means that all content is freely available without charge to the user or his/her institution under the terms of the Creative Commons Attribution Non-Commercial License (<http://creativecommons.org/licenses/by-nc/4.0>). Users are allowed to read, download, copy, distribute, print, search, or link to the full*

texts of the articles, without asking prior permission from the publisher or the author.

Copyright (c) 2021: Author (s).

References

- [1] Boisselier E, Astruc D. Gold nanoparticles in nanomedicine: preparations, imaging, diagnostics, therapies and toxicity. *Chemical Society Reviews*. 2009; 38 (6):1759-82.
- [2] Kim CS, Tonga GY, Solfiell D, et al. Inorganic nanosystems for therapeutic delivery: Status and prospects. *Adv Drug Deliver Rev*. 2013; 65 (1):93-99.
- [3] Camilo DE, Miyazaki CM, Shimizu FM, et al. Improving direct immunoassay response by layer-by-layer films of gold nanoparticles - Antibody conjugate towards label-free detection. *Mater Sci Eng C Mater Biol Appl*. 2019; 102:315-23.
- [4] Hamdy ME, Del Carlo M, Hussein HA, et al. Development of gold nanoparticles biosensor for ultrasensitive diagnosis of foot and mouth disease virus. *J Nanobiotechnology*. 2018; 16 (1):48.
- [5] Betzer O, Perets N, Angel A, et al. In Vivo Neuroimaging of Exosomes Using Gold Nanoparticles. *ACS Nano*. 2017; 11 (11):10883-93.
- [6] Ruttala HB, Ramasamy T, Poudel BK, et al. Multi-responsive albumin-Ionidamine conjugated hybridized gold nanoparticle as a combined photothermal-chemotherapy for synergistic tumor ablation. *Acta Biomater*. 2020; 101:531-43.
- [7] Wu D, Wang H, Hou X, et al. Effects of gold core size on regulating the performance of doxorubicin-conjugated gold nanoparticles. *Nano Research*. 2018; 11 (6):3396-410.
- [8] Cebrian V, Martin-Saavedra F, Yague C, et al. Size-dependent transfection efficiency of PEI-coated gold nanoparticles. *Acta Biomater*. 2011; 7 (10):3645-55.

- [9] Ghosh R, Singh LC, Shohet JM, et al. A gold nanoparticle platform for the delivery of functional microRNAs into cancer cells. *Biomaterials*. 2013; 34 (3):807-16.
- [10] Fratoddi I, Venditti I, Cametti C, et al. How toxic are gold nanoparticles? The state-of-the-art. *Nano Research*. 2015; 8 (6):1771-99.
- [11] Chompoosor A, Saha K, Ghosh PS, et al. The role of surface functionality on acute cytotoxicity, ROS generation and DNA damage by cationic gold nanoparticles. *Small*. 2010; 6 (20):2246-49.
- [12] Cui W, Li J, Zhang Y, et al. Effects of aggregation and the surface properties of gold nanoparticles on cytotoxicity and cell growth. *Nanomedicine*. 2012; 8 (1):46-53.
- [13] Coradeghini R, Gioria S, Garcia CP, et al. Size-dependent toxicity and cell interaction mechanisms of gold nanoparticles on mouse fibroblasts. *Toxicol Lett*. 2013; 217 (3):205-16.
- [14] Brandenberger C, Muhlfeld C, Ali Z, et al. Quantitative evaluation of cellular uptake and trafficking of plain and polyethylene glycol-coated gold nanoparticles. *Small*. 2010; 6 (15):1669-78.
- [15] Zhao F, Zhao Y, Liu Y, et al. Cellular uptake, intracellular trafficking, and cytotoxicity of nanomaterials. *Small*. 2011; 7 (10):1322-37.
- [16] Wang X, Hu X, Li J, et al. Influence of cell size on cellular uptake of gold nanoparticles. *Biomater Sci*. 2016; 4 (6):970-78.
- [17] Shahbazi R, Ozcicek I, Ozturk G, et al. Functionalized gold nanoparticles manifested as potent carriers for nucleolar targeting. *Nanotechnology*. 2017; 28 (2).
- [18] Abdelhalim MAK, Jarrar BM. Histological alterations in the liver of rats induced by different gold nanoparticle sizes, doses and exposure duration. *J Nanobiotechnol*. 2012; 10.
- [19] Khlebtsov N, Dykman L. Biodistribution and toxicity of engineered gold nanoparticles: a review of in vitro and in vivo studies. *Chem Soc Rev*. 2011; 40 (3):1647-71.
- [20] Turkevich J, Stevenson PC, Hillier J. A Study of the Nucleation and Growth Processes in the Synthesis of Colloidal Gold. *Discuss Faraday Soc*. 1951 (11):55-&.
- [21] Perrault SD, Chan WCW. Synthesis and Surface Modification of Highly Monodispersed, Spherical Gold Nanoparticles of 50-200 nm. *J Am Chem Soc*. 2009; 131 (47):17042-+.
- [22] Song WJ, Du JZ, Sun TM, et al. Gold nanoparticles capped with polyethyleneimine for enhanced siRNA delivery. *Small*. 2010; 6 (2):239-46.
- [23] Shahbazi R, Asik E, Kahraman N, et al. Modified gold-based siRNA nanotherapeutics for targeted therapy of triple-negative breast cancer. *Nanomedicine*. 2017; 12 (16):1961-73.
- [24] Lasagna-Reeves C, Gonzalez-Romero D, Barria MA, et al. Bioaccumulation and toxicity of gold nanoparticles after repeated administration in mice. *Biochem Bioph Res Co*. 2010; 393 (4):649-55.
- [25] Ganguly P, Breen A, Pillai SC. Toxicity of Nanomaterials: Exposure, Pathways, Assessment, and Recent Advances. *ACS Biomater Sci Eng*. 2018;4(7):2237-75.
- [26] Ma X, Sun J, Zhong L, et al. Evaluation of Turning-Sized Gold Nanoparticles on Cellular Adhesion by Golgi Disruption in Vitro and in Vivo. *Nano Lett*. 2019; 19 (12):8476-87.
- [27] Elci SG, Jiang Y, Yan B, et al. Surface Charge Controls the Suborgan Biodistributions of Gold Nanoparticles. *ACS Nano*. 2016; 10 (5):5536-42.

- [28] Fraga S, Brandao A, Soares ME, et al. Short- and long-term distribution and toxicity of gold nanoparticles in the rat after a single-dose intravenous administration. *Nanomedicine*. 2014; 10 (8):1757-66.

The relationship of monocyte to high density lipoprotein-cholesterol ratio and complete blood count parameters with radiologic staging of knee osteoarthritis

Mustafa Fatih Yasar,  Elif Yaksi 

Department of Physical Medicine and Rehabilitation, Bolu Abant Izzet Baysal University, Faculty of Medicine, Bolu, Turkey

ABSTRACT

Aim: To evaluate the predictive ability of bioindicators derived from complete blood count (CBC) parameters and monocyte-high density lipoprotein-cholesterol ratio (MHR) in the diagnosis of radiological stage of knee osteoarthritis (OA) in this study.

Method: This cross-sectional retrospective study was carried out between November 2017 and June 2021, in our physical therapy and rehabilitation clinics. 65 patients knee x-rays and routine laboratory results were included in the study. Each knee x-rays were assigned a grade from 0 to 4 (Kellgren-Lawrence Classification System (KL)). Patients were divided into two groups according to severity of the knee OA as follows. Group 1: Mild-moderate OA (KL Grade 1-2), Group 2: Severe OA (KL Grade 3-4).

Results: Independent T test and Mann Whitney U test were used to assess whether there was a difference in CBC parameters and their derivatives between two groups. Platelet lymphocyte ratio (PLR), red cell distribution width (RDW) to platelet ratio (RPR) and platelet (PLT) counts indicated statistically significant differences between the groups, *p*-values were 0.04, 0.03 and 0.04 respectively. There were no significant differences in terms of MHR score between the groups.

Conclusions: We could not find a relationship between MHR and radiological degree of knee osteoarthritis. However, there is a correlation between radiological stage of knee osteoarthritis and hemogram parameters like PLT and their derivatives such as PLR and RPR.

Key words: Knee, osteoarthritis, monocyte, high density lipoprotein, cholesterol, platelet, lymphocyte, red cell distribution.

✉ Dr. Mustafa Fatih Yasar

Department of Physical Medicine and Rehabilitation,
Bolu Abant Izzet Baysal University, Faculty of Medicine,
Bolu, Turkey

E-mail: mustafafy@hotmail.com

Received: 2021-09-28 / Revisions: 2021-10-14

Accepted: 2021-10-28 / Published online: 2022-01-01

Introduction

Osteoarthritis (OA) is the most common cause of arthritis, characterized by progressive degeneration and destruction of joint cartilage. Genetic factors, old age, trauma, high body

mass index (BMI), and deterioration of biomechanical properties are the main conditions that accelerate the process of osteoarthritis development. OA may remain silent for a long time or manifest slow progression. The disorder most commonly affects the knee joint symptomatically. Symptoms of OA include pain, joint dysfunction, and deformities. Knee OA is detected in approximately 80% of patients over 65 years old on plain radiographs; however, only one in three of these patients has

symptoms [1]. Early diagnosis of the disease and estimation of the clinical course and prognosis is difficult due to long asymptomatic periods. Recent studies have focused on discovering reliable biomarkers in the diagnosis and progression of OA [2,3]. Until recently, OA was accepted as a degenerative disease caused by joint abrasion and degeneration of periarticular soft tissue due to aging and increased mechanical load. Novel studies have proven that OA is associated with low-grade chronic inflammation [4-7]. Low-grade inflammation contributes to the pathogenesis of OA by inducing the production of pro-inflammatory cytokines. This process involves mononuclear cell (monocytes, macrophages, and activated T and B lymphocytes) infiltration in joint space and the release of pro-inflammatory mediators, such as IL-1 β and TNF. These mediators stimulate the production of matrix-metalloproteinases (MMPs), prostaglandin E2 (PGE2), nitric oxide (NO), and some other cytokines (IL-6, IL-8, IL-15, IL-17, IL-21). IL-1, IL-6, and TNF, which are key cytokines involved in the inflammatory process, may also lead to platelet activation. Platelets release inflammatory mediators and growth factors during hemostasis, inflammation, and tissue repair [8,9]. Monocytes and neutrophils contribute to inflammatory process steps and oxidative stress by releasing pro-inflammatory and pro-oxidative cytokines [10]. In recent years, various hematologic parameters, including mean platelet volume (MPV), neutrophil-lymphocyte ratio (NLR), platelet-lymphocyte ratio (PLR), and monocyte-high density lipoprotein-cholesterol ratio (MHR), have been evaluated as indicators of inflammation [11,12]. Previous studies have shown that high density lipoprotein-cholesterol (HDL-C) has anti-inflammatory, anti-oxidant effects and

protects endothelial cells [13,14]. Parameters such as MHR and NLR and red cell distribution width-platelet ratio (RPR) can be utilized by routine laboratory tests. These ratios can be computed by using complete blood count (CBC) results and biochemical profiles easily and inexpensively.

These parameters have been evaluated as indicators of inflammation and oxidative stress for systemic inflammatory diseases and cardiovascular disorders [15].

NLR has been introduced as a marker of inflammation in irritable bowel syndrome, ulcerative colitis, thyroiditis, and type 2 diabetes mellitus [16-19]. PLR has also been increased in various inflammatory conditions, including malignancy [20].

There is a paucity of research about the clinical and radiological progression of OA. Therefore, we aimed to assess the predictive ability of bioindicators derived from CBC parameters and the MHR ratio in the diagnosis of the radiological stage of knee OA in this study.

Materials and methods

Ethics statement

This cross-sectional retrospective study was carried out between November 2017 and June 2021, in our physical therapy and rehabilitation clinics. The study protocol was approved by our Institutional Review Board (Ethics Committee Approval Date and Number: 08.06/2021-148) and conducted in accordance with the Declaration of Helsinki.

Study design and population

Inclusion criteria

Patients with primary knee OA according to the clinical criteria of the American College of Rheumatology (ACR) and between the ages of 40-80 were included in the study. If OA wasn't unilateral, only the patients with an equal degree of OA on both knees were included.

All diagnostic decisions were made by the same physician. 65 patients with standing, weight bearing anteroposterior and lateral knee x-rays and routine laboratory results were included in the study. Each knee x-rays was assigned a grade from 0 to 4 (Kellgren-Lawrence Classification System (KL)). Demographic information and body mass index of the patients with knee OA were recorded.

Patients were divided into two groups according to severity of the knee OA as follows.

Group 1: Mild-moderate OA (KL Grade 1-2)

Group 2: Severe OA (KL Grade 3-4)

Kellgren-Lawrence classification system

The Kellgren-Lawrence system is applied specifically to classify the severity of knee OA using five grades and originally described using AP knee radiographs. This classification system was accepted by WHO in 1961. Below is the original description.

Grade 0: No radiographic features of OA are present

Grade 1: Doubtful joint space narrowing (JSN) and possible osteophytic lipping

Grade 2: Definite osteophytes and possible JSN on anteroposterior weight-bearing radiograph

Grade 3: Multiple osteophytes, definite JSN, sclerosis, possible bony deformity

Grade 4: Large osteophytes, marked JSN, severe sclerosis and definite bony deformity

Exclusion criteria

Participants with hematologic disorders which may affect blood parameters, patients with diagnosis of diabetes mellitus, acute decompensation and organ failure, inflammatory diseases, rheumatic diseases, acute or chronic infection, cardiovascular diseases, secondary osteoarthritis, oncologic diseases, patients who are receiving intra-articular steroid or hyaluronic acid treatment, patients with history of severe knee trauma or operation last 6 months, patients during the

pregnancy and lactation period were excluded from participation.

Laboratory analysis

While low density lipoprotein cholesterol [LDL-C] (mg/dL), and high density lipoprotein cholesterol [HDL-C] (mg/dL) levels were obtained from biochemical analysis (Architect CI4100, Chicago, USA), white blood cell (WBC) (K/uL), neutrophil (K/uL), lymphocyte (K/uL), monocyte (K/uL), hemoglobin (Hb) (g/dL), red blood cell distribution width (RDW), platelet (K/uL) (PLT) and mean platelet volume (MPV) (fl), platelet distribution width (PDW) values were acquired from CBC analysis using an XT1800i Kobe, JAPAN hematology analyzer. On the basis of these test results, NLR, PLR, LMR and MHR were calculated as dividing by different parameters. All assays were performed according to the manufacturer's instructions.

Statistical analyses

The data obtained in the study were analyzed on SPSS statistical package (IBM SPSS Statistics for Windows, Version 26.0. Armonk, NY: IBM Corp). Mean values, standard deviation values were calculated for all parameters. Kolmogorov-Smirnov test is used to assess normality of the variables. Independent T tests were used to compare the means between the groups for normally distributed data. Chi-square test is performed to understand the relationship of categorical variables. A p-value less than 0.05 is considered statistically significant.

Results

Demographic characteristics

Overall, 65 patients between the ages of 40-80, including 35 with mild-moderate OA and 30 with severe OA, were assigned to our study. Patients ranged in age from 44 to 80, with a mean age of 65.7 ± 9.4 . Most participants were

Table 1: Demographic information.

Parameters	Group 1 (Mild-Moderate Osteoarthritis)	Group 2 (Severe Osteoarthritis)	Total	<i>p</i>
Age				
Mean ± SD	62.5±8.6	69.4±9.1	65.7±9.4	0.79
Min-Max	46-77	44-80	44-80	
Gender				
Female (n, %)	21 (60%)	21 (70%)	42 (64%)	0.10
Male (n, %)	14 (40%)	9 (30%)	23 (35%)	
Admission status				
In-patient (n, %)	11 (31%)	7 (23%)	18 (28%)	
Out-patient (n, %)	24 (67%)	23 (77%)	47 (72%)	

SD: standard deviation, Min: minimum, Max: maximum

female (64%). Demographic characteristics were similar between the two groups ($P > 0.05$). Most patients (72%) were admitted to our outpatient clinics, and the remaining patients were hospitalized. Detailed information about the demographics of the participants is available in Table 1.

Prediction of OA grade according to hemogram parameters and MHR

Independent T test and Mann Whitney U test were used to assess whether there was a difference in CBC parameters and their derivatives between the two groups. PLR, RPR ratios, and PLT counts indicated statistically significant differences between the groups; *p*-values were 0.04, 0.03, and 0.04, respectively. The area under the curve for PLR and RPR was computed as 0.644 and 0.374, respectively (Figure 1). There were no significant differences in terms of MHR score between the groups; *p*-values were 0.07. The rest of the factors did not show a statistically significant difference between the groups (Table 2).

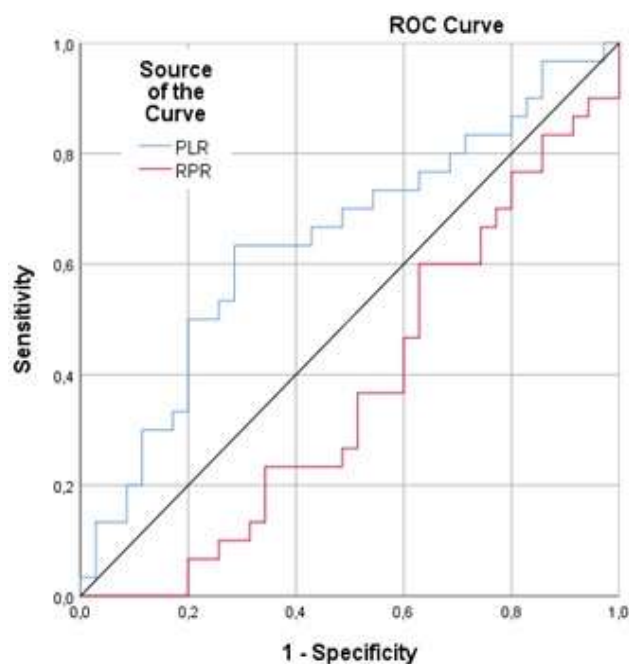


Figure 1. ROC curve analysis of the test (PLR curve:blue line, RPR curve:red line, reference: black line).

Discussion

The major findings of our study, in which we evaluated the predictive performance of bioindicators like blood parameters and MHR in the diagnosis and staging of knee osteoarthritis, were as follows:

Table 2. Comparison of the laboratory test results of the groups.

Parameters	Group 1 (n=35)	Group 2 (n=30)	P
WBC	6.70±1,5	7.04±1,8	0.75
Neu	3.75±1,3	4.18±1,5	0.47
Lym	2.13±0,5	2.10±0,7	0.87
Mono	0.46±0,1	0.52±0,2	0.17
HB	13.4±1,5	13.2±1,3	0.37
RDW	14.58±1,3	14.65±1,2	0.85
PLT	221.4±56,6	252.0±53,2	0.04
HDL	50.6±11,2	47.5±10,3	0.34
LDL	129.3±34,9	119.4±28,9	0.27
NLR	1.82±0,7	2.11±0,9	0.25
PLR	110.50±40,2	132.6±47,8	0.04
RPR	0.07±0.022	0.06±0.01	0.03
MHR	0.009±0.003	0.011±0.005	0.07
MLR	0.22±0.08	0.26±0.10	0.18

Values: Mean±SD. Group 1: Grade 1, 2 osteoarthritis. Group 2: Grade 3, 4 osteoarthritis. SD: Standard deviation, WBC: White blood cell. Lym: Lymphocyte. Mono: Monocyte. Neu: Neutrophil. HB: Hemoglobin. RDW: Red cell distribution width. PLT: Platelet. HDL: High density lipoprotein. LDL: Low density lipoprotein. NLR: Neutrophil/Lymphocyte ratio. PLR: Platelet/Lymphocyte ratio. RPR: RDW/Platelet ratio. MHR: Monocyte/HDL ratio. MLR: Monocyte/Lymphocyte ratio.

1. A significant difference was detected in terms of PLT, PLR and RPR values.

2. There were no significant differences in terms of MPV, MHR, NLR score between the groups.

3. There were no significant differences in terms of HDL and LDL levels between the groups.

Previous studies showed that hemogram parameters and their derivatives, such as MPV, NLR, and PLR, could indicate systemic inflammation in various etiologies [21-23].

MPV is one test run during the CBC; NLR and PLR can be easily calculated by dividing neutrophil or platelet count by lymphocyte count. In the literature, there seem to be limited studies on the relationship between OA and PLT parameters. PLT indices may reflect subclinical inflammation in OA and disease activation. What is known about the PLT activation process is not only that the number of PLT increases, but also that to reach a larger surface area, their morphology changes from discoid to spherical patterns [24]. Also, larger

platelets are likely to be more active at releasing pro-inflammatory and thrombotic mediators, and increased demand is seen during acute phase response [25].

Several studies have been conducted on the diagnostic and prognostic ability of CBC parameters and their derivatives, such as MPV, RDW, and RPR, during infectious and inflammatory disorders [26,27]. It has been proposed that there is a link between high MPV and RDW values and mortality or morbidity due to vascular events affecting the heart and kidneys, resulting in infectious disease [28-30]. Although many attempts have been made to assess the relationship between MPV and systemic inflammatory disorders, the results are contradictory [31,32]. It has been reported that MPV values in patients with active rheumatoid arthritis (RA) or ankylosing spondylitis (AS) are lower than in healthy controls. However, it is recommended to be careful when interpreting the MPV values, because this ratio is not consistently related to disease activity indexes, and tests may be influenced by technical settings [33,34]. Balbaoglu et al. compared patients with a diagnosis of OA, patients with synovitis related to OA, and a control group; there was no statistically significant difference detected between all groups. On the contrary, MPV values in patients with synovitis related to OA were lower than in the other groups [31].

Koca et al. reported that MPV value was increased in patients with severe osteoarthritis [32]. Despite the Koca et al. findings, a recent study conducted by Atar et al. found that NLR, PLR, and MPV values were similar between 92 knee OA patients and 52 healthy controls [32,35]. Our results share a similarity with Atar et al.'s findings; no significant correlation was observed between MPV values and OA grades. PLR, which is calculated as absolute platelet count dividing by absolute lymphocyte count,

is another principal factor with an influence on systemic inflammatory response pathogenesis [36].

In contradiction with earlier findings, we found a relationship between PLR ratio, knee osteoarthritis degree, PLT, and RPR levels in patients with advanced knee osteoarthritis [35]. NLR, as a marker of systemic inflammation, may reflect the neutrophil & lymphocyte balance and immune system status of the patient [37].

Tasoglu et al. compared NLR ratios of 176 patients with OA according to the Kellgren-Lawrence classification and found higher NLR values in patients with severe OA (grade 4). They suggest that the NLR ratio can be used as a predictor tool to estimate the radiological grade of knee OA [3]. Büyükavcı et al. proposed using blood platelet distribution width (PDW) and NLR to predict the severity of knee OA in clinical practice [38]. Atar et al. did not find a significant correlation between NLR ratio and radiological severity of knee osteoarthritis [3,35-38]. Similar to Atar et al.'s study, we did not find a relationship between the radiological stage of knee OA and NLR [35]. Contradictory results may be explained by local inflammation without systemic response. Future studies with larger populations should concentrate on this topic.

To the best of our knowledge, this is the first study in the literature evaluating the association between the MHR ratio, which is a novel bioindicator recently used as a marker of inflammation, and knee osteoarthritis.

The mononuclear phagocyte system plays a fundamental role in the inflammatory response during the development and progression of atherosclerosis. In the premature steps of the process, circulating monocytes migrate to the subendothelial matrix of the arterial wall, mature into macrophages, and internalize

oxidized LDLs and other lipids. Subsequently, these cells transform to foam cells, which release immunoregulatory cytokines, trigger inflammation, and invite T-lymphocytes, platelets, and further monocytes [39]. However, HDL-C disrupts monocyte functions, interferes with the conversion of monocytes to macrophages, and removes cholesterol from them, which reduces the inflammatory response [40]. Therefore, it is appropriate to utilize the combination of both parameters (MHR) in a single index as a pro-inflammatory marker. Previous studies recommended using MHR as a predictive marker of cardiovascular disease due to its ability to demonstrate systemic inflammation [41]. Demirbaş et al. showed a significant decrease in MHR, monocyte to lymphocyte ratio (MLR), and NLR levels after colchicine treatment [42].

Sirin et al. revealed that the Psoriasis Area and Severity Index score (PASI) was associated with C-reactive protein, serum amyloid A, and MHR in their study of 60 psoriasis vulgaris patients and 50 healthy controls. Our findings do not support previous studies, and we did not find a relationship between MHR and radiological grade of knee osteoarthritis [43]. The retrospective design of the study and the limited number of participants may be the reason for this concordance.

Recently, it has been thought that osteoarthritis may be a metabolic disease and lipid metabolism defects may be one of the underlying mechanisms [44,45]. Schwager et al. investigated the effects of serum cholesterol, low-density lipoprotein, and high density lipoproteins on the risk of knee osteoarthritis. As a result, they reported that they did not find a significant relationship between HDL, LDL and total cholesterol levels, and cartilage loss or worsening pain. [46]. Irshad et al. reported that serum cholesterol and triglyceride levels were

associated with osteoarthritis, but there was no relationship between serum HDL and LDL levels and osteoarthritis [47]. Like these studies, no significant correlation was found with HDL and LDL levels in our study.

Advanced age is a non-modifiable risk factor associated with OA. It is predictable that radiologically advanced OA patients will be older than those with low-grade OA; hence, age-dependent alterations in patients' laboratory results show concomitance with radiologic advanced stages.

We know our study may have a few limitations. The first is that the retrospective design of the study may have influenced the assessment of the clinical presence of inflammation. Another limitation is that there was no control group to compare the results with patients. The small sample size is also a limitation of this study.

Conclusions

The evidence from our study suggests that there is a correlation between the radiological stage of knee osteoarthritis and hemogram parameters like PLT and their derivatives such as PLR and RPR. However, we could not find a relationship between NLR, MHR, MPV, and radiological degree of knee osteoarthritis. Further work needs to be carried out in a larger patient group with more clinical evaluation parameters.

Funding: *The author(s) received no financial support for the research, authorship, and/or publication of this article.*

Conflict of Interest: *The authors declare that they have no conflict of interest.*

Ethical statement: *This study protocol was approved by Bolu Abant İzzet Baysal University Clinic Review Board (Date and Number: 08.06/2021-148), and conducted in accordance with the Declaration of Helsinki.*

Open Access Statement

This is an open access journal which means that all content is freely available without charge to the user or his/her institution under the terms of the Creative Commons Attribution Non-Commercial License (<http://creativecommons.org/licenses/by-nc/4.0>). Users are allowed to read, download, copy, distribute, print, search, or link to the full texts of the articles, without asking prior permission from the publisher or the author.

Copyright (c) 2021: Author (s).

References

- [1] Felson DT, Naimark A, Anderson J, et al. The prevalence of knee osteoarthritis in the elderly. The Framingham Osteoarthritis Study. *Arthritis Rheum.* 1987; 30(8):914-18.
- [2] Zhai G, Randell EW, Rahman P. Metabolomics of osteoarthritis: emerging novel markers and their potential clinical utility. *Rheumatology (Oxford).* 2018; 57 (12): 2087-95.
- [3] Tasoglu O, Boluk H, Sahin Onat S, et al. Is blood neutrophil-lymphocyte ratio an independent predictor of knee osteoarthritis severity? *Clin Rheumatol.* 2016; 35(6): 1579-83.
- [4] Sellam J, Berenbaum F. The role of synovitis in pathophysiology and clinical symptoms of osteoarthritis. *Nat Rev Rheumatol.* 2010; 6 (11):625-35.
- [5] Goldring MB, Otero M. Inflammation in osteoarthritis. *Curr Opin Rheumatol.* 2011; 23 (5): 471-78.
- [6] Benito MJ, Veale DJ, FitzGerald O, et al. Synovial tissue inflammation in early and late osteoarthritis. *Ann Rheum Dis.* 2005;64 (9): 1263-67.
- [7] Robinson WH, Lepus CM, Wang Q, et al. Low-grade inflammation as a key mediator of the pathogenesis of osteoarthritis. *Nat Rev Rheumatol.* 2016; 12(10): 580-92.
- [8] Dan K, Gomi S, Inokuchi K, et al. Effects of interleukin-1 and tumor necrosis factor on megakaryocytopoiesis: mechanism of reactive thrombocytosis. *Acta Haematol.* 1995; 93(2-4): 67-72.
- [9] Unsal E, Aksaray S, Koksall D, et al. Potential role of interleukin 6 in reactive thrombocytosis and acute phase response in pulmonary tuberculosis. *Postgrad Med J.* 2005; 81 (959): 604-7.
- [10] Ancuta P, Wang J, Gabuzda D. CD16+ monocytes produce IL-6, CCL2, and matrix metalloproteinase-9 upon interaction with CX3CL1-expressing endothelial cells. *J Leukoc Biol.* 2006; 80(5): 1156-64.
- [11] 36th International Symposium on Intensive Care and Emergency Medicine: Brussels, Belgium. 15-18 March 2016 (2016). *Crit Care* 20 (Suppl 2):94.
- [12] Imtiaz F, Shafique K, Mirza SS, et al. Neutrophil lymphocyte ratio as a measure of systemic inflammation in prevalent chronic diseases in Asian population. *Int Arch Med.* 2012; 5(1): 2.
- [13] Hessler JR, Robertson AL Jr, Chisolm GM, 3rd. LDL-induced cytotoxicity and its inhibition by HDL in human vascular smooth muscle and endothelial cells in culture. *Atherosclerosis.* 1979; 32(3): 213-29.
- [14] Parthasarathy S, Barnett J, Fong LG. High-density lipoprotein inhibits the oxidative modification of low-density lipoprotein. *Biochim Biophys Acta.* 1990; 1044 (2): 275-83.
- [15] Canpolat U, Cetin EH, Cetin S, et al. Association of Monocyte-to-HDL Cholesterol Ratio with Slow Coronary Flow is Linked to Systemic Inflammation. *Clin Appl Thromb Hemost.* 2016; 22(5): 476-82.

- [16] Aktas G, Duman TT, Atak BM, et al. Irritable bowel syndrome is associated with novel inflammatory markers derived from hemogram parameters. *Fam Med Prim Care Rev.* 2020; 22(2): 107–110.
- [17] Posul E, Yilmaz B, Aktas G, et al. Does neutrophil-to-lymphocyte ratio predict active ulcerative colitis? *Wien Klin Wochenschr.* 2015;127(7-8):262-65.
- [18] Aktas G, Sit M, Dikbas O, et al. Elevated neutrophil-to-lymphocyte ratio in the diagnosis of Hashimoto's thyroiditis. *Rev Assoc Med Bras (1992).* 2017;63(12):1065-68.
- [19] Bilgin S, Aktas G, Zahid Kocak M, et al. Association between novel inflammatory markers derived from hemogram indices and metabolic parameters in type 2 diabetic men. *Aging Male.* 2020;23(5):923-27.
- [20] Atak Tel BM, Kahveci G, Bilgin S, et al. Platelet to lymphocyte ratio in differentiation of benign and malignant thyroid nodules. *Exp Biomed Res* 2021; 4(2):148-53.
- [21] Kilincalp S, Coban S, Akinci H, et al. Neutrophil/lymphocyte ratio, platelet/lymphocyte ratio, and mean platelet volume as potential biomarkers for early detection and monitoring of colorectal adenocarcinoma. *Eur J Cancer Prev.* 2015; 24(4): 328-33.
- [22] Kuyumcu ME, Yesil Y, Ozturk ZA, et al. The evaluation of neutrophil-lymphocyte ratio in Alzheimer's disease. *Dement Geriatr Cogn Disord.* 2012; 34 (2): 69-74.
- [23] Boyraz I, Koc B, Boyaci A, et al. Ratio of neutrophil/lymphocyte and platelet/lymphocyte in patient with ankylosing spondylitis that are treating with anti-TNF. *Int J Clin Exp Med.* 2014; 7(9): 2912-15.
- [24] Jagroop IA, Clatworthy I, Lewin J, et al. Shape change in human platelets: measurement with a channelyzer and visualisation by electron microscopy. *Platelets.* 2000; 11(1): 28-32.
- [25] Schmitt-Sody M, Metz P, Gottschalk O, et al. Platelet P-selectin is significantly involved in leukocyte-endothelial cell interaction in murine antigen-induced arthritis. *Platelets.* 2007; 18 (5): 365-72.
- [26] Zareifar S, Farahmand Far MR, Golfeshan F, et al. Changes in platelet count and mean platelet volume during infectious and inflammatory disease and their correlation with ESR and CRP. *J Clin Lab Anal.* 2014; 28(3): 245-48.
- [27] Cetinkaya E, Senol K, Saylam B, et al. Red cell distribution width to platelet ratio: new and promising prognostic marker in acute pancreatitis. *World J Gastroenterol.* 2014; 20 (39):14450-54.
- [28] Patel KV, Semba RD, Ferrucci L, et al. Red cell distribution width and mortality in older adults: a meta-analysis. *J Gerontol A Biol Sci Med Sci.* 2010; 65(3): 258-65.
- [29] Zampieri FG, Ranzani OT, Sabatoski V, et al. An increase in mean platelet volume after admission is associated with higher mortality in critically ill patients. *Ann Intensive Care.* 2014; 4:20.
- [30] Atakan-Erkcal F, Sepin-Özen N, Emek M, et al. Increased mean platelet volume, red blood cell distribution width and platelet / red blood cell distribution width in patients with Hepatitis B. *Turk Hij Den Biyol Derg.* 2019; 76(1): 53-58.
- [31] Balbaloglu O, Korkmaz M, Yolcu S, et al. Evaluation of mean platelet volume (MPV) levels in patients with synovitis associated with knee osteoarthritis. *Platelets.* 2014; 25(2): 81-85.

- [32] Koca TT, Baykara M, Koçyiğit BF. Relation of complete blood count parameters and derivatives with radiologic staging of knee osteoarthritis. *Cukurova Med J.* 2019; 44 (4):1364-70.
- [33] Kisacik B, Tufan A, Kalyoncu U, et al. Mean platelet volume (MPV) as an inflammatory marker in ankylosing spondylitis and rheumatoid arthritis. *Joint Bone Spine.* 2008; 75 (3): 291-4.
- [34] Sahin A, Yetisgin A, Sahin M, et al. Can Mean Platelet Volume Be a Surrogate Marker of Inflammation in Rheumatic Diseases? *West Indian Med J.* 2015; 65(1): 165-69.
- [35] Atar E, Aşkın A. Diz osteoartrit hastalarında nötrofil/lenfosit oranı, trombosit/lenfosit oranı ve ortalama trombosit hacminin değerlendirilmesi. *Cukurova Med J.* 2017; 42 (2): 329-36.
- [36] Liu H, Wu Y, Wang Z, et al. Pretreatment platelet-to-lymphocyte ratio (PLR) as a predictor of response to first-line platinum-based chemotherapy and prognosis for patients with non-small cell lung cancer. *J Thorac Dis.* 2013; 5(6): 783-89.
- [37] Lissoni P, Brivio F, Fumagalli L, et al. Efficacy of cancer chemotherapy in relation to the pretreatment number of lymphocytes in patients with metastatic solid tumors. *Int J Biol Markers.* 2004;19 (2): 135-40.
- [38] Buyukavci R, Akturk S, Sag S. Comparison of blood platelet distribution width and neutrophil-lymphocyte ratio in patients with different grades of knee osteoarthritis. *J Back Musculoskelet Rehabil.* 2018; 31(6): 1035-39.
- [39] Ganjali S, Gotto AM, Jr., Ruscica M, et al. Monocyte-to-HDL-cholesterol ratio as a prognostic marker in cardiovascular diseases. *J Cell Physiol.* 2018; 233(12): 9237-46.
- [40] Enhos A, Cosansu K, Huyut MA, et al. Assessment of the Relationship between Monocyte to High-Density Lipoprotein Ratio and Myocardial Bridge. *Arq Bras Cardiol.* 2019; 112 (1): 12-17.
- [41] Ekizler FA, Cay S. A novel marker of persistent left ventricular systolic dysfunction in patients with peripartum cardiomyopathy: monocyte count- to- HDL cholesterol ratio. *BMC Cardiovasc Disord.* 2019; 19 (1):114.
- [42] Demirbas A, Kaya Islamoglu ZG. Can decreased monocyte to HDL-cholesterol ratio be a marker indicating the anti-inflammatory effect of the colchicine in Behcet's disease? A preliminary study. *Dermatol Ther.* 2020; 33(6): e14013.
- [43] Sirin MC, Korkmaz S, Erturan I, et al. Evaluation of monocyte to HDL cholesterol ratio and other inflammatory markers in patients with psoriasis. *An Bras Dermatol.* 2020; 95 (5):575-82.
- [44] Katz JD, Agrawal S, Velasquez M. Getting to the heart of the matter: osteoarthritis takes its place as part of the metabolic syndrome. *Curr Opin Rheumatol.* 2010; 22 (5): 512-19.
- [45] Gkretsi V, Simopoulou T, Tsezou A. Lipid metabolism and osteoarthritis: lessons from atherosclerosis. *Prog Lipid Res.* 2011; 50 (2):133-40.
- [46] Schwager JL, Nevitt MC, Torner J, et al. Is there an association of serum low density lipoprotein, high density lipoprotein or total cholesterol with development of knee osteoarthritis? *Arthritis Care Res (Hoboken).* 2020;10.1002/acr.24455.
- [47] Irshad K, Afzal MN. Comparison of serum lipid levels among patients suffering from osteoarthritis in Pakistan. *Rawal Med J.* 2014; 39(1): 6-9.

Evaluation of the effect of intravenous ibuprofen use on postoperative pain and opioid consumption after abdominoplasty operation

Mustafa Turkoglu¹, Isa Yildiz¹, Ali Gokkaya², Akın Dişikırık¹, Abdullah Demirhan¹

¹Department of Anesthesiology and Reanimation, Bolu Abant İzzet Baysal University, Faculty of Medicine, Bolu, Turkey

²Department of Plastic and Aesthetic Surgery, Bolu Abant İzzet Baysal University, Faculty of Medicine, Bolu, Turkey

ABSTRACT

Aim: Abdominoplasty is a common cosmetic procedure that is one of the most painful aesthetic surgery and has been used increasingly in recent years. Ibuprofen is a non-steroidal anti-inflammatory (NSAID) with antipyretic and analgesic effects. In this study, we aimed to evaluate the effectiveness of the intravenous (IV) form of ibuprofen on postoperative pain control and opioid requirement in patients who underwent abdominoplasty.

Methods: The patients were divided into 3 groups as Group 1 (Tramadol), Group 2 (Ibuprofen) and Group 3 (Tramadol HCL + Ibuprofen). Tramadol HCL was given continuous infusion at a concentration of 4mg / ml via IV Patient Controlled Analgesia to Group 1. Ibuprofen 800 mg IV was administered to Group 2 at 30 minutes before the end of the operation. Patients were followed up by administering 800 mg IV every 6 hours for 24 hours. In Group 3, 30 minutes before the end of the operation, tramadol was administered via PCA with continuous infusion at a concentration of 4mg / ml and 800 mg IV ibuprofen was administered as 4x1.

Results: VAS values were found to be significantly lower in Group 3 compared to Group 2 at every hour and at the 4th hour compared to Group 1. Group 3 was found to be significantly lower than Group 1 in total analgesic consumption in all time zones.

Conclusion: We think that IV ibuprofen, which will be given in addition to tramadol after abdominoplasty, can provide effective analgesia and reduce analgesic consumption.

Key words: Abdominoplasty, postoperative pain, ibuprofen, opioids.

✉ Dr. Isa Yildiz

Department of Anesthesiology and Reanimation, Bolu Abant İzzet Baysal University, Faculty of Medicine, Bolu, Turkey

E- mail: dr.isayildiz@hotmail.com

Received: 2021-09-28

Accepted: 2021-11-15

Published online: 2022-01-01

Introduction

Abdominoplasty surgery is an operation that aims to improve the contour of the abdominal wall by removing excess skin and fat from the abdominal region, rectus sheath plication and

umbilical transposition [1]. Abdominoplasty is one of the most painful procedures in aesthetic surgery and has been used increasingly in recent years [2].

Effective management of postoperative analgesia can prevent many of the complications, such as respiratory, cardiovascular complications, delayed mobilization, and prolonged hospitalization [3]. Safe and effective postoperative pain control for abdominoplasties can result in early mobilization, shorter hospital stay, reduced

hospital costs, quicker return to normal activities, and increased patient satisfaction [4]. Pharmacological and regional methods can be used for pain control after abdominoplasty. Patient-controlled analgesia (PCA), non-steroidal anti-inflammatory drugs (NSAID), opioids, multimodal analgesia are among these methods [5]. Patient-controlled analgesia is a closed-circuit system that allows the patient to self-inject drugs as needed and not exceeding a certain amount. PCA applications in the treatment of postoperative pain are more effective than conventional analgesia methods and are frequently preferred today due to higher patient satisfaction, less sedation, less postoperative complications and positive contributions to the healing process of the patients [6].

Although opioids are widely used in postoperative pain management, they do not block the pain-inflammation relationship [7]. Therefore, non-steroidal anti-inflammatory drugs are used together with opioids for postoperative pain management. NSAIDs block the conversion of arachidonic acid to prostaglandins and inhibit the response of pain receptors to injury [8]. Multimodal analgesia therapy can reduce the total amount of opioids required, and opioid-related side effects can be minimized by effectively treating pain [9]. Ibuprofen is an NSAID with anti-inflammatory, antipyretic and analgesic effects [10]. The oral form of the drug has been used safely for a long time and is one of the most preferred NSAIDs. Ibuprofen has been shown to be effective in the treatment of post-operative pain.

In this study, we aimed to evaluate the effectiveness of the intravenous (IV) form of ibuprofen on postoperative pain control and opioid requirement in patients undergoing abdominoplasty.

Materials and methods

After the approval of Bolu Abant İzzet Baysal University Clinical Studies Ethics Committee dated 04/08/2020 and numbered 2020/190, 60 patients at risk of ASA I-II between the ages of 18-65 who were scheduled for elective abdominoplasty were included in the study.

The patients were divided into 3 groups by the randomized, prospective and closed envelope method. In Group 1 (Tramadol), Tramadol HCL (Tramosel 100 mg / 2 ml Haver Pharma Drugs Inc, Istanbul) was given continuous infusion at a concentration of 4mg / ml via IV Patient Controlled Analgesia. Doses that could be administered 20 mg of tramadol HCL at each push with a lock-in interval of 20 minutes were adjusted. The patient was instructed to press the button whenever he had pain. In Group 2, 800 mg IV Ibuprofen (Dorifen 800mg/8ml VEM Drugs Inc., Turkey) was administered 30 minutes before the end of the operation. Patients were followed up by administering 800 mg IV every 6 hours for 24 hours. In Group 3 (Ibuprofen + Tramadol), 30 minutes before the end of the operation, tramadol was administered via PCA at a concentration of 4mg/ml with continuous infusion and 20 mg tramadol HCL doses per press were adjusted with a 20-minute locking interval. The patient was instructed to press the button whenever he had pain. In addition, 800 mg IV ibuprofen was administered as 4 times every 6 hours.

The patients were taken to the operating room and their electrocardiography (ECG), heart rate (HR), non-invasive blood pressure (NIBP) and peripheral oxygen saturation (SpO₂) values were monitored. Peripheral vascular access was established with an 18-gauge intravenous cannula. In the induction of anesthesia, 2 mg/kg of propofol (Propofol Lipuro %1 ampoule, B.Braun, Melsungen, Germany), 1mcg/kg of fentanyl (Fentanyl amp 0,05 mg/ml, Jansenn,

Belgium), 0.5 mg/kg of rocuronium (Esmeron flk 50 mg/5 ml) were given intravenously to induce unconsciousness and muscle relaxation, and then the patients were intubated. Anesthesia was maintained with Desflurane 6-7% (Suprane Liquid, Baxter, USA) + 50% oxygen + 50% air. According to the randomization result in Group 1 (Tramadol), Tramadol HCL was given continuous infusion at a concentration of 4mg / ml via IV Patient Controlled Analgesia. Doses that could be administered 20 mg of tramadol HCL at each push with a lock-in interval of 20 minutes were adjusted. The patient was instructed to press the button whenever he had pain. In Group2 800 mg IV ibuprofen was administered 30 minutes before the end of the operation. Patients were followed up by administering 800 mg IV every 6 hours for 24 hours. The 800 mg IV ibuprofen was administered as 4 times every 6 hours. In Group 3 (Ibuprofen + Tramadol), 30 minutes before the end of the operation, tramadol was administered via PCA at a concentration of 4mg/ml with continuous infusion and 20 mg tramadol HCL doses per press were adjusted with a 20-minute locking interval. The patient was instructed to press the button whenever he had pain. In addition, 800 mg IV ibuprofen was administered 4 times every 6 hours.

At the end of the operation, 0.01-0.02 mg/kg atropine and 0.04-0.08 mg/kg neostigmine were administered for muscle relaxant antagonization, and all patients were admitted to the postoperative anesthesia care unit (PACU) after extubation.

Patients with hypersensitivity to the drugs to be used in the study or to the substances in their composition, pregnant women, patients with severe cardiac, pulmonary, hepatic and renal disease, patients with a history of chronic opioid use and chronic pain syndrome, patients with low socio-cultural and mental capacities,

who cannot apply patient-controlled analgesia was excluded from the study. Demographic data (gender, age, weight, height, BMI, comorbidities) of all patients were recorded before the surgical procedure. Postoperative SAP, DAP, MAP, HR, VAS values at 30 minutes, 1st hour, 2nd hour, 4th hour, 8th hour, 12th hour, 18th hour and 24th hour; tramadol consumption, nausea, vomiting, and patient satisfaction at 0-1, 1-12, 12-24 hours were evaluated and recorded. Patients with nausea and vomiting were treated with ondansetron (ZOFTRAN ampoule IV 8mg/4mg/ml GlaxoSmithKline SpA, Italy) and, patients with rash and itching were treated with Pheniramine hydrogen maleate (Avil ampoule IM/IV 45.5 mg/2 ml Sandoz İlaç San. ve Tic. A.Ş. Turkey). When the VAS was above 4, 0.05 mg/kg morphine (Morphine HCL® 0.01 g/ml amp Galen İlaç AŞ./ Turkey) in 100 ml saline was administered intravenously as a rescue analgesic.

Statistical analyses

The information collected from the patients was entered into the SPSS 21.0 package program and statistical analyzes were made. Descriptive statistics of the variables (Frequency, Percentages, Mean \pm Standard Deviation, Median (interquartile range) were presented with tables. Three group comparisons were performed with one-way ANOVA test. Pairwise comparisons were continued with the post-hoc Bonferroni pairwise comparison test. For parametric repeated measures, repeated measures ANOVA test was applied.

Three group comparisons were performed with the Kruskal Wallis H test. For those with significant differences between the groups, pairwise comparisons were continued with Dunn-Bonferoni paired comparison test in order to determine which group the difference originated from.

Pearson Chi-Square test or Fisher's exact test was used to compare categorical variables.

Value of $p < 0.05$ was considered statistically significant. Data lists for each group were summarized with summary statistics.

Results

60 patients were included in the study. However, 8 patients whose operation was postponed due to the Covid-19 pandemic and 5 patients who were re-operated due to postoperative complications were excluded from the study. The study was completed with 47 patients, including 16 patients in Group 1, 16 patients in Group 2, and 15 patients in Group 3. There was no statistically significant difference between the groups in terms of age, weight, height, BMI, duration of surgery, duration of

anesthesia, ASA classification score ($p > 0.05$) (Table 1).

When the resting VAS scores were compared, the resting VAS scores at each hour were found to be statistically significantly lower in Group 3 compared to Group 2 ($p < 0.05$). The resting VAS score at the 4th hour in Group 3 was found to be statistically significantly lower compared to Group 1 ($p < 0.001$). Resting VAS scores at the 8th, 12th, 16th, 20th and 24th hours were found to be statistically significantly lower in Group 1 compared to Group 2 ($p < 0.001$) (Figure 1). When tramadol consumption amounts were examined, it was determined that the amount of tramadol consumed in Group 3 was statistically lower in 0-1, 1-12, 12-24 hours and total consumption compared to Group 1 ($p < 0.05$) (Figure 2).

Table 1. Comparison of the parameters of the groups.

Variables	Group 1 (Tramadol)	Group 2 (Ibuprofen)	Group 3 (Ibuprofen + Tramadol)	p-value
Gender				
Female	14 (%87,5)	13 (%18,8)	10 (%)	0,35
Male	2 (%12,5)	3 (%81,3)	5 (%33,3)	
Age	42,75±13,17	40,13±11,13	38,13±7,88	0,508
Weight (kg)	80,44±10,87	80,25±16,45	82,33±13,39	0,898
Height (cm)	159±4	161±6	162±6	0,817
BMI (kg/m²)	31,1±4,25	30,67±4,67	31,26±3,98	0,923
ASA score				
1/2	6-10	10-6	9-6	0,212
Duration of anesthesia (min.)	181,56±33,25	163,44±51,63	190,33±28,88	0,223
Duration of surgery (min.)	164,38±34,25	147,5±51,41	172±29,14	0,127

Values: n=number of patients, n (%), given as average ± standard deviation. BMI: Body Mass Index

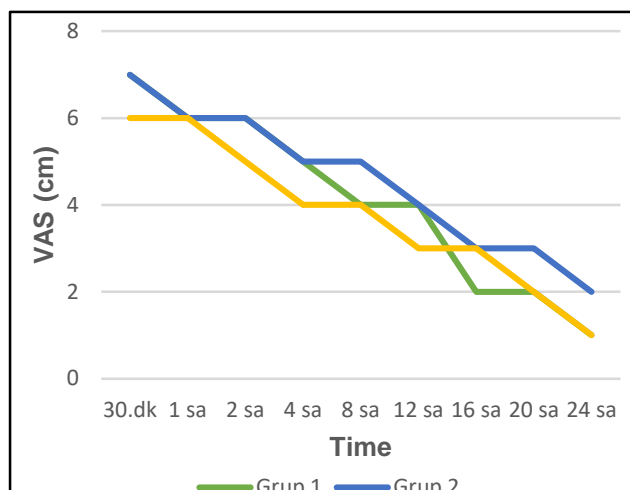


Figure 1. Resting VAS scores of the groups.

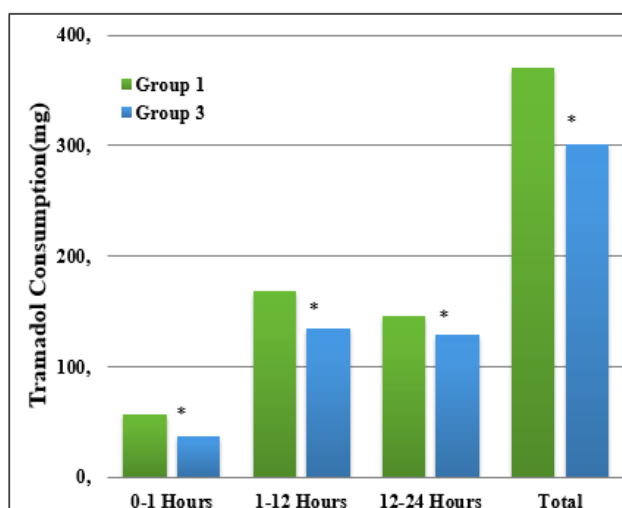


Figure 2. Tramadol Consumption Amount (mg).
*Statistically significant difference at $p < 0.05$ significance level according to independent groups *t*-test.

There was no statistically significant difference between the groups in terms of the use of morphine as a rescue analgesia ($p > 0.05$). In terms of side effects, nausea was seen at a rate of 6.3% in the ibuprofen group, and at a rate of 50% in the tramadol group and 40% in the group in which tramadol and ibuprofen were administered together. When this rate was compared between the groups, it was found to be statistically lower in Group 2 compared to Group 1 and Group 3 ($p < 0.05$).

Discussion

This study showed that; Tramadol and IV ibuprofen given as analgesics after abdominoplasty operation alone can provide analgesia by reducing the postoperative VAS values. However, when tramadol and IV ibuprofen are used together, they provide analgesia by reducing VAS values more effectively and lead to less opioid consumption. In addition, the frequency of nausea and vomiting in IV ibuprofen administered patients is less than in opioid administered patients.

Abdominoplasty is one of the most painful procedures in plastic surgery. In recent years, the number of operations due to reconstruction after obesity and aesthetic reasons has been increasing. Moderate to severe pain lasting longer than 24 hours can be seen, usually due to the need for extensive tissue mobilization, folding of the smooth abdominal muscles for deformities of the myoaponeurotic layer, and intense liposuction [11]. If pain is not adequately controlled, it can lead to heart, lung and kidney problems due to metabolic, endocrine and inflammatory responses. In addition, it may lead to deterioration in patient comfort, delayed mobilization, prolongation of hospital stay and increased cost [12]. Traditional postoperative pain management often uses opioids. Although opioids provide satisfactory relief of moderate to severe pain, there are risks of respiratory depression, sedation, nausea, vomiting, constipation and addiction [13,14]. Therefore, clinical guidelines recommend multimodal analgesia, which includes reducing the dose and duration of opioid use, plus the use of non-opioid analgesics [14,15]. Ibuprofen is an NSAID drug that is frequently used as a part of multimodal analgesia, especially in the treatment of low and moderate pain. Compared to other NSAIDs,

ibuprofen has a COX-1/COX-2 inhibition ratio of less than one. In this way, ibuprofen has a lower side-effect profile. With the widespread use of the IV form of ibuprofen, it has gained an important place among the agents used in postoperative analgesia [16]. The recommended dose of IV ibuprofen is 400-800 mg every six hours. The maximum daily dose is 3200 mg [17]. Kroll et al. investigated the postoperative analgesic efficacy of IV ibuprofen in 319 patients undergoing abdominal hysterectomy. They reported that it provided more effective analgesia and faster ambulation time, was well tolerated and safe in the group given 800 mg every 6 hours [18]. Martinez et al. investigated the efficacy and safety of IV ibuprofen in the treatment of postoperative pain in 206 patients undergoing abdominal and orthopedic surgery. They found that there was a significant decrease in VAS scores and total morphine consumption in the group in which ibuprofen was added as a part of multimodal analgesia compared to the group that was given only morphine. They reported that the use of 800 mg IV ibuprofen every 6 hours in patients who will undergo abdominal surgery reduces morphine consumption and pain scores, reduces opioid-related side effects, and can be used effectively and safely [10]. Minkowitz et al. evaluated tramadol and morphine in terms of postoperative analgesia and side effect profile in their study, which included 370 patients who had abdominoplasty operation. When the postoperative analgesia and side effects were examined, they reported that the incidence of opioid-related side effects was lower in the tramadol group in terms of side effects with similar analgesic effects [19]. In our study, we preferred tramadol because of its similar analgesic effect and low side-effect profile. We found that VAS values were lower

in the group that added ibuprofen to tramadol, similar to other studies. At the same time, we found that the addition of ibuprofen to the opioid reduced the frequency of side effects.

As a result; we believe that adding IV form of ibuprofen to opioids as part of multimodal analgesia provides adequate analgesia, reducing total opioid consumption and the incidence of opioid-related side effects.

Funding: *The author(s) received no financial support for the research, authorship, and/or publication of this article.*

Conflict of Interest: *The authors declare that they have no conflict of interest.*

Ethical statement: *The study was approved by Bolu Abant İzzet Baysal University Clinical Studies Ethics Committee. (Date and number: 04/08/2020 and 2020/190).*

Open Access Statement

This is an open access journal which means that all content is freely available without charge to the user or his/her institution under the terms of the Creative Commons Attribution Non-Commercial License (<http://creativecommons.org/licenses/by-nc/4.0>). Users are allowed to read, download, copy, distribute, print, search, or link to the full texts of the articles, without asking prior permission from the publisher or the author.

Copyright (c) 2021: Author (s).

References

- [1]Friedland JA, Maffi TR. MOC-PS(SM) CME article: Abdominoplasty. *Plast Reconstr Surg.* 2008;121(4 Suppl):1-11.
- [2]Abo-Zeid MA, Al-Refaey AK, Zeina AM. Surgically-assisted abdominal wall blocks for analgesia after abdominoplasty: A prospective randomized trial. *Saudi J Anaesth.* 2018;12(4):593-98.

- [3] American Society of Anesthesiologists Task Force on Acute Pain Management. Practice guidelines for acute pain management in the perioperative setting: an updated report by the American Society of Anesthesiologists Task Force on Acute Pain Management. *Anesthesiology*. 2004;100(6):1573-81.
- [4] Morales R Jr, Mentz H 3rd, Newall G, et al. Use of abdominal field block injections with liposomal bupivacaine to control postoperative pain after abdominoplasty. *Aesthet Surg J*. 2013;33(8):1148-53.
- [5] Kurşun YZ, Yıldız F, Kaymaz Ö, et al. Ağrılı kanser hastalarının tedavisinde analjezik basamak tedavisinin yeri [Analgesic step ladder treatment in cancer patients with pain]. *Agri*. 2015;27(1):26-34.
- [6] Hanna MN, Murphy JD, Kumar K, et al. Regional techniques and outcome: what is the evidence?. *Curr Opin Anaesthesiol*. 2009;22(5):672-77.
- [7] Rathmell JP, Wu CL, Sinatra RS, et al. Acute post-surgical pain management: a critical appraisal of current practice, *Reg Anesth Pain Med*. 2006;31(4):1-42.
- [8] Svensson CI, Yaksh TL. The spinal phospholipase-cyclooxygenase-prostanoid cascade in nociceptive processing. *Annu Rev Pharmacol Toxicol*. 2002;42:553-83.
- [9] Kehlet H, Dahl JB. The value of "multimodal" or "balanced analgesia" in postoperative pain treatment. *Anesth Analg*. 1993;77(5):1048-56.
- [10] Gago Martínez A, Escontrela Rodriguez B, Planas Roca A, et al. Intravenous Ibuprofen for Treatment of Post-Operative Pain: A Multicenter, Double Blind, Placebo-Controlled, Randomized Clinical Trial. *PLoS One*. 2016;11(5):e0154004.
- [11] Hurvitz KA, Olaya WA, Nguyen A, et al. Evidence-based medicine: Abdominoplasty. *Plast Reconstr Surg*. 2014;133(5):1214-21.
- [12] Kubra Turkoglu, Isa Yildiz, Kutay Engin Ozturan, et al. Comparison of Analgesic Effects of Pure Bupivacaine and Morphine Added as Bupivacaine Adjuvant in USG Guided Adductor Canal Block Following Total Knee Arthroplasty. *EJMI* 2020;4(3):327-31.
- [13] Stein C. New concepts in opioid analgesia. *Expert Opin Investig Drugs*. 2018;27(10):765-75.
- [14] Singla NK, Skobieranda F, Soergel DG, et al. APOLLO-2: A Randomized, Placebo and Active-Controlled Phase III Study Investigating Oliceridine (TRV130), a G Protein-Biased Ligand at the μ -Opioid Receptor, for Management of Moderate to Severe Acute Pain Following Abdominoplasty. *Pain Pract*. 2019;19(7):715-31.
- [15] Wardhan R, Chelly J. Recent advances in acute pain management: understanding the mechanisms of acute pain, the prescription of opioids, and the role of multimodal pain therapy. *F1000Res*. 2017;6:2065.
- [16] Erdogan Kayhan G, Sanli M, Ozgul U, et al. Comparison of intravenous ibuprofen and acetaminophen for postoperative multimodal pain management in bariatric surgery: A randomized controlled trial. *J Clin Anesth*. 2018 ;50:5-11.
- [17] Southworth S, Peters J, Rock A, et al. A multicenter, randomized, double-blind, placebo-controlled trial of intravenous ibuprofen 400 and 800 mg every 6 hours in the management of postoperative pain. *Clin Ther*. 2009;31(9):1922-35.
- [18] Kroll PB, Meadows L, Rock A, et al. Multicenter, randomized, double-blind,

placebo-controlled trial of intravenous ibuprofen (i.v.-ibuprofen) in the management of postoperative pain following abdominal hysterectomy. *Pain Pract.* 2011 11(1):23-32.

- [19] Minkowitz H, Salazar H, Leiman D, et al. Intravenous Tramadol is Effective in the Management of Postoperative Pain Following Abdominoplasty: A Three-Arm Randomized Placebo- and Active-Controlled Trial. *Drugs R D.* 2020;20(3):225-36.

The association between postoperative corneal edema and phacoemulsification level

Enes Uyar 

Department of Ophthalmology, Aksaray Training and Research Hospital, Aksaray University, Aksaray, Turkey

ABSTRACT

Aim: To evaluate the effect of phacoemulsification level on postoperative central corneal thickness (CCT) differences and to assess the effects of demographic characteristics, biometric values and surgical parameters of patients on postoperative corneal edema.

Methods: This prospective study included 232 eyes of 232 patients who underwent phacoemulsification surgery. Biometric values, phacoemulsification time, phacoemulsification power and effective phacoemulsification time (EPT) were evaluated. CCT measurements were repeated at follow-ups on days 1, 7 and 30 after surgery. Phaco-chop technique was performed in all patients and phacoemulsification level changes that occurred during surgery were recorded. Patients were grouped as Group 1: >75% of lens nucleus emulsified in capsular bag; Group 2: >75% of lens nucleus emulsified in iris plane; and Group 3: >50% of lens nucleus emulsified in anterior chamber.

Results: Increase in the mean CCT values on the first day (incCCT1) and at the first week after surgery were more pronounced in Group 3 as compared with both Groups 1 and 2 ($p < 0.05$ for all). In addition, incCCT1 was higher in Group 2 than Group 1 ($p=0.040$). In the final model of multiple linear regression ($R^2=0.31$), it was determined that EPT, aqueous depth (AD) and phacoemulsification level significantly affected incCCT1 (p range: <0.001 to 0.009).

Conclusions: The present study showed that more anterior phacoemulsification levels than the capsular bag caused higher CCT increase postoperatively. In addition, AD, EPT and phacoemulsification level were found as the most significant factors that influence postoperative corneal edema.

Key words: Central corneal thickness, corneal edema, phacoemulsification level, surgery.

✉ Dr. Enes Uyar

Department of Ophthalmology, Aksaray Training and Research Hospital, Aksaray University, Aksaray, Turkey

E-mail: enuyar@gmail.com

Received: 2021-10-26 / Revisions: 2021-11-24

Accepted: 2021-12-04 / Published online: 2022-01-01

Introduction

Currently, phacoemulsification surgery is being routinely used to treat cataract [1-3]. Although this is a safe and effective procedure, ultrasound energy used during the surgery can damage the corneal endothelium, and endothelial cell loss (ECL) can cause corneal edema [4-6]. Although

corneal edema is generally transient and mild, it cannot be recovered in some cases involving excessive ECL [6-8]. Several factors that may affect postoperative corneal edema have been proposed such as phacoemulsification time, manipulation of devices, nucleus hardness, surgery technique, surgeon experience, fluid and vacuum dynamics, Descemet's membrane detachment, and baseline endothelial cell count [5-7,9]. Another factor that may affect postoperative corneal edema and ECL is the depth of phaco probe in the anterior segment while the lens nucleus is emulsified. This factor

has been termed as “phacoemulsification level” in this study. When phacoemulsification level approaches the endothelium, the harmful effect of ultrasound energy on the endothelium may increase [5,10,11]. Previous studies that did not use the ophthalmic viscoelastic device (OVD) demonstrated higher ECL in anterior chamber phacoemulsification [12,13]. Koch et al. [14] have also found that iris plane phacoemulsification causes more ECL than the posterior chamber phacoemulsification even if OVD is used. In contrast, there is no considerable difference in postoperative central corneal thickness (CCT) between the pure posterior chamber techniques and some supracapsular techniques that involve more maneuvers and phacoemulsification in the anterior chamber [4,15].

The surgical technique during the phacoemulsification procedure may require modification owing to several factors such as patient compliance, surgeon comfort, intraoperative pupil changes, anterior chamber dynamics, diameter of the capsulorhexis, prolapses of the lens to the anterior chamber during hydrodissection, catch of the nuclear fragments by OVD in the anterior chamber, avoiding posterior capsule rupture, and surgeon experience. Therefore, phacoemulsification level may change during surgery when the same surgical technique is used. The present study aimed to determine the effect of phacoemulsification level changes occurring during the surgery on postoperative CCT differences. In addition, the effect of demographic characteristics, biometric values, and surgical parameters of patients on postoperative corneal edema was evaluated.

Materials and methods

The present study was designed on a prospective pattern, and it was performed on

232 consecutive patients who were operated in Ophthalmology Clinic between October 3, 2019 and December 31, 2020. Informed consent was obtained from all participants. The study was conducted with the approval of Aksaray University Ethical Committee in accordance with the Helsinki Declaration (Protocol number: 2019/10-02).

All patients underwent complete ophthalmologic examinations preoperatively, including best corrected visual acuity assessment, slit-lamp and fundus examinations, and intraocular pressure (IOP) measurement. Nuclear sclerosis was evaluated clinically according to the Lens Opacities Classification System 3. Biometric parameters, aqueous depth (AD), axial length (AL), lens thickness (LT), and pupil diameter measurements after full dilatation were evaluated using a low-coherence optical biometry device (Haag-Strait Diagnostics Biometer LS-900; Haag-Strait AG, Switzerland). Scheimpflug imaging instrument (Sirius, Costruzione Strumenti Oftalmici, and Florence, Italy) was used to evaluate CCT. Ophthalmologic examinations, CCT, and IOP measurements were repeated after surgery on day 1, 7, and 30. Measurements were performed by an experienced examiner who was blinded to the surgical data of patients.

The inclusion criteria were as follows: NO3 NC3 or NO4 NC4 grade senile cataract according to LOCS scale, best corrected visual acuity of lower than 10/20 with the decimal notation, age above 40 years, not having an acute or chronic eye disease (glaucoma, uveitis, diabetic retinopathy, etc.) and no previous ophthalmological surgery history. The exclusion criteria were as follows: preexisting corneal pathology, i.e. cornea guttata, corneal dystrophy, corneal degenerations and other corneal inflammations, pseudoexfoliation syndrome, using iris hooks during surgery

because of small pupil and any eye pathology preventing preoperative and postoperative measurements. Patients who developed intraoperative complications were also excluded from the statistical analysis.

The same surgeon (EU) performed all operations using the same phacoemulsification machine (OS4, Oertli Instrumente AG, Berneck, Switzerland). Preoperatively, tropicamide 1%, cyclopentolate hydrochloride 1.0%, and phenylephrine hydrochloride 2.5% eye drops were applied to ensure full pupil dilatation. Before the operation, proparacaine hydrochloride 0.5% eye drops were topically administered for topical anesthesia. After 5% povidone iodine solution was instilled to the conjunctival sac, the periocular skin was cleaned with 10% povidone iodine. The eye was covered with a sterile drape and opened with a lid speculum. Paracenteses were performed both temporally and nasally, and sodium hyaluronate 2.0% (Protectalon[®]) OVD was injected into the anterior chamber. Clear corneal main incision was made with a 2.75 mm blade at 11 o'clock position. Then, a continuous curvilinear capsulorhexis (approximately 5.5 - 6 mm diameter) and hydrodissection were completed. After the central cortical and epinuclear materials were removed, the phaco tip was buried with burst energy mode (50% cycle, 30 msec length) into the superior part of nucleus, and occlusion was performed under a high vacuum setting (400 mmHg). The bottle height was 90 cm. A chopper was placed underneath the anterior capsule at 6 o'clock position and moved through the phaco tip to crack the nucleus initially. After the first crack, the chopper and phaco tip were moved in opposite directions to separate the nuclear halves. Then, the nucleus was rotated, and half of it was impaled by the phaco tip. Chopping was performed, and the first free nuclear piece

was emulsified. This process was repeated under the same energy and vacuum settings in the capsular bag as much as possible until the nuclear material was completely consumed. If the moving lens fragments were emulsified closer to the anterior chamber than the capsular bag, the changes in phacoemulsification level were recorded. Patients were classified into three groups according to the percentage of lens nucleus emulsified at a particular phacoemulsification level (Table 1). Patients who did not meet any of the group criteria were excluded from the study.

Table 1. Group classification according to phacoemulsification level.

Group 1	75%–100% of the lens nucleus was emulsified in the bag, 0%–25% of the lens nucleus was emulsified in the iris plane.
Group 2	75%–100% of the lens nucleus was emulsified in the iris plane, 0%–25% of the lens nucleus was emulsified in the anterior chamber or in the bag.
Group 3	50%–75% of the lens nucleus was emulsified in the anterior chamber, 25%–50% of the lens nucleus was emulsified in the iris plane.

Epinucleus was cleared with low vacuum and ultrasound power settings. Cortex removal was performed by bimanual irrigation/aspiration. After all lens materials were cleared, sodium hyaluronate 1.4% (Protectalon[®]) OVD was injected into the capsular bag. Same foldable one-piece hydrophobic acrylic intraocular lens (Sensar AR40, AMO, Mineapolis, USA) was inserted to each patient. Then OVD was removed from anterior and posterior chamber

and corneal incisions were closed by stromal hydration without any suturing. At the end of surgery, intracameral cefuroxime 1mg/0.1 ml was applied and corneal incisions were checked in order to ensure that there was no leakage.

The phacoemulsification time (s), phacoemulsification power (%), and effective phacoemulsification time (EPT) were recorded. EPT was computed as follows: $\text{phacoemulsification time} \times \text{phacoemulsification power}/100$. Total operation time was calculated as the time between the opening of the first paracentesis and the closure of corneal incisions by stromal hydration. Postoperatively, patients were treated with moxifloxacin 0.5% and dexamethasone 0.1% eye drops 6 times daily for 1 week, after which only dexamethasone 0.1% was instilled over 3 weeks with a gradually decreasing dosage.

Statistical analyses

All data was analyzed using the SPSS statistical software package, version 24.0 (SPSS Inc., Chicago, IL, USA). Parametric data was compared using analysis of variance (ANOVA), followed by a Tukey's honestly significant difference test for post hoc comparisons, and non-parametric data was compared using the chi-square test. The associations with continuous and categorical variables were assessed using Pearson's and Spearman's-Rho bivariate correlation analyses, respectively. The factors that could affect the central corneal edema on the postoperative first day were evaluated using multiple linear regression analysis. The statistical significance level was set at $p < 0.05$. Normal distribution of the data was checked by Kolmogorov-Smirnov test. For all of the studied parameters, the p value for the Kolmogorov-Smirnov test was >0.05 .

Results

In total, 232 eyes of 232 patients were included in this study. Of these patients, 129 were male (55.6%) and 103 were female (44.4%), with an average age of 69.8 ± 7.4 years. Of the 232 eyes, 107 (46.1%) were right and 125 (53.9%) were left. Overall, 104 patients had NO3 NC3 (44.8%) and 128 patients had NO4 NC4 (55.2%) cataract. There were 87 patients (37.5%) in Group 1, 79 patients (34.1%) in Group 2, and 66 patients (28.4%) in Group 3. Regarding intraoperative complications, two cases of posterior capsule ruptures without vitreous loss, one of zonular dehiscence, six of small detachments of Descemet's membrane, and two of radial capsulorhexis tears were noted. No postoperative complication was observed during the follow-up.

Biometric and surgical data of patients are provided in Table 2. The mean values of CCT along with mean differences between preoperative CCT (preCCT) and postoperative CCT values of groups are shown in Table 3. There was no difference among the groups in IOP values as well as among IOP differences on days 1, 7, and 30 after surgery ($p > 0.05$ for all). Biometric and surgical data were similar in all groups ($p > 0.05$ for all) (Table 2). There were statistically significant differences between groups in postoperative CCT values on the first day (postCCT1) and postoperative CCT values at the first week ($p < 0.001$ for both). Postoperative CCT values in the first month were not different among the groups ($p = 0.352$) (Table 3).

In post hoc comparisons, an increase in the mean CCT values after surgery on the first day and at the first week were more pronounced in Group 3 than in Group 1 and Group 2 ($p < 0.05$ for all). One month after the surgery, these differences were not statistically significant ($p > 0.05$ for all). In addition, an increase in the

Table 2. Biometric and surgical parameters of the groups.

Parameters		Group 1 (n=87)	Group 2 (n=79)	Group 3 (n=66)	P
Age (years)		69.1 ± 7.7	71.0 ± 7.2	69.9 ± 6.9	0.284*
EPT (sec)		3.8 ± 2.2	3.8 ± 1.5	3.9 ± 1.5	0.992*
Phaco time (sec)		14.0 ± 7.5	14.1 ± 5.7	14.8 ± 5.1	0.862*
Phaco power (%)		28.1 ± 4.9	28.2 ± 5.6	26.3 ± 4.7	0.213*
Total operation time (min)		13.5 ± 2.9	12.8 ± 2.8	12.7 ± 2.3	0.269*
Preoperative IOP (mmHg)		14.1 ± 2.8	14.5 ± 3.7	13.7 ± 3.0	0.436*
AL (mm)		23.5 ± 0.8	23.5 ± 0.9	23.6 ± 1.0	0.869*
AD (mm)		2.8 ± 0.4	2.9 ± 0.4	2.9 ± 0.3	0.422*
LT (mm)		4.4 ± 0.4	4.3 ± 0.4	4.4 ± 0.5	0.817*
PD (mm)		6.9 ± 1.0	6.8 ± 0.9	7.0 ± 1.0	0.600*
NS	Grade 3 n=126	50	39	37	0.494**
	Grade 4 n=106	37	40	29	

*One-way ANOVA, ** Chi-Square test.
AD: Aqueous depth, AL: Axial length, EPT: Effective phacoemulsification time, LT: Lens thickness, NS: Nuclear sclerosis, PD: Pupil diameter with full dilatation.

mean CCT values on the postoperative first day (incCCT1) was higher in Group 2 than in Group 1 ($p = 0.040$).

In the correlation analyses, the factors that could be associated with incCCT1 were as follows: age, sex, EPT, AD, phacoemulsification level, phacoemulsification time, and phacoemulsification power (r range: -0.246 to 0.420 , p range: <0.001 – 0.027). No significant relationship was noted among NS grade, AL, pupil diameter, total operation time, LT, and incCCT1 (r range: -0.121 to 0.131 , p range: 0.093 – 0.950). A multiple linear regression analysis, in which all independent variables were entered into the model simultaneously, was conducted to define independent factors associated with incCCT1. The first model was developed with factors that

were associated with postoperative ECL or corneal edema in previous studies [5,6,9,16]. Next, phacoemulsification level was added into the model. The final multiple linear regression model indicated that EPT, AD, and phacoemulsification level significantly affected incCCT1. The model explained 31% of the variation in incCCT1 and revealed that the effect of phacoemulsification level accounted for 13%.

Discussion

The present study reported that the increase in postoperative CCT values was higher in the anterior chamber phacoemulsification than in the posterior chamber phacoemulsification or the iris plane phacoemulsification. The effect of the anterior chamber phacoemulsification

Table 3. CCT values and postoperative CCT differences of the groups.

Parameters	Group 1 (n=87)	Group 2 (n=79)	Group 3 (n=66)	P
PreCCT (μm)	531.5 \pm 27.4	534.3 \pm 29.0	540.2 \pm 25.3	0.322*
PostCCT1 (μm)	573.7 \pm 35.6	594.7 \pm 45.4	627.2 \pm 56.3	<0.001*
PostCCT7(μm)	545.8 \pm 33.8	545.0 \pm 32.9	576.6 \pm 45.9	<0.001*
PostCCT30 (μm)	533.1 \pm 27.2	539.8 \pm 29.7	544.2 \pm 25.2	0.352*
PostCCT1-PreCCT (μm)	42.2 \pm 17.3	60.4 \pm 32.7	81.4 \pm 50.3	<0.001*
PostCCT7-PreCCT (μm)	12.0 \pm 11.5	14.2 \pm 13.3	29.9 \pm 28.4	<0.001*
PostCCT30-PreCCT (μm)	1.1 \pm 2.9	1.4 \pm 2.8	3.0 \pm 5.0	0.181*
Percentage of (PostCCT1-PreCCT) / PreCCT (%)	7.9 \pm 3.2	11.3 \pm 6.2	15.3 \pm 9.6	<0.001*
Percentage of (PostCCT7-PreCCT) / PreCCT (%)	2.3 \pm 2.2	2.7 \pm 2.5	5.5 \pm 5.1	0.002*
Percentage of (PostCCT30-PreCCT) / PreCCT (%)	0.2 \pm 0.6	0.3 \pm 0.5	0.5 \pm 0.9	0.198*

*One-way ANOVA. PostCCT1: Central corneal thickness on postoperative first day, PostCCT7: Central corneal thickness at postoperative first week, PostCCT30: Central corneal thickness on postoperative first month, PreCCT: Preoperative central corneal thickness.

persisted for more than a week. In addition, AD, EPT, and phacoemulsification level were factors significantly affecting incCCT1. Recent studies have revealed that anterior chamber phacoemulsification or supracapsular techniques can be used safely and have certain advantages [4,15,17-19]. Hwang et al. [4] compared the retro-chop and stop-and-chop techniques according to the postoperative ECL and CCT increase. In the retro-chop group, phacoemulsification was performed in the iris plane, which resulted in lower ECL than in the stop-and-chop group. The authors have proposed that reduced phacoemulsification time used in the retro-chop group caused less ECL. In addition, Alio et al. [17] found no difference in postoperative CCT and ECL between the stop-and-chop and the phaco-out groups, in which phacoemulsification was

performed entirely in the anterior chamber. The authors have attributed these findings in the phaco-out group to the use of copious dispersive OVD [17]. However, clinical examinations revealed that the corneal edema was more pronounced in the phaco-out group during the postoperative first 2 weeks [17]. In the half-moon technique used by Can et al. [18], the lens nucleus was prolapsed at the supracapsular level at the start of the operation; after the first crack, it was pushed back into the capsular bag. The authors suggested that the half-moon technique can be used as safely as posterior phacoemulsification strategies. However, the CCT values on the first day after surgery were higher in the half-moon group, even though EPT was less than the stop-and-chop group. The authors attributed this difference to the fact that chopping was

performed closer to the corneal endothelium at the beginning of the surgery [18]. In contrast, Kosrirukvongs et al. [20] found that the ECL percentage in postoperative first week was significantly higher in the chip-and-flip group (21%) than in the divide-and-conquer group (12.6%). The authors did not detect a difference in mean postoperative CCT values between two groups; however, CCT values on the postoperative first day were not evaluated in this study. The authors specified that more surgical trauma occurred in the chip-and-flip group, even though OVD was used to protect the corneal endothelium [20]. Likewise, Koch et al. [14] deduced that iris plane phacoemulsification caused more endothelial injury than posterior chamber phacoemulsification, particularly when cohesive OVD was used instead of dispersive OVD. Although different phacoemulsification techniques have been thoroughly compared in above mentioned studies, the present study assessed the effect of possible phacoemulsification level changes on postoperative corneal edema while the same technique is used. The phaco-chop technique was used for nuclear fragmentation in all patients, and we observed that phacoemulsification performed at levels closer to the anterior chamber than the capsular bag lead to more corneal edema. In regression analyses, the phacoemulsification level of Group 3 had the most significant effect on inducing incCCT1, whereas that of Group 1 resulted in significantly reduced incCCT1.

In previous studies that investigated similar preoperative and intraoperative factors, phacoemulsification time, phacoemulsification power, age, AL, NS grade, pupil diameter, total infusion volume, implanted IOL type, surgeon experience and total operation time were found to be determinants of postoperative corneal

edema [3,5,6,9,16,21]. In this study, however, we detected that AL did not have a remarkable effect on corneal edema whereas AD values were negatively correlated with postoperative CCT increase. Several studies suggested that the phacoemulsification closer to corneal endothelium might have much harmful effect on cornea, however no significant association between AD and postoperative ECL was found [5,11,16]. Walkow et al. [5] have explained their results by the deepening of anterior chamber during surgery. O'brien et al. [16] have attributed the lack of association between shallow anterior chamber and ECL to the contribution of reduced wound leakage during surgery. This difference might be due to the non-use of dispersive OVD which caused the effect of shallow AD on corneal edema to become more pronounced [11,14,22]. Another reason of dissimilar results might be the differences in bottle heights or total infusion volumes.

Many studies have reported an association between phacoemulsification time and postoperative corneal edema or ECL [5,6,16,21,23,24].

Likewise, phacoemulsification time and EPT were significantly related with incCCT1 in the present study. Several mechanisms have been proposed how ultrasound energy may damage corneal endothelium [23,25,26]. Moreover, it has been shown that NS grade might affect corneal edema by increasing EPT [5,9]. In the present study, the absence of a significant relationship between LT or NS grade and incCCT1 may be caused by the inclusion of only grade NO3 NC3 and NO4 NC4 cataracts. The literature may have possible explanations for the different results observed regarding the factors affecting affect corneal edema. Firstly, there were differences in measurement devices, evaluated postoperative parameters, surgery

techniques, phaco machines, OVD types, surgeon experience, and methods used in the studies. Additionally, many intraoperative dynamics such as bottle height, total infusion volume, and wound leakage might yield different results in studies that evaluated how preoperative biometric parameters of patients affect the corneal damage. Especially, the type and amount of OVD used during surgery might affect the relationship between AD, AL, EPT, NS grade, and postoperative corneal edema or ECL. The regression model of the present study explained 31% of the variation in incCCT1; thus, there may be other factors influencing incCCT1, which could not be identified by regression models. These factors include OVD types, baseline endothelium cell count, surgeon experience, total infusion volume, and phaco tip position [3,5,6,9,11,16,22-24].

The present study possesses the following limitations: CCT values could have been measured in earlier hours postoperatively and follow-ups could have been arranged more frequently. The durations of surgery steps were not calculated separately. The surgeon observed the percentage of emulsified lens nucleus during surgery to decide the phacoemulsification level. This method can be criticized as not being objective enough. Few possible predictors of the postoperative corneal edema such as total infusion volume, the amount of OVD used, the position of phaco tip, and baseline endothelium cell count were not evaluated. One more limitation of the study is that only CCT measurements were used to evaluate the effect of phacoemulsification procedure on the corneal edema, and postoperative ECL was not assessed. However, previous studies have suggested that CCT measurements have greater availability, accuracy, and importance clinically to reveal endothelial damage [6,18]. In addition, a

significant correlation has already been observed between the increase in CCT and ECL after surgery [8,27,28]. In contrast, the present study has certain advantages. The effect of phacoemulsification level on the cornea was evaluated objectively with the contribution of standardized variables, i.e., nuclear fragmentation technique, NS grade, used OVD, surgeon, and phaco machine. In addition to these, as the phacoemulsification time, phacoemulsification power, demographic, and biometric parameters of the groups were similar, the effect of phacoemulsification level could be evaluated independently. Furthermore, the study method could adequately represent cataract surgery practice, because phacoemulsification level changes were evaluated during live surgery.

Conclusion

In conclusion, the current study showed that phacoemulsification levels closer to the anterior chamber than the capsular bag resulted in more negative effect on the cornea. Moreover, this effect might continue longer than 1 week. Thus, phacoemulsification in the capsular bag may be safer for the corneal endothelium and can still be a primary choice in routine cataract cases. At the same time, advances in modern surgical techniques and instruments have made supracapsular techniques, which have a relatively shorter learning curve, more preferable, especially in cases such as zonular dehiscence, lens subluxation, hard cataracts with posterior plate, small pupil, and advanced pseudoexfoliation. However, if more than half of the lens nucleus is to be emulsified in the anterior chamber, abundant use of dispersive OVD is strongly recommended.

Funding: The author(s) received no financial support for the research, authorship, and/or publication of this article.

Conflict of Interest: The authors declare that they have no conflict of interest.

Ethical statement: The study was conducted with the approval of Aksaray University Ethical Committee in accordance with the Helsinki Declaration (Protocol number: 2019/10-02).

Open Access Statement

This is an open access journal which means that all content is freely available without charge to the user or his/her institution under the terms of the Creative Commons Attribution Non-Commercial License (<http://creativecommons.org/licenses/by-nc/4.0>). Users are allowed to read, download, copy, distribute, print, search, or link to the full texts of the articles, without asking prior permission from the publisher or the author.

Copyright (c) 2021: Author (s).

References

- [1] Linebarger EJ, Hardten DR, Shah GK, et al. Phacoemulsification and modern cataract surgery. *Surv Ophthalmol.* 1999;44(2):123-47.
- [2] Olson RJ, Mamalis N, Werner L, et al. Cataract treatment in the beginning of the 21st century. *Am J Ophthalmol.* 2003;136(1):146-54.
- [3] Wong T, Hingorani M, Lee V. Phacoemulsification time and power requirements in phaco chop and divide and conquer nucleofractis techniques. *J Cataract Refract Surg.* 2000;26(9):1374-78.
- [4] Hwang HS, Lee JH, Jeon SJ, et al. Stop-Chop versus Retro-Chop Nucleotomy During Phacoemulsification. *Curr Eye Res.* 2016;41(11):1454-59.
- [5] Walkow T, Anders N, Klebe S. Endothelial cell loss after phacoemulsification: relation to preoperative and intraoperative parameters. *J Cataract Refract Surg.* 2000;26(5):727-32.
- [6] Lhuillier L, Jeancolas AL, Renaudin L, et al. Impact of Ophthalmic Surgeon Experience on Early Postoperative Central Corneal Thickness After Cataract Surgery. *Cornea.* 2017;36(5):541-45.
- [7] Sharma N, Singhal D, Nair SP, et al. Corneal edema after phacoemulsification. *Indian J Ophthalmol.* 2017;65(12):1381-89.
- [8] Lundberg B, Jonsson M, Behndig A. Postoperative corneal swelling correlates strongly to corneal endothelial cell loss after phacoemulsification cataract surgery. *Am J Ophthalmol.* 2005;139(6):1035-41.
- [9] Hayashi K, Hayashi H, Nakao F, et al. Risk factors for corneal endothelial injury during phacoemulsification. *J Cataract Refract Surg.* 1996;22(8):1079-84.
- [10] De Bernardo M, Rosa N. Central corneal thickness measurement after cataract surgery. *Cornea.* 2018;37(4):e19-e20.
- [11] Pereira ACA, Porfirio Jr F, Freitas LL, et al. Ultrasound energy and endothelial cell loss with stop-and-chop and nuclear preslice phacoemulsification. *J Cataract Refract Surg.* 2006;32(10):1661-66.
- [12] Kraff MC, Sanders DR, Lieberman HL. Specular microscopy in cataract and intraocular lens patients: a report of 564 cases. *Arch Ophthalmol.* 1980;98(10):1782-84.
- [13] Sugar J, Mitchelson J, Kraff M. The effect of phacoemulsification on corneal endothelial cell density. *Arch Ophthalmol.* 1978;96(3):446-48.
- [14] Koch DD, Liu JF, Glasser DB, et al. A comparison of corneal endothelial changes after use of Healon or Viscoat during phacoemulsification. *Am J Ophthalmol.* 1993;115(2):188-201.

- [15] Jeancolas A-L, Lhuillier L, Renaudin L, et al. Central corneal thickness assessment after phacoemulsification: Subluxation versus Divide-and-Conquer. *J Fr d'Ophtalmol.* 2017;40(9):744-50.
- [16] D O'Brien P, Fitzpatrick P, Kilmartin DJ, et al. Risk factors for endothelial cell loss after phacoemulsification surgery by a junior resident. *J Cataract Refract Surg.* 2004;30(4):839-43.
- [17] Alió JL, Mulet ME, Shalaby AM, Attia WH. Phacoemulsification in the anterior chamber. *J Cataract Refract Surg.* 2002;28(1):67-75.
- [18] Can İ, Takmaz T, Genç İ. Half-moon supracapsular nucleofractis phacoemulsification: safety, efficacy, and functionality. *J Cataract Refract Surg.* 2008;34(11):1958-65.
- [19] Gross FJ, Garcia-Zalisnak DE, Bovee CE, et al. A comparison of pop and chop to divide and conquer in resident cataract surgery. *Clinical ophthalmology.* 2016;10:1847-51.
- [20] 20. Kosrirukvongs P, Slade SG, Berkeley RG. Corneal endothelial changes after divide and conquer versus chip and flip phacoemulsification. *J Cataract Refract Surg.* 1997;23(7):1006-12.
- [21] Dick HB, Kohlen T, Jacobi FK, et al. Long-term endothelial cell loss following phacoemulsification through a temporal clear corneal incision. *J Cataract Refract Surg.* 1996;22(1):63-71.
- [22] Behndig A, Lundberg B. Transient corneal edema after phacoemulsification: comparison of 3 viscoelastic regimens. *J Cataract Refract Surg.* 2002;28(9):1551-56.
- [23] Faramarzi A, Javadi MA, Karimian F, et al. Corneal endothelial cell loss during phacoemulsification: bevel-up versus bevel-down phaco tip. *J Cataract Refract Surg.* 2011;37(11):1971-76.
- [24] Pirazzoli G, D'Eliseo D, Ziosi M, et al. Effects of phacoemulsification time on the corneal endothelium using phacofracture and phaco chop techniques. *J Cataract Refract Surg.* 1996;22(7):967-69.
- [25] Packer M, Fishkind WJ, Fine IH, et al. The physics of phaco: a review. *J Cataract Refract Surg.* 2005;31(2):424-31.
- [26] Raskin E, Paula JS, Cruz AAV, et al. Effect of bevel position on the corneal endothelium after phacoemulsification. *Arquivos brasileiros de oftalmologia.* 2010;73(6):508-10.
- [27] Cheng H, Bates AK, Wood L, et al. Positive correlation of corneal thickness and endothelial cell loss: serial measurements after cataract surgery. *Archives of ophthalmology.* 1988;106(7):920-22.
- [28] Perone JM, Boiche M, Lhuillier L, et al. Correlation between postoperative central corneal thickness and endothelial damage after cataract surgery by phacoemulsification. *Cornea.* 2018;37(5):587-90.

Does mean platelet volume and neutrophil to lymphocyte ratio increase in primary hyperparathyroidism arising from a single adenoma

Isilay Kalan Sari¹, Serkan Ceylan²

¹Department of Endocrinology and Metabolic Disorders, University of Health Sciences, Antalya Training and Research Hospital, Antalya, Turkey

²Department of General Surgery, University of Health Sciences, Antalya Training and Research Hospital, Antalya, Turkey

ABSTRACT

Aim: Primary hyperparathyroidism (PHP) is commonly caused by adenomas. Studies have shown mild inflammation in PHP and elevated levels of some inflammatory markers to support this. In addition, excess parathyroid hormone (PTH) and calcium (Ca) cause atherosclerosis by disrupting endothelial function. Mean platelet volume (MPV) describes the size and indirect activity of platelets and its value is expected to increase with inflammation and associated atherosclerosis. Neutrophil to lymphocyte ratio (NLR) is another parameter associated with inflammatory response. This study was performed to investigate the MPV and NLR levels in PHP developing from a single parathyroid adenoma.

Method: Patient records from 2016-2021 were retrospectively scanned from the computer system and 40 patients with PHP developing from a single parathyroid adenoma were selected based on exclusion criteria. The values of PTH, Ca, 25-Hydroxyvitamin D, phosphorus, MPV and number of blood cells were recorded. NLR was calculated. The results were compared with the results of 36 healthy controls.

Results: MPV (8.7 ± 0.6 fl and 7.6 ± 0.6 fl, respectively; $p=0.001$) and NLR (2.6 ± 1.7 and 1.7 ± 0.8 , respectively; $p=0.000$) were higher in the PHP group compared to the control group. Ca and PTH correlated positively with MPV ($p=0.003$ and $p=0.000$, respectively) and NLR ($p=0.011$ and $p=0.023$, respectively).

Conclusion: MPV and NLR were found to be higher in patients with PHP developing from a single adenoma than in healthy individuals.

Key words: Mean platelet volume, neutrophil to lymphocyte ratio, primary hyperparathyroidism, parathyroid adenoma, calcium.

✉ Dr. Isilay Kalan Sari

Department of Endocrinology and Metabolic Disorders,
University of Health Sciences, Antalya Training and
Research Hospital, Antalya, Turkey

E-mail: isilaykalan@gmail.com

Received: 2021-05-13 / Revisions: 2021-11-04

Accepted: 2021-12-14 / Published online: 2022-01-01

Introduction

Parathyroid adenomas are the most common cause of primary hyperparathyroidism (PHP)

and are increasingly encountered in clinical practice with increased ultrasound experience and widespread measurement of calcium (Ca), 25-hydroxyvitamin D (25OHD), and parathyroid hormone (PTH). Early diagnosis also allows patients to be caught mostly in the asymptomatic phase. Therefore, clinical studies have focused on investigating whether high PTH and Ca levels cause other pathologies in this group of patients without typical bone and

renal involvement [1-7]. In these studies, the PTH-1 receptor has also been observed outside of bone and kidney which are typical sites of PTH action [3]. Apart from these two regions, the PTH-1 receptor was most frequently detected in the heart and vascular network, which is why the cardiac effects of PTH have begun to be studied [3-7]. These studies showed that PTH exerts chronotropic and inotropic effects on the heart and is a causative factor for left ventricular hypertrophy and hypertension [4,5]. Studies have shown mild inflammation in PHP and increased levels of some inflammatory markers (interleukin-6, high-sensitivity C-reactive protein) supporting this [6,7]. Moreover, excess PTH and Ca cause atherosclerosis by disrupting endothelial function [8,9]. Platelets are involved in the development of inflammation and play a special role in hemostasis and thrombosis [10]. Platelets express and secrete CD40 ligand, which stimulates inflammation in the endothelium, and platelet cytoplasmic granules contain numerous inflammatory products, including leukotrienes, prostaglandins, platelet-activating factor, beta-thromboglobulin, and interleukin-1 [11-13]. MPV describes the size and indirectly the activity of platelets [14]. Therefore, its value is expected to increase in inflammation and associated atherosclerosis, in which platelet activity increases [15-16]. Studies have also supported this idea, and MPV has been found to be increased in chronic inflammatory diseases such as ankylosing spondylitis, rheumatoid arthritis, and inflammatory bowel disease, as well as in acute inflammatory processes such as unstable angina and myocardial infarction [17-20]. MPV has also been associated with infections such as coronavirus 2019 (Covid-19), obesity, diabetes mellitus, frailty, and coronary artery disease [21-24]. The neutrophil to lymphocyte ratio

(NLR) is obtained by dividing the neutrophil count by lymphocyte count in the complete blood count and is one of the markers of the inflammatory response [25]. The positive association between high-sensitivity C-reactive protein and systemic inflammation also supports this finding [25]. NLR has been found to help predict prognosis in some diseases, indicating poor prognosis in cardiovascular disease, solid tumors, and infections [26-28]. This study was conducted to investigate the level of MPV and NLR in PHP developing from a single parathyroid adenoma.

Materials and methods

After obtaining ethics committee approval (date: 10/06/2021; decision number: 8/21), the data of subjects who visited the endocrinology and/or general surgery departments of Antalya Training and Research Hospital between January 2016 and April 2021 were reviewed. The exclusion criteria were as follows: PHP due to hyperplasia of the parathyroid glands, PHP patients with multiple adenomas, cases with surgical pathologies of parathyroid cancer, younger than 18 and older than 70 years, with cardiovascular or cerebrovascular diseases, taking medications that affect platelet function (e.g., acetylsalicylates, heparin, antiepileptic drugs, etc.), and with infections or inflammatory diseases. Patient records were retrospectively scanned from the computer system, and 40 PHP patients with solitary parathyroid adenoma who met the exclusion criteria were identified and included in the study. The study population was formed by selecting 36 controls of similar age and gender with normal serum PTH and Ca levels. In all patients, PHP diagnosis had been based on at least two separate measurements of Ca, phosphorus (P), albumin, and PTH, and at least one measurement of 25OHD and 24-hour urine

Ca and creatinine. The diagnosis of adenoma was confirmed by the presence of adenoma on Technetium (^{99m}Tc) sestamibi scintigraphy in addition to the ultrasound image, and by PTH washout from the lesion on ultrasound if the scintigraphy was negative. Ca, P, albumin, and other biochemical tests results were obtained by the traditional spectrophotometric method using commercial kits from Beckman Coulter with a Beckman Coulter AU5800 autoanalyzer (Beckman Coulter Inc., CA, USA), and the result of whole blood parameters (hemogram) were obtained with a Beckman Coulter LH780 hematology autoanalyzer. PTH, 25OHD and other necessary hormone tests were performed using the chemiluminescence method on a Beckman Coulter DxI800 instrument (Beckman Coulter Inc.). The reference ranges in our hospital were 8.8-10.6 mg/dl for Ca, 2.5-4.5 mg/dl for P, 12-88 ng/l for PTH, and 3.6-12 fl for MPV between the study dates. Serum levels of Ca, P, albumin, PTH, 25OHD and hemogram of total population were recorded. If the patient's albumin is low, it was analyzed by calculating the corrected Ca for albumin [Corrected Ca (mg/dl) = measured Ca (mg/dl) + 0.8 (4-patient albumin)]. 25OHD level below 20ng/ml was considered as insufficient. We statistically compared the MPV and NLR values of patients and controls and examined the correlation between these parameters and PTH, 25OHD and Ca.

Statistical analysis

All results were given as numbers and percentages for categorical parameters and means and standard deviations for continuous variables. Analyzes were obtained in SPSS 20.0 program. Whether the distribution of the data was normal or not was determined by performing the Shapiro-Wilk test. The comparison of the means of the two groups that met the parametric analysis conditions was

made with the Student's T-test and the Mann Whitney U test was used when comparing the means of nonparametric variables. Spearman correlation test was used to identify possible relationships among the parameters. It was considered significant when the p value was below 0.05.

Results

40 PHP patients with a mean age of 50.6 ± 7.3 years and 36 controls with a mean age of 49.8 ± 8.1 years were studied. 29 (72.5%) of the PHP patients were female, while 26 (72.2%) of the control subjects were female. Mean PTH level was significantly higher in patients than control subjects (214.9 ± 112.6 ng/l and 49.0 ± 6.3 ng/l, respectively; $p=0.001$). The mean 25OHD level in the PHP group indicated insufficiency, while the 25OHD level in the control group was adequate (18.1 ± 7.6 $\mu\text{g/l}$ and 26.6 ± 4.0 $\mu\text{g/l}$, respectively; $p=0.024$). The mean Ca level was 11.6 ± 0.9 mg/dl in patients, 9.2 ± 1.0 mg/dl in controls ($p=0.012$). P level was lower in patients than in controls as expected (2.4 ± 0.02 mg/dl and 3.5 ± 0.4 mg/dl, respectively; $p=0.002$). Red blood cell count and hemoglobin content were similar in the 2 groups. While platelet count did not change between patients and controls, MPV was significantly higher in patients compared to controls (8.7 ± 0.6 fl, and 7.6 ± 0.6 fl, respectively; $p=0.001$), supporting our hypothesis. The white blood cell count did not differ between the groups, but the neutrophil count was significantly increased in the PHP patients ($p=0.000$). In addition, NLR was significantly higher in the PHP group than in the control group (2.6 ± 1.7 and 1.7 ± 0.8 , respectively; $p=0.000$). The comparison of study parameters between patients and controls is shown in Table 1. We found a significant correlation between PTH and MPV ($r=0.476$,

Table 1. Table 1. Comparison of the parameters between patients and controls.

Parameters	PHP group	Control group	<i>p</i>
Number (n)	40	36	
Male/Female (n) (%)	11/29 (27.5/72.5)	10/26 (27.8/72.2)	0.986
Age (yrs.)	50.6±7.3	49.8±8.1	0.812
PTH (ng/l)	214.9±112.6	49.0±6.3	0.001*
25OHD (µg/l)	18.1±7.6	26.6±4.0	0.024*
Calcium (mg/dl)	11.6±0.9	9.2±1.0	0.012*
Phosphorus (mg/dl)	2.4±0.02	3.5±0.4	0.002*
MPV (fl)	8.7±0.6	7.6±0.6	0.001*
Neutrophil (10 ³ /µl)	5.7±1.4	4.2±1.9	0.000*
Lymphocyte (10 ³ /µl)	2.2±1.0	2.5±0.6	0.267
NLR	2.6±1.7	1.7±0.8	0.000*

**p*<0.05 is statistically significant PTH, parathyroid hormone; PHP, primary hyperparathyroidism; MPV, mean platelet volume; NLR, neutrophil to lymphocyte ratio; 25OHD, 25-hydroxyvitamin D.

p=0.000) positive, between Ca and MPV (*r*=0.292, *p*=0.003) positive and between MPV and 25OHD (*r*=-0.367, *p*=0.024) negative. In addition, NLR showed significant positive correlation with serum Ca (*r*=0.214, *p*=0.011) and PTH (*r*=0.347, *p*=0.023) and negative correlation with 25OHD which was not

statistically significant (*r*=-0.072, *p*=0.131). The correlation results are shown in Table 2.

Discussion

In our study, we found that MPV, which was expected to increase in platelet activation, and NLR, which is positively correlated with inflammatory parameters were significantly higher in PHP patients than in healthy controls. MPV was found to be increased in chronic inflammatory diseases, many cancer types including thyroid papillary carcinoma as well as in cardiovascular diseases such as coronary artery disease and myocardial infarction (MI) [16-18,29]. Butterworth RJ et al., showed that MPV is also increased in ischemic stroke and that MPV on admission is significantly higher in patients who died or became dependent at 3 months after stroke [30]. In another study, an increase in MPV was observed after MI,

Table 2. The result of correlation analysis.

Parameters	MPV	NLR
PTH	<i>r</i> :0.476 <i>p</i>:0.000*	<i>r</i> :0.347 <i>p</i>:0.023*
Calcium	<i>r</i> :0.292 <i>p</i>:0.003*	<i>r</i> : 0.214 <i>p</i>: 0.011*
25OHD	<i>r</i> :-0.367 <i>p</i>:0.024*	<i>r</i> :-0.072 <i>p</i> :0.131

PTH, parathyroid hormone; MPV, mean platelet volume; NLR, neutrophil to lymphocyte ratio; 25OHD, 25-hydroxyvitamin D. **p*<0.05 is statistically significant, spearman correlation tests.

suggesting that it may be a predictor of death or other ischemic events after MI [18]. The study, which compared thyroid cancer patients who underwent surgery with healthy controls and operated thyroid patients with benign goiter pathology, concluded that the MPV increase in thyroid papillary cancer was significant compared to other groups (29). Another study by Kuzu F et al., on thyroid nodules found that MPV and NLR were high in malignant nodules (31). Also, in studies on MPV in thyroid patients, it was observed that MPV increased in autoimmune thyroid diseases irrespective of TSH level (32). An increase in MPV was also observed in Graves' orbitopathy, which is also an autoimmune inflammatory process (33). In patients with PHP, inflammation, endothelial dysfunction, and the atherosclerosis cascade are activated by pathways whose mechanisms are not clearly understood. The consequence of this process is a poor prognosis and an increased risk of death from cardiovascular disease [3-9]. To elucidate this etiopathogenesis, platelet functions have been brought to the forefront and it has been suggested that changes in coagulation parameters, susceptibility to thrombosis and increased platelet activation may occur in PHP [34,35]. It is known that the number of studies investigating platelet function and activation in PHP is quite limited. In these studies, some factors of the coagulation cascade, coagulation and adhesion molecules were measured. One study found that the levels of the factor VII and D-dimer were higher in PHP patients than in control subjects [34], while in another study, P-selectin levels and aggregation parameters did not differ between PHP and control groups [35]. In studies that investigated MPV in PHP, the results were consistent with ours [36-38]. Yılmaz et al, on the other hand, found that MPV values decreased significantly in the 6th month after

adenoma surgery [37]. Baradaran et al., studied MPV levels in secondary hyperparathyroidism in dialysis patients and found that there was a direct correlation between MPV and PTH in this group of patients, and observed that platelet count decreased with increasing PTH [38]. Some studies hypothesized that increased Ca levels, rather than PTH, affected platelets in PHP, leading to an increase in platelet Ca levels by altering platelet shape and activation [39,40]. It has also been suggested that increased inflammation and oxidative stress may cause platelet activation in PHP [41,42]. Similar to our results, Cure et al. [42] and Arpacı D et al., [36] found a negative correlation between MPV and 25OHD levels. In agreement with previous reports [43,44], females in this study were more likely to have a PHP than males. Another finding of our study is that NLR is higher in subjects with PHP than in healthy subjects. NLR, which can be derived from leukocyte count, increases in systemic inflammation [45]. Some data suggest that NLR may be related to cardiovascular disease prognosis [26,45]. In a few studies investigating the influence of PHP on NLR, a positive correlation between PTH and NLR was documented [46,47]. In this study, Zeren S et al., found that NLR increased with increasing parathyroid adenoma size [47]. In another study that focused attention on NLR in patients who developed primary or secondary PTH elevation, it was highlighted that due to the positive correlation between PTH and Ca and NLR, elevated PTH would indicate a proinflammatory state [48]. Our study has some limitations. The study population was small, the study was retrospective, and we did not measure other atherosclerotic or inflammatory markers and platelet activation parameters.

Conclusion

The significance of this study is that it

demonstrates increased platelet activation and inflammatory propensity in PHP and paves the way for new studies to assess inflammatory markers and adhesion and aggregation molecules in relation to platelet activity. In our study, we found that MPV, which is an indicator of platelet activation, and NLR, which correlates with inflammatory parameters, increase in PHP due to a single parathyroid adenoma, but new studies on the clinical significance of these findings are needed. There is no conflict of interest.

Funding: *The author(s) received no financial support for the research, authorship, and/or publication of this article.*

Conflict of Interest: *The authors declare that they have no conflict of interest.*

Ethical statement: *The study was conducted with the approval of Local Ethical Committee in accordance with the Helsinki Declaration After obtaining ethics committee approval (date: 10/06/2021; decision number: 8/21).*

Open Access Statement

This is an open access journal which means that all content is freely available without charge to the user or his/her institution under the terms of the Creative Commons Attribution Non-Commercial License (<http://creativecommons.org/licenses/by-nc/4.0>). Users are allowed to read, download, copy, distribute, print, search, or link to the full texts of the articles, without asking prior permission from the publisher or the author.

Copyright (c) 2021: Author (s).

References

[1] Marx SJ. Hyperparathyroid and hypoparathyroid disorders. *N Engl J Med.* 2000;343(25):1863-75.
[2] Solomon BL, Schaaf M, Smallridge RC. Psychologic symptoms before and after

parathyroid surgery. *Am J Med.* 1994;96(2):101-6.
[3] Choev M. Parathyroid hormone 1 receptor: insights into structure and function. *Recept Channels.* 2002;8(3-4):219-42.
[4] Taylor EN, Curhan GC, Forman JP. Parathyroid hormone and the risk of incident hypertension. *J Hypertens.* 2008;26(7):1390-94.
[5] van Ballegooijen AJ, Visser M, Kestenbaum B, et al. Relation of vitamin D and parathyroid hormone to cardiac biomarkers and to left ventricular mass (from the Cardiovascular Health Study). *Am J Cardiol.* 2013;111(3):418-24.
[6] Grey A, Mitnick MA, Shapses S, et al. Circulating levels of interleukin-6 and tumor necrosis factor-alpha are elevated in primary hyperparathyroidism and correlate with markers of bone resorption--a clinical research center study. *J Clin Endocrinol Metab.* 1996;81(10):3450-54.
[7] Emam AA, Mousa SG, Ahmed KY, et al. Inflammatory biomarkers in patients with asymptomatic primary hyperparathyroidism. *Med Princ Pract.* 2012;21(3):249-53.
[8] Rashid G, Bernheim J, Green J, et al. Parathyroid hormone stimulates endothelial expression of atherosclerotic parameters through protein kinase pathways. *Am J Physiol Renal Physiol.* 2007;292(4):1215-18.
[9] Bonet J, Bayés B, Fernández-Crespo P, et al. Cinacalcet may reduce arterial stiffness in patients with chronic renal disease and secondary hyperparathyroidism - results of a small-scale, prospective, observational study. *Clin Nephrol.* 2011;75(3):181-87.
[10] Pitchford SC, Momi S, Giannini S, et al. Platelet P-selectin is required for pulmonary eosinophil and lymphocyte recruitment in a

- murine model of allergic inflammation. *Blood*. 2005;105(5):2074–81.
- [11] Grove EL, Hvas AM, Kristensen SD. Immature platelets in patients with acute coronary syndromes. *Thromb Haemost*. 2009;101(1):151–56.
- [12] Ranjith MP, Divya R, Mehta VK, et al. Significance of platelet volume indices and platelet count in ischaemic heart disease. *J Clin Pathol*. 2009;62(9):830-33.
- [13] Henn V, Slupsky JR, Grafe M, et al. CD40 ligand on activated platelets triggers an inflammatory reaction of endothelial cells. *Nature*. 1998;391(6667): 591-4.
- [14] Aktas G, Sit M, Tekce H, et al. Mean platelet volume in nasal polyps. *West Indian Med J*. 2013;62(6):515-18.
- [15] van der Loo B, Martin JF. Megakaryocytes and platelets in vascular disease. *Baillieres Clin Haematol*. 1997;10(1):109-23.
- [16] Kiliçli-Camur N, Demirtunç R, Konuralp C, et al. Could mean platelet volume be a predictive marker for acute myocardial infarction? *Med Sci Monit*. 2005;11(8):387-92.
- [17] Kapsoritakis AN, Koukourakis MI, Sfiridaki A, et al. Mean platelet volume: a useful marker of inflammatory bowel disease activity. *Am J Gastroenterol*. 2001;96(3):776–81.
- [18] Kisacik B, Tufan A, Kalyoncu U, et al. Mean platelet volume (MPV) as an inflammatory marker in ankylosing spondylitis and rheumatoid arthritis. *Joint Bone Spine*. 2008;75(3):291-94.
- [19] Choi CU, Seo HS, Kim YK, et al. Can mean platelet volume predict coronary vasospasm? *Platelets*. 2011;22(3):173-78.
- [20] Endler G, Klimesch A, Sunder-Plassmann H, et al. Mean platelet volume is an independent risk factor for myocardial infarction but not for coronary artery disease. *Br J Haematol*. 2002;117(2): 399-404.
- [21] Aktas G, Kocak MZ, Duman TT, et al. Mean Platelet Volume (MPV) as an inflammatory marker in type 2 diabetes mellitus and obesity. *Bali Med J*. 2018;7(3):650-53.
- [22] Bilgin S, Aktas G, Kahveci G, et al. Does mean platelet volume/lymphocyte count ratio associate with frailty in type 2 diabetes mellitus? *Bratisl Med J*. 2021;122(2):116-19.
- [23] Aktas G. Hematological predictors of novel coronavirus infection. *Rev Assoc Med Bras*. 2021;67(1):1-2.
- [24] Sincer I, Gunes Y, Mansiroglu AK, et al. Association of mean platelet volume and red blood cell distribution width with coronary collateral development in stable coronary artery disease. *Adv Interv Cardiol*. 2018;14(3):263-69.
- [25] Sen BB, Rifaioglu EN, Ekiz O, et al. Neutrophil to lymphocyte ratio as a measure of systemic inflammation in psoriasis. *Cutan Ocul Toxicol*. 2014;33(3):223-27.
- [26] Kaya H, Ertas F, Islamoglu Y, et al. Association between neutrophil to lymphocyte ratio and severity of coronary artery disease. *Clin Appl Thromb Hemost*. 2013;20(1):50-4
- [27] Templeton AJ, McNamara MG, Šeruga B, et al. Prognostic role of neutrophil-to-lymphocyte ratio in solid tumors: a systematic review and meta-analysis. *J Natl Cancer Inst*. 2014;106(6):124.
- [28] Liu X, Shen Y, Wang H, et al. Prognostic Significance of Neutrophil-to-Lymphocyte Ratio in Patients with Sepsis: A Prospective Observational Study. *Mediators Inflamm*. 2016;2016:8191254.
- [29] Baldane S, Ipekci SH, Sozen M, et al. Mean platelet volume could be a possible biomarker for papillary thyroid carcinomas.

- Asian Pac J Cancer Prev. 2015;16(7):2671-74.
- [30] Butterworth RJ, Bath PM. The relationship between mean platelet volume, stroke subtype and clinical outcome. *Platelets.* 1998;9(6):359-64.
- [31] Kuzu F, Arpaci D, Cakmak GK, et al. The value of blood cell markers in patients with thyroid nodules including atypia of undetermined significance/follicular lesion of undetermined significance cytology. *Medicine.* 2018;7(2):386-90.
- [32] Carlioglu A, Timur O, Durmaz SA. Mean platelet volume in euthyroid patients with Hashimoto's thyroiditis. *Blood Coagulation & Fibrinolysis.* 2015;26(3):282-84.
- [33] Atilgan CU, Şendül SY, Kösekahya P, et al. Evaluation of Neutrophil-to-Lymphocyte Ratio and Mean Platelet Volume in Patients with Active and Inactive Thyroid Orbitopathy. *Sisli Etfal Hastan Tip Bul.* 2018;52(1):26-30.
- [34] Erem C, Kocak M, Hacıhasanoğlu A, et al. Blood coagulation, fibrinolysis and lipid profile in patients with primary hyperparathyroidism: increased plasma factor VII and X activities and D-Dimer levels. *Exp Clin Endocrinol Diabetes.* 2008;116(10):619-24.
- [35] Yorulmaz G, Akalın A, Akay OM, et al. The Effect of Hyperparathyroid State on Platelet Functions and Bone Loss. *Turk J Haematol.* 2016;33(4):293-98.
- [36] Arpaci D, Kuzu F, Emre AU, et al. Elevated mean platelet volume in patients with primary hyperparathyroidism. *Int J Clin Exp Med.* 2016;9(3):6330-35.
- [37] Yilmaz H. Assessment of mean platelet volume (MPV) in primary hyperparathyroidism: effects of successful parathyroidectomy on MPV levels. *Endocr Regul.* 2014;48(4):182-88.
- [38] Baradaran A, Nasri H. Impact of parathormone Hormone on Platelet Count and Mean Volume in End-stage Renal Failure Patients on regular Hemodialysis. *J Med Sci.* 2005;5(4): 266-71.
- [39] Fliser D, Franek E, Fode P, et al. Subacute infusion of physiological doses of parathyroid hormone raises blood pressure in humans. *Nephrol Dial Transplant.* 1997;12(5):933-38.
- [40] Salzman EW, Ware JA. Ionized calcium as an intracellular messenger in blood platelets. *Prog Hemost Thromb.* 1989;9:177-202.
- [41] Rashid G, Bernheim J, Green J, et al. Benchetrit S. Parathyroid hormone stimulates the endothelial nitric oxide synthase through protein kinase A and C pathways. *Nephrol Dial Transplant.* 2007;22(10):2831-37.
- [42] Cure CM, Cure E, Yuce S, et al. Mean platelet volume and vitamin D level. *Ann Lab Med.* 2014;34(2):98-103.
- [43] Walker MD, Fleischer J, Rundek T, et al. Carotid vascular abnormalities in primary hyperparathyroidism. *J Clin Endocrinol Metab.* 2009;94(10):3849-56.
- [44] Christensen MH, Fenne IS, Nordbo Y, et al. Novel inflammatory biomarkers in primary hyperparathyroidism. *Eur J Endocrinol.* 2015;173(1):9-17.
- [45] Shen XH, Chen Q, Shi Y, et al. Association of neutrophil/ lymphocyte ratio with long-term mortality after ST elevation myocardial infarction treated with primary percutaneous coronary intervention. *Chin Med J.* 2010;123(23):3438-43.
- [46] Lam H, Yang P, Chien M, et al. Association between neutrophil-to-lymphocyte ratio and parathyroid hormone in patients with primary hyperparathyroidism. *Archives of Medical Science.* 2019;15(4):880-86.

- [47] Zeren S, Yaylak F, Ozbay I, et al. Relationship between the neutrophil to lymphocyte ratio and parathyroid adenoma size in patients with primary hyperparathyroidism. *Int Surg.* 2015;100(7-8):1185-89.
- [48] Toraman A, Aras F, Hekimsoy Z, et al. Is there a relationship between parathyroid hormone and neutrophil lymphocyte ratio or platelet lymphocyte ratio? *Acta Endocrinol (Buchar).* 2019;5(1):96-101.

The role of diffusion-weighted imaging on 3 tesla magnetic resonance in the clinical staging and pathological grading of clear cell renal carcinoma

Hasan Gundogdu¹, Recep Bedir², Huseyin Eren³, Berrin Erok⁴

¹Department of Radiology, Recep Tayyip Erdogan University, Faculty of Medicine, İslampasa, Rize, Turkey

²Department of Pathology, Recep Tayyip Erdogan University, Faculty of Medicine, İslampasa, Rize, Turkey

³Department of Urology, Recep Tayyip Erdogan University Faculty of Medicine, İslampasa, Rize, Turkey

⁴Department of Radiology, Health Sciences University, Okmeydanı Cemil Taşçı City Hospital, Istanbul, Turkey

ABSTRACT

Aim: To evaluate the contribution of the apparent diffusion coefficient (ADC) to distinguish between the four clinical stages and pathological grading in patients with clear cell renal cell carcinoma (RCC) on 3T MRI.

Methods: MRI of 93 patients with histopathological diagnosis of clear cell RCC were evaluated retrospectively. Clinical stage was evaluated according to American Joint Committee on Cancer and histopathological examination was evaluated according to the Fuhrman grading system. ADC values were compared for each clinical stage and pathological grade.

Results: Clinical stages were I in 51 patients (54.8%), II in 14 patients (15%), III in 15 patients (16.1%), and IV in 13 patients (13.9%). The Fuhrman grade of the patients were I in 8 (8.6%) patients, II in 55 (59.1%) patients, III in 23 (24.7%) patients and IV in 7 (7.5%) patients. Clinical stage I and Fuhrman grade I had significantly higher ADC values than all groups ($p < 0.001$). The sensitivity was 81% and the specificity was 80.4% when the optimum cut-off value of ADC was taken as $1.41 \times 10^{-3} \text{ mm}^2/\text{s}$ to differentiate between clinical stage I and other stages (II, III, and IV) (AUC:0.910; 95CI:0.855-0.964; $p < 0.001$). The optimum cutoff value of ADC was taken as $1.67 \times 10^{-3} \text{ mm}^2/\text{s}$ to differentiate between Fuhrman grade I and other grades (II, III and IV), the sensitivity was 88.2% and the specificity was 100% (AUC: 0.927; 95CI: 0.872- 0.983; $p < 0.001$).

Conclusions: In patients with renal mass suggestive of clear cell RCC in imaging studies; The possibility of lymph node or distant metastatic lesion should be considered in patients with an ADC of the primary tumor site less than $1.41 \times 10^{-3} \text{ mm}^2/\text{s}$, and the presence of distant metastasis in patients with an ADC less than $1.22 \times 10^{-3} \text{ mm}^2/\text{s}$.

Key words: Clear cell renal cell carcinoma, apparent diffusion coefficients, clinical stage, Fuhrman grade, MRI

✉ Dr. Hasan Gundogdu

¹Department of Radiology, Recep Tayyip Erdogan University, Faculty of Medicine, İslampasa, Rize, Turkey

E- mail: hasan.gundogdu@erdogan.edu.tr

Received: 2021-12-09 / Revisions: 2021-12-20

Accepted: 2021-12-23 / Published online: 2022-01-01

Introduction

Renal cell carcinoma (RCC) is the most frequent malignant renal tumor with a

prevalence of approximately 2% among adult cancers, accounting for about 80-90% of all parenchymal kidney tumors [1, 2]. The age of presentation is typically 50-70 years, with a moderate male predilection of 2:1 [3]. Most clinical manifestations are nonspecific, and many patients are recognized incidentally in earlier stages on imaging studies performed for other reasons. The classic triad of hematuria,

flank pain, and mass is seen in only 10% of patients with advanced tumors [4].

RCC represents a heterogeneous group of tumors with many different histological varieties. Clear cell, papillary, and chromophobe RCCs constitute the three main histological subtypes with the malignant course, of which ~75% are the clear cell subtype in the adult population [5,6]. The prognosis of RCC is closely related to the pathological subtypes. Clear cell RCC originates from the proximal tubule epithelium and is the most common and malignant subtype of RCCs. The five-year cancer-related survival rate is the lowest compared to other subtypes at 68.9% [7-8]. These main pathological subtypes of RCC can often be noninvasively differentiated by imaging characteristics [9]. Clear cell RCC has a more heterogeneous appearance due to multiple areas of hemorrhage, internal necrosis, and cystic changes, in addition to a tremendous amount of enhancement.

At the microscopic evaluation, clear cell RCCs are characterized with tumor cells having clear cytoplasm due to the accumulation of glycogen and lipids accompanying in varying proportions to the cells with granular eosinophilic cytoplasm [4]. Diffusion-weighted imaging (DWI), a magnetic resonance (MR) imaging technique based on the molecular mobility of water molecules, demonstrates high signal intensity in the lesions with dense cellularity and weak interstitium that limit the mobility of water molecules, as in tumoral processes. The apparent diffusion coefficient (ADC) is a parameter that allows the quantification of restricted diffusion. It is used as an indicator of cell proliferative activity and provides insight into the nature of the lesions in various parts of the body [10,11]. DWI is a valuable tool in detecting metastatic lymph nodes and

differentiating high-grade tumors from low-grade ones [12-14].

Various studies have shown that ADC is significantly different between clear-cell RCC and non-clear-cell RCC subtypes [9, 15,16]. Recently, the utility of ADC has been suggested in predicting the clinical stage of clear cell RCC [17, 18]. However, studies reporting the relationship between ADC and the clinical stage of clear cell RCC are few in the literature, and most of them were performed on 1.5 Tesla (T) MR imaging [18]. Our study aims to investigate the utility of DWI with ADC measurement on 3T MR imaging in clinical staging and pathological grading of clear cell RCCs.

Materials and methods

The study was approved by the Recep Tayyip Erdoğan University Faculty of Medicine Clinical Research Ethics Committee (Date: 2021-11-11/No:2021/195). All the procedures were carried out in accordance with ethical rules and the principles of the Declaration of Helsinki. Due to the design of our study, an informed consent form could not be obtained from the patients. Demographic characteristics, medical history, surgical notes, and pathology results of all patients, in whom 3T MR imaging was performed for the evaluation of the kidney masses with pathological diagnosis of clear cell RCC made by examining the tissues obtained in radical/partial nephrectomy between February 2016 and September 2021 were retrospectively analyzed from the hospital information system. Patients under 18, patients who had MR imaging or nephrectomy surgery in another center, patients who underwent MR imaging with 1.5 T MR device, patients with poor MR imaging quality, and patients whose medical information could not be reached were excluded from the study.

MR Imaging

MR imaging was performed with the patient in the supine position, using a 3 T MR scanner (Discovery w750, GE Healthcare, United States). Antecubital intravenous access was established before the examination, and a bolus injection of contrast material was administered intravenously, following the precontrast images. Conventional, dynamic, and DWI were obtained using standard abdominal coils. For all patients, axial and coronal section T2-weighted (T2w) single-shot fast spin-echo (FSE) sequences, axial section T1-weighted (T1w) dual-echo in-phase and out-of-phase sequences, diffusion-weighted images were taken before contrast agent injection. Diffusion-weighted images were obtained by applying diffusion-sensitizing gradients with different b values (50 sec/mm², 800 sec/mm²) in all three directions (x, y, z) to the echo-planar SE T2w sequence in the axial plane. For each b-value, isotropic diffusion-weighted images that eliminate directional signal flares were generated. ADC maps were generated automatically by the instrument using each cross-sectional image.

After diffusion-weighted images were obtained, the gadolinium contrast agent was administered intravenously at a dose of 0.1 mmol/kg with an automatic injector at a rate of 3 ml/sec through the vascular access established before the examination, and high-resolution T1w fat-suppressed TSE axial and coronal section images were obtained (Table 1). For the evaluation of kidneys, all sequences were obtained at breath-holding. After the images were obtained, they were recorded in our hospital's PACS (Picture Archiving and Communication System).

Image analysis

Imaging data for each of the 93 renal masses were evaluated prior to reviewing the pathological data by a single reviewer (H.G) with 7 years of experience. The ADC was manually calculated by setting a region of interest (ROI) within the tumor using a workstation. ROIs were placed in a single location within the solid components of the tumor based on visual evaluation, which was seen as the brightest on DWI and the darkest on ADC maps, avoiding areas of necrosis, cystic

Table 1. Parameters for MR imaging.

Parameters	Axial T2W imaging	Coronal T2W imaging	In-phase/out of phase imaging	CE MRI	DWI
Echo time (m)	84	84	2.4/5.6	1.5	56
Repetition time (ms)	3768	3000	230	3.5	2700
Flip angle (degrees)	90	90	90	15	90
Intersection gap (mm)	1	1	1	-2.5	1
Section thickness (mm)	5	5	5-6	5	5-6
Field of view (mm)	360-400	360-400	360-400	340-400	360-400
Matrix	320x224	288x192	256x192	288x224	128x128
Parallel imaging acceleration factor	2	-	2	2	2

MR: Magnetic resonance, DWI: Diffusion-weighted imaging, CE MRI: Contrast-enhanced magnetic resonance imaging.

degeneration, and hemorrhage that typically show no enhancement on dynamic contrast-enhanced MR images. The ROI was set in an as large area as possible with the ROI size between 90–110 mm² (mean ROI area; 98 mm²). The ADC value from a single ROI was accepted as the representative ADC of the renal lesion and expressed as mean ± standard deviation in the form of X x10⁻³ mm²/s.

Clinical staging

The clinical stage was determined and recorded according to the 2010 TNM classification of the American Joint Committee on Cancer (AJCC) [19]. The relationship between DWI findings and the clinical stages of the patients was investigated.

Pathological analysis

A nuclear grade for each tumor using the Fuhrman nuclear grading system, the most widely used histopathological grading system defined by Furhman et al. [20], was assigned, unaware of MR imaging findings. In the Fuhrman classification, a grade is given to the tumors between grade I-IV; grade I indicates the best prognosis and grade IV the worst (Table 2).

Table 2. Fuhrman grading system.

Grade	Fuhrman nuclear grading
Grade 1	Nucleoli are absent or inconspicuous and basophilic at 400x
Grade 2	Nucleoli are conspicuous and eosonophilic at 400x and visible but not prominent at 100x
Grade 3	Nucleoli are conspicuous and eosonophilic at 100x
Grade 4	Extreme nuclear pleomorphisim, multinucleate giant cell and /or rhabdoid sarcomatoid differentiation

In 3 patients with renal masses in both kidneys, clinical staging and Fuhrman grading were performed based on the tumor of the larger size.

Statistical Analysis

Statistical analyses were performed using the IBM SPSS Statistics, Version 23.0 (SPSS Inc., Chicago, USA) program. Descriptive statistics of both groups were reported as frequency and percentages within the groups (n, %). Continuous numerical variables were analyzed by normality analyses. Accordingly, those with normal distribution were reported as mean ± standard deviation, and those without normal distribution were reported as median (min-max). Difference analyzes between groups were performed with Student's t-test or Mann-Whitney U test. The distribution of categorical data between the groups was evaluated with the Chi-square test. Relationships between parameters were evaluated with Spearman correlation analysis and reported with rho coefficient. ROC curve analyzes were performed to evaluate the parameters' clinical stage and pathological grading performances and determine the appropriate threshold values. Accordingly, area under curve (AUC), sensitivity and specificity values were reported. A *p*-value < 0.05 was considered statistically significant.

Results

164 patients who underwent nephrectomy for RCC were retrospectively evaluated. 29 patients diagnosed with non-clear cell RCC were excluded. After that, 35 patients who did not have preoperative MR imaging or had MR imaging but at 1.5 T MR Device were also excluded. Lastly, 7 patients were excluded due to the poor quality of DWI (Figure 1).

The remaining 93 cases, of whom 73 (%78, 5) were male, and 20 (%21, 5) were female, with a mean age of 60, 25±11, 65 (39-77), were

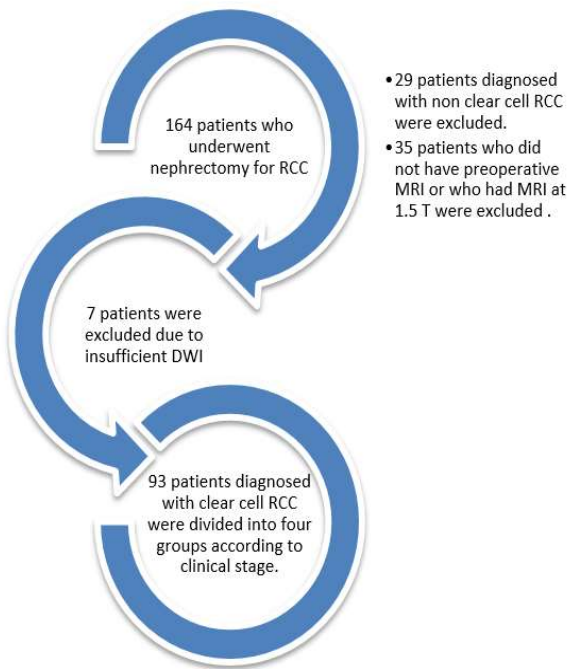


Figure 1. Flowchart for patient selection.

recruited for the study. Left (54.8%) nephrectomy was performed in 51 (45.2%) patients, and right nephrectomy was performed in 42 (% 45.2) patients. Partial nephrectomy was performed in 27 (29%) patients and radical nephrectomy in 66 (71%) patients. According to clinical stages and Fuhrman grades, these 93 cases were divided into four groups according to clinical stages.

Clinical stages were I in 51 patients (54.8%), II in 14 patients (15%), III in 15 patients (16.1%), and IV in 13 patients (13.9%). The Fuhrman grade of the patients were I in 8 (8.6%) patients, II in 55 (59.1%) patients, III in 23 (24.7%) patients, and IV in 7 (7.5%) patients. There was a moderate positive correlation between clinical stage and Fuhrman grade ($\rho=0.618$; $p<0.001$). For all 93 patients, the median ADC of clear cell RCC was 1.42×10^{-3} mm²/sec (min-max: $0.97-1.86 \times 10^{-3}$ mm²/s).

The mean ADC value for stage I was $1.59 \pm 0.18 \times 10^{-3}$ mm²/s, for stage \geq II was $1.23 \pm 0.18 \times 10^{-3}$ mm²/s, for stage \geq III was

$1.15 \pm 0.14 \times 10^{-3}$ mm²/s and for stage IV was $1.07 \pm 0.64 \times 10^{-3}$ mm²/s. Stage I had significantly higher ADC values than all groups ($p<0.001$) (Figure 2). ADC values for each stage are given in table 3.

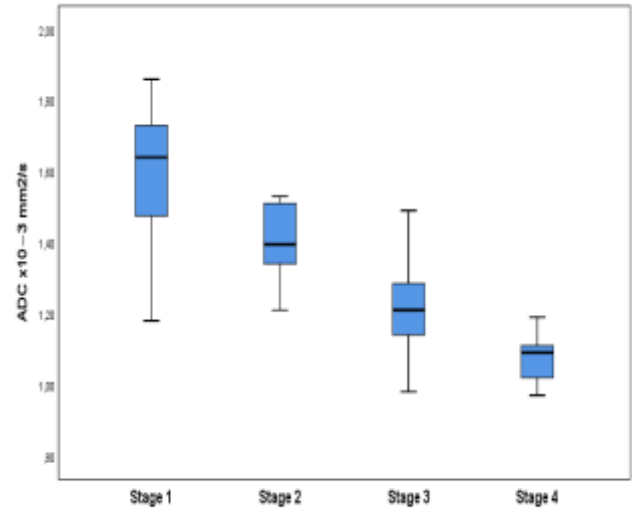


Figure 2. The box plot of ADC values in clinical stages.

Table 3. ADC values according to clinical stage and pathological grades of clear cell RCCs.

Parameters	ADC $\times 10^{-3}$ mm ² /s				
	Mean	SD	Min	Max	
Clinical stage	1	1.59	0.18	1.18	1.86
	2	1.40	0.10	1.21	1.53
	3	1.22	0.16	0.98	1.49
	4	1.07	0.06	0.97	1.19
Fuhrman grade	1	1.76	0.07	1.68	1.85
	2	1.52	0.18	1.13	1.86
	3	1.17	0.14	0.97	1.48
	4	1.19	0.21	0.99	1.49

The sensitivity was 81%, and the specificity was 80.4% when the optimum cut-off value of ADC was taken as 1.41×10^{-3} mm²/s to differentiate between clinical stage I and other stages (II, III, and IV) (AUC:0.910;

95CI:0.855-0.964; $p<0.001$). The sensitivity was 93%, and the specificity was 80.4% when the optimum cut-off value of ADC was similarly taken as 1.41×10^{-3} mm²/s to distinguish between clinical stages I and more advanced stages (III and IV). (AUC: 0.964; 95CI:0.927-1.000; $p<0.001$). The sensitivity was 100%, and the specificity was 98.1% when the optimum threshold value of the ADC was taken as 1.22×10^{-3} mm²/s to distinguish between clinical stage I and stage IV (AUC:0.998; 95CI:0.994-1.000; $p<0.001$) (Figure 3).

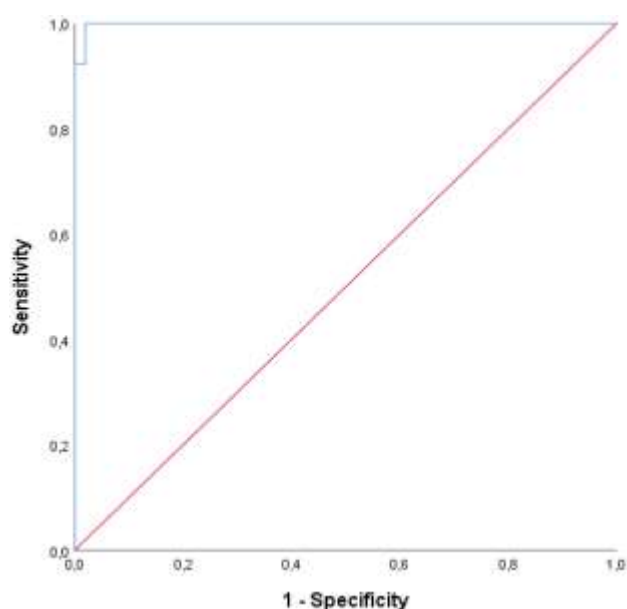


Figure 3. ROC curve showing success in discrimination between clinical stage I and stage IV of clear-cell RCC for and $ADC \leq 1.22 \times 10^{-3}$ mm²/s.

The mean ADC value for Fuhrman Grade I was $1.76\pm 0.68 \times 10^{-3}$ mm²/s, $1.40\pm 0.24 \times 10^{-3}$ mm²/s for grade \geq II, $1.17\pm 0.16 \times 10^{-3}$ mm²/s for grade \geq III and $1.19\pm 0.21 \times 10^{-3}$ mm²/s for grade IV. Grade I had significantly higher ADC values than all groups ($p<0.001$). When the optimum cut-off value of ADC was taken as 1.67×10^{-3} mm²/s to differentiate between Fuhrman grade I and other grades (II, III, and IV), the sensitivity was 88.2%, and the specificity was

100% (AUC: 0.927; 95CI: 0.872- 0.983; $p<0.001$). When the optimum cut-off value of ADC was taken as 1.59×10^{-3} mm²/s to differentiate between Fuhrman grade I and more advanced grades (II, III and IV), the sensitivity was 100%, and the specificity was 100% (AUC:1.000; 95CI:1.000-1.000; $p<0.001$)) The sensitivity was 100%, and the specificity was 100% when the optimum cut-off value of ADC was taken as 1.59×10^{-3} mm²/s to differentiate between grade I and grade IV (AUC:1.000; 95CI:1.000-1.000; $p=0.001$).

Discussion

The stage of RCC is based on the tumor diameter and extent of the invasion, which is defined in the AJCC Cancer Staging guidelines as follows: T1a tumor is ≤ 4 cm in greatest dimension and limited to the kidney; T1b tumor is between 4 cm and 7 cm; T2a tumor is >7 cm but ≤ 10 cm in size and limited to the kidney; T2b tumor is >10 cm in size but confined within the kidney; T3 tumor extends into major veins or invades adrenal gland or perinephric tissues, but not beyond Gerota's fascia; and T4 tumor invades beyond Gerota's fascia (includes a contiguous extension into ipsilateral adrenal gland) [21, 22].

In the management of patients with RCC, minimally invasive ablative treatments can be used in stage I disease without lymph node or distant metastatic lesions, which may sometimes be challenging to detect on imaging studies, especially when they are small. Therefore, imaging parameters that can be used in the preoperative estimation of the clinical stage, which is one of the main parameters of the prognostic evaluation together with the pathological grade, have critical importance in guiding optimal management of the patients, particularly in the accurate differentiation of

stage I clear cell RCC from advanced disease. Although studies performed to estimate the role of ADC in this differentiation are limited in number, they are suggestive of its potential utility as a quantitative method in preoperative clinical staging [18, 23]. In this regard, we tried to determine the association of ADC values of clear cell RCC with every clinical stage on 3T MR imaging.

Our study revealed that when the cut-off value of ADC is taken as 1.41×10^{-3} mm²/s, the sensitivity is 90% and the specificity is 80.4% to differentiate between clinical stage I and more advanced stages (III and IV) and when it is taken as 1.22×10^{-3} mm²/s the sensitivity is 100%. The specificity is 98.1% to differentiate between clinical stage I and stage IV. Previously, Nakamura et al. evaluated 49 patients with pathologically proven RCCs to compare the ADC values between each clinical stage and reported statistically significant differences in ADC values between stage I and more advanced stages (III and IV) [18]. In the study of Yoshida et al., 51 patients with 51 pathologically confirmed clear-cell RCCs who underwent 1.5T MR imaging were retrospectively evaluated. A statistically significant difference in ADC values was reported between stages I clear-cell RCC and more advanced stage clear-cell RCCs with lymph node metastasis or distant metastasis. They found a sensitivity of 80.0% and a specificity of 81.0% for the optimal cut-off ADC value of 1.552×10^{-3} mm²/s [23].

In addition to clinical staging, the nuclear grade of clear cell RCC also correlates with survival, particularly the Furhman grade [20, 24-26]. Previous studies reported a significant difference between ADC values of high grade and low-grade clear cell RCCs, particularly Furhman grades [18, 27-28]. In our study, we also tried to compare the ADC values for each

Furhman grade. Our study population was composed mainly of Furhman grade 2 clear cell RCCs. Similarly, in the study of Gürsoy et al., more than half of the patients were Furhman grade 2 with the rate of 61% among all four grades [29]. We found that Furhman grade I clear cell RCCs had significantly higher mean ADC values than all groups. The cut-off ADC value of 1.59×10^{-3} mm²/s in our study was found to differentiate between Furhman grade I and advanced grades with sensitivity and specificity of 100%. In one study, ADC values at b-value of 500 s/mm² were found to be significantly lower in Furhman grade III-IV clear cell RCC cases compared with Furhman grade I-II group, while no significant difference was found the difference was found between the groups at b value of 1000 s/mm². The authors concluded that this could be explained to some extent by the explicitness of the perfusion effect at lower b values [9].

In a meta-analysis regarding the relationship between b value and the detectability of RCC, standard b-value (800–1000 s/mm²) showed a superior specificity but an approximately equivalent sensitivity to low b-value (400–500 s/mm²), which had an overall superior diagnostic accuracy [30]. The b value we preferred in our study was 50 and 800 s/mm². The limitations of our study included the following; first, this was a single-center and a retrospective study. Second, evaluations were performed by only one single observer. Third, only two b-values (50 and 800 mm²/s) were used to calculate the ADC. Fourth, the reproducibility of the ADC values were not assessed. On the other hand, when compared with the present studies, our study stands out with its following features; we evaluated a relatively larger number of patients, we performed the MR imaging on 3T MR device, and ADC values were detailed for every clinical

stage. Moreover, the ADC values were also compared for each Furhman grade.

Conclusion

In conclusion, we assessed the utility of ADC in a relatively large number of patients with clear cell RCC for differentiating preoperative clinical stages and Furhman grades. We found a statistically significant difference in ADC values between early-stage clear cell RCC and advanced stages of the disease. In patients with kidney masses suggestive of clear cell RCC on imaging studies, the ADC of primary tumor site less than $1.41 \times 10^{-3} \text{ mm}^2/\text{s}$ should be considered for the possibility of lymph node or distant metastatic lesions, and the values less than $1.22 \times 10^{-3} \text{ mm}^2/\text{s}$ should be strongly suggested for distant metastasis. The accurate preoperative characterization of clear cell RCC is essential to ensure appropriate clinical management of patients and contributes to the prognosis. Therefore, the ADC value of the primary tumor site should be evaluated in predicting the clinical stage of clear cell RCC.

Funding: *The author(s) received no financial support for the research, authorship, and/or publication of this article.*

Conflict of Interest: *The authors declare that they have no conflict of interest.*

Ethical statement: *The study was approved by the Recep Tayyip Erdoğan University Faculty of Medicine Clinical Research Ethics Committee (Date: 2021-11-11/No: 2021/195).*

Open Access Statement

This is an open access journal which means that all content is freely available without charge to the user or his/her institution under the terms of the Creative Commons Attribution Non-Commercial License (<http://creativecommons.org/licenses/by-nc/4.0>). Users are allowed to read, download,

copy, distribute, print, search, or link to the full texts of the articles, without asking prior permission from the publisher or the author.

Copyright (c) 2021: Author (s).

References

- [1]NG CS, Wood CG, Silverman PM, et al. Renal cell carcinoma: diagnosis, staging, and surveillance. *Am J Roentgenol.* 2008;191(4):1220-32.
- [2]Siegel RL, Miller KD, Jemal A. Cancer statistics, 2018. *CA Cancer J Clin.* 2018;68(1):7-30.
- [3]Federle MP, Jeffrey RB, Woodward PJ, et al. Diagnostic Imaging: Abdomen. Lippincott Williams & Wilkins, Amirsys; 2009. P.2-02.
- [4]Hsieh JJ, Purdue MP, Signoretti S, et al. Renal cell carcinoma. *Nat Rev Dis Primers.* 2017;9(3):17009.
- [5]Graham TM, Stevens TM, Gordetsky JB. Pathology of renal tumors. In *Diagnosis and surgical management of renal tumors.* Springer, Cham; 2019. p. 13-38.
- [6]Escudier B, Porta C, Schmidinger M, et al. Renal cell carcinoma: ESMO Clinical Practice Guidelines for diagnosis, treatment and follow-up. *Ann Oncol.* 2016;27 (suppl 5):58-68.
- [7]Beck SD, Patel MI, Snyder ME, et al. Effect of papillary and chromophobe cell type on disease-free survival after nephrectomy for renal cell carcinoma. *Ann Surg Oncol.* 2004;11(1):71–77.
- [8]Cheville JC, Lohse CM, Zincke H, et al. Comparisons of outcome and prognostic features among histologic subtypes of renal cell carcinoma. *Am J Surg Pathol.* 2003;27(5):612–24.
- [9]Kıs N, Erok B. Diffusion weighted imaging in differentiation of the clear cell RCC from the major non-clear cell RCC subtypes. *Eur J Clin Exp Med.* 2021;19(3):215–20.

- [10] Koh DM, Collins DJ. Diffusion-weighted MRI in the body: applications and challenges in oncology. *Am J Roentgenol.* 2007;188(6):1622–35.
- [11] Elmi A, Hedgire SS, Covarrubias D, et al. Apparent diffusion coefficient as a non-invasive predictor of treatment response and recurrence in locally advanced rectal cancer. *Clin Radiol.* 2013;68(10):524–31.
- [12] Arvinda HR, Kesavadas C, Sarma PS, et al. Glioma grading: sensitivity, specificity, positive and negative predictive values of diffusion and perfusion imaging. *J Neurooncol.* 2009;94(1):87–96.
- [13] Tamada T, Sone T, Jo Y, et al. Apparent diffusion coefficient values in peripheral and transition zones of the prostate: comparison between normal and malignant prostatic tissues and correlation with histologic grade. *J Magn Reson Imaging.* 2008;28(3):720–26.
- [14] Yılmaz E, Erok B, Atca AÖ. Measurement of apparent diffusion coefficient in discrimination of benign and malignant axillary lymph nodes. *Pol J Radiol.* 2019;84:592-97.
- [15] Er HÇ, Peker E, Erden A, Öztürk E. The utility of diffusion-weighted imaging in differentiation of papillary and clear cell subtypes of renal cell carcinoma. *Acta Oncol Tur.* 2015;48(1):8-14.
- [16] Yu X, Lin M, Ouyang H, et al. Application of ADC measurement in characterization of renal cell carcinomas with different pathological types and grades by 3.0T diffusion-weighted MRI. *Eur J Radiol.* 2012;81(11):3061–66.
- [17] Maruyama M, Yoshizako T, Uchida K, et al. Comparison of utility of tumor size and apparent diffusion coefficient for differentiation of low- and high-grade clear-cell renal cell carcinoma. *Acta Radiol.* 2015;56(2):250–56.
- [18] Nakamura T, Yoshizako T, Araki H, et al. The relation between apparent diffusion coefficient and clinical stage of clear-cell renal cell carcinoma. *Clin imaging.* 2015;39(1):72-75.
- [19] Edge SB, Byrd DR, Compton CC, et al. *AJCC Cancer Staging Manual.* 7th ed. New York: Springer; 2010.
- [20] Fuhrman SA, Lasky LC, Limas C. Prognostic significance of morphologic parameters in renal cell carcinoma. *Am J Surg Pathol.* 1982;6(7):655–63.
- [21] Motzer RJ, Jonasch E, Agarwal N, et al. Kidney cancer, version 3. *J Natl Compr Canc Netw.* 2015;13(2):151-59.
- [22] Swami U, Nussenzeig RH, Haaland B, Agarwal N. Revisiting AJCC TNM staging for renal cell carcinoma: quest for improvement. *Ann Transl Med.* 2019;7(Suppl 1):S18.
- [23] Rika Yoshida, Takeshi Yoshizako, Araki Hisatoshi, et al. The additional utility of apparent diffusion coefficient values of clear-cell renal cell carcinoma for predicting metastasis during clinical staging. *Acta Radiol Open.* 2017;6(1):2058460116687174.
- [24] Delahunt B. Advances and controversies in grading and staging of renal cell carcinoma. *Mod Pathol.* 2009;22(Suppl 2):24-36.
- [25] Medeiros LJ, Jones EC, Aizawa S, et al. Grading of renal cell carcinoma: Workgroup No. 2. Union Internationale Contre le Cancer and the American Joint Committee on Cancer (AJCC). *Cancer.* 1997;80(5):990-91.
- [26] Delahunt B, Cheville JC, Martignoni G, et al. The International Society of Urological Pathology (ISUP) grading system for renal cell carcinoma and other prognostic parameters. *Am J Surg Pathol.* 2013;37(10):1490-504.

- [27] Goyal A, Sharma R, Bhalla AS, et al. Diffusion-weighted MRI in renal cell carcinoma: a surrogate marker for predicting nuclear grade and histological subtype. *Acta Radiol.* 2012;53(3):349–58.
- [28] Paudyal B, Paudyal P, Tsushima Y, et al. The role of the ADC value in the characterisation of renal carcinoma by diffusion-weighted MRI. *Br J Radiol.* 2010;83(988):336–43.
- [29] Gürsoy D, Seçinti İ.E., Hakverdi S., Görür S. Renal Cell Carcinoma: Epidemiological Profile and Histopathological Features. *Bulletin of Urooncology.* 2020;19(2):68-73.
- [30] Tang Y, Zhou Y, Du W, et al. Standard b-value versus low b-value diffusion-weighted MRI in renal cell carcinoma: a systematic review and meta-analysis. *BMC Cancer.* 2014;14:843.

Evaluation of silent cerebral ischemia and cognitive functions in young and middle-aged patients with metabolic syndrome

Gulmine Dundar¹,  Sehnaz Basaran² 

¹Department of Neurology, Kocaeli State Hospital, Kocaeli, Turkey

²Department of Neurology, Health Sciences University, Derince Training and Research Hospital, Kocaeli, Turkey

ABSTRACT

Aim: Metabolic syndrome (MetS) risk factors and accompanying silent cerebral ischemia (SCI) may cause cognitive decline. The aim of this study is to investigate the characteristics and association between SCIs and cognitive functions in young and middle-aged patients with MetS.

Methods: A total of 91 patients who were aged between 20-60 years with a diagnosis of metabolic syndrome were prospectively enrolled. Silent cerebral infarcts (SCIs) were analyzed by performing 3 Tesla magnetic resonance imaging (MRI) of the brain. Attention and executive functioning were assessed with the Wechsler Adult Intelligent scale-Revised (WAIS-R), verbal fluency, Stroop, and clock drawing test. Wechsler Memory Scale-Revised (WMS-R) visual reproduction and Öktem verbal memory processes tests were conducted to determine visual and verbal memory performance, whereas visuospatial functions were evaluated by the Benton judgment of line orientation test.

Results: Diagnosis of hypertension and diabetes mellitus were significantly higher, while educational level was lower in patients with SCIs than without SCIs. ($p < 0.001$, $p = 0.034$, $p = 0.05$, respectively). Cognitive test scores regarding attention and executive functioning, verbal, visual, and visuospatial memory showed no significant difference between patients with SCIs and without SCIs. However, hyperhomocysteinemia was negatively correlated with executive functions in MetS patients with SCI ($p = 0.038$).

Conclusions: SCIs may be associated with hypertension and diabetes mellitus in young and middle-aged patients with MetS. In addition, controlling homocysteine levels might be beneficial in MetS patients with SCI in terms of improving cognitive functions.

Key words: Metabolic syndrome, silent cerebral infarcts, cognition, executive functions, memory.

✉ Dr. Sehnaz Basaran

Department of Neurology, Health Sciences University,
Derince Training and Research Hospital, Kocaeli,
Turkey

E-mail: basaransehnaz@yahoo.com

Received: 2021-12-09 / Accepted: 2021-12-26

Published online: 2022-01-01

Introduction

Metabolic syndrome (MetS) is an endocrinopathy characterized by a prothrombotic and proinflammatory process resulted in abdominal obesity, hyperlipidemia,

high blood pressure, and insulin resistance [1]. MetS and its components are associated with an increased risk of cardiovascular and cerebrovascular diseases [2,3]. Moreover, in the last few decades, a combination of genetic tendency and unhealthy lifestyle choices such as low physical activity, and progressive weight gain leading MetS as a prominent public health issue [4, 5].

Silent cerebral infarct (SCI) is an incidental condition detected by neuroradiologic

evaluation [as performed with computed tomography (CT) or magnetic resonance imaging (MRI)] without any neurological symptoms or deficits. This term was first described by Chodosh et al. in 1988, and classified as a subtype in “cerebrovascular diseases III” by the National Institute of Neurological Disorders and Stroke (NINDS 1990) [6, 7]. The prevalence of SCIs in the general population ranging from 10% to 28% [8, 9].

Previous studies have suggested the significant association between SCIs, periventricular, and subcortical white matter hyperintensities, and MetS [10, 11]. Additionally, the presence of SCIs may be an initial process for cognitive dysfunction and vascular dementia [12-14]. However, studies about the relationship between vascular changes and cognitive functions in patients with MetS have been highly controversial due to the variabilities in neurocognitive assessment tools and sampling methods [13-15]. Based on our knowledge, no study has assessed SCIs and cognitive functions in young and middle-aged people with MetS. Hence, we aimed to explore the possible association between MetS components, SCIs, and cognitive performance on these subjects.

Materials and methods

Study design

Our study was performed at endocrinology and neurology outpatient clinic in Kocaeli University Medicine Faculty. The study protocol was approved by the local ethics Committee which is in line with the Helsinki Declaration (2009/98, AEK-12/17). Written and informed consent was obtained from all subjects prior to participating.

Study population

All subjects were prospectively recruited from endocrinology clinic in a tertiary care hospital.

Before the initiation of neuroradiologic and cognitive assessment, the diagnosis of MetS was made in accordance with the NCEP ATP-III criteria [16]. This syndrome was defined by an alteration in ≥ 3 of the following 5 criteria: (i) waist circumference of the males >102 cm, and females >88 cm; (ii) fasting blood glucose concentration ≥ 110 mg/dl or receiving drugs for diabetes medication; (iii) triglyceride levels ≥ 150 mg/dl; (iv) HDL-cholesterol levels less than < 40 mg/dl in males, <50 mg/dl in females; or receiving medications for dyslipidemia (v) systolic blood pressure value ≥ 130 mmHg and/or diastolic ≥ 85 mmHg; and/or receiving antihypertensive agents.

Neuroradiological evaluation

Cranial magnetic resonance imaging (MRI) was performed using 3T MR system (Achieva; Philips Medical Systems, Netherlands). All images including axial T1 and axial T2 weighted images and fluid-attenuated inversion recovery (FLAIR) sequences were acquired. SCIs were documented while the lesions had were ≤ 15 mm in diameter, hyperintensity on a T2 sequence and FLAIR scan, hypointensity on a T1 sequence, without neurological symptoms and findings. Neuroradiologic assessment were performed by using Fazekas White Matter Lesion Scale [17]. In this scale, white matter hyperintensities were classified into four grades; Grade 0 = lack of hyperintensities on periventricular white matter; Grade 1 = frontal or occipital cap or thin line surrounding lateral ventricle; Grade 2 = halo image around lateral ventricles; Grade 3 = asymmetric deep white matter hyperintensities. All sequences were interpreted by an experienced neuradiologist.

Cognitive assessment

An experienced clinical psychologist applied the neuropsychological tests including various cognitive domains, such as executive functioning, verbal, and visual memory, and

visuospatial abilities. All participants performed the selected tests for all cognitive skills. Neuropsychological tests were defined below:

Wechsler adult intelligent scale-revised (WAIS-R) digit span and similarities test: WAIS-R digit span test evaluates the attention, short-term, and working memory performance. Under normal circumstances, an adult could repeat seven digits in a forward sequence which indicates the mean limit of the human information storage capacity. No more than two digits should differ from forward digit span scores when performing backward digit span test. It has been adapted to Turkish by Epir and İskit et al. [18].

WAIS-R similarities test determines the abstract verbal reasoning of the frontal lobe. Subjects are responded how two seemingly dissimilar items could be similar. Patients with decline in abstract verbal reasoning could not identify the differences between these items [19].

Verbal fluency test: This test is a tool to assess executive and linguistic functions [20]. It has been standardized to Turkish by Tumac et al. Participants say the words beginning with the letter F, A, and S (in Turkish K, A, and S) on their own in a one-minute period [21]. Semantic fluency test has performed by asking the subjects to name as many different animals, fruits, and professions as they could in one minute time per category. The final score is the total number of responded items during three minutes [20].

Stroop test: This test evaluated the susceptibility to interference and the inability to inhibit inappropriate automatic responses by tasks that provoke competing responses [22]. It has been adapted to Turkish and is called "Tubitak Bilnot Battery" by Karakaş et al. [23]. Prolonged response time and the presence of

many errors and corrections in this test represent frontal dysfunction [22].

Clock drawing test: This test is used for screening verbal, visuoconstructive, and spatial abilities. Various application methods have been developed and could be used for the assessment. In a classic method, patients performed to draw a clock, then put all the numbers with setting the hands for a time of 11.10 [24]. Turkish validation and reliability were performed by Cangöz et al. [25].

Öktem verbal memory processes test: This test contains a word-list learning scheme that performed in two steps. In the first step, 15 words were read 10 times to the patient by the clinician. In the second step, patients respond to these 15 words after 45 minutes (free recall). After both of these steps, the total response time that a patient could remember and repeat the words defined by the total learning score. This test measures working memory, retrieval skills, learning, and retention of learned information [26].

Wechsler Memory Scale-Revised visual memory test (WMS-R): This scale is a comprehensive psychometric test that evaluates attention, verbal and visual memory. In addition, the visual reproduction subtest of WMS-R reflects visual perceptual or constructional functioning performance [27]. Turkish reliability and validity of this test was performed by Mollahasanoglu et al. [28].

Benton Judgment of line orientation test: This test assesses visuospatial functions that are commonly related to right parietal lobe [29]. Turkish validity and reliability were established by the project of BİLNOT battery [30].

Statistical analysis

The statistical package for social sciences (SPSS) 17.0 (IBM Corporation, USA) was used for the analysis. Descriptive data was defined by numbers (n), mean \pm standard deviation

(SD), and percentages (%). Chi-square test was performed to analyze categorical parameters. Normality tests were carried out for all variables. Independent sample t-test and Mann-Whitney U test were performed for normally and non-normally distributed variables, respectively. For the comparison of cognitive test performances between the patient groups, all subscales were transformed into z scores and composite z scores were measured to determine the decline in each cognitive domain (executive functions, memory, and visuospatial functions). The z-scores of negative components in the cognitive tests were multiplied by -1 and added to positive components of the scales to prevent biased scores. Partial correlation analysis was used to evaluate the association between cognitive test scores and syndrome-related

variables in patients with MetS. In this analysis, we adjusted confounding factors such as age, gender, and educational level. Conditions with a *p*-value of ≤ 0.05 were considered statistically significant.

Results

Demographic and clinical characteristics

We analyzed 91 consecutively patients with MetS [47 patients with SCIs (36 women, 11 men) and 44 patients without SCIs (33 women, 11 men)] who were admitted to the endocrinology clinic between July 2009-September 2010. No statistical difference was found between sociodemographic parameters such as gender, smoking status among the groups. However, age was significantly higher, and educational level was lower in MetS

Table 1. Sociodemographic, clinical, and cognitive features of MetS patients with and without silent cerebral infarcts (SCIs).

Variables	Patients with SCI (n=47)	Patients without SCI (n=44)	<i>p</i>
Age (years)	45.85±6.83	40.14±8.96	0.001
Gender (female, n, %)	36 (76.6)	33 (75)	0.86
Education (years)	7.08±2.91	8.47±3.67	0.05
Current or past smoker (n, %)	21 (44.7)	18 (40.9)	0.59
Waist circumference (cm)	113.35±12.21	115.47±13.42	0.52
Family history of MetS (n, %)	27 (57.4)	30 (68.2)	0.29
Hypertension (n, %)	30 (63.8)	10 (22.7)	<0.001
Diabetes mellitus (n, %)	23 (48.9)	12 (27.3)	0.034
Dyslipidemia (n, %)	45(95.7)	42 (95.5)	0.94
Homocysteine (5–15 µmol/l.)	15.01±5.38	14.77±3.97	0.71
Protein C	118.38±25.66	115.75±15.82	0.85
Protein S	101.13±15.64	99.91±17.97	0.73
Executive functions	-.54.34±23.27	-52.52±22.01	0,703
Memory functions	0.17±4.12	-0.18±3.98	0,672
Visuospatial functions	0.06±1.34	0.06±1.93	0.756

Variables are presented mean ± standard deviation. MetS= metabolic syndrome, SCIs=silent cerebral infarcts.

patients with SCI (+) ($p=0.001$, and $p=0.05$, respectively). The diagnosis of hypertension and diabetes mellitus were significantly frequent ($p < 0.001$, and $p=0.034$, respectively) in SCI (+) patients, while family history of MetS, waist circumference, dyslipidemia, serum homocysteine, protein C, and protein S levels did not differ among SCI (+) and SCI (-) groups. Comparison of demographic and clinical features of MetS patients with and without SCIs was given in Table 1.

Neuroradiologic evaluation

Based on the Fazekas scale, 47 patients were SCI (+) 44 patients were SCI (-) in subjects with MetS. Four patients had grade 1 (caps or pencil-thin lining), and 1 patient had grade 2 (smooth halo) periventricular white matter hyperintensities (PVWM). In addition, 32 patients had grade 1 (punctate foci), and 4 patients had grade 2 (beginning confluence of foci) deep white matter hyperintense signals (DWMH). Table 2 shows the frequency and localization of SCIs on cranial MRI of the patients with MetS.

Age distribution of the SCI (+) MetS patients; 3.29 % were ≤ 34 years, 5.49 % were between 35-39 years, 13.19 % were between 40-44 years, and 12.09 % were between 45-49 years, and 17.58 % were 50 or older (Table 3).

Table 2. Frequency and localization of SCIs on cranial MRI of patients with MetS.

SCI	n	%
Negative	44	48.35
Positive	47	51.65
PVWM		
Grade 1 (caps or pencil-thin lining)	4	8.51
Grade 2 (smooth halo)	1	2.12
Grade 3 (irregular PVH extending into the deep white matter)	-	0
DWMH		
Grade 1 (punctate foci)	32	68.08
Grade 2 (beginning confluence of foci)	2	4.25
Grade 3 (large confluent areas)	-	0
PVWM Grade 1+ DWMH Grade 1	6	12.77
PVWM Grade 1+ DWMH Grade 2	2	4.25

SCIs = silent cerebral infarcts; MRI= magnetic resonance imaging; MetS= metabolic syndrome; PVWM= periventricular white matter hyperintensities; DWMH= deep white matter hyperintense signals.

Cognitive assessment

No significant differences were detected regarding executive, memory, and visuospatial cognitive domains between subjects with SCI (+) and SCI (-) MetS groups. In a partial correlation analysis, serum homocysteine levels were negatively correlated with executive performance in SCI (+) patients with MetS ($r =$

Table 3. Age distribution of MetS patients with and without silent cerebral infarcts

Age groups	SCI (+)	SCI (-)	Total
≤ 34 years	3 (3.29%)	11 (12.08%)	14 (15.38%)
35-39 years	5 (5.49%)	9 (9.89%)	14 (15.38%)
40-44 years	12 (13.19%)	11 (12.09%)	23 (25.27%)
45-49 years	11 (12.09%)	8 (8.79%)	19 (20.87%)
50-60 years	16 (17.58%)	5 (5.49%)	21 (23.07%)

Table 4. Partial correlation analysis between cognitive domains (as presented with composite z scores) and syndrome related variables in metabolic syndrome patients with SCIs.

Parameters	Executive functions	Memory functions	Visuospatial functions
Waist circumference (cm)	r= -,196 p= ,201	r= ,805 p= ,42	r=,006 p=,968
Smoking	r= -,044 p=,683	r=,056 p=,606	r=,025 p=,817
Systolic blood pressure (mmHg)	r= -,018 p= ,910	r= -,063 p=,687	r= -,045 p=,770
Diastolic blood pressure (mmHg)	r= -,029 p= ,853	r= -,018 p=,910	r= -,023 p=,883
Fasting blood glucose (mg/dl)	r= ,198 p= ,197	r=,121 p=,434	r=,076 p=,625
Hba1c (%)	r= -,017 p= ,915	r= -,099 p=,523	r=,041 p=,792
TG (mg/dL)	r=,175 p=,255	r= -,011 p=,942	r=,048 p=,755
LDL (mg/dL)	r= -,151 p= ,329	r= -,282 p=,064	r= ,135 p=,383
Total cholesterol (mg/dL)	r= -,085 p= ,581	r= -,259 p=,089	r=,138 p=,371
HDL (mg/dL)	r= ,017 p= ,915	r= -,100 p=,517	r=,133 p=,390
Homocysteine (mcmol/L)	r= -,314 p=,038	r= -,231 p=,132	r= -,143 p=,353
Protein C (IU/dL)	r=,108 p=,486	r=,284 p=,061	r= -,141 p=,360
Protein S (IU/dL)	r=,117 p=,450	r= -,155 p=,314	r=,214 p=,162

SCIs= Silent cerebral infarcts; Hba1c= Hemoglobin A1c; TG= triglyceride; LDL= low-density lipoprotein; HDL= high-density lipoprotein.

-.314, p = .038). No correlation was found between other MetS components and cognitive domains in this group (Table 4).

Discussion

In this study, we explored clinical factors and cognitive performances of MetS patients with and without SCIs. Additionally, we evaluated possible associations between syndrome-

related factors and cognitive functions regarding executive, memory, and visuospatial domains in young and middle- aged SCI (+) patients with MetS.

SCIs are the possible neurological consequences of the prothrombotic and proinflammatory pattern of the MetS components such as; hypertension, atherogenic dyslipidemia, insulin resistance, and abdominal

obesity. Increased free radicals, alterations of neurotrophic factors, impaired insulin-stimulated glucose transport into the brain may contribute to both atherothrombotic and lacunar ischemic processes in patients with MetS [31-34].

Strong association between MetS risk factors and SCIs have been well-established in epidemiologic and clinical studies [8, 31-35]. In a population-based Rotterdam Scan study, cranial MRI of 1077 non-demented participants between 60 to 90 years was compared. They found that 20 % of the population had shown SCIs, and the frequency increased per year with age: 8 % in the group aged between 60-65 years and 35 % at age 85 to 90 years old. In their study, there was a strong association between SCIs and hypertension (OR= 2.4; 95 % CI, 1.7 to 3.3), whereas no association was found between SCIs, DM, and smoking [8]. In addition, community-based Framingham Study evaluated the risk factors and the prevalence of SCI among middle-aged and elderly participants. They showed that SCI prevalence increased with age; < 8 % in the 30– 49 year's age, and > 15 % at 70– 89 years. Furthermore, higher systolic blood pressure (SBP), elevated plasma homocysteine, atrial fibrillation, carotid stenosis, and increased carotid intimal-medial thickness were associated with SCIs [35]. Consistent with this report, we found that the frequency of SCIs increases with age (17.1 % at age \leq 39 years, and 82.9 % at age \geq 40 years, respectively). In Cardiovascular Health Study, 3,324 elderly subjects without a history of cerebrovascular disease underwent a cranial MRI scan. They reported that, 28% of these subjects had SCIs, and higher systolic and diastolic blood pressure values, carotid wall thickness, and atrial fibrillation were associated with a higher risk for cerebrovascular events [36].

However, only a few studies have been focused on the association between the risk factors and SCIs among young and middle-aged people in clinical practice. In Atherosclerosis Risk in Communities (ARIC) study, hypertension, smoking, age, alcohol use, educational level, and being African American were independently associated with white matter hyperintensities in middle-aged healthy subjects [37,38]. In our study, age was significantly higher ($p=0.001$), educational level was significantly lower ($p=0.05$), and diagnosis of hypertension and DM were more frequent ($p<0.001$, and $p=0.034$, respectively) in young and middle aged MetS patients with SCIs than without SCI. In a study by Park et al., higher blood pressure, abnormal glucose regulation, hypertriglyceridemia and large waist circumference were significantly related to SCIs in MetS patients aged between 40 and 59 years [39]. Similarly, Kwon and colleagues confirmed the significant role of high blood pressure and abnormal glucose regulation on SCI risk in a wide spectrum of ages (between 20-86 years) [40]. In addition, Atherosclerosis Risk in Communities Neurocognitive Study (ARIC-NCS) reported that patients with more severe diabetes (defined as elevated HbA1c levels and longer disease duration) were at high risk for white matter hyperintensities in the middle aged group [41]. Taking these into account, previous studies reported conflicting results due to the sampling strategies (differences in age groups, variability between radiological techniques, casual interferences, having a history of cerebrovascular event before the enrollment) during the methodologic process.

MetS components such as; insulin resistance, glucose intolerance, dyslipidemia, arterial hypertension, and morbid obesity *constitute an important* part of cognitive decline [42-44].

Episodes of hypoglycemia and insulin-resistance in DM, arteriolosclerosis, and lipohyalinosis in small vessels due to hypertension, neuroinflammation, and altered *adipokine* levels in obesity may facilitate the development of cognitive impairment in patients with MetS [43-45]. Although, the exact mechanism has not been elucidated, the pathogenesis is explained with a multifactorial process regarding vascular injury caused by cerebral ischemia and non-ischemic neuronal death via neurodegeneration [45]. Recent studies have demonstrated poorer executive and memory functions in both middle-aged and elderly people with MetS [46-49]. In addition, previous research has emphasized the contributing effect of cerebral ischemia on the relationship between cognitive decline and MetS components [33,50]. In our study, we observed decline in executive functions, memory performance, and visuospatial functions in 37.3 %, 8.8 %, and 29.7 % of MetS patients, respectively. Nevertheless, cognitive test scores did not differ between MetS patients with and without SCIs. These results may be related to the existence of a younger age population in our study. In the MetS patients with SCIs group, a significant correlation between elevated serum homocysteine levels and decline in executive functioning was observed ($r = -.314, p = .038$). Previous studies emphasized the role of increased homocysteine levels on the risk of cognitive impairment regarding episodic memory, speed of information processing, spatial learning and executive functions in elderly subjects [51-54]. However, these studies are limited to the geriatric population, and the exact mechanism of homocysteine levels on cognitive processes remained unclear. This study was limited in several ways. First, our study was carried out in a tertiary referral

center with a relatively small sample size. Second, depending on the hospital's distance between densely populated areas and frequent admissions of chronic and palliative care patients to our hospital, we could not reach the targeted number of patients during the enrollment process. Third, consecutive and nonrandomized sampling may possibly cause biased results on neuropsychological test scores. Despite these limitations, this is the first prospective study comparing the possible association between syndrome-related factors, SCIs, and cognitive performance in young and middle aged subjects with MetS. Additionally, all reliable and validated cognitive tests were applied by an experienced clinical psychologist.

Conclusion

In sum, our results suggest that older age, lower educational status, hypertension, and DM are more frequent, and serum homocysteine levels are associated with executive functions in SCI (+) patients with MetS. Further longitudinal studies are needed to clarify syndrome-related factors, cognitive phenotypes, and dementia risk in patients with SCIs and MetS.

Funding: *The author(s) received no financial support for the research, authorship, and/or publication of this article.*

Conflict of Interest: *The authors declare that they have no conflict of interest.*

Ethical statement: *All procedures performed in studies involving human participants were in accordance with the ethical standards of the clinical Research Ethics Committee of Kocaeli University Hospital (approval number 2009/98, AEK-12/17) and adhered to the tenets of the Declaration of Helsinki. Written and informed consent was obtained from all participants.*

Acknowledgements: We would like to thank Prof. Dr. Faik Budak for his permanent support and scientific guidance. In addition, we sincerely thank all patients and healthy volunteers who participated in our study.

Open Access Statement

This is an open access journal which means that all content is freely available without charge to the user or his/her institution under the terms of the Creative Commons Attribution Non-Commercial License (<http://creativecommons.org/licenses/by-nc/4.0>). Users are allowed to read, download, copy, distribute, print, search, or link to the full texts of the articles, without asking prior permission from the publisher or the author.

Copyright (c) 2021: Author (s).

References

- [1] McCracken E, Monaghan M, Sreenivasan S. Pathophysiology of the metabolic syndrome. *Clin Dermatol*. 2018;36(1):14-20.
- [2] Alberti KG, Eckel RH, Grundy SM, et al. International Diabetes Federation Task Force on Epidemiology and Prevention; National Heart, Lung, and Blood Institute; American Heart Association; World Heart Federation; International Atherosclerosis Society; International Association for the Study of Obesity. Harmonizing the metabolic syndrome: a joint interim statement of the International Diabetes Federation Task Force on Epidemiology and Prevention; National Heart, Lung, and Blood Institute; American Heart Association; World Heart Federation; International Atherosclerosis Society; and International Association for the Study of Obesity. *Circulation*. 2009;120(16):1640-45.
- [3] Bangen KJ, Armstrong NM, Au R, Gross AL. Metabolic Syndrome and Cognitive Trajectories in the Framingham Offspring Study. *J Alzheimers Dis*. 2019;71(3):931-43.
- [4] Simmons RK, Alberti KG, Gale EA, et al. The metabolic syndrome: useful concept or clinical tool? Report of a WHO Expert Consultation. *Diabetologia*. 2010;53(4):600-5.
- [5] Kahn R, Buse J, Ferrannini E, et al. The metabolic syndrome: time for a critical appraisal. Joint statement from the American Diabetes Association and the European Association for the Study of Diabetes. *Diabetologia*. 2005;48(9):1684-99.
- [6] Chodosh EH, Foulkes MA, Kase CS, et al. Silent stroke in the NINCDS Stroke Data Bank. *Neurology*. 1988;38(11):1674-79.
- [7] Special report from the National Institute of Neurological Disorders and Stroke. Classification of cerebrovascular diseases III. *Stroke*. 1990;21(4):637-76.
- [8] Vermeer SE, Koudstaal PJ, Oudkerk M, et al. Prevalence and risk factors of silent brain infarcts in the population-based Rotterdam Scan Study. *Stroke*. 2002;33(1):21-25.
- [9] Price TR, Manolio TA, Kronmal RA, et al. Silent brain infarction on magnetic resonance imaging and neurological abnormalities in community-dwelling older adults. The Cardiovascular Health Study. CHS Collaborative Research Group. *Stroke*. 1997; 28(6):1158-64.
- [10] Jiménez-Balado J, Riba-Llena I, Abril O, et al. Cognitive Impact of Cerebral Small Vessel Disease Changes in Patients With Hypertension. *Hypertension*. 2019; 73(2):342-49.
- [11] Bokura H, Yamaguchi S, Iijima K, et al. Metabolic syndrome is associated with silent ischemic brain lesions. *Stroke*. 2008;39(5):1607-9.
- [12] Zhao J, Tang H, Sun J, et al. Analysis of cognitive dysfunction with silent cerebral

- infarction: a prospective study in Chinese patients. *Metab Brain Dis.* 2012; 27(1):17-22.
- [13] Shibata K, Nishimura Y, Otsuka K, et al. Influence of cerebral white matter hyperintensities on cognitive impairment in elderly medical patients. *Geriatr Gerontol Int.* 2017;17(10):1488-93.
- [14] Wardlaw JM, Valdés Hernández MC, Muñoz-Maniega S. What are white matter hyperintensities made of? Relevance to vascular cognitive impairment. *J Am Heart Assoc.* 2015, 4(6):001140.
- [15] Bokura H, Nagai A, Oguro H, et al. The association of metabolic syndrome with executive dysfunction independent of subclinical ischemic brain lesions in Japanese adults. *Dement Geriatr Cogn Disord.* 2010;30(6):479-85.
- [16] Expert Panel on Detection, Evaluation, and Treatment of High Blood Cholesterol in Adults. Executive Summary of The Third Report of The National Cholesterol Education Program (NCEP) Expert Panel on Detection, Evaluation, And Treatment of High Blood Cholesterol In Adults (Adult Treatment Panel III). *JAMA.* 2001; 285(19):2486-97.
- [17] Mäntylä R, Erkinjuntti T, Salonen O, et al. Variable agreement between visual rating scales for white matter hyperintensities on MRI. Comparison of 13 rating scales in a poststroke cohort. *Stroke.* 1997;28(8):1614-23.
- [18] Epir S, Iskit Ü. Wechsler Yetişkinler Zeka Ölçeği Türkçe çevirisinin ön analizi ve üniversite danışmanlık merkezlerindeki uygulama potansiyeli. *Hacettepe Sosyal ve Beşeri Bilimler Dergisi,* 1972; 4: 198-205.
- [19] Wechsler D, Manual for the Wechsler Adult Intelligence Scale-Revised. In: Psychological Corporation, New York; 1981.
- [20] Benton A. Differential behavioral effects on frontal lobe disease. *Neuropsychologia.* 1968; 6: 53- 60.
- [21] Tumaç A. Normal deneklerde, frontal hasarlara duyarlı bazı testlerde performansa yaş ve eğitimin etkisi, yüksek lisans tezi, İstanbul 1997.
- [22] Golden, CJ (1978) Stroop Color and Word Test: A Manual for Clinical and Experimental Uses. Chicago, Illinois; 1978. p.1-32.
- [23] Karakas S, Eski R, Basar E. BILNOT Battery, Standardized neuropsychological tests for Turkish culture. 32nd National Congress of Neurology Congress Book. 1997. p. 43-70.
- [24] Freedman MI, Leach L, Kaplan E, et al. Clock Drawing. Oxford: Oxford University Press, 1994.
- [25] Cangöz B, Karakoç E, Selekler K. Saat Çizme Testinin 50 yaş ve üzeri Türk yetişkin ve yaşlı örnekleminde norm belirleme ve geçerlik-güvenirlilik çalışmaları. *Turkish J Geriatrics* 2006; 9: 136-42.
- [26] Öktem Ö. Sözel bellek süreçleri testi (SBST): Bir ön çalışma. *Nöropsikiyatri Arşivi,* 1992; 29: 196-206.
- [27] Wechsler D: Wechsler Memory Scale-Revised Manual. San Antonio, Psychological Corporation, 1987.
- [28] Mollahasanoğlu A, Normal deneklerde bir grup görsel ve sözel bellek testleri performansına yaş ve eğitimin etkisi. yüksek lisans tezi, İstanbul 2002.
- [29] Michael D. Franzen. Reliability and Validity in Neuropsychological Assessment. Springer Science & Business Media.2000. p. 156.

- [30] Karakaş S. Bilnot Bataryası El Kitabı: Araştırma ve Geliştirme Çalışmaları, Ankara: Dizayn Ofset 2. Baskı, 2006.
- [31] Eguchi K, Kario K, Hoshida S, et al. Greater change of orthostatic blood pressure is related to silent cerebral infarct and cardiac overload in hypertensive subjects. *Hypertens Res.* 2004; 27(4):235-41.
- [32] Dearborn JL, Schneider AL, Sharrett AR, et al. Obesity, Insulin Resistance, and Incident Small Vessel Disease on Magnetic Resonance Imaging: Atherosclerosis Risk in Communities Study. *Stroke.* 2015; 46(11):3131-36.
- [33] Alkan E, Taporoski TP, Sterr A, et al. Metabolic syndrome alters relationships between cardiometabolic variables, cognition and white matter hyperintensity load. *Sci Rep.* 2019; 9(1): 4356.
- [34] Friedman JI, Tang CY, de Haas HJ, et al. Brain imaging changes associated with risk factors for cardiovascular and cerebrovascular disease in asymptomatic patients. *JACC Cardiovasc Imaging.* 2014; 7(10):1039-53.
- [35] Das RR, Seshadri S, Beiser AS, et al. Prevalence and correlates of silent cerebral infarcts in the Framingham offspring study. *Stroke.* 2008; 39(11): 2929-35.
- [36] Bernick C, Kuller L, Dulberg C, Longstreth WT Jr, Manolio T, Beauchamp N, Price T; Cardiovascular Health Study Collaborative Research Group. Silent MRI infarcts and the risk of future stroke: the cardiovascular health study. *Neurology.* 2001; 57(7): 1222-29.
- [37] Liao D, Cooper L, Cai J, et al. Presence and severity of cerebral white matter lesions and hypertension, its treatment, and its control. The ARIC Study. Atherosclerosis Risk in Communities Study. *Stroke.* 1996; 27(12): 2262-70.
- [38] Power MC, Deal JA, Sharrett AR, et al. Smoking and white matter hyperintensity progression: the ARIC-MRI Study. *Neurology.* 2015; 84(8): 841-48.
- [39] Park K, Yasuda N, Toyonaga S, et al. Significant associations of metabolic syndrome and its components with silent lacunar infarction in middle aged subjects. *J Neurol Neurosurg Psychiatry.* 2008; 79(6): 719-21.
- [40] Kwon HM, Kim BJ, Lee SH, et al. Metabolic syndrome as an independent risk factor of silent brain infarction in healthy people. *Stroke.* 2006; 37(2):466-70.
- [41] Biessels GJ, Despa F. Cognitive decline and dementia in diabetes mellitus: mechanisms and clinical implications. *Nat Rev Endocrinol.* 2018;14(10):591-604.
- [42] J. Jimenez-Balado, I. Riba-Llena, O. Abril, et al. Cognitive impact of cerebral small vessel disease changes in patients with hypertension. *Hypertension.* 2019;73(2): 342-49.
- [43] Cournot M, Marquie JC, Ansiau D, et al. Relation between body mass index and cognitive function in healthy middle-aged men and women. *Neurology.* 2006; 67(7): 1208-14.
- [44] Schneider ALC, Selvin E, Sharrett AR, et al. Diabetes, Prediabetes, and Brain Volumes and Subclinical Cerebrovascular Disease on MRI: The Atherosclerosis Risk in Communities Neurocognitive Study (ARIC-NCS). *Diabetes Care.* 2017; 40(11):1514-21.
- [45] Borshchev YY, Uspensky YP, Galagudza MM. Pathogenetic pathways of cognitive dysfunction and dementia in metabolic syndrome. *Life Sci.* 2019; 237:116932.
- [46] Foret JT, Oleson S, Hickson B, et al. Metabolic Syndrome and Cognitive

- Function in Midlife. Arch Clin Neuropsychol. 2021;36(6):897-907.
- [47] Rouch I, Trombert B, Kossowsky MP, et al. Metabolic syndrome is associated with poor memory and executive performance in elderly community residents: the PROOF study. Am J Geriatr Psychiatry. 2014; 22(11):1096-104.
- [48] Segura B, Jurado MA, Freixenet N, et al. Mental slowness and executive dysfunctions in patients with metabolic syndrome. Neurosci Lett. 2009;462(1):49-53.
- [49] Lai MMY, Ames DJ, Cox KL, et al. Association between Cognitive Function and Clustered Cardiovascular Risk of Metabolic Syndrome in Older Adults at Risk of Cognitive Decline. J Nutr Health Aging. 2020; 24 (3):300-304.
- [50] Yamawaki M, Wada-Isoe K, Yamamoto M, et al. Association of cerebral white matter lesions with cognitive function and mood in Japanese elderly people: a population-based study. Brain Behav. 2015; 5(3): e00315.
- [51] Hooshmand B, Solomon A, Kåreholt I, et al. Associations between serum homocysteine, holotranscobalamin, folate and cognition in the elderly: a longitudinal study. J Intern Med. 2012; 271 (2): 204-12.
- [52] Nurk E, Refsum H, Tell GS, et al. Plasma total homocysteine and memory in the elderly: the Hordaland Homocysteine Study. Ann Neurol. 2005; 58(6):847-57.
- [53] van den Kommer TN, Dik MG, Comijs HC, et al. Homocysteine and inflammation: predictors of cognitive decline in older persons? Neurobiol Aging. 2010; 31(10):1700-9.
- [54] Narayan SK, Saxby BK, Firbank MJ, et al. Plasma homocysteine and cognitive decline in older hypertensive subjects. Int Psychogeriatr. 2011; 23(10):1607-15.